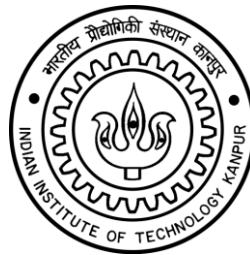


HYBRID METHODOLOGIES FOR HEALTH MANAGEMENT OF INTERNAL COMBUSTION ENGINES

Prashanth Dalawai



**DEPARTMENT OF MECHANICAL ENGINEERING
INDIAN INSTITUTE OF TECHNOLOGY KANPUR
INDIA**

HYBRID METHODOLOGIES FOR HEALTH MANAGEMENT OF INTERNAL COMBUSTION ENGINES

A Thesis Submitted
in Partial Fulfillment of the Requirements
for the Degree of
DOCTOR OF PHILOSOPHY

by

Prashanth Dalawai

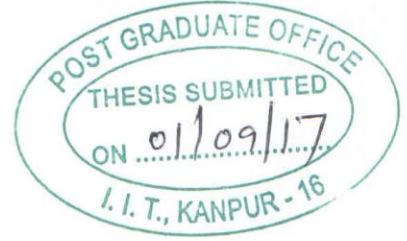
to the

DEPARTMENT OF MECHANICAL ENGINEERING
INDIAN INSTITUTE OF TECHNOLOGY KANPUR
August, 2017









Certificate

It is certified that the work contained in the thesis entitled “**Hybrid Methodologies for Health Management of Internal Combustion Engines**”, by “**Prashanth Dalawai**”, Roll No. 10105136 has been carried out under our supervision and that this work has not been submitted elsewhere for a degree.

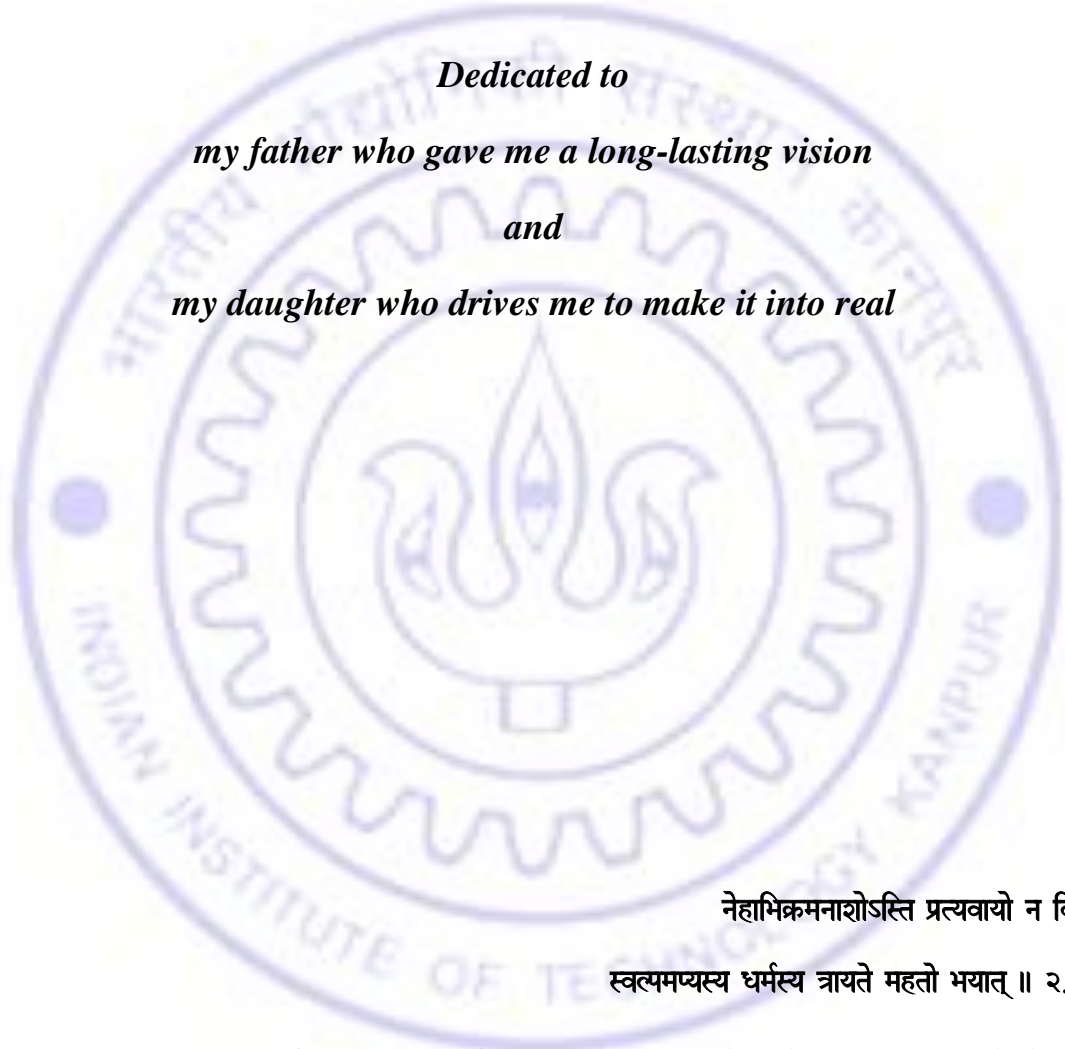
August, 2017

Dr. N. N. Kishore

Dr. N. S. Vyas

Department of Mechanical Engineering,
Indian Institute of Technology, Kanpur





*Dedicated to
my father who gave me a long-lasting vision
and
my daughter who drives me to make it into real*

नेहाभिक्रमनाशोऽस्ति प्रत्यवायो न विद्यते ।
स्वल्पमप्यस्य धर्मस्य त्रायते महतो भयात् ॥ २.४० ॥

On the path of endeavors, there is neither loss nor diminution.

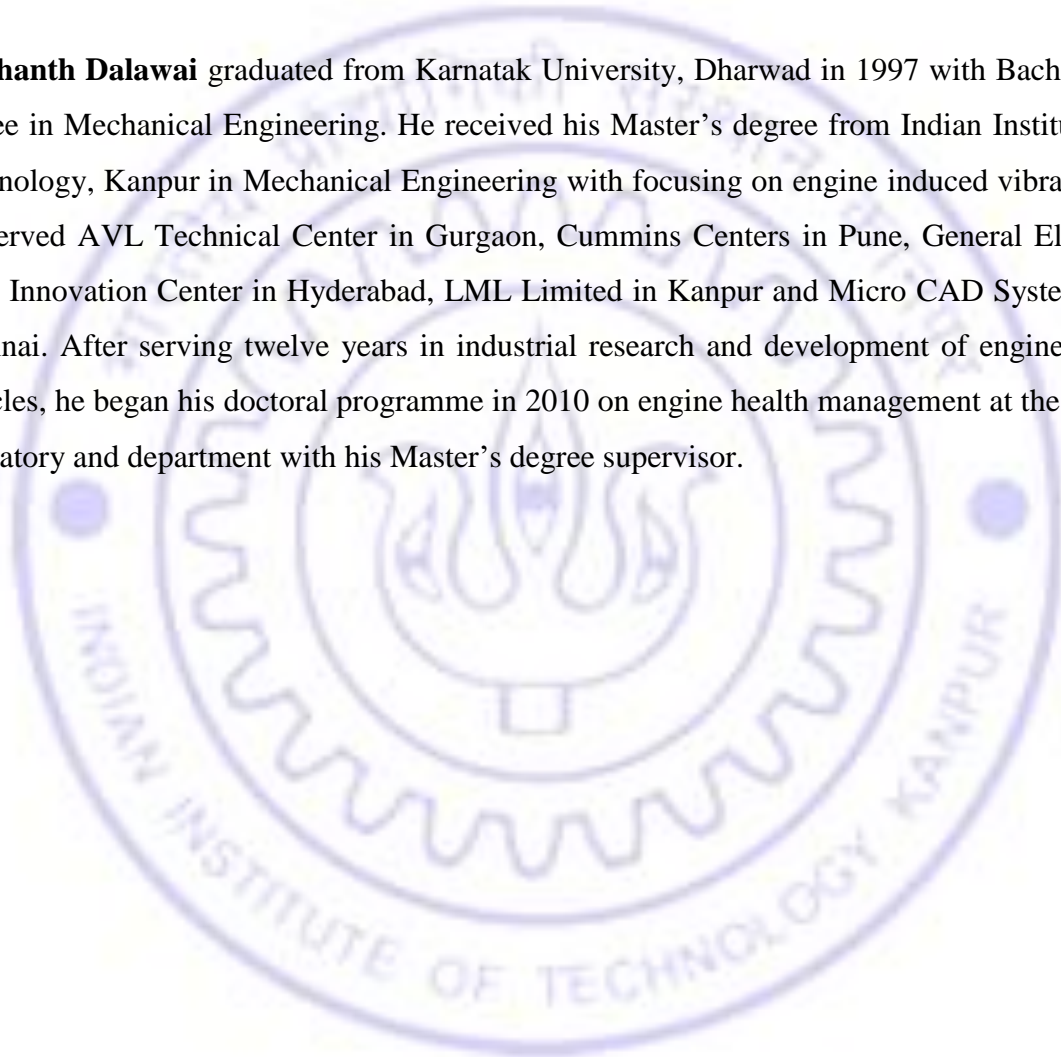
Even a little progress eliminates one's most dangerous fear.

Bhagavad Gita - 2.40



BIOGRAPHICAL SKETCH

Prashanth Dalawai graduated from Karnatak University, Dharwad in 1997 with Bachelor's degree in Mechanical Engineering. He received his Master's degree from Indian Institute of Technology, Kanpur in Mechanical Engineering with focusing on engine induced vibrations. He served AVL Technical Center in Gurgaon, Cummins Centers in Pune, General Electric India Innovation Center in Hyderabad, LML Limited in Kanpur and Micro CAD Systems in Chennai. After serving twelve years in industrial research and development of engines and vehicles, he began his doctoral programme in 2010 on engine health management at the same laboratory and department with his Master's degree supervisor.





ABSTRACT

Technologies for Integrated Vehicle Health Management (IVHM) are being vigorously pursued by automobile, railway and aerospace communities to ensure safety, reliability and availability of the vehicles. Health management of engines is critical to these technologies. Its structural faults occur internally due to minute geometric, material or operational causes, which are challenging to detect and cure. They continue to degrade the health and may lead to catastrophic failure, if left unattended.

In this work, some physics-based and data-driven health management methodologies are built and a hybrid procedure is developed on an internal combustion engine. An engine test bed has been built to study the emulated fault and failure conditions. Set-up is evaluated to select the sensitive operating and measurement conditions. Dimensionality of the database is reduced to few important signals. Procedures for signal processing and parameter estimation are developed on numerically constructed signals, and implemented on engine vibro-acoustic signals. Physics-based models are built using lumped mass discretization and flexible multi-body dynamics. Reduced models are explored to investigate fault diagnosis using vibration, and estimate life using fatigue and fracture techniques. Data-driven (statistical and intelligent) and model-based reasoning techniques are built and automated. Remaining useful life is estimated by correlating the signals to the idealized crack and degradation is predicted using state estimators. Some of these models are combined in a hybrid approach for a comprehensive scheme.



SYNOPSIS

Name of the Student: Prashanth Dalawai, Roll Number: 10105136
Degree for which Submitted: Ph.D., Department: Mechanical Engineering
Thesis Title: Hybrid Methodologies for Health Management
of Internal Combustion Engines
Name of the Thesis Supervisor: Dr. Nalinaksh S. Vyas and Dr. N. N. Kishore
Month and Year of Submission: August, 2017
Month and Year of Defense: April, 2018

Increasing system complexity and demand for higher reliability are consistently enforcing to manage the health of a vehicle. It is largely affected by faults such as mis-alignments, bends, cracks, erodes, and unbalances, which cause abnormal behaviour that can grow over time, and lead to a catastrophic failure, if left unattended. Faults originate in the material, geometry and assembly either due to minute defect, ill-operation, or overuse. They can be identified by monitoring the signatures such as vibration, noise and oil debris, and inferring the health conditions. Survivability can be predicted by assessing fault conditions, their threshold limits for failure and degradation rates. They require a framework to, gather exact knowledge, detect crucial faults, predict potential failures and activate appropriate maintenance remedies.

Engine failure, which is a major cause of a vehicle breakdown and challenging due to its complexity, is taken for this study. A health management procedure is developed by investigating, enhancing and combining typical transforms, reasoning and estimation techniques on an internal combustion engine. Symptoms to detect structural faults and predict the remaining survival life are established and automated.

A study on the state-of-the-art indicated that engine signals have non-stationary, non-linear and noise constituents due to the system complexity and practical nature. Engines have large number of rotating and reciprocating components; they undergo a varying configurations and largely uncertain cycle process. Rotating component fault diagnosis from stationary signal is well established (Jardine et al. [1], Walker et al. [2] and Lee et al. [3]), while failure prognosis (Zhang et al. [4] and An et al. [5]) is being studied. Few researchers (DeBotton et al. [6] and Liu et al. [7]) have attempted to diagnose engine faults by extracting statistical and Fourier features from stationary vibration signals as fault symptoms. For non-stationary signals, above features are less effective and it is difficult to interpret faults in time-frequency contours (Wu and Chen [8], Zheng and Leung [9] and Albarbar et al. [10]). Staszewski and Giacomini [11], and Peng et al. [12] attempted to quantify fault symptoms by estimating parameters of the time-frequency ridges. In most of these cases, only externally introduced structural and process faults are being studied. Which are easy to, introduce, detect, and can be cured automatically in a regular service. Structural faults are chronic, occur inside the engines, almost cureless and challenging to detect and emulate using conventional methods. They are being assessed by data-driven (statistical and intelligent), model-based (that uses precise rules from physics or knowledge and uncertainties of variables from measurement) or hybrid reasoning methods (Srivastava and Han [13]). Physics-based (Novotny and Pistek [14], and Ma and Perkins [15]) techniques provide understanding of dynamics and modes of failure, but inadequate to study actual faults and failures of a complex machinery. Advances in flexible multibody (Ricci [16]) with rotor dynamics (Markert et al. [17] and Friswell et al. [18]) simulate the detailed behaviour. It can even capture changes caused by few local geometrical and material defects. Data-driven techniques (Heng et al. [19] and Pascual [20]) can map and learn the real environment, but they consumes significant time and restricted to machine under consideration. Several sensors and cases make database very large, so signals must be used with optimum locations, dimensions, resolutions and parameters. Model-based techniques (Wu et al. [21]) have less computational time, but difficult to develop a generic logic. A hybrid method has an ability to eliminate the individual deficiencies and may provide better tools to monitor complex systems effectively with optimal resources (Siddique and Adeli [22]). Therefore, the present work attempts to investigate, enhance, and combine these techniques appropriately to form an effective engine health management protocol.

In this research, an engine test bed is built to simulate the emulated fault and failure conditions. Instrumentation is developed to measure vibration, noise and shaft motion. They are calibrated with common practices to eliminate few inherent faults and ensure repeatability. Evaluation is carried out for different resolutions, sensors, mounting locations, directions, fuels and speed conditions to select most sensitive operating and measurement conditions. Dimensionality of the database is reduced by using multivariate principal and independent component analysis. Important events and running orders are identified by superimposing operational information in the signals to extract fault inherent characteristics from collision excitations and responses. Few modal and order parameters are estimated. Estimation is conducted by formulating and evaluating Orbital, Wavelet transform, Hilbert-Huang transform and Vold-Kalman filter on numerically simulated signals. Most appropriate methods are implemented on the engine to study fault diagnosis and failure prognosis.

Physics-based models are built using lumped mass discretization and multibody dynamics approach. Load profiles are estimated from thermodynamic, hydrodynamic and engine dynamic models, which are independently validated through test, literature and commercial tools. Material hysteresis is incorporated through Rayleigh damping model. In lumped mass approach, the engine structure is idealized with different models and studied by including rotor dynamic effects. In multibody dynamics approach, a detailed rigid multibody model is developed through MSC/ADAMS software and is converted into flexible multibody model using Craig-Bampton model reduction method. Simulations are carried out to extract vibration response and compare it with experiment, and select appropriately reduced model. Fault diagnosis is investigated on the reduced models by deliberately modelling realistic bend, crack, unbalance and erosion defects. Simulated responses under these faults and their Wavelet transforms are compared. Physics-based fault diagnosis approach is compared with experiment for a cut fault case and differences are justified. Survivability in terms of remaining useful life is predicted using a fatigue life analysis in MSC/FATIGUE software. Life for crack initiation and fracture are predicted and fracture life is compared with the experiments, where accelerated run-to-fail trials are conducted in the engine by treating crack as a series of increasing cut lengths in connecting rod, till it fractures. A close match with test indicates that some physics-based models are good enough to predict the faults and failures.

In the fault simulation on the engine test bed, the field rejected samples are re-used directly and in few cases used to emulate faults on fresh components. Faulty main bearing, cracked connecting rod, gear with broken tooth, and worn samples of valve, cam, journal and piston ring are introduced in the engine by replacing their healthy one. Engine with faulty samples is simulated in the test bed and signals are acquired. Fault diagnosis is initially carried out manually by comparing the plots of statistical moments, fast Fourier transforms and Wavelet transform for a selected speed case. Statistical and Fourier transform features for entire speed range are used to automate the fault diagnosis. Diagnosis procedure is built with statistical, intelligent and model-based classifiers using a multiple discriminant method, an artificial neural network and fuzzy logic respectively. For failure prognosis, an accelerated fatigue test is conducted by treating crack propagation as a series of cuts made in an incremental step along the crack path till the fracture. Healthy connecting rod in the engine is replaced with the samples that have increasing cut lengths. In every increased cut length, signals are acquired and the acquisition is repeated with incremented step till the connecting rod finally fractures. A correlation between cut length and crack length of its fracture mechanics model is established and measured signals are plotted against cycles for crack propagation. Engine degradation in terms of remaining useful life is estimated for the measured signals and speed stages. In predicting the general degradation states, a model-based particle filter is proposed with incorporating few initial measurements and uncertainty of the vibration signals.

Hybrid methodologies by combining the above studied data-driven and model-based techniques are proposed. Hybridization of Wavelet and Neural Network extracts fault symptoms from the sampled signals, while adaptive neuro-fuzzy inference system extracts rules and knowledge from experimental data. Hence these models are developed and evaluated for engine fault classification. Capability of each classifier in terms of handling different features, resource utilization and robustness are explored.

To summarise, the thesis formulates a health management methodology and validates it for an internal combustion engine. Literature review concluded that managing a health requires careful selection, enhancement and integration of knowledge, diagnosis and prognosis techniques, and use of suitable maintenance schemes. Survey indicated that highest failures

of an engine occur in its powertrain components. Vibro-acoustic signals, superior data reduction techniques and transforms, parameterization and hybridization of reasoning techniques can provide effective results. Comparison of different data reduction transforms and reasoning techniques provides strong validation and criteria for their selection. Engine set-up is capable of acquiring signals and simulating the emulated structural faults and failure conditions. Evaluation of sensor types, locations, directions, engine fuels and speeds indicated accelerometer signals in vertical direction at cylinder head for 2000 rpm engine speed with diesel fuel as sensitive conditions, which can facilitate distinguishable responses for easy fault diagnosis. Estimated parameters from different signal processing techniques provided a simple, few degree, order and event systems that can represent the actual engine system with certain error. Wavelet transform found to be more effective in parameter estimation and it requires less prior knowledge. Physics-based models are able to predict faults that have significantly large geometrical dimensions. Lumped mass models provided quick results, while flexible multibody models simulated few minute geometrical defects. An unclear trend and difficulty in manual comparison of actual fault features demands for an automatic diagnosis tool. Neural network proved to be a simple classifier with less user involvement, while it recorded a low performance. Fuzzy logic classified the faults with less computational time but requires rules that are difficult to generate. Hybrid ANFIS found to be more effective and reliable with providing few simple rules. Classifiers have successfully separated the fault features from their healthy condition. Physics-based crack propagation estimated the fracture of connecting rod over 7 mm crack length, while intermittent cut based accelerated fatigue test conformed its fracture in the trial of 6 mm cut length step. A close match between the lengths conform the validation and potentiality of these approaches for further use. The difference is mainly due to unaccounted damage accumulation in the experimental trials and idealisation of the test sample. Information of cut lengths correlated to the measured signals gave a methodology to detect crack directly and assess degradation. A close match of degradation predicted using Particle filter and experimental values at which connecting rod actually fractured indicates the model is sufficiently good enough to predict remaining survivability of the engine.



ACKNOWLEDGEMENTS

I express all my gratitude to thesis main advisor, Prof. Nalinaksh S. Vyas for formulating thesis topic and guiding to move in its natural direction. He was also my M.Tech advisor, through which he created interest in ‘engine dynamics and vibrations’ that motivated me to continue in industry in the same area and return for this programme. Hope his mentorship and association will continue. I studied FEM course during my M.Tech programme under Prof. N. N. Kishore, serving at IIT Tirupati since 2016. I am influenced by his meticulous problem solving nature. I also, mostly, worked as a teaching assistant under him. I thank him for associating and advising me during the deputation of my main advisor, and continued to advise as and when needed. I feel fortunate to have two senior most researchers as my advisors. Their combined expertise in Vibration, Finite Element Methods, Dynamics, Rotor Dynamics, Numerical Methods, Fatigue and Fracture, Instrumentation, Non-Destructive Testing and Condition Monitoring have helped me in finding key solutions of this research. They have/had addition roles (Prof. Kishore was Registrar during 2014-2015. Prof. Vyas was Chairman, Automotive NPMSS for 2008-2015, Head mechanical engineering for 2008-2011, Vice-chancellor RTU, Kota for 2013-2015 and is Chairman-Indian railway technology since 2015) so drawing time was a challenge, but it was great thrill to discuss the progress and deploy their experience. Their genuine care and supervision of all the academic and professional activities have supported me in many ways. They will now last with me forever.

Support from our department heads, especially Prof. P. K. Panigrahi and Prof. P. Venkitanarayanan was immense. I would like to thank Prof. Bishakh Bhattacharya, J. Ramkumar, Sumit Basu, Nachiketa Tiwari and Bhaskar Dasgupta for their help. Classes of Prof. Amit Mitra and Prof. Nishchal Verma on multivariate analysis, statistical inference neural network and fuzzy logic were valuable in the formulation of statistical and intelligent part of this thesis. NPTEL resource was immense to grab.

I acknowledge Soni Machinery Stores for the supply of genuine engine and spares, and 4i lab, central work shop and manufacturing lab for fabricating test rig fixtures and faults. I am thankful to several un-listed mechanics, who took extra effort in explaining the potential faults of engine and their failure modes. Their approaches in giving simple yet valuable suggestions and finding a joy in every bit of work have encouraged me.

My friends Servesh, Anshul and Vaibhav have supported during my stay here, they made research environment healthy by providing criticism and suggestions. I am thankful to Venugopala and Siddharth for proof reading of the thesis. Discussion with my several juniors such as Bishikh, Suman, Nitin, Mateen and Shahnawaz on this research was very helpful. I acknowledge the troubleshooting support of equipments from my lab-mates and laboratory-in-charge. Mr. Anil Kumar Arya and Mr. Shobit have helped in moving the office papers on-time. Moral support from Laxmikant Trivedi and Rajeshwar Tripathi is much appreciated.

I was brought up very close to my father, as a high school teacher he seeded interest in academics, cleared fundamentals with patience and supported me beyond his limits. I lost him during this programme, 'Appa, your thoughts still keep me active'. Mentorship that I received from my Lallu (Lakshminarayana) mama during start of my carrier has continued to help me. Several teachers have seeded academic interest in me; most influential are, Prof. Shrinivas Balli and Prof. Prashant Kumar. I wish to thank all my managers who encouraged me to take these post-graduate studies. Quotes of several geniuses were priceless; they helped to condense the theme of each chapter in few words.

I am thankful to my wife Vijaya for providing a supportive environment and proof reading every manuscript this programme. Inspiration in solving these problems is my five year old daughter Lakshmi. Her spontaneous energy and approach towards exploring the life has motivated me, and reflected in every corner of this research. I would like to thank my in-laws and my whole family for their constant support, love and encouragement.

Prashanth Dalawai

August 2017

CONTENTS

CONTENTS	xxi
LIST OF FIGURES	xxvii
LIST OF TABLES	xxxii
NOMENCLATURE	xxxiii
ABBREVIATIONS	xxxv

CHAPTERS:

1. INTRODUCTION	1
1.1 Background	1
1.2 Research Topic.....	4
1.3 Objectives of this Research.....	7
1.4 Outline of this Research.....	7
1.5 Approach and Validation	9
1.6 Significance.....	10
1.7 Thesis Structure	11
1.8 Summary	12
2. LITERATURE REVIEW	13
2.1 Introduction.....	13
2.2 Common Faults in an IC Engine.....	15
2.2.1 Process Faults.....	16
2.2.2 Structural Faults	17
2.2.3 Rotating Component Faults	20
2.3 Engine Health Monitoring	22
2.3.1 Performance Health Monitoring	23
2.3.2 Tribological Health Monitoring.....	24
2.3.3 Structural Health Monitoring.....	24

2.4 Engine Health Management.....	27
2.4.1 System Overview	28
2.4.2 Knowledge Management	28
2.4.2.1 Feature Extraction.....	29
2.4.2.2 Feature Selection.....	33
2.4.2.3 Dimensionality Reduction	33
2.4.3 Diagnostics.....	35
2.4.3.1 Fault Detection.....	35
2.4.3.2 Fault Isolation	35
2.4.4 Prognostics.....	35
2.4.4.1 Failure Mode, Effects and Criticality Analysis.....	35
2.4.4.2 Component Life Tracking.....	36
2.4.4.3 Remaining Useful Life.....	36
2.4.4.4 Performance Trending	36
2.4.4.5 Fault Prediction.....	36
2.4.5 Maintenance Management.....	36
2.4.5.1 Fault Assessment	37
2.4.5.2 Fault Reporting	37
2.4.5.3 Supply Chain Integration	37
2.4.5.4 Fault Accommodation.....	37
2.4.6 Reasoning Techniques	37
2.4.6.1 Physics-based Reasoning.....	38
2.4.6.2 State-based Reasoning	39
2.4.6.3 Case-based Reasoning	40
2.4.6.4 Data-driven Reasoning.....	42
2.4.6.5 Rule-based Reasoning.....	42
2.4.7 Knowledge Discovery and Data Mining.....	43
2.4.8 Data Fusion – Hybrid Techniques	43
2.5 Research Gaps in the Engine Health Management.....	44
2.5.1 Physics-based Models.....	45
2.5.1.1 Lumped Mass Approach	45
2.5.1.2 Multibody Dynamics Approach.....	45
2.5.2 Data-driven Models	46
2.5.2.1 Statistical Approach	46
2.5.2.2 Intelligent Approach	47
2.5.3 Model-based Models.....	47
2.5.4 Hybrid Models	48
2.6 Conclusions.....	49

3. ENGINE SET-UP, EVALUATION AND ESTIMATION.....	51
3.1 Introduction.....	51
3.2 Experimental Set-up.....	52
3.2.1 Engine Test Rig.....	52
3.2.2 Engine Instrumentation.....	54
3.2.3 Engine Faults and Failure Samples.....	55
3.2.4 Data Collection.....	56
3.2.5 Engine Event Identification.....	57
3.3 Set-up Evaluation.....	59
3.3.1 Different Type of Measurements.....	59
3.3.2 Measurements with Different Speeds.....	60
3.3.3 Measurements with Different Fuels.....	61
3.3.4 Measurements with Different Locations.....	62
3.4 Dimensionality Reduction.....	64
3.4.1 Principal Components Analysis.....	64
3.4.2 Independent Component Analysis.....	66
3.5 Parameter Estimation Procedure.....	67
3.5.1 Crankshaft Displacement.....	69
3.5.2 Engine Vibration and Noise.....	70
3.5.2.1 Wavelet based Parameter Estimation.....	70
3.5.2.2 Hilbert-Huang based Parameter Estimation.....	74
3.5.2.3 Vold-Kalman Filter based Parameter Estimation.....	76
3.6 Estimation of Engine Signal Parameters.....	77
3.6.1 Numerical Simulation.....	77
3.6.1.1 Estimation of Shaft Orbit Parameters.....	77
3.6.1.2 Estimation of Engine Event Parameters.....	79
3.6.1.3 Estimation of Engine Ramp Parameters.....	84
3.6.2 Implementation on Engine Signals.....	91
3.6.2.1 Crankshaft Displacement Parameters.....	91
3.6.2.2 Vibration Parameters of Engine Events.....	92
3.6.2.3 Noise Parameters of Engine Events.....	94
3.6.2.4 Noise and Vibration Parameters from Ramp-up Analysis.....	97
3.7 Conclusions.....	99
4. PHYSICS-BASED HEALTH MANAGEMENT.....	103
4.1 Introduction.....	103
4.2 Engine Mechanism and its Actual Failures.....	105
4.3 Engine Physics-based Models.....	107
4.3.1 Simulation Methodology.....	111
4.3.3 Model Idealization.....	113

4.3.3 Material Description	121
4.3.4 Load Estimation	121
4.4 Model Solution for Fault Diagnosis.....	127
4.4.1 Free Vibration Response.....	127
4.4.2 Forced Vibration Response.....	128
4.5 Model Evaluation, Reduction and Selection.....	129
4.5.1 Comparison of Model Responses	129
4.5.2 Comparison with Experiments.....	134
4.6 Engine Fault Diagnosis	135
4.6.1 Fault Cases	135
4.6.2 Fault Response Comparison	140
4.6.3 Fault Diagnosis Comparison with Experiments	141
4.7 Model Solution for Failure Prognosis.....	142
4.7.1 Fatigue Life	142
4.7.2 Fracture Life	144
4.8 Engine Failure Prognosis	145
4.8.1 Failure Cases.....	146
4.8.2 Failure Life Comparison	148
4.9 Conclusions.....	150
5. DATA-DRIVEN AND MODEL-BASED HEALTH MANAGEMENT	151
5.1 Introduction.....	151
5.2 Fault and Failure Samples.....	153
5.2.1 Fault Cases	153
5.2.2 Failure States.....	155
5.3 Signals from Faulty Samples	155
5.3.1 Comparison of Statistical Moments.....	157
5.3.2 Comparison of Fourier Spectrums	159
5.3.3 Comparison of Wavelet Contours.....	159
5.3.4 Feature Selection and Extraction	164
5.4 Engine Fault Classification	166
5.4.1 Statistical Classification.....	166
5.4.2 Intelligent Classification	169
5.4.3 Model-based Classification.....	174
5.5 Signals from Failure Samples	180
5.5.1 Features Correlation.....	180
5.5.2 RUL from the Features	184
5.6 Engine Failure Prediction	185
5.6.1 Kalman Filter based Degradation	186
5.6.2 Particle Filter based Degradation.....	188

5.7 Conclusions.....	190
6. HYBRID METHODOLOGY HEALTH MANAGEMENT	193
6.1 Introduction.....	193
6.2 Hybrid Models	194
6.2.1 Wavelet Neural Network	195
6.2.2 Adaptive Neuro-Fuzzy Inference System.....	198
6.3 Engine Fault Classification using Hybrid Models.....	202
6.3.1 WNN for Engine Fault Classification.....	202
6.3.2 ANFIS for Engine Fault Classification.....	203
6.4 Comparison of Classifiers.....	207
6.5 Conclusions.....	210
7. CONCLUSIONS AND SUGGESTIONS	211
7.1 Summary	211
7.2 Chapter wise Conclusions.....	211
7.2.1 Chapter 1 Introduction	211
7.2.2 Chapter 2 Literature Review	212
7.2.3 Chapter 3 Engine Set-Up, Evaluation and Estimation.....	214
7.2.4 Chapter 4 Physics-based Health Management.....	216
7.2.5 Chapter 5 Data-driven and Model-based Health Management.....	217
7.2.6 Chapter 6 Hybrid Methodology Health Management	218
7.3 Overall Conclusions.....	218
7.4 Suggestions for Future Work.....	220
PUBLICATIONS	223
REFERENCES.....	225



LIST OF FIGURES

1.1	P-F Curve for Deterioration and a Fault Life Cycle	3
1.2	Schematic of an IC Engine with Defect Causes and their Effects	5
1.3	Flow Chart of Engine Hybrid Methodology Health Management	8
1.4	Chapter Organization Scheme	12
2.1	Review of Techniques-Topics Listed in Quadrants	14
2.2	IC Engine Faults	15
2.3	Condition-based Health Monitoring Techniques	22
2.4	Engine Faults and Monitoring Techniques	26
2.5	Functions of a Health Management System	28
2.6	Signal Processing Techniques	29
2.7	Types of Reasoning Techniques	38
2.8	Classifiers and Predictors	38
3.1	Experimental Set-up and Instrumentation	53
3.2	Sensor Locations	54
3.3	Engine Instrumentation	55
3.4	Samples Failed in the Field	55
3.5	Engine Signals	56
3.6	Superposition of Simulated Pressure and Valve Lifts with Measured Signals	58
3.7	Types of Signals in Different Directions	59
3.8	Signals for Speed Trials	61
3.9	Effect of Speed and Direction	61
3.10	Signals for Fuel Trials	62
3.11	Effect of Fuel	62
3.12	Measurement Locations and Directions for Vibration and Sound Signals	63
3.13	Signals for Location Trials	63
3.14	Effect of Locations	64
3.15	Principal Components	65
3.16	ICA of Engine Signals	66
3.17	Shaft Motion	69
3.18	Wavelet-based Parameter Estimation Procedure	73
3.19	Shaft Motion Parameters	78
3.20	Simulated Engine Cycle Vibration Signal	79
3.21	Transforms of Simulated Engine Cycle Vibration Signal	80

3.22	Simulated Engine Cycle Sound Pressure Signal.....	82
3.23	Transforms of Simulated Engine Cycle Sound Pressure Signal.....	83
3.24	Simulated Ramp-up Signal.....	86
3.25	Transforms of Simulated Ramp-up Signal.....	87
3.26	Vold Kalman Filter Order.....	87
3.27	Simulated Ramp-up Signal for Engine Shaking.....	89
3.28	Transforms of Simulated Ramp-up Signal for Engine Shaking.....	90
3.29	Vold Kalman Filter Orders.....	90
3.30	Crankshaft Displacements.....	91
3.31	Crankshaft Orbits for Orders at 1500 rpm.....	91
3.32	Crankshaft 3 rd Order Orbits at Engine Speed.....	91
3.33	System Parameters from Orbit Plots.....	92
3.34	Cylinder Head Vibration Signal for a Full Cycle.....	93
3.35	Transforms of Cyl. Head Vibration Signal.....	94
3.36	Near Field Sound Pressure Signal for a Full Cycle.....	95
3.37	Transforms of Near Field Sound Pressure Signal.....	96
3.38	Engine Ramp-up Signals.....	97
3.39	Transforms of Cyl. Head Vibration and Near Field Sound Pressure Signal.....	98
4.1	Engine Models.....	105
4.2	Solid Model of the Powertrain.....	106
4.3	Typical Catastrophic Failures in Cranktrain.....	107
4.4	Framework for Physics-based Engine Health Management.....	113
4.5	Crankshaft Solid Model and its LMD.....	114
4.6	Conn.Rod and Valvetrain Solid Models and LMD.....	115
4.7	Cranktrain Solid Model and its LMD.....	115
4.8	Cranktrain MBD Models.....	119
4.9	Valvetrain MBD Models.....	119
4.10	Engine Cycle Simulation.....	123
4.11	Tuned Parameters-Simulated v/s Test.....	123
4.12	Powertrain Dynamic Models.....	125
4.13	Net Forces on Crankshaft-MATLAB v/s Commercial Tools.....	125
4.14	Total Ring Frictional Force.....	126
4.15	Crankshaft and Slider Vibrations of LMD Model.....	131
4.16	Camshaft and Valve Vibrations of LMD Model.....	131
4.17	Accelerations of Crankshaft and Slider MBD Model.....	132
4.18	Accelerations of Camshaft and Valve MBD Model.....	133
4.19	Measured Vertical Vibrations.....	134
4.20	Simulated Vertical Vibrations.....	134
4.21	Added Fault in Connecting Rod FE Models.....	137
4.22	Fault Response from LMD.....	138
4.23	Con. Rod Fault Response from FMBD.....	138
4.24	WT Plots of LMD Faults.....	139
4.25	WT Plots of FMBD Faults.....	140
4.26	WT Plots of FMBD and Experiments.....	142
4.27	Fatigue Life Curves.....	143
4.28	Cranktrain Responses at 26° CA.....	145

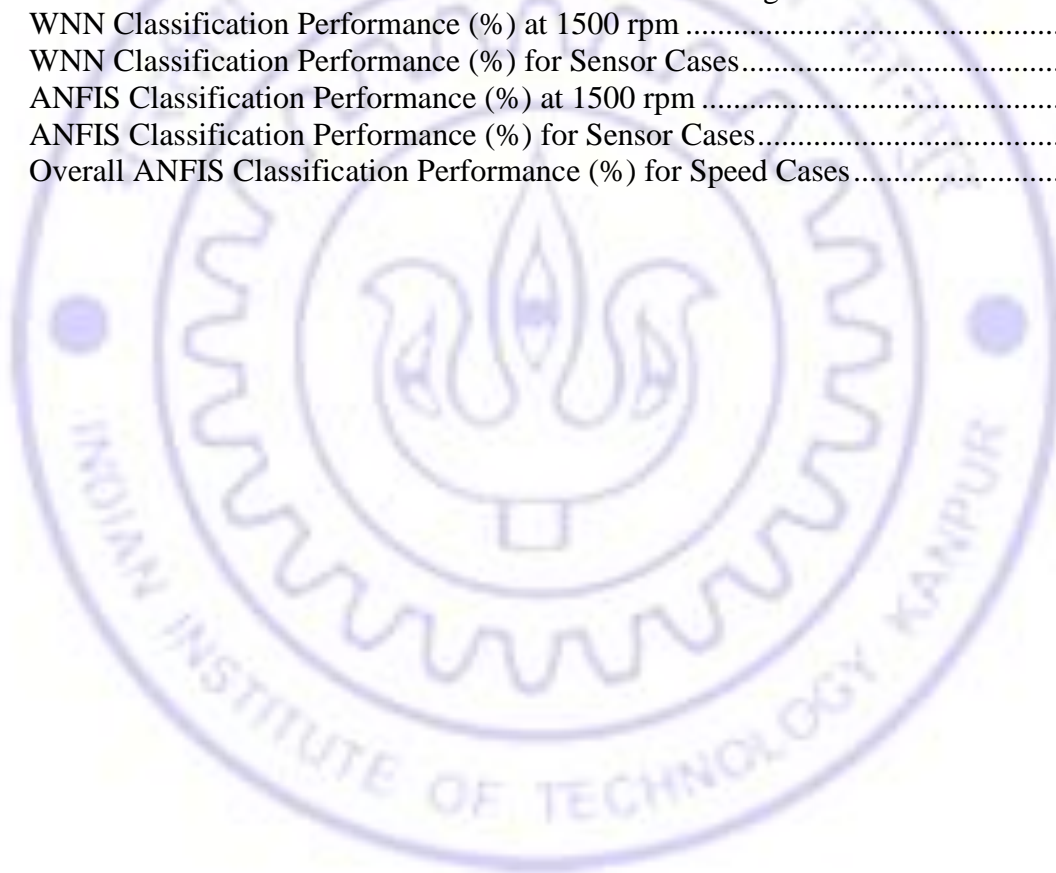
4.29	Crack Progression Models for the Connecting Rod	147
4.30	Engine Fatigue Life.....	148
4.31	Crack Growth Curve of Connecting Rod.....	148
5.1	Healthy and Defective Components	154
5.2	Connecting Rod Cut Length States.....	155
5.3	Proximity, Vibration and Sound Pressure Signals	156
5.4	Statistical Moment Plots	158
5.5	Cyl. Head Vertical Vibration FFT Plots	160
5.6	Near Field. Sound Pressure FFT Plots.....	161
5.7	WT Plots for Cyl. Head Vibration Signal	162
5.8	WT Plots for Near Field Sound Pressure Signal.....	163
5.9	Discrimination of Faults from Vib. and Sound Pr. Data.....	168
5.10	Perceptron Model Mapped to Biological Neuron and Fed to Multi Layers	170
5.11	Activation Functions	170
5.12	ANN Performance Plots	173
5.13	Membership Functions.....	175
5.14	Illustration of Fuzzy Inference System	175
5.15	Engine Fuzzy Logic System	177
5.16	Membership Functions.....	178
5.17	Proximity, Vibration and Sound Pressure Signals for Cut Length	181
5.18	Signals Features v/s Cut lengths	182
5.19	Connecting Rod Crack.....	183
5.20	Signals Features v/s Number of Cycles	183
5.21	RUL for Engine Features	185
5.22	Illustration of Transitions in Kalman Filter process	187
5.23	Illustration of Transitions in Particle Filter process.....	188
5.24	Estimation of New States using Particle Filter	190
6.1	Wavelet Neural Network	195
6.2	ANFIS Network	199
6.3	WNN Performance.....	202
6.4	Engine ANFIS Structure	204
6.5	ANFIS Performance.....	205
6.6	Rules Generated by the ANFIS model for Entire FFT Data.....	206
6.7	Classifier Performance.....	208



LIST OF TABLES

1.1	Trial Cases Matrix.....	9
2.1	Symptoms of Common Faults	21
2.2	Overview of Transformation Techniques	31
2.3	Overview of Dimensionality Reduction Techniques	34
2.4	Overview of Physics-based Reasoning Techniques	39
2.5	Overview of State-based Reasoning Techniques.....	40
2.6	Overview of Case-based Reasoning Techniques.....	41
2.7	Overview of Data-based Reasoning Techniques	41
2.8	Overview of Rule-based Reasoning Techniques	42
2.9	Overview of Knowledge Discovery and Data Mining Techniques	43
2.10	Literature on I.C. Engine Health Management.....	44
3.1	Specification of the Engine.....	52
3.2	Measurement Specifications	54
3.3	Overall Levels at 1500 rpm.....	60
3.4	Properties of the Engine Fuels	61
3.5	WT and HHT based System Parameters of Simulated Noise Free Signal	81
3.6	WT and HHT based System Parameters of Simulated Noisy Signal	84
3.7	Simulated Parameters for Inertia Ramp-up.....	85
3.8	System Parameters from Inertia Ramp-up Analysis.....	87
3.9	Simulated Parameters for Shaking Force Ramp-up.....	88
3.10	System Parameters from Shaking Force Ramp-up Analysis	90
3.11	Engine System Parameters of Vibration Signals at Cylinder Head.....	94
3.12	Engine System Parameters of Near Field Sound Signal	97
3.13	Engine System Parameters from Ramp Signal Analysis	99
4.1	System Parameters of the Engine	117
4.2	Materials of the Engine Components.....	121
4.3	Summary of the Cranktrain Responses.....	146
4.4	Connecting Rod Crack Progression Model Results.....	149
5.1	Statistical Moments for Fault Comparison	158
5.2	Vibration and Sound Pressure Symptoms of the Engine Faults	159

5.3	Statistical Moment Training Data.....	165
5.4	Harmonic Order Training Data.....	165
5.5	Fault Share (%) for MDA Training	168
5.6	MDA Classification Performance (%) at 1500 rpm	168
5.7	MDA Classification Performance (%) for Sensor Cases.....	169
5.8	Overall MDA Classification Performance (%) for Speed Cases	169
5.9	ANN Classification Performance (%) at 1500 rpm	173
5.10	ANN Classification Performance (%) for Sensor Cases.....	173
5.11	Overall ANN Classification Performance (%) for Speed Cases.....	173
5.12	Fuzzy Rules for Inference and True Memberships for Each Fault.....	177
5.13	Membership Values for CCR Data at 1500 rpm with Triangular Function	178
5.14	Fuzzy Classification Performance (%) at 1500 rpm	178
5.15	Fuzzy Classification Performance (%) for Sensor Cases	179
5.16	Correlation Coefficient between Growth of Crack and Engine Sensors	184
6.1	WNN Classification Performance (%) at 1500 rpm	203
6.2	WNN Classification Performance (%) for Sensor Cases.....	203
6.3	ANFIS Classification Performance (%) at 1500 rpm	206
6.4	ANFIS Classification Performance (%) for Sensor Cases.....	206
6.5	Overall ANFIS Classification Performance (%) for Speed Cases.....	206



NOMENCLATURE

α	Speed ramp rate, Inclination	$\Im \cdot $	Imaginary part
β	Inclination, Degree of fulfillment	$\Re \cdot $	Real part
ε	Gaussian noise, Strain		
ζ	Damping ratio	a	Crack length
η	Learning rate	$a_k(t)$	Complex envelope
θ	Crank angle, Inclination	$\bar{a}_k(t)$	State equation
λ	Eigen value, Length ratio, Lagrange multiplier, Slope	b	Bias, Length dimensions, Exponent
μ	Mean, Fuzzy measure, Friction constant, Dynamic viscosity, Membership function	c	Damping, Independent source, Exponent
ρ	Correlation coefficient	d	Desired value
σ	Std. deviation, Surface roughness, Stress amplitude	e	Eccentricity, Error
τ	Time length	$f(\cdot)$	Non-linear transition function
φ	Angular displacement, Flow and share factors	$f(t)$	Force signal in time domain
ϕ	Phase functions, Shape function	f, f_s	Fourier frequency, sampling Frequency
χ_t	Particle set	$g(\cdot)$	Higher order moment, Non-linear transition function
$\psi^*(t)$	Complex conjugate of mother Wavelet	h	Confidence function, Film thickness, Enthalpy
ω	Angular frequency in rad/sec Excitation frequency	k	Discretization, Integer Stiffness, No. of stress levels
ω_0	Central frequency or resolution Parameter	m	Mass, material constant
	Initial angular velocity	n	No. of cycles, Accuracy factor
Δf	Bandwidth	n_v	No. of voices, Frequency bins at dyadic interval of frequency
Λ	Eigen value matrix	o	Actual output
Σ	Covariance matrix	p	Cylinder pressure
Φ	Jacobian matrix, Activation function		Natural frequency, Consequent parameters
Ω	Angular velocity	$p(t)$	Complex harmonic signal
		p_d	Damped natural frequency
		p_k	Complex phasor

q	Generalized coordinate	D	Discriminant score, Cylinder diameter, Friction parameter
r	Frequency ratio, Radius, Residue	E	Error, Modulus of elasticity
r^f	Forward harmonic components	EA, EI	Elastic properties
r^b	Backward harmonic components	F	Force, Fifth Moment
s	Wavelet dilation, Scale, Variance	G	Gyroscopic couple, Geometric Mean
t	Time	$H_i(t)$	Instantaneous amplitude, Harmonic Mean
u	Unbalance, Internal energy, sliding velocity, Output	I_d	Diametral moment of inertia
$v(t)$	Broadband signal, measurement noise	I_p	Polar moment of inertia
w	Weight, Eigenvector, Process noise	K	Kalman gain, Stiffness matrix, Kurtosis
$w^*(t)$	Window function	L	Likelihood
x, \dot{x}, \ddot{x}	Displacement, velocity and acceleration respectively	M	State transition matrix, Mass matrix, No. of rules
$x(t)$	Response signal in time domain	N	Mother wavelet shape parameter, RPM, No. of cycles
x_0, \dot{x}_0	Impact initial conditions	N_b	No. of balls
x_d and x_q	Direct and quadrature parts	N_t	No. of tooth
x_e	Signal envelope	O	Data
$x_i(t)$	IMF of the signal	P	Participation factor matrix
$y_i(t)$	Hilbert transform of IMF	$P(H_t)$	Probability of hypothesis at time t
$\bar{y}_k(t)$	Data equation	Q	Transformation matrix, Heat energy
$z_i(t)$	Analytic function	S	Shape Factor, Skewness, Stress
A	Area, Friction parameter, State transition matrix	V	Coefficient of Variation
B	Measurement matrix, Friction parameter, Class scatter, State transition matrix	W	Weight Matrix, Scatter within the class, Width
B_{ω_0}	Normalization constant	X	Amplitude, Discourse, Frequency ratio, Orders, Running frequency
C	Damping matrix, Friction parameter, Material constant, Crest Factor, Class, Measurement transition matrix	Y	Compliance function

ABBREVIATIONS

aBDC	after Bottom Dead Center	CBM	Condition-based Maintenance
ADAC	Allgemeiner Deutscher Automobil-Club (General German Automobile Club)	CBR	Case-Based Reasoning
ADAMS	Automated Dynamic Analysis of Mechanical Systems	CCR	Cracked Connecting Rod
AE	Acoustic Emission	CDU	Cylinder Diagnostic Unit
AI	Artificial Intelligence	CE	Combustion Excitation
AIR	Aerospace Information Report	CI	Computational Intelligence
ANFIS	Adaptive Neuro Fuzzy Inference System	COG	Center of Gravity
ANN	Artificial Neural Networks	CVA	Cylinder Head Vibration Axial
API	American Petroleum Institute	CVL	Cylinder Head Vibration Lateral
ARP	Aerospace Recommended Practice	CVV	Cylinder Head Vibration Vertical
AS	Aerospace Standards	CWD	Choi-William Distribution
ASM	American Society for Materials	CWT	Continuous Wavelet Transform
aTDC	after Top Dead Center	DAQ	Data Acquisition
B&K	Brüel & Kjær	DC	Direct current
bBDC	before Bottom Dead Center	DDR	Data-driven Reasoning
BBN	Bayesian Belief Networks	DFT	Discrete Fourier Transform
BC	Boundary Conditions	DLKAPP	Apparent Stress Intensity
BCR	Bent Connecting Rod	DLKEFF	Effective Stress Intensity
BDC	Bottom Dead Centre	DOF	Degree of Freedom
BNC	Bayonet Neill–Concelman	DSTFT	Discrete Short Time Fourier Transformation
bTDC	before Top Dead Center	DWT	Discrete Wavelet Transform
BVA	Base Vibration Axial	ECG	Electrocardiography
BVL	Base Vibration Lateral	ECU	Engine Control Unit
BVV	Base Vibration Vertical	EGR	Exhaust Gas Recirculation
CA	Crank Angle in Degree	EHM	Engine Health Management
CAD	Computer Aided Design	EMD	Empirical Mode Decomposition
CB	Craig - Bampton	EOM	Equation Of Motion
		EPFM	Elasto-plastic Fracture Mechanics
		EVC	Exhaust Valve Closing
		EVD	Eigen Value Decomposition

EVO	Exhaust Valve Opening	MAD	Mean Absolute Dev
EVP	Eigen Value Problem	MATLAB	Matrix laboratory
FDA	Fisher Discriminant Analysis	MBD	Multibody Dynamics
FE	Finite Element	MBF	Main Bearing Fault
FFT	fast Fourier transform	MANOVA	Multivariate Analysis of Variance
FI	Fuzzy Integral	MBR	Model Based Reasoning
FIS	Fuzzy Inference System	MDA	Multiple Discriminant Analysis
FL	Fuzzy Logic	MDOF	Multi Degree of Freedom
FMBD	Flexible Multi Body Dynamics	MK	Mark
FMECA	Failure Mode, Effects and Criticality Analysis	MLPN	Multi-Layer Perceptron Network
FT	Fourier Transform	MNF	Modal Neutral File
FWNN	Fuzzy Wavelet Neural Network	MR	Mid Range
HCF	High Cycle Fatigue	MRO	Maintain Repair and Overhaul
HM	Health Management	MSC	MacNeal-Schwendler Corporation
HMM	Hidden Markov Mode	MUF	Mass Unbalance Fault
HHT	Hilbert-Huang Transform	NASA	National Aeronautic and Space Administration
HSMF	High Speed Multi Fuel	NASTRAN	NASA STRucture ANALysis
HT	Hilbert Transform	NI	National Instruments
IC	Initial Conditions	NOR	Normal i.e. Healthy Engine
ICA	Independent Component Analysis	NVH	Noise, Vibration, Harshness
ICE	Internal Combustion Engine	OBD	On-board Diagnostics
IMF	Intrinsic Mode Functions I-P-F Installation-Potential-Function	ODE	Ordinary Differential Equation
IQR	Inter-Quartile Range	OEM	Original Equipment Manufacturer
ISO	International Organization for Standardization	OS	Occurrence of the Spark
IVC	Inlet Valve Closing	PBR	Physics-based Reasoning
IVHM	Integrated Vehicle Health Management	PCA	Principal Components Analysis
IVO	Inlet Valve Opening	pdf	probability density function
KDD	Document Knowledge Discovery	PDL	Proximity Displacement Lateral
KF	Kalman Filter	PDV	Proximity Displacement Vertical
LabVIEW	Laboratory Virtual Instrument Engineering Workbench	PF	Particle Filter
LCF	Low Cycle Fatigue	P-F	Potential to Function
LDA	Linear Discriminant Analysis	PHC	Hollow shaft Powder Clutch
LEFM	Linear Elastic Fracture Mechanics	PHM	Prognostic Health Management
LMD	Lumped Mass Discretization	PS	Piston Slap
LVDT	Linear Variable Differential Transformer	PSFA	Partial Sampling and Feature Averaging
		QDA	Quadratic Discriminant Analysis
		RBE	Rigid Body Element
		RBF	Radial Basis Function

RBR	Rule-based Reasoning	SVM	Support Vector Machine
RMBDR	Rigid Multibody Dynamics	TAN	Total Acid Number
RMSE	Root Mean Squared Error	TBN	Total Base Number
RPM	Revolutions per minute	TC	Technical Committee
RUL	Remaining Useful Life	TDC	Top Dead Centre
SAE	Society of Automotive Engineers	TET	Tetrahedron
SBR	State-based Reasoning	TK	Keyphasor Conditioner
SC	Sub Committee	TMG	Tooth Missing Primary Gear
SDI	Shape and Directivity Index	TSA	Time Synchronous Average
SDOF	Single Degree of Freedom	VKF	Vold Kalman Filter
SDP	Symmetrized Dot Pattern	WCL	Worn Cam Lobe
SENB	Singe Edge Notched Bending	WCJ	Worn Crank Journal
SHM	Structural Health Management	WEV	Worn Exhaust Valve
SI	Spark Ignition	WNN	Wavelet Neural Networks
SIF	Stress Intensity Factor	WPR	Worn Piston Ring
SKF	Svenska Kullagerfabriken AB	WT	Wavelet Transform
S-N	Stress Cycle	WVD	Wigner-Ville Distribution
SNR	Signal to Noise Ratio	1D	One Dimensional
SO	Occurrence of Spark	1DOF	Single Degree of Freedom
SPF	Sound Pressure Far Field		
SPN	Sound Pressure Near Field		
SR	Sweep Rate		
STFT	Short Time Fourier Transformation		





CHAPTER 1

INTRODUCTION

Imagination is more important than knowledge.

Knowledge is limited. Imagination encircles the world.

- Albert Einstein (1879 - 1955)

1.1 Background

Reliability of the vehicles is gaining increased attention due to their growing volumes and complexity. A survey by [Becker \[23\]](#) and [Tyler \[24\]](#) shows that there is a 6% year-over-year growth in the volumes of automotive and aircraft. Mechanical complexities have also increased by 2% ([Berger \[25\]](#)) yearly, which have increased the accidents by 3% ([Tews \[26\]](#)) yearly. ADAC breakdown statistics reveals that around 47.5% ([Markl \[27\]](#)) of vehicle breakdowns can be traced to engine and its surroundings. This point out that the engine failure is a major source for accidents, while other sources are: battery (31.7%), chassis (7.5%), wheels (6.7%), brakes (1.9%), suspension (0.4%) and steering (0.3%). A survey for the cause of an accident shows the mechanical failure is dominated by, first (38%, [Davies \[28\]](#)) in top 100 largest plant accidents during 1958-87, second (20%, [Kebabjian \[29\]](#)) in major flight accidents during 1950-2010 and third (10%, [Rumar \[30\]](#)) in major road accidents. Other considerable causes are design, manufacturing, assembly and operation, which can be reduced by minimizing the defects and error in the operations.

Government norms and competition between OEMs ensures only best vehicles in use and scraps aged one much before the end of their useful live. It reduces ageing failures, but adds inventory, unavailability, recycling issues. Safety instructions can ensure reliable operation however technology limitation, operational error, sabotage and natural hazard are inevitable. Monitoring and curing their ill-health requires a methodology, which is being evolved under

Integrated Vehicle Health Management (IVHM) concept, that reduces potential failures and improve reliability by offering schemes for real-time monitoring and maintenances. [Benedettini et al. \[31\]](#) has presented its future challenges.

Actual failures are much complex; they are driven by a critical combination of different faults and several uncertainties. Mechanical faults are caused by minute deviation in the geometry and material properties, which grow with time and result into failures, and are observable in appropriate signals. Monitoring such faults in an engine requires knowledge of fault life cycle, cyclic operational information, signal acquisition and processing to extract effective features. Health management requires a decision making agent to learn the data, deal uncertainty and integrate knowledge from multiple domains. The main challenge is to formulate a procedure for an effective management of such faults and failures.

An asset failure (P-F, i.e. potential to function) curve from reference [\[32-35\]](#) is shown in Figure 1.1 for deterioration growth instead of asset condition. It presents fault life cycle and health monitoring techniques, intervals and appropriate maintenance strategies with cost to repair. Point 'I' is a condition at machinery installed with precision, it has high asset condition i.e. low deterioration. Point 'P' corresponds to a condition at which potential defect enters the system. Defect arises from micron level geometric issues or accumulated damages. With time, defect matures and seeds other faults, and finally accelerates towards functional failure point 'F'. Corrosion leads to micron level wear and pits, which aggravate to cracks and bends. Bent or deviated component can collide and cause accidents. Solid circles show the conditions and tests that are capable to detect the deteriorations. Explosion marks indicate the conditions for a defect to grow into a noticeable fault. Fixing the fault at higher stage can exponentially increase un-availability and repair cost. Ignoring the issues and warnings, and continuing to operate without attending the faults can result into sudden catastrophic failures.

Fault can be detected by mounting a suitable sensor at appropriate location, acquiring and processing the signal for a pre-defined abnormality and isolating it to a particular component. Its failure modes can be assessed, remaining survivability can be predicted with respect to functional failure and suitable remedies can be recommended by integrating the information

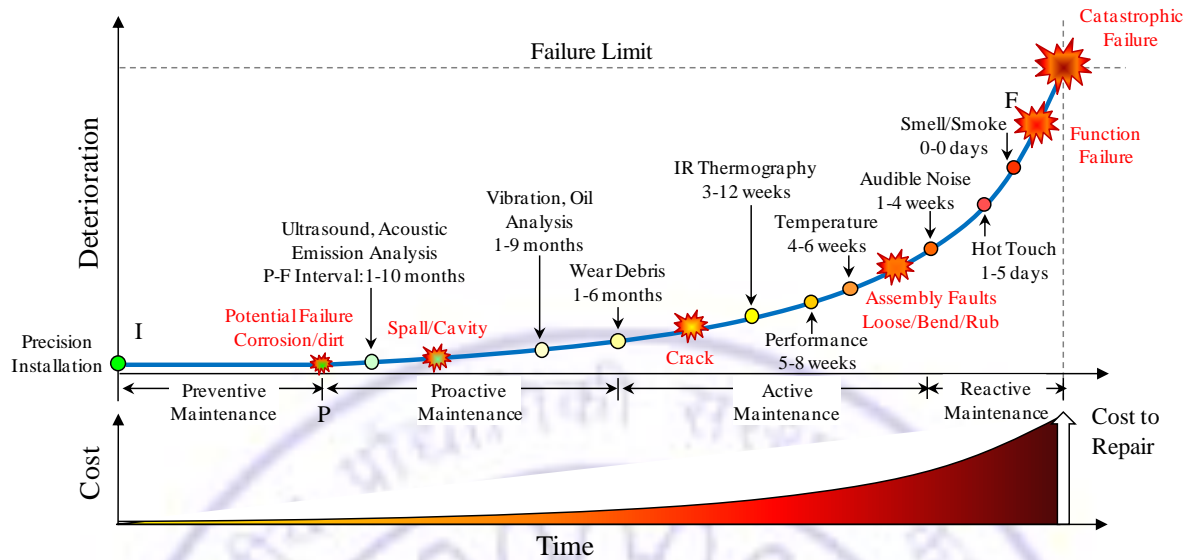


Figure 1.1: P-F Curve for Deterioration and a Fault Life Cycle [32-35]

from multiple disciplines. They are adopted from medical treatment approaches and referred as health management technique, which has monitoring, diagnosis, prognosis and maintenance activities. Diagnosis involves fault detection, it identifies a cause and localizes to a component, while prognosis predicts evolving time of detected incipient fault for a failure condition, thus allow estimating remaining useful life (RUL). Based on the information, maintenance is carried out to manage deterioration, reduce risk of failures, and improve health with increase in the availability and low downtime. It is divided into preventive, reactive, proactive and active maintenance based on increased functionality and logistic support. Usually preventive is conducted without any prior knowledge of faults, at a particular schedule that has a very small likelihood of failure between services. Due to the increasing machine complexity, preventive approach is becoming less effective. Proactive predicts the impending failures and activates maintenance program by least disturbing the process. Active maintenance accumulates real time damage, assesses the situation, and eliminates redundant systems and loads. In reactive maintenance, less critical or run-to-fail components are inspected in the trial tests. Health management is becoming more accurate due to increased real-time, on-board, wireless sensors and telemetry monitoring strategies. Based on actual conditions, a Condition-based Maintenance (CBM) program under Prognostic Health Management (PHM) domain (Vachtsevanos et al. [36], and Mrad and Mrad [37]) is carried out with an active contribution from multiple disciplines. It increases

availability of a machine and utilizes skill and resources optimally by performing precise fault diagnosis, failure prognosis and maintenance based on actual machine condition.

The causes of a failure are often investigated (Matthews [38], Bloch and Geitner [39]) if significant casualty, economy and resource are involved. Usually to claim the insurance, liability and technical improvement; it can be biased. Errors in the product either originated during design, manufacturing, assembly or exhaustive usage results into wear, corrosion, fouling or fatigue defects. Ill operations, negligence of early alarms and avoiding of timely maintenance can cause service related failures. Though condition monitoring helps to identify the causes at early stages and offers several benefits, but it has certain security and reliability issues. Real time on-board monitoring with wireless sensors and telemetries raises the security concerns. Faulty sensor and false alarm can add panic. Complete automation can cause fatal accidents, so human intervention is still needed. Unnecessary and repeated troubleshooting can increase unavailability and lose reliability of the system. Monitoring and assessing of conflicting information, intimation and blocking of in-active sensors and fault tolerant system can reduce the probability of such failures. It still requires miniaturization, inexpensive and reliable instrumentation technologies. It is not feasible to cover all the above discussed issues in this research, so the current research is restricted to formulate a management methodology to monitor and improve the structural health.

1.2 Research Topic

Topic of the research is “Hybrid Methodologies for Health Management of Internal Combustion Engines”. Primary goal is to formulate a procedure and manage the structural health accurately. The study investigates, enhances and implements structural health monitoring (SHM) and management techniques on an Internal Combustion (IC) engine.

A modern IC engine is a complex multi-disciplinary system that operates in a changing environment with varying configurations. It consists of:

1. Reciprocating components - pistons, rings, valves, push rods etc.
2. Rotating components – crankshafts, cams, bearings, gears, pulleys and sprockets.

3. Oscillating components - connecting rods, rocker arms and fork shifts.
4. Accessories - filters, pumps, injectors, exhaust gas recirculation units, governors, turbochargers, control units, sensors and actuators.

These components interact with each other and forms sliding, revolving and intermittent contact joints. Defect in the product, overuse and ageing cause wear and tear, cracks, bends and misalignments, which degrade over time and finally lead to breakdown of the system. Fault can be studied experimentally by injecting and observing the changes in the measured vibration, noise, shaft motion, oil contamination and wear debris. Duration for a failure can be predicted by measuring threshold and growth rate. Alternatively, they can be studied using physics-based models, where geometry is simplified, fault location is known and entire resources are invested around its front region to predict the growth. There exist only few fault (rub, crack and misalignment) models on a highly simplified rotor system. An IC engine system is a multibody superstructure as shown in Figure 1.2 that houses thousands of complex components; they have several sources of defects and can affect severely. Engine cycle process is highly uncertain due to uneven administration of fuel, charge and transient operations within and over a cycle. This makes both experimental and physics-based models challenging for detecting faults and predicting their exact duration for failures.

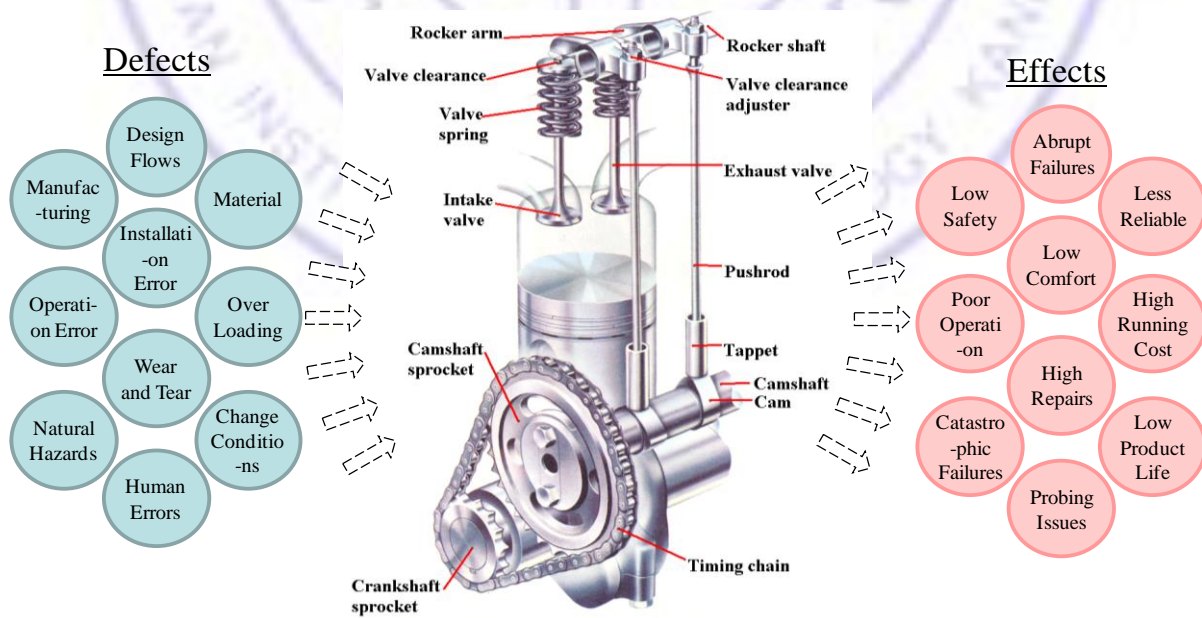


Figure 1.2: Schematic of an IC Engine [40] with Defect Causes and their Effects

A pre-defined symptoms database of healthy and defects can be used to distinguish a fault. Operating conditions and threshold limits for failures can indicate the growth rates. Database of common symptoms, operating conditions and threshold limits can be experimentally generated by introducing known defects and run-to-fail trials. Features extracted by processing responses in time, frequency and time-frequency domains can provide characteristics of the fault and failure. Inferring the database can detect actual faults and predict failures. However, its successful implementation depends on reliability of the characteristics, which can be ensured by tracking sensitive features at error free operation, fewer sensors and important measurements. A speed sensor at idle speed condition is always desirable, but system complexity and measurement limitation demands for several sensors and operating conditions. So, exercises are required to select optimal number and cases. Fault can be quantified by estimating parameters of a signal. Models with few parameters are easy to handle, but large number can represent faults accurately. Hence it is required to evaluate appropriate signal processing technique, effective and optimal number of parameters for representing a fault. Due to heavy involvement of time and cost, and availability of scant information from the experiments, the physics-based models are preferable. A virtual engine rig employing advanced physics-based simulations can also generate such database.

Minute defects in a large assembly and huge uncertainty within the cycles make physics-based models as highly challenging to use for studying fault detection and failure prediction. Till date physics-based models are not available to study real faults and failures of an engine; lumped mass and commercial multibody models can be proposed. Carefully built models can investigate faults and failures by accommodating advanced dynamics and geometric details.

Fault diagnosis and failure prognosis can be carried out manually by comparing fault and failure features with the database or can be automated with data-driven (statistical and intelligent), model based or hybrid techniques. So, capability of manual approach and need for automation process requires evaluation. An effective automation demands selection of most suitable statistical, intelligent and model-based classifiers and predictors based on their capabilities. Individual deficiencies of the above techniques can be eliminated by formulating and enhancing a hybrid framework.

1.3 Objectives of this Research

The research formulates a health management framework using an internal combustion engine. Literature review presented in next chapter discusses the engine fault symptoms, existing and recent maintenance techniques, possible gaps and challenges. Based on the review, primary objectives for health modeling and maintenance are formed as,

1. Build and evaluate an experimental rig to simulate common faults and failures.
2. Develop an effective signal processing, dimensionality reduction and transform techniques, and parameters estimation for shaft motion and vibro-acoustic signals.
3. Build and reduce physics-based models, and study realistic faults and failures.
4. Formulate data-driven and model-based models, and study real faults and failures.
5. Integrate the above models into the hybrid models for a comprehensive scheme.

1.4 Outline of this Research

Figure 1.3 shows flow chart of the physics and experimental based procedure that has been followed for this work. Models are evaluated and superior statistical, intelligent, model-based and physics-based models are integrated into hybrid model for an effective framework. Table 1.1 lists the cases and trials that are carried out. First row of trials emphasize on building and calibrating the models, and procedures; second row represents the list of diagnostic tasks that are carried out iteratively; finally, third row indicates trials for failure prognosis that are carried out on the diagnostic models.

Keyphasers, proximities, accelerometers and microphones are installed on the test-rig and speed, shaft motion, vibration and sound pressure signals respectively are collected for steady and transient conditions. Rig is evaluated for sensors and their locations, engine speeds and fuels. Later, suitable data reduction, transforms and parameter estimation techniques are selected. In fault injection process, a healthy component in the engine is replaced by its faulty one. Features under faulty bearing, worn valve, cam, piston ring and journal, cracked connecting rod and tooth missing gear faults are extracted from the acquired data. Fault diagnosis is investigated using manual and statistical, intelligent and model-based techniques. Engine life is usually above 15,000 running hours or 1 million running kilometers i.e. around

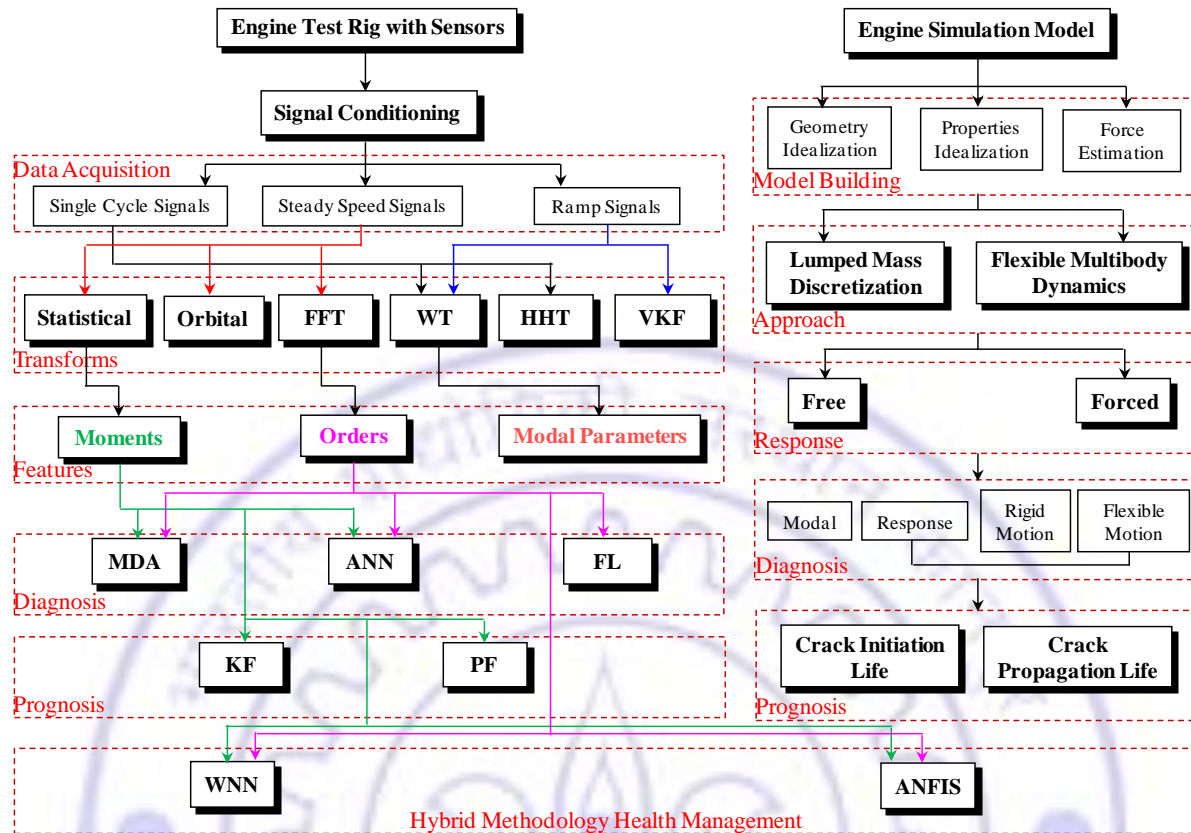


Figure 1.3: Flow Chart of Engine Hybrid Methodology Health Management

400 to 1000 hours deepening on the type of test in durability test cell. So, structural damage accelerates very slowly and fault takes years to get initiated, which is not feasible for present study. Hence, an accelerated fatigue test, i.e., component is forced to deteriorate and fracture within the duration of study is conducted. For this, a cut is initiated and its length is manually progressed in the stages of millimeters until it completely fractures. RUL is estimated by correlating cut to crack and degradation states are predicted using state estimators.

In physics-based approach, dynamics of cranktrain is simulated using lumped mass and multibody dynamics (MBD) models. A thermodynamic layout correlated with its performance parameters, engine dynamics model calibrated with commercial software and hydrodynamic model validated with literature, are used to estimate gas, inertia and friction loads respectively. They are employed on physics-based models. Lumped mass models are built by extending rotor and structural dynamics concepts to cranktrain, and resulting equations are solved numerically. MBD models idealized with different flexibility are used to

Table 1.1: Trial Cases Matrix

Objectives	Lumped Mass Discretization			Flexible Multibody Dynamics			Data-driven, Model-based				
Model	Discrete Geom.	Response	Signal	Parameters	Tool	MBD Flex.	Speed, rpm	Parameters	Locations	Fuel	Dim'ty
Idealization and Evaluation	i) Crank (4 dof), Con Rod (2 dof)	i) Free Lat.	I) Non- stationary	i) Vibration	I) Pro- Mechanism	i) Rigid	i) 1000 ii) 1500	i) Orbits ii) Vibration	i) Cyl. Head ii) Base	i) Petrol ii) Kerosene	i) PCA ii) ICA
	ii) Crank excited Con Rod	ii) Forced Lat.	ii) Engine vibration	ii) Stress	ii) ADAMS- Rigid	ii) Flex. Crank, Con Rod, Piston, Pin	iii) 2000 iv) 2500	iii) Sound	iii) Bl. Ex. iv) Bl. Tank	iii) Diesel	
	iii) Crank (20 dof) excited Con Rod		iii) Engine acoustic	iii) Initi. Life	iii) ADAMS- Flex	iii) All Comp Flex.	v) 3000 vi) Ramp		v) Bl. Fl. vi) Bl. Cup.		
	iv) Fully Coupled			iv) Prop. Life	iv) MATLAB						
Diagnosis	Effects			Faults			Faults	Transforms	Int. Diag.	Stat. Diag.	
	i) Unbalance Fault			i) Crack Conn. Rod			i) Normal	i) FT	i) FS	i) MDA	
	ii) Lack of Lubrication			ii) Bend Conn. Rod			ii) Worn Valve iii) Faulty Bearing	ii) WT iii) HHT	ii) ANN		
							iv) Cracked Con. Rod v) Worn Cam vi) Missing Tooth Gear vii) Worn Piston Ring viii) Worn Crank Journal	iv) SDI			
Prognosis	Life Prediction			RUL			Crack in Connecting Rod		Failure Predictor		
	i) Crack Initiation			i) Crank Shaft			i) Normal		i) Kalman Filter		
	ii) Crack Propagation			ii) Connecting Rod			ii) 1.0 mm		ii) Particle Filter		
				iii) Piston Pin			iii) 2.0 mm				
			iv) Piston			iv) 3.0 mm					
			v) Cracked Conn. Rod-SENT			v) 4.0 mm					
			vi) Cracked Conn. Rod-SENB			vi) 5.0 mm					
						vii) 6.0 mm					

study the model reduction. Responses from these models are compared with measurements. On the selected models, faults such as unbalance, lack of lubrication, crack, bend are modeled and studied for possible symptoms of the defect. The results are then extended to a fatigue and fracture mechanics computational models to predict failure prognosis. Finally, fault symptoms and RUL is generated and database is formed.

1.5 Approach and Validation

Experimental trials and their comparative evaluations provided a realistic base for fault diagnosis and failure prognosis study. Physics-based modeling for the realistic systems has been confirmed by starting with simple rotor and oscillator models and use of correlated inputs, and calibration of responses mentioned in the literature. Validated models are gradually extended to complex with addition of more and more details of the real systems. Finally, the response from the experiment and physics-based model that is developed for the real complex systems is compared for a particular case and differences

between them are justified. Then the physics-based models are employed to study faults and failures. Experiments consume higher time, money and effort, in a few cases they have been attempted to study actual faults and failures. Features from the experimental response are extracted and compared manually in different domain, and automated with statistical, intelligent, modal-based and hybrid reasoning techniques. Finally, classifiers are compared, that ensures the validation of the approach for effective health management system.

1.6 Novelty and Significance

The thesis attempts to explore new approaches, methodologies and make important knowledge contribution to health management technology. A few novelties can be seen in,

1. Condenses state-of-the-art and contributes knowledge to the health management.
2. Evaluates the test-rig for multiple sensors and cases, and formulates a methodology to select sensitive operating conditions, and reduces dimensions.
3. Formulates a systematic methodology to use time-frequency transforms for non-stationary engine signals and quantify the event parameters.
4. Validates parameter estimation techniques at a bulk level and deploys practically.
5. Builds physics-based engine models to study realistic faults and failures. Formulates a methodology with including recent developments. Establishes various symptoms of fault and failures in different domain.
6. Comprehensive health modeling from data-driven, model-based and hybrid models.
7. Condition monitoring technology that is ready for an industrial implementation.

Health management techniques are extensively used in aircraft engines to Maintain Repair and Overhaul (MRO) process, being executed under IVHM platform. Several maintenance processes are common in medical treatments, vehicles and machineries. Information on a chronic fault and failure are easily available in automotive systems, while heavy cost and human involved in other disciplines make it difficult. This thesis attempts to adopt and improve the techniques by addressing actual and impending faults in an IC engine. Results are useful to ensure reliability at design stage and troubleshoot during usage. Some of the observations are applicable to resolve issues in general machinery and other applications.

1.7 Thesis Structure

The thesis contains seven chapters; Figure 1.4 shows its organization and highlights the work carried out in the following chapters. Chapter two discusses the health management concepts and literature review. It briefs the current state-of-the-art of health management and its application to engines. Research on signal monitoring, processing, reduction and models for fault diagnostics and failure prognostics are discussed in this section. Various structural faults, failures and their symptoms of an engine are discussed.

Chapter three discusses experimental set-up, test methodology, data acquisition, signal processing, and parameter estimation under steady and transient conditions. Set-up is evaluated for different operating conditions and lists the most effective conditions. Engine database is reduced using multivariate principal and independent component analysis. Parameter estimation is proposed, evaluated on numerical signals and implemented on actual signals using orbits, Wavelet and Hilbert-Huang transforms, and Vold-Kalman filters.

Chapter four proposes the physics-based dynamical models for engine health management. Loads required for simulation are estimated using thermodynamic, simplified hydrodynamic lubrication and engine dynamics approach. Lumped mass and flexible multibody models are simulated for vibration and fatigue response, and fracture growth. A modal reduction technique is iterated to select the reduced model. Experimental and physics-based simulation results are compared for a speed case. Faults and failure symptoms are discussed by investigating the symptoms in time, frequency and time-frequency domains.

Chapter five discusses the data-driven and model-based methods. A manual fault diagnosis is attempted by comparing statistical moments, Fourier transform and Wavelet plot features. Statistical and Fourier features are used to automate diagnosis. Statistical-Multiple Discriminant Analysis (MDA), intelligent-Artificial Neural Networks (ANN) and model based-Fuzzy Logic (FL) are built and used/trained to classify faults. Remaining useful life (RUL) is assessed with run-to-fail experiments. A model-based particle filter is employed to predict the degradation states in the connecting rod using few measured signals.

Model Idealization and Evaluation	Chapter 2 Literature Review Engine Health Management, Identifying the Research Gaps	Chapter 3 Engine Set-up, Evaluation and Estimation Experimental Set-up Model Evaluation for Operating Conditions, Dimensionality Reduction using Principal and Independent Components, Estimation of Engine Signal Parameters	Chapter 4 Physics-based Health Management Model Idealization, Force Estimation, Solution Comparison with Experiments	Chapter 6 Hybrid Methodology Health Management Hybrid Model Formulation and Evaluation	Chapter 7 Conclusions and Suggestions Drawing Conclusions and Future Work
Diagnosis	Faults Monitoring	Chapter 5 Data-driven and Model-based Health Management Statistical and Intelligent Models, Classification and Failure Prediction. Statistical: Discernment Analysis, Intelligent: Neural Network, Model: Fuzzy Logic	Simulation by introducing Faults,	Hybrid Classification based on Wavelet Neural Network and ANFIS	Conclusions on individual chapters Conclusions on overall Thesis
Prognosis	Failure Monitoring	Degradation Rates using Kalman and Particle Filter	Simulation of Failure Models		
Maintenance			Logistic Support		Suggestions for Future Work

Figure 1.4: Chapter Organization Scheme

Chapter six discusses the Wavelet Neural Network (WNN) and Adaptive Neuro Fuzzy Inference System (ANFIS) hybrid systems. They are proposed for engine fault classification and used to explore the fault characteristics. The performance of MDA, ANN, FL, WNN and ANFIS classifiers are compared and effectiveness in terms of handling different features, classification, resource utilization and robustness are discussed.

The chapter seven discusses the conclusions of each chapter and overall conclusions. Logistic support to manage the engine health is recommended and suggestions for future work are discussed.

1.8 Summary

The chapter briefs the need to study health degradation issues, of course common to any machine, in an engine. It introduces the mechanical components of IC engine in brief, and causes of defects and their effects. Objectives, basic outline, and a methodology of the work have been covered. Approach and validation, significance and possible applications are discussed. The chapter ends with organizing the thesis structure.

CHAPTER 2

LITERATURE REVIEW

Knowing yourself is the beginning of all wisdom.

- Aristotle (384 BC - 322 BC)

2.1 Introduction

In Chapter 1, the degradation issues of an IC engine are briefed and methods that are studied in this thesis are outlined. Some of these methods are in use, and some are being proposed to solve medical, aircraft and other machinery problems (Mrad and Mrad [37]). Techniques for managing aircraft health are growing rapidly due to high involvement of casualty and consequences (Yu et al. [41]). They detect abnormality, predict survival life, recommend remedy and initiates logistic support by taking active contribution from multiple disciplines. Developments in sensors, battery, field-ready electronic control units and wireless communication has enhanced their capability. Techniques that are managing rotating machinery health often fail when applied to an automotive/engines due to system complexity, non-stationary, non-linearity and strong noise signals (Wang and Chen [42]). But affordability and growing demand are enforcing for their enhancement. Purpose of this literature review is to understand HM constituents and summarize the state-of-the-art to,

1. Identify gaps and propose models to study faults and failures of an IC engine.
2. Build and evaluate different models (physics-based, data-driven and hybrid) and select sensitive models for studying health management.
3. Introduce defects in the most sensitive models to generate fault symptoms.
4. Propagate faults into failures to get information on survivability conditions.
5. Select appropriate methods and make decisions on engine health.

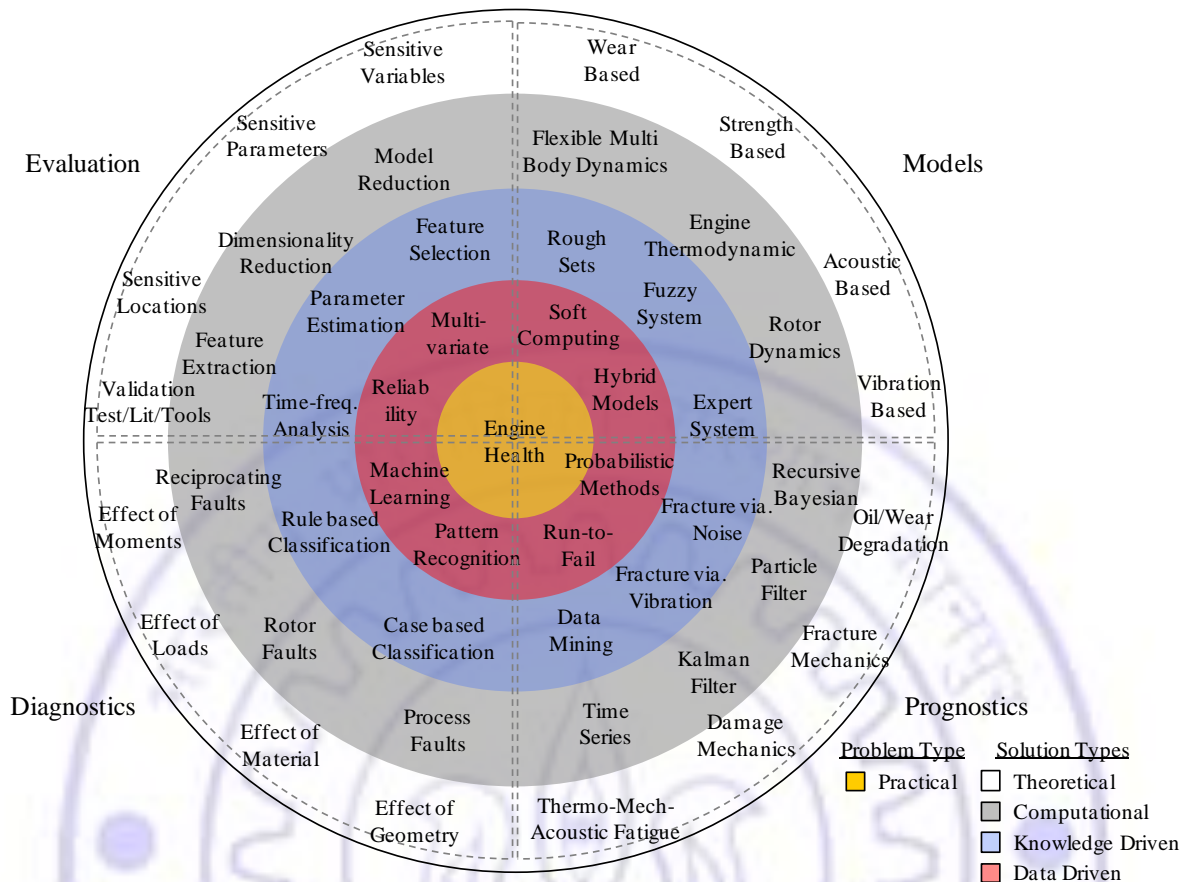


Figure 2.1: Review of Techniques-Topics Listed in Quadrants

Figure 2.1 shows topics that are covered in literature review; they are arranged based on their capability to evaluate engine health. Techniques placed far away from the center are less effective in managing the health. They focus on theoretical, computational, knowledge and data driven approaches from outer ring to innermost ring respectively. Theoretical i.e. physics-based techniques poorly represent the health, provide less expensive, high fidelity and quick trials and explore a wide range of conditions virtually. They can accommodate recent advances but their reliability depends on amount of correlation with experiments. Computational techniques have well capability to represent geometry and predict certain faults but require huge resources. Knowledge driven methods are expensive, requires condensation of knowledge or experience into simple tests/rules but their success depends on perfect match of trial with available library. Data driven techniques are highly capable, uses direct measurement and soft computing models to predict the health with certain probability. First to fourth quadrant of the figure indicates models for HM study, model evaluation to

explore the range of their capability, evaluated models for diagnostics, and diagnostic models to study prognostic respectively. To a certain extent, HM is an art rather than science, since practical solutions are often chosen by the operator depending on the available time, logistics and nature of severity assessed at the situation. Above techniques are reviewed to adopt, formulate a procedure, assess engine health, and extract fault symptoms and failure rates.

Section 2.2 of this chapter discusses the IC engine faults and few rotating machinery faults that are in common. Recent techniques for monitoring the health of an engine are covered in Section 2.3. Section 2.4 discusses the EHM using above techniques. It gives appropriate standards, technological components and a framework; data processing (extraction, selection and reduction of feature) and reasoning techniques for decision making. Section 2.5 reviews the IC EHM and identifies the technological gaps. Lastly, the conclusions are listed.

2.2 Common Faults in an IC Engine

Faults in engine can be mainly grouped as process and structural as shown in Figure 2.2, depending on their nature. Zima and Greuter [43] and Denton [44] listed its reciprocating component faults. Davies [28], Collacott [45], Ehrlich [46] and Walker et al. [2] listed a variety of rotating machinery faults, while most of them are also applicable to an IC engine.

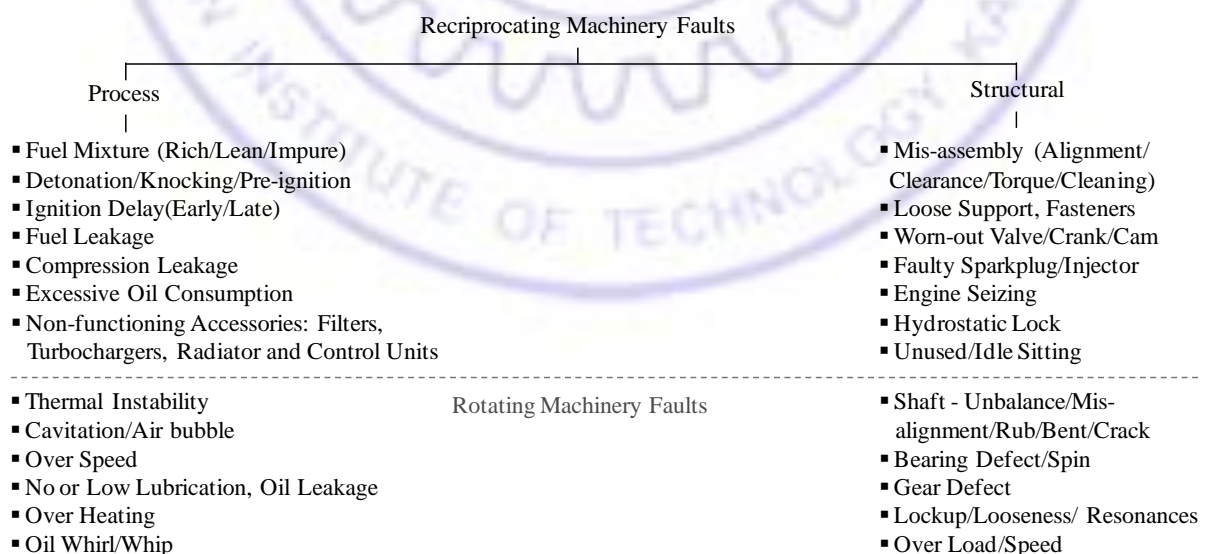


Figure 2.2: IC Engine Faults

2.2.1 Process Faults

Process faults occur quite frequently and survive for short duration. They are caused by dysfunctioning of sub systems (e.g. fouling, change in settings, dirt or flow obstacle, loose electrical connections, defects in sensor, actuators and control units). It leads to fluctuation of thermodynamic properties such as pressure, temperature and speed. They can be identified by misfire, hard to start, low performance and high emission, but they are less harmful, less critical to resolve and have low downtime in maintenance. Such faults may eliminate automatically or being removed in usual proactive maintenance. In engines, they occur due to inability of fuel supply, ignition, injection, air supply and exhaust control systems to manage their appropriate timings. Symptoms are characterized by early or delayed functions, such as loss of compression, spark and change in emission characteristics. Process faults are analogous to acute illness in humans, such as common cold, cough and fever.

Engine Knocking: It occurs when pockets of air/fuel mixture explodes by compression outside the envelope of normal combustion front. Shock wave creates a metallic pinging sound with drastic increase in cylinder pressure and temperature. A high knock can damage engine completely by damaging piston ring, grooves, punching holes at piston tops, smashing connecting rod, bearings and blowing the head gaskets. Detonation occurs near peak cylinder pressure with intensity much larger than the knock. It occurs due to pre-ignition, ignition timing, lean fuel mixture, low octane fuel and excessive use of manual transmission. Proper regulation of the air/fuel mixture and spark plugs can prevent these issues.

Rich/Lean Fuel Mixture: Due to rich fuel mixture, oil and carbon deposits heavily in the combustion chamber and valves. Frequent fluctuation in engine speeds can accelerate the deposition. Burning of excessive oil can wear the valve guides and seats. Excessive pressure in the fuel injector or a faulty sensor can cause fuel mixture to run rich, which can deposit the carbon on the spark electrodes and lead to dysfunction of spark plug and produce misfire.

Pre-ignition: Unnatural combustion ignites much before the spark due to enough pressure and temperatures within the cylinder. It results in knocks and drops the power output and efficiency that increases the noise and vibration. Hot exhaust valve causes insufficient valve

lashes, weak valve spring, excessive wear of valve stem or guide, or retarded ignition timing. Pre-ignition is one of the contributing factors for the detonation.

Excessive Oil Consumption: An engine that burns oil can foul the spark plugs, cause ignition misfire and high emissions. It is caused by high clearance between the valve stems and guides, cracked or broken valve and seat, worn or broken rings, and wear in the cylinders. It results in low compression and high blow-by loss.

Impurity in Fuel: Hydrocarbons either gets dissolve with the fuel or can have an entry of a foreign object in the cylinder that can become ash or solid particles in the chamber. Such particles can block the injectors and seize the engine.

Over Heating: It occur as the result of a failed or underperforming cooling system and that can cause pre-ignition. Excessive heat can expand metals, lower the clearances, gall and stick valve stems, melt and glue the rings on the piston to walls of cylinder, scuff piston and seize the engine. Too much of heat can cause cylinder heads to swell, warp and/or crack and blow the head gasket, misalign the cam or seize the cam bearings, or even break the cam. Entry of coolant into crankcase can deteriorate the engine components.

A variety of process faults such as leaks in EGR and manifold, defective EGR and manifold pressure sensor, throttle sensor, air mass flow sensor in an automotive engine was studied by [Nyberg \[47\]](#). [Ding \[48\]](#) and [Isermann \[49\]](#) developed a model-based fault diagnosis for manifold (misfire, knock, gas recirculation, catalyst, leaks). Common process faults in an aero engine are blade tip clearance change, variable geometry wear, fuel system faults and nozzle blowing ([Kurz and Brun \[50\]](#)). Root causes for these degradations are fouling, erosion, deposits and corrosion.

2.2.2 Structural Faults

Structural faults normally occur due to the chronic degradation such as corrosion, crack and wear in the components. They affect the dependent components and alter the structural health characteristics. These faults are difficult to isolate and require high downtime for

maintenance. They can be identified by a change in engine noise, vibration, overheating and loss of power. Ignorance of such warnings for longer duration may lead to engine seizure. Cause may be minor or major; it requires rigorous detection methods and treatments, often lead to replacement of complete components or sub-assemblies. The structural faults are analogous to chronic diseases in humans such as cancer, heart and kidney related issues.

Engine Misassembly: Misalignment, incorrect clearances and inappropriate torque on critical fasteners can result in engine misassembly. Galling or seizure indicates the bearing has tight clearances, while fatigue failure points to excessive clearances. Too much of torque on the critical fasteners like head bolts, rod and main bearing cap bolts can crush the head gasket, deform bearings or cause the bolts to fail. While too little or uneven torque can lead to leaks. Wrong assembly may occur in a newly built engine or during re-assembly. Wear in a bearing indicates possible bend in the shafts or misaligned bores. Failure to clean and lubricate properly parts during the assembly or deposition of rust and corrosion that can scour bearings and wear the surfaces. They need to be coated with oil to prevent a dry start.

Hydrostatic Lock: In situations like leak of coolant chamber, extreme weather, heavy rain, flash or flood, coolant or water enters into the combustion chamber. Due to incompressible nature, it gets lock during compression stroke and lead to catastrophic failure. Usually these failures are characterized by bend in connecting rods, shear of cylinder heads, blow of crank cases, bend or breaking of crankshaft, valve, stretch of head studs and blow the head gaskets.

No or Low Lubrication: Processes like excessive oil leak or blow-by can heat the engine, breath the oil out from the crankcase and makes engine to run with low quantity of oil. Oil enters the combustion chamber through worn valve guides and seals, worn or broken piston rings and worn cylinders. Pistons gets expand and rub the cylinder walls that make scratches and deep cuts on the liner and piston walls and fuse, which lead to engine seizure. Blow-by deposits black wet on the back of intake valves, combustion chambers and oil-fouled spark plugs. Foreign material in the oil embeds at the surface, erode the debris and ruin the bearings. Plugged oil filter, air filter and breather pumps the oil out. Usually this occurs due to ignoring the replacement of oil on regular intervals.

Oil Starvation: Worn or failed oil pump causes bearings to lose the oil lubrication and wipe away the bearing material. In cold start, low oil pressure or high oil viscosity can delay the arrival of oil long enough that causes starvation and seize the cam. Bearing suffered due to lack of lubrication can lose its function and fuse to the shaft. This can damage the crank journals, connecting rod and even fly off the pistons from the block.

Not in Function for Long Time: In the unused engines, dust and moist air forms rust, which degrades the engine oil and lead to dysfunction and deterioration. Rust on the engine liner can cause to seize the bearings and engine liners.

[Matthews \[38\]](#) surveyed the machinery faults and their failure mechanism. Failures by percentage are: welds (30%), shafts (20%), castings (15%), fasteners (13%), others (9%) and gears (7%). Around 60% of failures are due to high cycle fatigue, 10% are low cycle fatigue and 10% are thermal cycle fatigue, while remaining failures are due to corrosion, creep and static loading. [Zima and Greuter \[43\]](#) surveyed the IC engine failures. They reported the component failures in percentage: piston and connecting rod (24.1%), worn crank (18.5%), cylinder sleeves (16.1%), bearings (14.9%), crankcase (9.6%), cylinder heads (7.6%), valve train (5.8%), cam and gears (5.4%). Dominant failures of an aero engine are due to blade damage, tip clearance change and variable geometry wear as reported by [Kurz and Brun \[50\]](#). Major causes for the mechanical degradations are corrosion, looseness and aging.

[Liu et al. \[7\]](#), [Li et al. \[51\]](#), [Denton \[44\]](#), [Kim and Lee \[52\]](#), [Albarbar \[53\]](#) and [Mohammadpour et al. \[54\]](#) listed most common faults of an IC engine. [Ben-Ari et al. \[55\]](#), and [DeBotton et al. \[6\]](#) studied the behavior of artificially created defective spark plugs, change in ignition timing by early, delaying the spark and loose engine mounting. [Liu et al. \[7\]](#) introduced the valve clearance defects and valve leaks. [Li et al. \[51\]](#) and [Albarbar \[53\]](#) investigated injector fault. [Lee and Kim \[56\]](#) investigated severe wear in cylinder liner. They studied few externally introduced faults and demonstrated vibration monitoring as powerful technique for health management. Statistical and Fourier features extracted from stationary signals can serve as symptoms. Due to the highly non-stationary engine signals and faults mostly internal to the engine they are difficult to introduce and challenging to monitor.

2.2.3 Rotating Component Faults

In the last three decades, study of rotating machinery faults has been an area of extensive research. Ehrlich [46], and Eisenmann and Eisenmann [57] have reported various faults of rotating machinery and their steady speed symptoms. This section discusses the most prominent rotating machinery faults, their causes and symptoms.

Shaft Defects: Deviation in the shaft geometry is a major cause in every rotating system. An unbalanced shaft exerts fluctuating centrifugal force on its support, which causes the machine to vibrate at frequencies equal to the shaft speed and its multiples. Vibration induces excessive wear and reduces service life in bearings, bushings, gears, cams and other machine elements. Shaft misalignment occurs due to the deviation of rotational centerlines between the driver and driven shaft. Coupling misalignment causes friction and deflection of bearing, which are characterized by twice, sometimes thrice or four times of the running speed. Shafts running into resonance show large amplitude of response at critical speeds and at its sub harmonics. Shafts with large excitation torque show torsional oscillations. Bent shaft shows symptoms that are similar to an unbalanced shaft. Cracked shaft has an asymmetric stiffness due to the breathing of crack; high response can be observed at first and sometimes, second or third multiples of rotational speed.

Bearing Defects: Bearing wear and excessive clearance result due to an application of high loads, shocks, or bearing attenuations. When an element of rolling bearing passes over a defect in its races, balls or cages, causes an impulsive excitation, which can be related to bearing geometry and rotational speed.

Gear Faults: Manufacturing error causes a shift in the geometric center from the rotating central axis that lead to an eccentricity. Uneven hardened flank and gear tooth face can lead to surface fatigue and result in flaking or spalling of material. Gears are subjected to shock and cyclic loading. Crack initiates at tooth root due to high stress concentration and propagates under service loads. This results in fracture of the tooth and giving rise to missing tooth. Errors in assembly or shifting of sliding gears into mesh without stopping the rotation of shafts can results in chipping or partial breakage of the gear tooth.

Distortion and Looseness Faults: Distortion in the foundation causes misalignment or rubbing in the shaft and bearing, which lead catastrophic failure at resonance. Loose disks, sleeves, collars cause internal friction and destabilization. Vibration of loose bolts occurs at frequency equal to the shaft speed. Loose bearing gives rise to sub-harmonic response. Physical contact between rotating elements and stationary machine parts can generate rub. Usually rub is observed at twice the rotational frequency of the shaft.

Table 2.1: Symptoms of Common Faults

Fault	Time Waveform	Frequency	Cause
Beats	Build-up and decreases periodically	Two close frequency	Excitations at almost same speed
Oil whirl and Oil whip	Sub synchronous instability, Self excited amplitudes	0.42~0.48% of 1X, Whirl locks at nat. freq	Journal bearings caused by excessive clearance
Looseness	Amplitude and frequency constantly change, rattling	0.5X, 1.5X, 2.5X, etc.	Internal friction
Resonance	Constantly increasing amplitude	Discrete peaks	A serious condition with very high amplitudes
Unbalance	Constant amplitude	Distinct 1X with much lower 2X, 3X, etc.	Unequal distribution of the weight and
Misalignment	Pulsation of amplitude	Distinct 1X with equal or high 2X and 3X; high axial	Casing and foundation distortion, incorrect alignment
Eccentricity	Cannot be corrected with weights	1X	Sudden increase in speed or an external shock
Bent shaft	Can be corrected with weights near the center	1X and 2X	Excessive heat, its length or it may be physically bent.
Rubs	Restricted amplitudes	0.25X, 1/3X, 0.5X etc. External loops in orbit	Severe mass unbalance, insufficient clearances
Soft foot	Dramatically decreases by loosening bolts	1x rpm	Hold down of foundation bolt
Bearings	Small spikes or impacts	0.4X, $0.4X \cdot N_b$ and $0.6X \cdot N_b$ respectively, High freq	Lubrication and shaft problems, Dirt and pit
Gears	Modulated signal	$1X \cdot N_t$, $2X \cdot N_t$ usually larger, Sidebands	Shaft and tooth problems, Overloading, backlash

1X is running frequency, N_b is no. of balls and N_t is no. of tooth

Oil Whirl and Oil Whip Faults: In journal bearings, oil whirl usually occurs at slightly less than half the running speed. It is a formation of pressurized load-carrying film to raise the shaft position to a stable altitude, angle and eccentricity depending on shaft speed, weight, oil pressure and pre-loads. Oil whip occurs when whirl frequency coincides and gets lock with the shaft natural frequencies, which can lead to catastrophic failure, if continued to run. Characteristics of oil whirl and whip can serve as symptoms of a specific fault.

Fault diagnosis is often restricted to steady speed, while transient analysis can reveal complete information of the system. Table 2.1 lists symptoms of few rotating machinery faults at steady speed. Asymmetry, rigorous fluctuations in loads and intermittent contacts of IC engine demands for transient analysis. IC engines are less expensive, easy to access, has exhaustive loading and have several faults in common to rotating machine. It helps to reveal clear symptoms at early stage and makes more convenient for EHM research.

2.3 Engine Health Monitoring

Mobley [58], Williams et al. [59] and Mohanty [60] reviewed various condition monitoring techniques. They concluded that the process/performance, tribological, structural and electrical parameters are good indicators of a machinery health. Figure 2.3 presents the monitoring techniques. Structural health can be monitored tracking fatigue cycles counts, crack, vibration, contact, acoustics, oil debris and contamination. Loss of power, consumption, drop or rise in fluid properties, gas particulate and leak can monitor process health. Electrical indicators such as current, voltage can record certain short term changes.

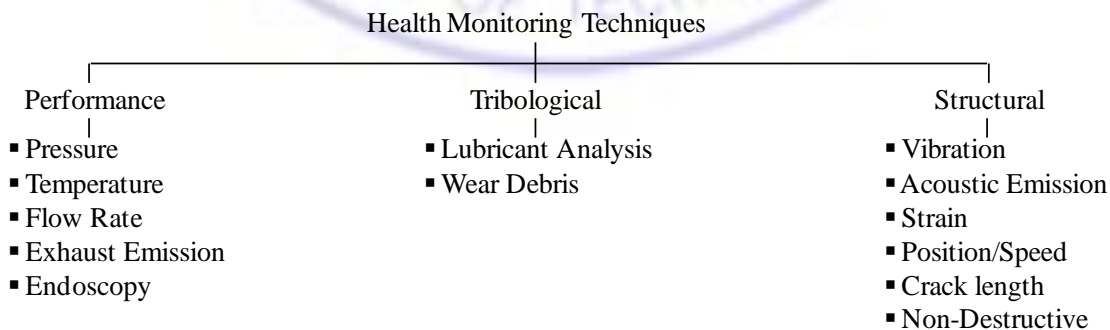


Figure 2.3: Condition-based Health Monitoring Techniques

2.3.1 Performance Health Monitoring

Monitoring of parameters such as temperatures, pressures, flow rates, humidity and air-fuel ratio can record the short-term changes of an engine. The block, leak and dysfunction of the process are quite often and are easy to detect and fix. Change in alignment, symmetry and valve clearance can affect the efficiency, dynamic nature of the system and increases the running expense. Direct online methodology for continuous monitoring can indicate the problem at source level so they are in demand.

Clearance: Change in clearance can detect the leakages due to variations in seal, speed, operation and temperature. Online monitoring schemes are more effective in assessing the leakages. Thermography monitors the thermal signatures and detects local hot spots. Increased thermal output can identify seal leaks, defective bearing and gear distress.

Hazard Performance Assessment: Change in overall performance of machines can be assessed by their operating hazardous environmental conditions. The change in shaft speed, temperature and pressure can be linked to the defect in flow path components. Measurement of flow path with a degraded model and a set of appropriate indicators/sensors specific to a machine can give fault symptoms database.

Gas Path Debris Monitoring: It detects the electrostatic charge carried by debris that engine has ingested or present in the exhaust gas. The debris is detected and potential to damage is assessed to determine the resultant effect of ingested object and identify nature of the fault. It also monitors the fault along flow path of the engine.

Till date, engine diagnostics is restricted to performance monitoring and carried-out by on-board checking the functionality of control units and sensors, and ensured by flashing. The process changes can be easily detected and well simulated by a simplified mathematical (Isermann [49] and Elhaj et al. [61]) model so a less sophisticated sensor is sufficient. A detailed survey on diagnostic and prognostic aspects of condition-based maintenance may be found in a review by Mohammadpour et al. [54]; they made a survey of the OBD methodologies for detecting the process and sensor faults by tracing the ECU systems. The

model-based fault diagnosis has been played a volatile role in fault diagnosis of process faults. [Ding \[48\]](#), [Nyberg \[47\]](#) and [Isermann \[49\]](#) developed a model-based fault diagnosis for manifold process faults (misfire, knock, gas recirculation, catalyst and leaks). They concluded that the different residuals between actual and theoretical parameters of manifold are sensitive to different faults that can serve as fault symptoms.

2.3.2 Tribological Health Monitoring

Monitoring oil contamination and debris can indicate damage accumulation and forecast the component failure. This method is effective and reliable, but changes are very slow and applicable only to oily systems.

Lubricant Analysis: It analysis the oil and monitors chemical changes of oil. The viscosity, total acid and base numbers (TAN and TBN) of oil are good indicators of the oil degradation.

Oil Debris Analysis: It monitors metallurgical changes of the material that are removed from the oil filter. It is a powerful method for metallic particulate, but unreliable to monitor non-metallic debris. Survey indicates that the online observations have more realistic results so they have a greater demand; however the accuracy depends on the capability of extending lab based methods to the actual field.

Jun et al. [\[62\]](#) predicted the time to change oil by analyzing its degradation status for the usage mode and mileage. They used viscosity, TAN and TBN, engine hours, number of engine start-ups and oil temperature as indicators for deciding the time. [Zhang et al. \[63\]](#), [Yonghui et al. \[64\]](#) and [Macian et al. \[65\]](#), developed a method to predict component wear by analyzing the particles, debris and contamination in the lubricant.

2.3.3 Structural Health Monitoring

Monitoring of the shaft motion, vibration, sound pressure, acoustic emission, crack and accumulated fatigue life from stresses can indicate the structural faults and failures. Reference [\[3, 66-70\]](#) discusses the measurements, damage identification and decision making methods for monitoring the structural health in civil, mechanical and aerospace systems.

Non-destructive Monitoring: NDT techniques such as visual inspection, hearing, smell, magnetic-particle, liquid penetration, radiographic, ultrasonic, shock and pulse, infrared thermography or acoustic emission evaluates material properties and cracks without causing any physical damage. AE sensor records plastic deformation and crack using radiation of high frequency (in the order of MHz) elastic waves within the material, caused by rapid release of localized stress energy. It is widely used in civil structure (Ettouney and Alampalli [67]) but it measures specific characteristics and not necessarily the effect or its extent.

Metallurgical Life Monitoring: The gradual cycle counts due to damage mode, low or high cycle fatigue (LCF or HCF), thermal fatigue, corrosion and creep can reveal remaining durations for a failure. A failure limit 10^5 load reversals decides the LCF. It is characterized by high stress fluctuations and local failures, due to flaw such as void, impurity or high stress concentration, machining flaw or service induced cracks. It is computed by monitoring the stress reversal counts, start-stop cycles or speed exceeding limits. Overlay of HCF condition makes computation difficult in transients. HCF has low average stress fluctuations and the failure progress rapidly, and characterized by majority of failures. Cyclic fluctuations in temperature results in thermal stresses and thermal fatigue, which is analogous to LCF stress environment. Prolonged periods of stress or temperature exposure can result in creep failure, which is characterized by permanent deformation in the components.

Vibration Monitoring: Vibrations can be linked to periodic events in the machine's operation. The symptoms such as order ratio, modal parameters and their limits can detect operational or component abnormality. It can pinpoint the source of vibration energy. Vibration symptoms for gear, shaft, bearings, and couplings using stationary signals have been well documented; however the symptoms from the transient and assembly level are gaining increased attention. In vibration based fault diagnosis, the symptom database of common faults is generated by deliberately introducing the faults in the healthy system.

Sound Monitoring: Sound pressure or levels recorded by a microphone can indicate the machine health condition and occupational hazard. Defective operation and collision in the machine changes the operational sound that can be referred to the specific fault.

Shaft Motion Monitoring: A non contact eddy current probes installed on bearing or around the shaft can record the actual motion of shaft inside the fluid film bearing. It is a net motion of the shaft assembly relative to the bearing, while vibration and sound measures the total motions of shaft mixed with oil wedge, bearing and foundation response, that can contains several minute impulsive excitations due to collisions. Shaft orbits and shaft centerline plots can indicate the condition of shaft stability and few most dominant shaft defects accurately.

DeBotton et al. [6] and Ben-Ari et al. [55] concluded that the vibration monitoring as a predictive maintenance tool for reciprocating machines. They listed most sensitive location on engine for data collection and studied by introducing some external faults. They proposed health evaluation criteria for defective spark plugs, change of ignition timing by early and delaying the spark, and loose engine mount. They concluded that the distinguished vibration symptoms can provide various malfunctions in the engine.

Figure 2.4 shows some of the engine faults discussed in Section 2.2 with their location and appropriate monitoring techniques. It indicates that the vibration monitoring is widely used technique for measuring structural defects.

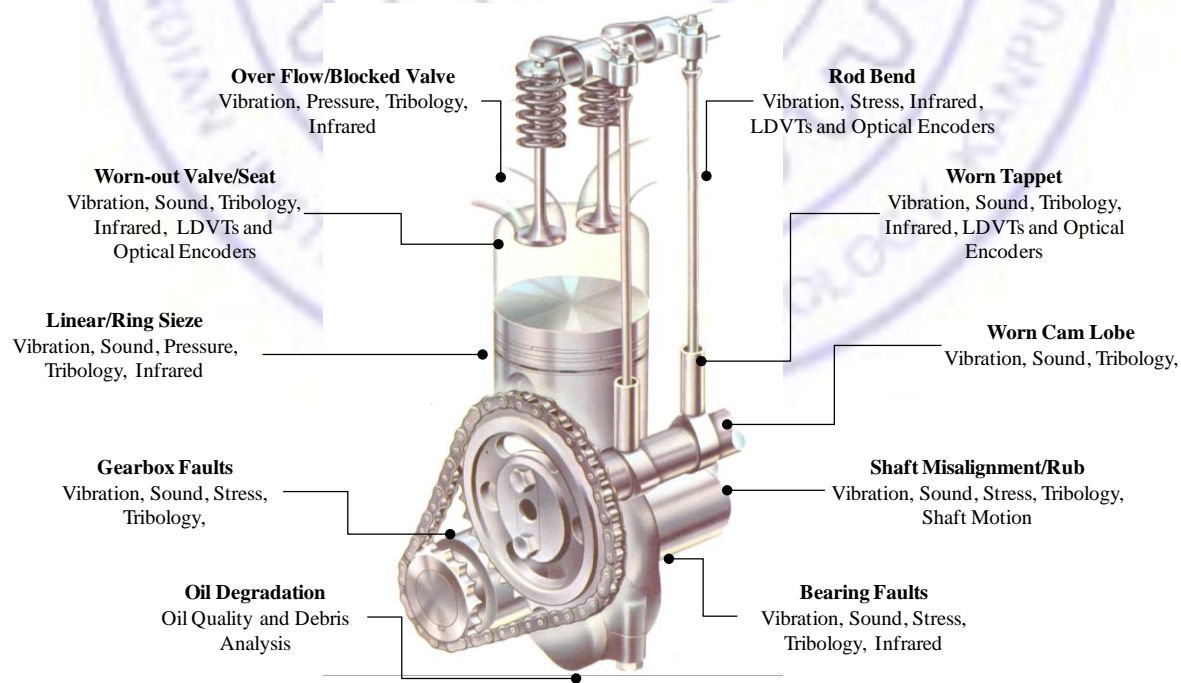


Figure 2.4: Engine Faults and Monitoring Techniques

2.4 Engine Health Management

Mobley [58] reported that only 33% of maintenance is effective; it is either due to unnecessary or improperly carried-out maintenance. About 50% of fully functional components are being removed in maintenance (Clutz [71]). Adopting a suitable maintenance strategy requires evaluation of different methods. Maintenance methods are grouped into preventive, reactive, proactive and active with increased functionality and logistic support (Moustapha [72] and Mobley [58]). Preventive is a maintenance that is scheduled for a small likelihood of failure between repairs or a breakdown. In reactive maintenance, less critical or run-to-fail components are inspected in the trial tests. Proactive maintenance predicts the impending failures and activates maintenance with minimum intervention to the process. Active maintenance accumulates real time damage, assesses the situation, and eliminates the redundant systems and loads.

International Organization for Standardization (ISO) has a few standards for the machinery condition monitoring. Section ISO/TC 108/SC 5 (Condition monitoring and diagnostics of machine systems, [73]) outlines the monitoring processes and requirements (such as service, training, contract, insurances and litigation) for certification. ISO standards 13380, 14830, 10816 1-7, 13373 1-2, 13381-1 lists the general guidelines for machine condition monitoring based on performance, tribology, vibration ratings and severity respectively. These standards neither focus on a particular application nor give any illustrative examples. Society of Automotive Engineers (SAE) has come up with a series of guidelines for aircraft engine condition monitoring and maintenance [74]. Guides such as AS 8054, AIR 1839, ARP 1587, 1872/873/900, 4061/175/4754, 6212/406/461/725/803/883, J1455/814/300/978/306/699/2602/1850/1939, 304, 2847/836/API 670 reviews the methods for engine life monitoring and component logistics. They are useful to monitor the process failures, while a few address the structural health. Employing new techniques, algorithms and enhancement of CBM can eliminate the removal of fully functional component. The following section reviews existing health management techniques.

2.4.1 System Overview

A health management system monitors the health conditions and initiates appropriate decisions for maintenance. HM uses sensor, instrumentation, signal processing, system identification and several reasoning techniques. It employs data collection, diagnosis, prognosis and maintenance techniques as shown in Figure 2.5. Diagnosis is a process of detecting the fault, based on observed symptoms and isolating it to a specific component. Prognosis predicts the RUL or operational time span of a component for the given working conditions. Maintenance management is the process of taking service decisions based on diagnostics and prognostics information, available resources and operational demand. [Jardine et al. \[1\]](#) and [Esperon-Miguez et al. \[75\]](#) has surveyed diagnostic and prognostic aspects of CBM, they reported the recent developments on data acquisition, data processing and decision making in mechanical systems. [Vachtsevanos et al. \[36\]](#) provides a holistic and integrated approach of fault diagnosis and failure prognosis for engineering systems.

2.4.2 Knowledge Management

It is the process of collecting data, capturing and developing knowledge, and sharing it to diagnostics, prognostics and maintenance functions that make evaluation and decisions. Data is collected using monitoring techniques and data that provide sufficient information are organized. In case of engines, data need to be acquired for the entire operating range from several different sensors and locations with sufficient resolutions. A suitable processing and extraction of unique and most valuable features can provide the knowledge. In communication process, data sets that demonstrate the progress are tracked.

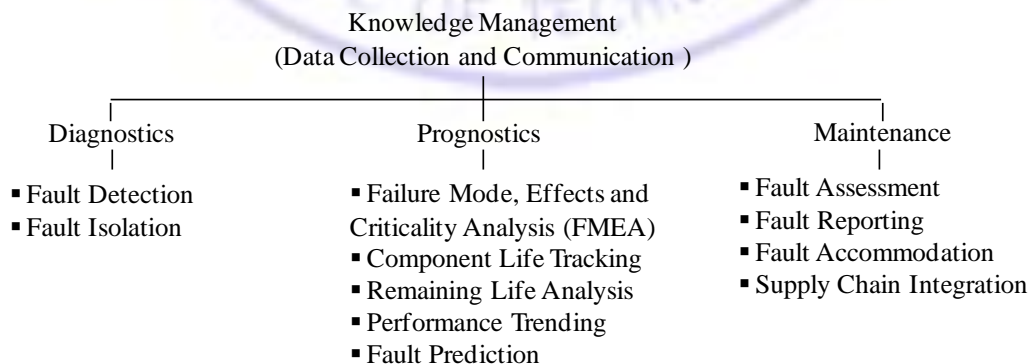


Figure 2.5: Functions of a Health Management System

2.4.2.1 Feature Extraction

It is the process of extracting silent features of a signal by processing in different domains as shown in Figure 2.6. Partial or down sampling, averaging, Empirical Mode Decomposition (EMD) and summarized dot pattern (SDP) operates in time domain, while fast Fourier Transform (FFT) operates in frequency domain. Transforms such as Short-time Fourier Transform (STFT), Wigner-Ville Distribution (WVD), Choi-William Distribution (CWD) and Continuous Wavelet transform (CWT), Hilbert-Huang transform (HHT) represents the signal in time-frequency domain. STFT extends the Fourier transform, but has a fixed resolution in both time and frequency, while WT has a varying resolution in time-frequency domain. WT works with the Heisenberg uncertainty, while HHT works on empirical approach and has complete reconstruction capability. Publication ([Mallat \[76\]](#), [Iatsenko et al. \[77\]](#) and [Huang \[78\]](#)) lists the works that are carried-out on time-frequency methods.

Time Domain Transforms: Statistical moments record the overall health of the signal. Information regarding periodic nature such as constant, slowly or rapidly changing process is not captured and parameters have poor reconstruction capability. In order to reduce the background noise the down sampling are usually carried out.

Orbital Domain Transforms: Change in shaft orbit and centerline motion within the journal can be used to detect faults. An orbit plot indicates the dynamic motion of the center of a rotating shaft, while a shaft centerline plot displays the path of shaft center during the start-up shut downs and transient maneuvers. Orbit shapes such as ellipse indicates unbalance; outer loop shows oil whip, banana and inner loop shows possibility of misalignment in the shaft.

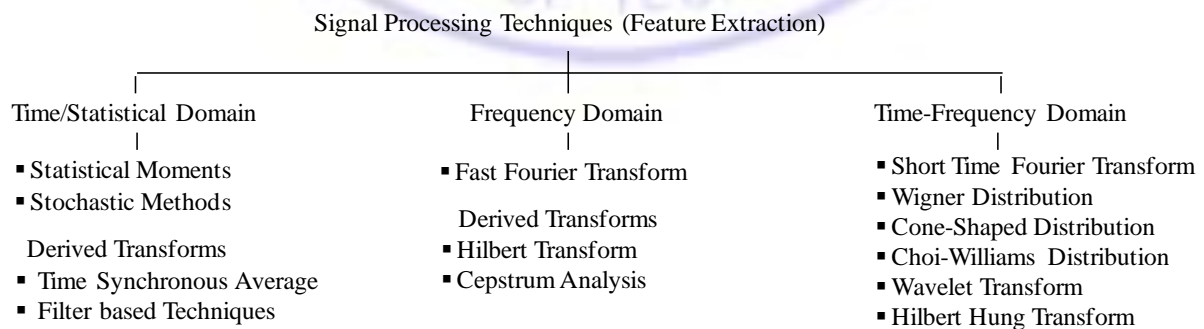


Figure 2.6: Signal Processing Techniques

Frequency Domain Transforms: It decomposes a time (a signal) function into a series of elementary functions that make it up. In doing so, frequency information is captured and time information is lost. Fourier transform $FT(\omega)$ and its discrete form (DFT) are,

$$FT(\omega) = \int_{-\infty}^{\infty} f(t) \cdot e^{-j\omega t} dt \quad 2.1$$

$$DFT(k) = \sum_{n=1}^N f_n \cdot e^{-j\cdot(k-1)(n-1)/N} \quad k = 1, 2, \dots, N \quad 2.2$$

where t is independent variable represents time (in sec), ω is angular frequency (rad/sec), f is an integrable function ($\int_{-\infty}^{\infty} |f(t)| \cdot dt < \infty$). In real case, signals are sampled and cannot be representable by elementary functions, so they can be approximated by discretization k on frequency ω axis. DFT iteratively fits signal by scaling the original sinusoidal wave. Characteristic values obtained can serve as the symptoms of a fault.

Time-Frequency Transforms: A STFT divides a longer time signal into shorter segments of equal length and then compute the Fourier transform separately on each shorter segment. STFT and its discrete form (DSTFT) are,

$$STFT_f^w(\tau, \omega) = \int_{-\infty}^{\infty} f(t) \cdot w^*(t - \tau) \cdot e^{-j\omega t} dt \quad 2.3$$

$$DSTFT_f^w(\tau_n, \omega_n) = h \sum_{k=0}^{N-1} f(t_k) \cdot w^*(t_k - \tau_n) \cdot e^{-j\omega_n t_k} \quad k = 1, 2, \dots, N - 1 \quad 2.4$$

where $\tau_k = t_k = kh$, $\omega_n = 2\pi n/Nh$ and $n = -N/2, \dots, N/2$. Wavelet is a function that divides a function of time into different scales; its coefficient refers the closeness to the signal at a particular location and scale. CWT and its discrete form (DWT) are,

$$CWT_f^\psi(\tau, s) = \frac{1}{\sqrt{s}} \int_{-\infty}^{\infty} f(t) \cdot \psi^*\left(\frac{t-\tau}{s}\right) dt; \quad s > 0, \tau \in \mathcal{R} \quad 2.5$$

$$DWT_f^\psi(k2^{-s}, 2^{-s}) = \sum_m 2^{s/2} f(t_m) \cdot \psi(2^s t_m - k). \quad 2.6$$

where $\psi_{\tau,s}^*(t) = \frac{1}{\sqrt{s}} \psi^*\left(\frac{t-\tau}{s}\right)$ is the complex conjugate of mother wavelet, which has to meet zero mean ($\int_{-\infty}^{\infty} \psi^*(t) dt = 0$) and finite energy ($\int_{-\infty}^{\infty} |\psi^*(t)|^2 \cdot dt < \infty$) conditions. Discrete

wavelet taking τ and s in the form of $k2^{-s}$ and 2^{-s} respectively; $k, s \in Z$ are set of integers. HHT transforms (Huang [78]) the non-stationary and non-linear signals. First step in HHT is EMD, which decomposes signal into simple oscillatory components called IMFs and a residue. It retains both non-linear and non-stationary effects in the individual IMF and helps to produce effective reconstruction. Time-frequency curves of HHT are analogues to the WT ridges. IMF of a HHT is almost a mono-component, so its instantaneous frequencies can be determined. However, an IMF seeks mathematical proof and justification. For a noise free signal $x(t)$, the Hilbert transform $y_i(t)$ of each IMF $x_i(t)$ are,

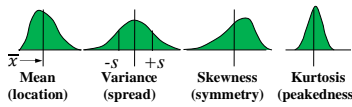
$$x(t) = \sum_{i=1}^n x_i(t); \quad y_i(t) = \int_{-\infty}^{\infty} \frac{x_i(\tau)}{\pi(t-\tau)} d\tau \quad 2.7$$

Modal characteristics for each mode can be obtained from the complex signal.

$$z_i(t) = x_i(t) + jy_i(t) \quad 2.8$$

Table 2.2 lists the comparison of these transforms. Time-frequency transforms have certain computational and resolution issue that needs justification for their optimal selection, but they have strong reconstruction capabilities so they are accurate in feature extraction.

Table 2.2: Overview of Transformation Techniques

Domain	Expression	Advantages	Challenges
Statistical	Descriptive statistics  <p>Mean (location) Variance (spread) Skewness (symmetry) Kurtosis (peakedness)</p>	<ul style="list-style-type: none"> Summarizes the bulk data into relatively few quantities Simple and straightforward 	<ul style="list-style-type: none"> Lack of frequency (constant, change-rapid/slow) information No reconstruction capability Unable to identify the cause
Frequency	$FT(\omega) = \int_{-\infty}^{\infty} f(t) \cdot e^{-j\omega t} dt$	<ul style="list-style-type: none"> Suitable for stationary signals Extracts dominant harmonics 	<ul style="list-style-type: none"> Event (time) information lost Not suitable for non-stationary
Orbital	$f(t) = x(t) + jy(t)$	<ul style="list-style-type: none"> True motion of the shaft Explains stability 	<ul style="list-style-type: none"> Applicable to rotating system Requires steady speed
Time-frequency	$TF(t, \omega) = \int_{-\infty}^{\infty} f(t) \cdot w(t, \omega) dt$	<ul style="list-style-type: none"> Strong re construction capability 	<ul style="list-style-type: none"> Optimal resolution issue High computational time

Due to non-stationary nature in IC engine signals, the time and FFT features are less effective. A few literatures demonstrate the use of FFT features under extremely controlled stationary scenario. [DeBotton et al. \[6\]](#) and [Ben-Ari et al. \[55\]](#) proposed FFT features as health evaluation criteria for engine defects, and their degradation. [Lee and Kim \[56\]](#) detected severe wear in cylinder liner with a specific frequency and amplitude of acoustic emission for different load conditions.

WT and HHT are widely applied in condition monitoring of rotating machineries ([Peng and Chu \[79\]](#), and [Lei et al. \[80\]](#)), while literature [\[8-9, 11, 53, 81-82\]](#) lists application of WT on an automotive vehicle and engine systems. [Wu and Chen \[8\]](#) applied WT based plots for various engine faults such as leakage, miss-firing and cooling fan rubbing. Time-frequency distribution of vibro-acoustic signals under an injector fault is studied by [Zheng and Leung \[9\]](#). [Staszewski and Giacomini \[11\]](#) employed frequency response based WT for analyzing acceleration transmissibility across an automobile seat. [Albarbar \[53\]](#) presented WT plots of engine acoustic signals for varying load, speed, and injection pressure and oil level. [Chang et al. \[81\]](#), and [Merkisz and Waligórski \[82\]](#) used WT plots to detect misfire and knock in spark ignition engine. [Zou et al. \[83\]](#) employed Wavelet packets to extract combustion, valve impacts and compression components from vibro-acoustic signature. HHT is receiving increased attention for detection of engine faults. [Li et al. \[84\]](#) used an IMF to detect abnormal clearance in rings and valves of an engine. [Yadav \[85\]](#) used cumulative IMFs to identify cam, chain, tappet and gear faults. [Xu et al. \[86\]](#) and [Yang \[87\]](#) used HHT to analyze the engine vibration signal. [Wang et al. \[88\]](#) used IMF energy moments to classify throttle sensor, ignition coil, hall sensor and injector faults. Application of WT in [\[8-9, 11, 53, 81-82\]](#) has been restricted to report scalogram contours for different faults; assessment of these contours is qualitative and subjective. It is difficult to differentiate the contours precisely and quantify the significant parameters of each fault. HHT contours of [\[84-88\]](#) also do not quantify time invariant parameters of the faults and justification of IMF is difficult due to existence of several unrealistic low frequency IMFs. [Peng et al. \[12\]](#) attempted to reduce such IMFs by amplitude correlation. It is necessary to look into the superiorities and claims of these transforms and propose enhancement for analysis and estimation of engine vibro-acoustic signal parameters for precise fault quantification.

2.4.2.2 Feature Selection

It is the process of selecting a subset of relevant variable or attributes. It reduces the number of attributes in the dataset by including and excluding attributes without changing them. It identifies and removes the unwanted, irrelevant and redundant attributes from data that hinders the accuracy of a predictive model. There are three general classes of feature selection algorithms: filter, wrapper and embedded methods.

Filter Methods: In this method, the features are either retained or removed from the dataset by scoring each feature based on statistical (Chi squared test and correlation coefficient) measure. These methods are usually feature independent or dependent of the variable.

Wrapper Methods: This method recursively eliminates the features by preparing, evaluating and comparing different combinations. A score is assign to the combination using the predictive model. Search process uses methods such as best-fit search, random hill-climbing or heuristics, like forward and backward passes to add or remove features.

Embedded Methods: In these methods, features that contribute to accuracy of model are selected by penalizing the complex model. Common type of embedded feature selection methods are regularization methods.

2.4.2.3 Dimensionality Reduction

Number of attributes in the dataset can be reduced by creating new combinations of attributes. A multivariate technique such as PCA, ICA, SVD and Sammon's mapping can reduce the data without losing valuable information or dependence. They group, sort and investigate inter-dependent relationship between many variables simultaneously. It gives key and collective information about the process and contribution of each variable. Table 2.3 lists the overview of few dimensionality reduction techniques

Profile Analysis: It tests performance of variables in a group to extract meaningful information from data. If performance profile is parallel, then tests are made for their coincidences, which are then tested for constant levels across the variables.

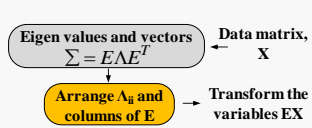
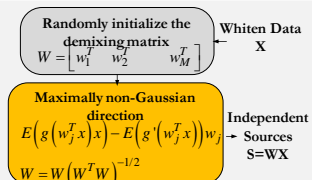
Multivariate Analysis of Variance (MANOVA): It is a procedure for analyzing the means of two or more populations. It tests the effect of independent variable on several dependent variables at once by creating new dependent variables that has linear combinations of measured dependent variables and they contribute in maximizing the group differences.

Principal Component Analysis (PCA): It uses an orthogonal transformation to convert a set of observations of possibly correlated variables into a set of values of linearly uncorrelated variables with total variance. It arranges uncorrelated principal components in the order of variability by a linear combination of the elements. They are constructed to visualize dimensional data that makes easy to select the highly versatile data.

Independent Component Analysis (ICA): It separates the sensor observations that are mixtures of unknown independent sources into independent, non-Gaussian signals using statistical independence assumption. ICA is a special case of blind source separation.

Liu et al. [7] concluded that the partial sampling and feature averaging (PSFA) of cylinder head vibration signals corresponding to the period of valve closing is more effective than cycle-by-cycle. Li et al. [51] and Albarbar et al. [10] investigated the source of weak events corrupted with background engine noise for injector fault and developed an ICA based enhancer for separation of the source signal. Yadav [85] proposed wavelet and empirical mode based de-noising to eliminate noise in the transient acoustic signals.

Table 2.3: Overview of Dimensionality Reduction Techniques

Techniques	Expression	Advantages	Challenges
PCA	 <p>Eigen values and vectors $\Sigma = E\Lambda E^T$</p> <p>Arrange A_i and columns of E</p> <p>Data matrix, X</p> <p>Transform the variables EX</p>	<ul style="list-style-type: none"> • Arranges based on amount of variance in leading directions. • Commonly used for dimensionality reduction. 	<ul style="list-style-type: none"> • Not suitable for fault classification. • Unsupervised, ignores class labels. • PCA is adequate if the data are Gaussian, linear, and stationary.
ICA	 <p>Whiten Data X</p> <p>Randomly initialize the demixing matrix $W = [w_1^T \ w_2^T \ \dots \ w_M^T]$</p> <p>Maximally non-Gaussian direction $E(g(w_j^T x) x) - E(g(w_j^T x)) w_j$</p> <p>Independent Sources $S = WX$</p> <p>$W = W(W^T W)^{-1/2}$</p>	<ul style="list-style-type: none"> • Maximizing the statistical independence of the estimated components. • Can handle several source data 	<ul style="list-style-type: none"> • Can't determine the variances (energies) of the IC's • Can't determine the order of the IC's

2.4.3 Diagnostics

It is the process of detecting a fault and isolating the fault to a specific component that hinders the system to perform its full operation.

2.4.3.1 Fault Detection

It involves identification of a fault that has occurred and causing system to dysfunction. It can be detected by observing abnormal symptoms from signatures, usually after filtering out the noise and extracting the characteristic features.

2.4.3.2 Fault Isolation

Causes of a fault can be hidden that can disturb the dependent components and has potential to affect the future performance. Its isolation involves testing of system or sub-system in an on-board or built-in-test and localizing the cause to a specific component.

2.4.4 Prognostics

Once the fault is detected, predicting chance of survival becomes important. It involves estimating remaining useful life using data-driven, model-based or physics-based approaches. RUL is the survival time span of a component for the desired operation. Survival statistics reveals probability of a detected fault that can continue to perform for a fixed period. Acceptable service life of a component is estimated by understanding component damage modes, tracking rate of damage accumulation and forecasting the dynamic operation demands. Prognostic is carried-out using failure mode effects and criticality analysis, component life tracking, remaining life analysis, performance trending and fault prediction.

2.4.4.1 Failure Mode, Effects and Criticality Analysis (FMECA)

It identifies the possible ways in which component fails and their consequences, and classifies according to the probability of their occurrence and severity. It involves: 1. Constructing block diagram of the system, 2. Identifying failure modes in each sub - systems, 3. Assessing effects of each failure mode, 4. Assessing severity of a fault, 5. Identifying probability of occurrence of the fault and 6. Arranging failure modes in terms of their severity and criticality.

2.4.4.2 Component Life Tracking

Usually, life of a component is estimated based on the worst case scenario, which removes the components much before their actual life. But advancement in memory data storage devices, increased life of battery and miniaturized sensors has allowed tracking of component damage accumulation in real-time. State of the components and their probability of satisfactory endurance for future loadings are estimated by monitoring component cycle fatigue counts, pressure and temperature profiles.

2.4.4.3 Remaining Useful Life

It is the useful life that is still remaining in a serving component at a particular time of operation till its dysfunction. It is predicted based on the damage mode life limits, real-time damage accumulation and the operational demands.

2.4.4.4 Performance Trending

It monitors a set of parameters that affect the performance with respect to an acceptable level. Performance of a new or repaired system has an output that exceeds the minimum required limits for its safe operation. With the subsequent degradation, the performance reaches to a point at which conditions such as expense, safety and risk are no longer acceptable. Based on the performance trending or operational observations or conditions that exceed the costs, the maintenance actions are recommended.

2.4.4.5 Fault Prediction

It is the prediction of a point in time, where the performance of a component becomes no longer unacceptable. On-board monitoring strategy can predict the faults accurately.

2.4.5 Maintenance Management

It initiates suitable maintenance and logistic decisions in terms of a set of options based on the diagnostic and prognostic information. It assesses and reports the fault, and activates supply chain integration and fault accommodation. Challenge is to assess large amount of automated diagnostic and prognostic information and make effective decisions on engine assets at the corporate level.

2.4.5.1 Fault Assessment

It assesses the impact of a fault and effect on current and future services. It estimates safety, fault growth rate and remaining duration of the operation within the acceptable limit, and provides best options to reduce the damage under such ill-fated conditions.

2.4.5.2 Fault Reporting

It documents the essential and informative features related to the severity of impending fault that is useful to operator and associated members. It also advises emergency actions and offers alternatives for continued safe operation.

2.4.5.3 Supply Chain Integration

Based on impending fault diagnostic, prognostics and logistics data, the component availability, shipping instructions, work bay and personnel requirements are formulated. Though it is helpful but final decisions are being taken by responsible personnel.

2.4.5.4 Fault Accommodation

It ensures the system for continuing its functionality even after the fault has occurred by identifying faulty components, sensors, redundant systems and software to reduce the collateral damage. The operating life is extended by sensing damage accumulation, mode and altering the operations without affecting functions. It intelligently uses redundant systems or operating procedures to accommodate the gradual system degradation. It reduces operation cost and increases life by altering the operation and eliminating redundant operations.

2.4.6 Reasoning Techniques

It derives the conclusions from available information. A variety of reasoning techniques are listed in Figure 2.7 for different type of problems. They can be classified as: physics-based, model-based and data-driven techniques. Physics-based approach uses theoretical governing equations and provides accurate solutions for analytical or computational models. Real life problems are too complex and difficult to solve by conventional physics-based approaches and require rigorous data to learn, logics to handle imprecision, knowledge and probability to deal uncertainty. So they are being solved using computational intelligence techniques.

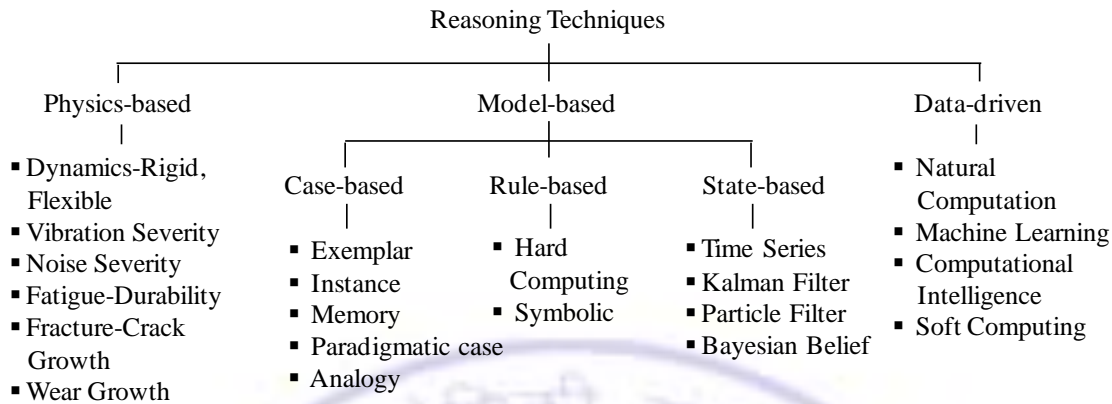


Figure 2.7: Types of Reasoning Techniques

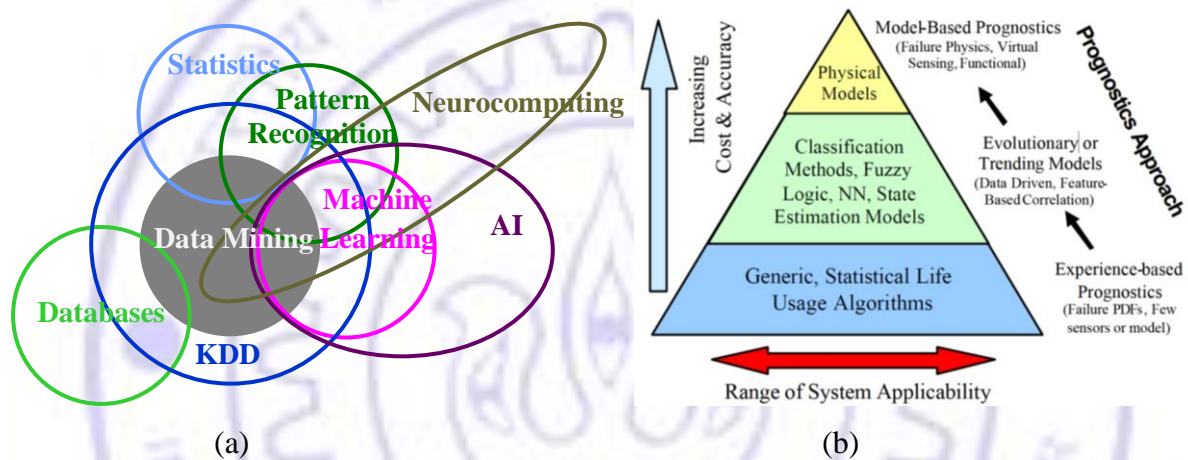


Figure 2.8: Classifiers and Predictors; (a) Types [89] and (b) Hierarchy [90]

Figure 2.8 shows the overview of these techniques for knowledge discovery in databases (KDD), they have certain overlaps. Model-based reasoning has a small application but results are highly accurate. Intelligent reasoning has moderate application and accuracy, while statistical techniques have vast application and have large uncertainty due to noise and repeatability issues in the signals. Hybridization can eliminate their individual deficiency.

2.4.6.1 Physics-based Reasoning (PBR)

It simulates a theoretical model of thermal, fluid, structural and acoustics etc., of a system at any operating conditions using detailed knowledge and enormous experimentally correlated inputs. Accurate vibration, wear, fatigue life, crack growth responses can detect and track the structural defect. Table 2.4 gives the summary of a few PBR techniques. Process simulation is accurate and there exist a variety of models, while structural faults doesn't have direct clue

Table 2.4: Overview of Physics-based Reasoning Techniques

Techniques	Expression	Advantages	Challenges
Analytical	$m \frac{d^2q}{dt^2} + (C + \Omega G) \frac{dq}{dt} + Kq = F \sin \omega t, \text{ BCs and ICs}$ $\frac{da}{dN} = C(\Delta K)^m$	<ul style="list-style-type: none"> •Highly accurate for simple system •Low computation and resources 	<ul style="list-style-type: none"> •Real-life system is highly complex and stochastic •Lot of crude assumptions
Discrete	$[M]\{\dot{q}\} + [C]\{\dot{q}\} + [K]\{q\} = \{F_t\}$ $\frac{q_{i,j}^{n+1} - q_{i,j}^n}{\Delta t}, \frac{q_{i+1,j}^n - 2q_{i,j}^n + q_{i-1,j}^n}{(\Delta t)^2}$	<ul style="list-style-type: none"> •Full control on the code •Improves with use 	<ul style="list-style-type: none"> •Has many variables •High maintenance
Software	-	<ul style="list-style-type: none"> •Accurate geometry •Low maintenance 	<ul style="list-style-type: none"> •Routine loading environments •Restricted source code/method •Computationally expensive

and often difficult to simulate due to complexity. However, few basic faults can be simulated in a highly approximated shaft/beam model with a highly simplified load history.

2.4.6.2 State-based Reasoning (SBR)

It is usually restricted to static knowledge and has a difficulty in simulating the actual behavior. Models with many parameters have large computational time, difficulty in reasoning and expensive to accommodate growing experimental data. State estimators such as Kalman, particle and time series are widely used. Table 2.5 gives their summary.

Kalman Filter: It combines a series of measurements, predictions from system dynamics and measurements for an accurate estimate. It estimates a joint probability distribution over the variables for each timeframe using Bayesian inference.

Particle Filter: It uses Monte Carlo simulations of the sample data from state and measurement updates. Instead of modeling with function, it is modeled with particles i.e. sample around the expected value. Each particle gets updated by an action command to a position with noise and updates the observations.

Time Series Analysis: It fits a parametric model to the time series waveform and extracts the model coefficients, and use the model to predict future values based on previously observed values. These models are difficult to use due to complexity and order estimation.

Table 2.5: Overview of State-based Reasoning Techniques

Techniques	Expression	Advantages	Challenges
Bayesian Belief Networks	<p>$P(H_t H_{t-1}, O_t)$</p>	<ul style="list-style-type: none"> • Easy to predict further states • Handles incomplete data sets • Captures knowledge on individuals than event • Visual link for dependents 	<ul style="list-style-type: none"> • A lot of state transition and fatal data are needed • Depends on the prior knowledge • Difficulty in determining the probabilities
Kalman filter	<p>$P(H_t H_{t-1}, A_t, O_t)$</p>	<ul style="list-style-type: none"> • Minimum error variance • Unbiased, Optimal • Incorporate latest measurement to maintain low error 	<ul style="list-style-type: none"> • Suitable for linear system • Complicated, linear, Gaussian • Requires system and measurement model information
Particle filter	<p>$P(H_t H_{t-1}, A_t, O_t)$</p>	<ul style="list-style-type: none"> • Non-linear and non-Gaussian noise • Works on sampling 	<ul style="list-style-type: none"> • Requires system and measurement model information • Large number of particles consume huge time
Time series	<p>$y = \varphi\theta + \varepsilon$</p>	<ul style="list-style-type: none"> • Handles incomplete information. • Simple and highly effective, uses the seasonal patterns 	<ul style="list-style-type: none"> • Costly because it is based on historical data • Restricted to non-stationary data

2.4.6.3 Case-based Reasoning (CBR)

It works on the principle that similar problems have similar solutions, which can be adopted by cognitive or computational analogy of the past problem types, their solutions and variations. It stores cases and solutions to encounter future problems. It consists of past cases database, their solutions, and a set of rules for measuring similarity and variations. New

problems are solved by retrieving the past and learning can be added to new case or modifying the recalled cases. Solutions are adopted by rules that capture domain theory about the impact of attribute values. Learned features of new case and failed solution are stored as new indices in the database. Table 2.6 gives the summary of CBR techniques.

Table 2.6: Overview of Case-based Reasoning Techniques

Techniques	Expression	Advantages	Challenges
Case-based models		<ul style="list-style-type: none"> • Easy and follows a reference model • System has learning capability. • Intuitive does not require experience 	<ul style="list-style-type: none"> • Takes large space for storage and processing time for actual model • Adaptation issues • Computationally expensive

Table 2.7: Overview of Data-based Reasoning Techniques

Techniques	Expression	Advantages	Challenges
Neural Network	$y = \sum w_i x_i + b$	<ul style="list-style-type: none"> • Handles complex, non-linear noisy, and instable process • Data are in pair of numbers • Adaptive system • Efficient for few inputs 	<ul style="list-style-type: none"> • Black box, difficult to understand the structure • Too many attributes can result in over fitting • Heuristic path with extensive experimentation
Support Vector Machine	$Mar = \min_{x \in D} (xw + b) / (\sum w_i^2)^{0.5}$ <p>Maximize the margin, $\max_{x,b} (Mar), x \in D, (xw + b) \geq 0$</p>	<ul style="list-style-type: none"> • Experiments follow the theory • Efficient for more inputs • Maximized boundary classifier • Easy to control complexity of rule and error 	<ul style="list-style-type: none"> • Difficult to find optimal parameters for non-linearly separable data • Difficult to understand structure of algorithm • No standard method to choose kernel function
Hidden Markov Model		<ul style="list-style-type: none"> • Well established, handles incomplete data sets. • Revel the hidden state change process • Suitable for multi-failure models 	<ul style="list-style-type: none"> • Relies on a failure threshold • Non-practical assumptions • Complex model and large data is required

2.4.6.4 Data-driven Reasoning (DDR)

Table 2.7 lists the tools that interpolates, approximates the complex data and learns new knowledge simultaneously to make predictions. They are fault tolerant and non-parametric, and require no prior knowledge but uses large amount of data. They consist of large number of relatively simple co-processors that are trained to reasoning and adopt new situations.

2.4.6.5 Rule-based Reasoning (RBR)

It searches for if-then-else rule statement patterns in the data. Rule ‘if’ checks the true condition, ‘then and else’ insist taking two different actions for true and false conditions. Rules can be forward or backward-chaining, data-driven or goal-driven. They (listed in Table 2.8) look for a set of rules either start with data/facts and applying rules until a goal is reached or start with goal and apply rules to that goal for a conclusion. Variables uncertainty modeled as probability densities decides their degree of association in execution of the rules.

Table 2.8: Overview of Rule-based Reasoning Techniques

Techniques	Expression	Advantages	Challenges
Rule-based expert systems		<ul style="list-style-type: none"> •Simple and easy to develop •Fast and consistent response •Increased availability and reusability of expertise 	<ul style="list-style-type: none"> •Difficult to acquire domain knowledge •Maintenance of dynamic rule base •Requires precise input
Fuzzy logic	$FI = \int h \cdot \mu$	<ul style="list-style-type: none"> •Deals with imprecision, uncertainty and stochastic rules •Fewer rules required than for expert systems 	<ul style="list-style-type: none"> •Result quality depends on prior knowledge •Solutions are not precise for unclear, directional decisions •Difficult to identify fuzzy measures
Rough Sets		<ul style="list-style-type: none"> •Handles vague, uncertainty and incomplete data sets •No assumptions or prior knowledge 	<ul style="list-style-type: none"> •Does not consider imperfections in the data •Can't handle large, continuous and noisy data

2.4.7 Knowledge Discovery and Data Mining (KDD)

Due to the increased monitoring systems and automation in modern HM system, huge data is being generated, so integrating the collected data with human experience is becoming extremely challenging. It requires a vast number of tools to transform the data automatically and intelligently into useful knowledge. Techniques such as machine learning, statistical and soft computing (listed in Table 2.9) are being used in diagnostic and prognostic models.

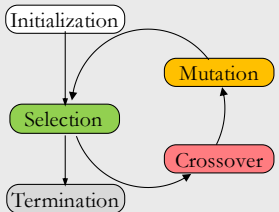
Discriminant Analysis and Classification: It identifies a discriminant function, which distinguishes the various multivariate populations in an optimal way with prediction of class membership. The function can be used to build classification models for various populations.

Cluster Analysis: It identifies a group of heterogeneous possible data, and then forms homogeneous groups in the object either with hierarchical or non-hierarchical clustering.

2.4.8 Data Fusion – Hybrid Methodologies

They integrate the heterogeneous data in a logical manner with condensing large quantities of different information into relevant information for effectively managing the health. Their success depends on the total number of dimensions in the learning domain. Integrated systems approach is being applied by defining data fusion requirements. The computational intelligence has a self-learning capability and accommodates new emerging problems.

Table 2.9: Overview of Knowledge Discovery and Data Mining Techniques

Techniques	Expression	Advantages	Challenges
Discriminant Analysis and Classification	Discriminant score $D = \sum w_i x_i + b$	<ul style="list-style-type: none"> •Classifies different groups on the dependent variable •Visual plots and maps •Suitable for feature selection 	<ul style="list-style-type: none"> •Quadratic discrimination requires more computation and data •Requires sufficient data for sample means
Genetic Algorithm	 <pre> graph TD Init([Initialization]) --> Sel([Selection]) Sel --> Term([Termination]) Term --> Sel Mut([Mutation]) --> Sel Cross([Crossover]) --> Sel </pre>	<ul style="list-style-type: none"> •Suitable for reinforced search/optimization •Can handle large, complex, multimodal spaces, Refines irrelevant and noisy features 	<ul style="list-style-type: none"> •Not most efficient method for some problems •Makes local optima rather than global, Complicated, Uses large time series data

2.5 Research Gaps in Engine Health Management

Table 2.10 shows summary of the literature on HM techniques for an IC engine application. The literatures are studied for identifying scopes and research gaps in each objective/topics and propose models. They are divided into physics-based, data-driven and model-based, depending on capability to deal high fidelity and uncertainty. These models are explored for their selection, diagnosis and prognosis.

Table 2.10: Literature on IC Engine Health Management

Objectives	Physics-based		Data-driven		Model-based	
	Discrete	Computational	Statistical	Intelligent	Qualitative	Imprecise
Model Idealization and Evaluation	Vibration models [56, 92]	Rotor model reduction [91]	Exploring engine events [7]. Fuel on vibrations [94]	-	-	-
	Engine signal models [83]	Efficient MBD models for engines [14-15]	Motion [93] Vibrations [94] Acoustic [52] PCA [95] ICA [10] Orbits [93] FFT [6, 52, 55] WT [8-9,56, 83]			
Diagnosis	Engine performance faults [97-98]	Rotor fault [17, 99-101]	FFT of engine faults [6-7, 52, 55]	NN based engine fault diagnosis [111-113, 119]	Model based process fault diagnosis [47, 114-115]	Expert Systems for engine fault diagnosis [21, 103]
Prognosis	-	Engine power-train faults [6-10, 102]	WT of engine faults [8-9]	-	Engine wear rate based on oil loss[65]	-
		Wear rate in joints[104-105], cam follower wear [106-107]	Prediction of time to change engine oil [62]			

2.5.1 Physics-based Models

These models predict the response by solving governing equations analytically, numerically or using empirical expressions to mimic the measured response directly. They are accurate, takes less time and few inputs, but their reliability depends on the amount of correlation with test results. Till-date, they are widely used in prediction of process faults and less employed for structural faults. They predict gross response of the system with larger approximation and inefficient to capture the effect of local minute geometrical defects. They are accurate but do not account uncertainty; while actual faults and failures requires consideration of uncertainty, hence they have a limited application.

2.5.1.1 Lumped Mass Approach

In this approach, the physical system is approximated into a series of spring, mass, damper elements or a set of empirical expressions. They highly simplify the structure and predict the gross response. Currently they are being investigated for additional complexity in dynamics. In rotating machine problems, the invariants of Jeff cot rotors are widely used, while in IC engines, solutions from structural dynamics are being used. [Ma and Perkins \[15\]](#) developed a multibody dynamics code for an IC engine and correlated the results with commercial multibody MSC/ADAMS tool. [Zou et al. \[83\]](#) generated the signal directly using discrete expressions to mimic the measured response; known parameters of the signal are used to calibrate the signal transform.

2.5.1.2 Multibody Dynamics Approach

Literature indicates that MBD models are being used to condense model effectively by including flexible effects. [Novotny and Pistek \[14\]](#) studied engine powertrain for vibration, noise and fatigue solution synchronously. They incorporated the inputs from analytical and FE models for multibody simulation. Such models are ideally suitable for development process, use of such models need to be explored to study small geometrical defects.

[Wagner et al. \[88\]](#) surveyed various model reduction options for rotor dynamic systems. Model reduction of crankshaft is carried out by [Ricci \[16\]](#) and [Ricci et al. \[92\]](#). They replaced the rigid crankshaft by flexible for optimal model size. [Rivola et al. \[102\]](#) studied design

optimization and diagnostics of valvetrain using elastodynamic simulation. [Mukras et al. \[104\]](#) and [Flores \[105\]](#) predicted the wear rate in a revolute joint by multibody simulation. Wear in cam follower was carried out [Nayak et al. \[106\]](#) and [Hugnell et al. \[107\]](#). [Macian et al. \[65\]](#) investigated engine wear rate based on oil loss computation. Increased geometrical, flexibility and dynamics details have a potential to respond for small geometrical defects.

2.5.2 Data-driven Models

These models are widely used for engine fault diagnosis. [Ajovalasit and Giacomini \[94\]](#) studied engine idling and steering wheel vibrations to identify engine fuel composition. [Lee and Han \[93\]](#), [DeBotton et al. \[6\]](#), [Kim and Lee \[52\]](#) and [Gao et al. \[96\]](#) respectively indicated that the engine vibrations, shaft orbit and sound pressure are good indicators of engine health, while [Liu et al. \[7\]](#) showed that partial sampling and averaging of most affected events measured at their nearest location indicate significant information. [DeBotton et al. \[6\]](#) and [Ben-Ari et al. \[55\]](#) showed that locations on engines affect the vibrations and should be measured at certain sensitive locations.

2.5.2.1 Statistical Approach

[DeBotton et al. \[6\]](#) presented the FFT symptoms of several externally introduced faults such as defective spark plug, loose engine mount, early and late timing in an engine. [Wu and Chen \[8\]](#) generated symptoms for externally introduced looseness, misfiring, and resonance faults. [Liu et al. \[7\]](#) extracted symptoms of valve clearance and leakages. [Zheng and Leung \[9\]](#) reported symptoms of injector faults. [Kim and Lee \[52\]](#) presented symptoms of engine liner wear. [Jun et al. \[62\]](#) predicted the time to change engine oil. They concluded that statistical amplitudes at stationary condition have some capability in engine fault diagnosis.

[Staszewski \[108\]](#) and [Slavič et al. \[109\]](#) proposed wavelet-based ridge for better accuracy in parameter estimation and to quantify fault effectively. [Wu and Chen \[8\]](#) applied CWT to distinguish externally introduced faults. [Zheng and Leung \[9\]](#) explored time-frequency contours of an injector fault. PCA was studied by [Chandroth et al. \[95\]](#) for diesel engine. [Lee and Kim \[56\]](#) developed an ICA based acoustic enhancer for diagnosis. [Albarbar et al. \[10\]](#) and [Albarbar \[53\]](#) employed PCA and ICA algorithm for engine fault diagnosis.

Statistical methods have shown great potential in diagnosing the engine faults; however the recent developments in signal analysis can increase the diagnosis capabilities. Combining different statistical models have shown better results.

2.5.2.2 Intelligent Approach

Zhang et al. [4] and Byington et al. [110] predicted time for a failure with the probabilistic networks. Wu and Liu [111-112] employed neural network to classify the engine faults. They used energy distribution from DWT to train the network. Antory et al. [113] proposed non-linear PCA for accurately classifying the engine faults. The review concludes that the neural network is extensively used as a tool for engine fault classification.

2.5.3 Model-based Models

Nyberg et al. [47] modeled the process fault of an automotive engine. Isermann [49] employed model-based fault diagnosis techniques for studying the pressure flow valve actuator and lateral behavior of passenger cars. Lakshminarasimha et al. [97] and Tabakoff et al. [98] and predicted the performance deterioration of aircraft engine compressor and turbine, due to fouling and erosion using thermodynamic simulation.

Markert et al. [17] proposed a model-based structural fault diagnosis of rotor system; they investigated unbalance, rub, misalignment and crack faults with computing the vibrations on a highly simplified beam with approximating harmonic load. Undamaged system matrices and measured vibrations, and damaged system measured vibrations were used to estimate the fault residual forces. Least square method was used to fit between the simulated residual and measured residuals in identifying the type, magnitude and location of the fault. Jalan and Mohanty [99] diagnosed misalignment and unbalance faults under steady-state. Darpe [100] detected the cracks in rotating shafts by vibrational analysis. He investigated an effect of shaft crack opening in beam model. Bachschmid et al. [101] studied shaft misalignment, bow and unbalance. Fuzzy sets (Wu et al. [21], and Celik and Bayir [114]) and rough sets (Tay and Shen [115]) are employed for engine fault diagnosis. They adopted rule based model for fault classification. Model-based approach built on physics uses extremely simple geometry while built on rules uses large data, which need to be explored for real engine faults.

2.5.4 Hybrid Models

Loutas et al. [116] monitored the progressive wear in a gear and concluded that the combined use of online vibration, acoustic and oil debris are more effective in monitoring the fault. Time, frequency and DWT data were fused with PCA and ICA to indicate the fault class and features were classified using ANN. Orsagh et al. [117] proposed an approach to model multi-fault (corrosion, spalling, and crack) progression. A fault is detected based on the degradation state and predefined threshold level. RUL of the component is predicted for each mode. Liu [118] presented a data fusion approach for machinery fault diagnosis. Different features of the signals were fused at both feature and decision levels using fuzzy measure and fuzzy integral data fusion techniques. Wu and Kuo [119] proposed wavelet packet transforms and neural network for reducing the complexity and an effective engine fault classification. The review on hybrid models concludes that combining different models are effective in monitoring the fault and it eliminates the deficiency of the individual model.

Research gaps can be summarized as: Till date research is restricted to investigate mainly externally introduced faults and majority of them are process faults, which can be detected easily and curable in a regular service. Internal faults such as crack and worn defects are chronic, originate over the period and gradually grow into failure. They are crucial and mostly not curable, difficult to identify and emulate. There is a strong need to study internal faults of an engine. Due to non-linear and non-stationary nature in engine signals, it forms a challenging problem for effective signal processing and parameter estimation, and seeks immediate attention. There is a very little research on physics based models for health management. Integrating recent developments such as flexible multi body, rotor dynamics and fatigue can make effective protocol for studying fault diagnosis and prognosis. Investigation of health management techniques on IC engines is more convenient, as they are less expensive, easy to access, has exhaustive loading at less speed that can reveal clear symptoms at early and has several faults in common and easily extendable to aero engine. A very little research has been progressed on prognostics; it identifies possible scope to explore new techniques. A library of engine degradation curves can be useful in handling standard degradation cases, so it needs to be explored. Combined parameters and hybrid models are more effective in CBM, hence a study is required to explore their effectiveness on engines.

2.6 Conclusions

In this chapter, a state-of-the-art review on EHM has been conducted, research gaps are identified, issues in existing techniques are discussed and a methodology is formulated for fault diagnosis and failure prognosis.

A wide verity of IC engine faults, monitoring techniques and their recent trends are assessed. Most commonly occurring faults of IC engines are listed that includes some rotating machinery faults, which are in common to IC engine. The symptoms of rotating machinery faults are discussed. Faults are categorized into process and structural, which can be monitored using various techniques at various stages. Capability and suitability of performance, tribological, structural and non-destructive techniques for HM for an engine are discussed. It concludes that vibration and acoustic are good indicators of engine structural health.

An overview of EHM is given, basic constituents of an EHM are discussed and their terminologies are briefed. They are categorized into diagnosis, prognosis and maintenance management components. They start with knowledge management, where data acquisition, signal processing and feature extraction are compared for efficiency. A framework for EHM system is discussed.

Various models, cases, rules and data based reasoning techniques are reviewed, their features are compared in applications to EHM are discussed for effective handling. It concluded that the hybridizing superior techniques can resolve actual issues of an IC engine effectively.

Technological gaps for health management components are identified and reviewed. It identifies as study of engine internal faults, prognostics, engine signal processing, parameter estimation and integrating recent dynamics advancements, and selection and hybridizing suitable reasoning techniques are immediate gaps to fill.



CHAPTER 3

ENGINE SET-UP, EVALUATION AND ESTIMATION

All identification is for control and ownership.

- Bryant McGill (1969 -)

3.1 Introduction

Chapter 2 reviewed the constituents of an EHM, their current trends and existing gaps. It concluded that the monitoring vibration, noise, oil debris and shaft motion signals together can make a reliable assessment (Loutas et al. [116]). Faults can alter excitation and response characteristics of collisions significantly. Processing of such collision events and orders can provide inherent information about the fault. Estimating few important parameters can help to simplify complex health process by a mathematical model. An engine is a multibody complex structure that operates at varying speed, abrupt and stochastic heat release, and noisy environment. They give rise to non-stationary, non-linear and noisy signals; processing them is a challenge. It requires an efficient set-up; acquisition with optimal resolution and identifying critical events, and processing them for few parameters. They can be used to detect faults and forecast catastrophic failures precisely. Purpose of this chapter is to,

1. Build an engine experimental set-up to study the field emulated faults and failures.
2. Acquire speed, shaft motion vibration, noise signals and identify the cycle events.
3. Evaluate the set-up for entire operating range under varied operating conditions.
4. Formulate an effective signal processing, data reduction and parameter estimation of events/orders on numerically simulated signals and implement on actual signals.
5. Select most sensitive signals and parameters for an effective EHM.

Section 3.2 describes an experimental setup, and the subsequent section evaluates its operating limits and sensitive conditions. Dimensionality reduction using principal and independent component techniques are discussed in Section 3.4. A procedure for parameter estimation from crankshaft orbit, engine vibrations and sound pressure using Wavelet, Hilbert-Huang transforms and Vold-Kalman Filter are discussed in Section 3.5. Later section validates the procedure numerically and implements them for estimating actual engine signal parameters. Last section of this chapter lists the conclusions.

3.2 Experimental Set-up

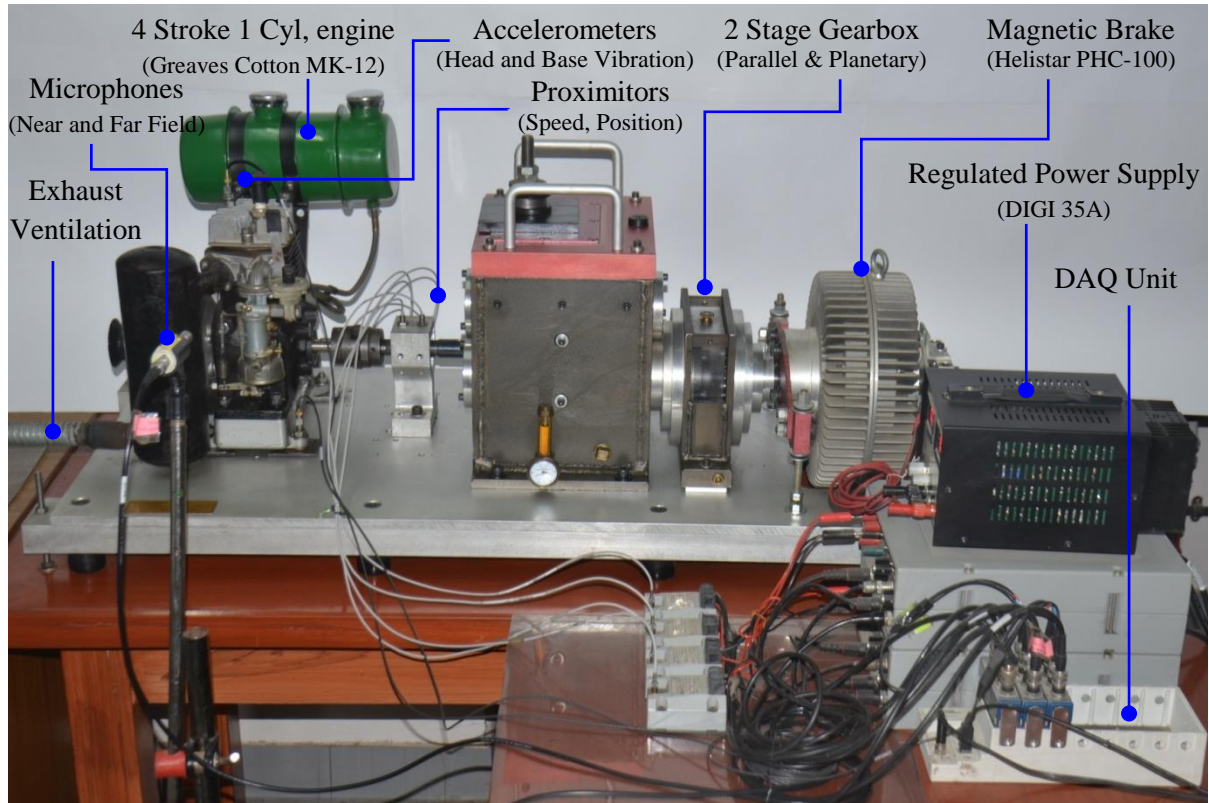
An experimental set-up is built to simulate the emulated field faults and failures conditions of the engine. Faults are deliberately introduced and forcefully propagated into failures. This section discusses the engine test rig, instrumentation, collection of field faults, failure samples, data acquisition, and identification of dominant engine events and orders.

3.2.1 Engine Test Rig

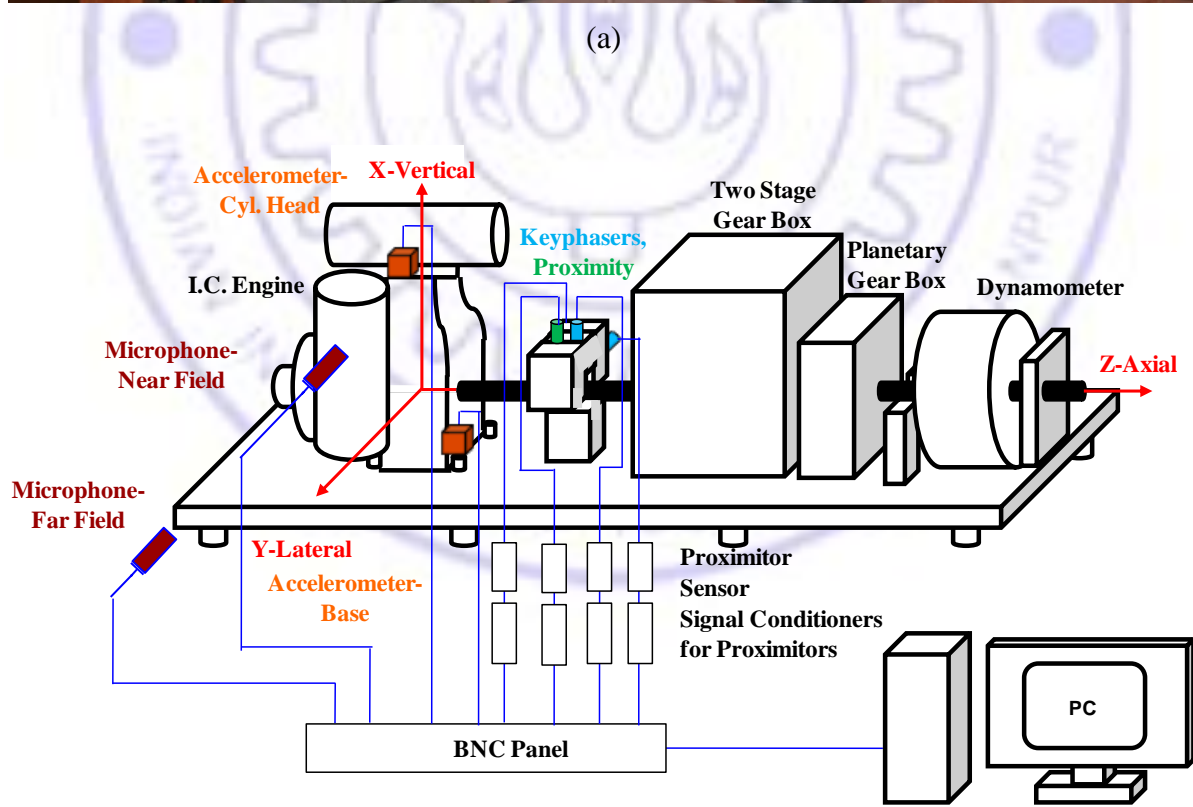
It is built with interfacing engine, dynamometer through a gearbox and mounting the sensors. DAQ card is configured for online monitoring and data logging. Engine is a small, single cylinder, vertical, air cooled, SI that runs on multi fuels by changing main jet of the carburetor. Specifications are listed in Table 3.1. Dynamometer is a magnetic particle clutch (Make: Helistar PHC-100) coupled through 2 stage and planetary gearboxes. It loads engine to its fullest extent by a DC power supply. Figure 3.1 (a-b) shows rig and its schematic diagram with a measurement coordinate system. Engine is operated for steady and transient speeds at loaded conditions. Faults are seeded and propagated to failures in a controlled manner. A ventilation system pumps out exhaust gases and blower is used to cool the engine.

Table 3.1: Specification of the Engine

Make and Model	Greaves Cotton Limited, HSMF MK-12
Type	Four Stroke, Spark Ignited, Single Cylinder, Side valves, Air Cooled, Horizontal Shaft engine
Bore X Stroke, Displacement	55.0 mm X 50.0 mm, 118 cc
Compression Ratio	4.5:1
Ignition Timing	28° bTDC
Exhaust valve open and close (measured)	27° bBDC and 10° aTDC
Inlet valve open and close (measured)	6° bTDC and 24° aBDC



(a)



(b)

Figure 3.1: Experimental Set-up and Instrumentation; (a) Rig, (b) Schematic Diagram

3.2.2 Engine Instrumentation

Accelerometers, microphones, keyphasors and proximity probes are mounted on engine set-up. Figure 3.2 and Table 3.2 gives the details of measurement location and sensor specifications respectively. Accelerometers are mounted on the engine base bolt and nearby surface of cylinder head and liner, and vibrations are measured in ‘g (0-p)’. Microphones are installed to capture sound pressures in ‘Pa (0-p)’. Proximity and keyphasors are mounted on the fixture in vertical and lateral direction as shown in Figure 3.2 (d) to record shaft motion in ‘ μm (0-p)’ and shaft rotations respectively. Top Dead Centre (TDC) position is marked on the crankshaft. Data acquisition is carried out in NI cDAQ-9172 chassis through NI-9215/34 modules by NI LabVIEW. Figure 3.3 shows sensor and instrument connections with chassis.

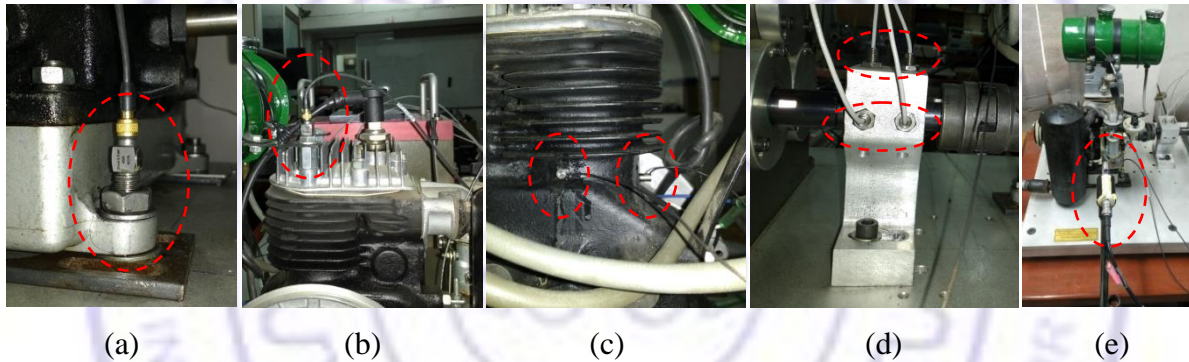


Figure 3.2: Sensor Locations; (a) Base, (b) Cyl. Head, (c) Linear, (d) Shaft, (e) Free Field

Table 3.2: Measurement Specifications

Sl. No.	Measurement	Sensor	Specification	Mounting Location
1	Cylinder head Vibrations	Tri-axial accelerometer	B&K DeltaTron, type 4520	Cylinder head mounting bolt, as in Figure 3.2-a
2	Engine Foundation Vibrations	"	"	Engine mounting bolt, as in Figure 3.2-b
3	Cylinder liner lateral Vibrations	Uni-axial accelerometer	B&K type 4374, Nexus conditioning amplifier type 2693	Linear wall - lateral, as in Figure 3.2-c
4	Cylinder liner long. Vibrations	"	"	Linear wall - longitudinal, as in Figure 3.2-c
5	Near field sound levels	Free field microphone	B&K type 4189, Preamplifier, type 2671	At 0.5 m from spark plug as in Figure 3.2-e
6	Far field sound levels	"	"	At 3.0 m from spark plug as in Figure 3.2-e
7	Horizontal shaft motion	Proximity probe	Bently Nevada Type 3300 XL, Conditioner Type TK15	At horz. locn. on mounting fixture as in Figure 3.2-e
8	Vertical shaft motion	"	"	At vert. locn. on mounting fixture as in Figure 3.2-e
9	Shaft speed	Keyphasor	"	"



Figure 3.3: Engine Instrumentation; (a) Instrument Front Panel, (b) BNC Connections

3.2.3 Engine Faults and Failure Samples

Figure 3.4 shows the samples that are rejected due to crack, bend, worn or eccentricity in service station during services and repairs. Re-usable sample with a single prominent fault are selected and in few cases used to fabricate faults on fresh as faulty sample for emulating field faults conditions much before its actual failure. In next section, set-up is evaluated to select sensitive conditions and estimate few parameters to serve effective HM methodology. In Chapter 5, selected faulty samples are re-introduced at sensitive conditions and features extracted from signals are studied for fault diagnosis and failure prognosis.



Figure 3.4: Samples Failed in the Field

3.2.4 Data Collection

After calibration using common practices, the signals of keyphaser, proximity, vibration and microphone are collected at steady and transient speeds. A steady speed ± 50 rpm is attained by adjusting governor lever position and regulating DC power supply to load through power clutch. In transient manoeuvres, engine is accelerated and decelerated at no-load condition by ramping governor position and cutting off the fuel supply. Data is collected in following sets,

Set No. 1: Steady speed 1000-3000 rpm at 500 rpm increments for cycle information, signals acquired with 10.24k samples/0.2s duration i.e. 1 - 5 cycles.

Set No. 2: Steady speed 1000-3000 rpm at 500 rpm increments for avg. information, signals acquired with 51.2k samples/2s duration i.e. 16 - 50 cycles.

Set No. 3: Transient manoeuvres between low idle and maximum rated speed 1000-3520-1000 rpm for ramp-up and coast-down information, signals acquired with 51.2k samples/5s duration.

Figure 3.5 shows the signals for data Sets No. 1-3 at 1500 rpm, variations of first 2.5 cycles and 25 cycle levels, and transient ramps respectively. Some events are seen in first set while second shows overall levels and third imply the presence of order or resonance information.

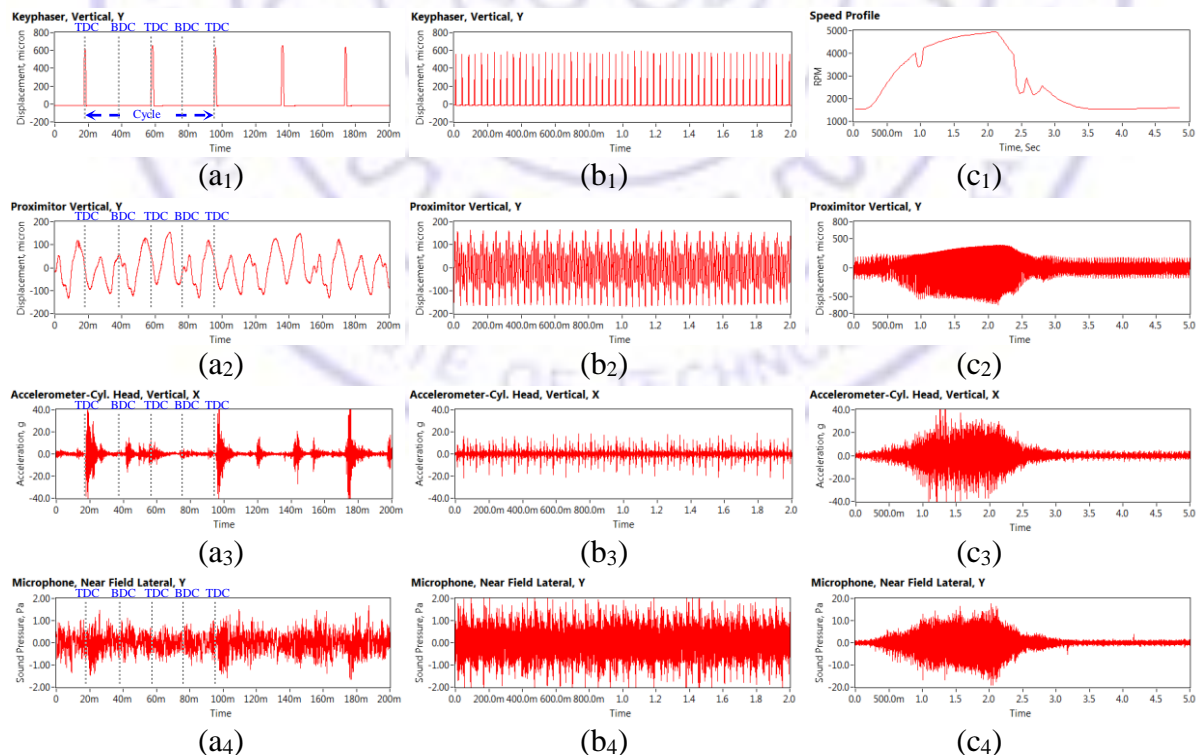


Figure 3.5: Engine Signals; (a.) 1500 rpm, 2.5 cycles, (b.) 1500 rpm, 25 cycles, (c.) Transient

Characteristics of events, levels and orders can be extracted from the above data sets, which can be used to assess engine health. Events are operational impulsive responses due to excitations of ignition, firing, collisions due to valve hitting the seat and piston slapping the liner etc. Such events are visible clearly in vibration cycle of Figure 3.5 (a₃), while in other signals they are less visible. Parameters of these events are inherent to a specific fault or condition, so identifying events and estimating its parameters can quantify fault. Due to cycle-to-cycle variations, overall levels can be estimated by averaging large number of cycles i.e. Set No 2. They can assess the process, evaluate the set-up and select sensitive operating conditions. Transient data contains running orders and resonance, so dominant orders, critical speed and modal parameters can give critical information of the set-up.

Figure 3.5 (c₁) indicates engine recorded a maximum speed of 5000 rpm. Specifications of 3300 XL proximity are inadequate to measure complete range of shaft displacements; at high speeds, asymmetric amplitudes are seen in Figures 3.5 (c₂). Measurable gap range of proximity is 1 mm (i.e. currently installed at 0.4 mm and -0.6mm measurable band location), while shaft is deflecting around 1.2 mm, hence symmetric information of signal is processed.

3.2.5 Engine Event Identification

Engine events in the measured signals can be identified by synchronizing time data to engine crank angle and locating operational information in a full cycle diagram. TDC positions are located by Keyphasor pulses of Figure 3.5 (a₁). Interval of two TDC positions i.e. two rotations of crank gives time period for a full cycle, speed and possible information of strokes i.e. after every TDC pulse, stroke can be either intake or power. In healthy conditions, high amplitude events similar to that are observed in Figure 3.5 (a₃ and a₄) indicates engine firing event, subsequent events can be identified as valve opening-closing and compression. Under defective conditions and depending on fault intensity, amplitudes of events are subjected to change, so they are unreliable for event identification. Additional operation information such as valve lift or cylinder pressure diagram can locate these events; a measured valve lift and pressure-crank diagram is more useful. Simulated valve lift, piston motion and pressure-crank diagrams are used to locate the events. Figure 3.6 shows superimposition of measured engine signals of Figure 3.5 (a₁, a₃ and a₄) filtered for a full cycle with simulated diagrams.

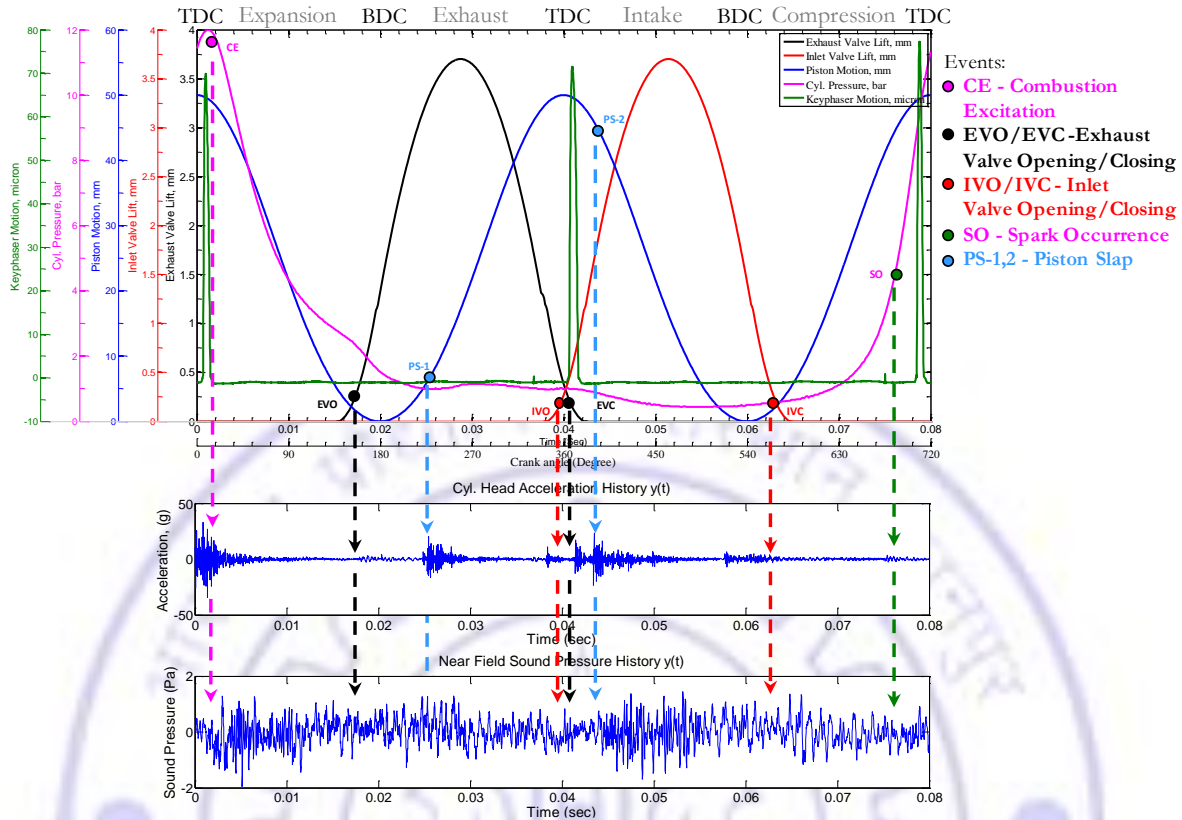


Figure 3.6: Superposition of Simulated Pressure and Valve Lifts with Measured Signals

Keyphaser signal aligned with simulated diagrams confirms respective strokes and events. Information of event duration of Table 3.1 is labeled in Figure 3.6 and signal corresponding to these durations are termed as respective events. Due to combustion and valve hitting (during opening/closing) effects, amplitudes of vibro-acoustic signal event correspond to these crank angles are high. Events are abbreviated (Heywood [120]) as Combustion Excitation (CE), Exhaust Valve Opening (EVO), Piston Slap (PS), Inlet Valve Opening (IVO), Exhaust Valve Closing (EVC), Inlet Valve Closing (IVC) and Occurrence of Spark (SO) i.e. ignition timing event. Rapid rise in pressure occurs due to occurrence of spark that results into combustion excitation, which induces engine vibrations and noise. Piston slap i.e. hitting of piston against side of liner wall can occur anywhere in the engine cycle duration, usually seen around dead centers. Quantification of parameters from these events requires a suitable processing and estimation. In sound pressure signal, firing event is slightly visible, while other events are not visible due to high noise in signal or inappropriate sensor location, so processing and parameter estimation should be good enough to deal such noisy signals.

3.3 Set-up Evaluation

Sensitive conditions exaggerate the system to produce completely different responses and easily distinguishable symptoms are useful in building an efficient health management system. So, the set-up is evaluated for varied operating conditions to assess operating limits, cycle peaks and overall levels. Operating and measurement conditions such as speed, fuel are varied to possible extent as cases. Speed is varied from low idle to rated in stages, fuel is changed based on volatility, and signals acquired from different sensors, mounting locations in principal directions. Cycle and overall levels are superimposed and discussions are made.

3.3.1 Different Type of Measurements

In this section, different types of signals and measurement directions are studied. Figure 3.7 (a-d) shows vertical and lateral keyphasor and proximity signals at 1500 rpm. Vibration and microphone signals in principal directions are shown Figure 3.7 (e-j). Fluctuations in lateral

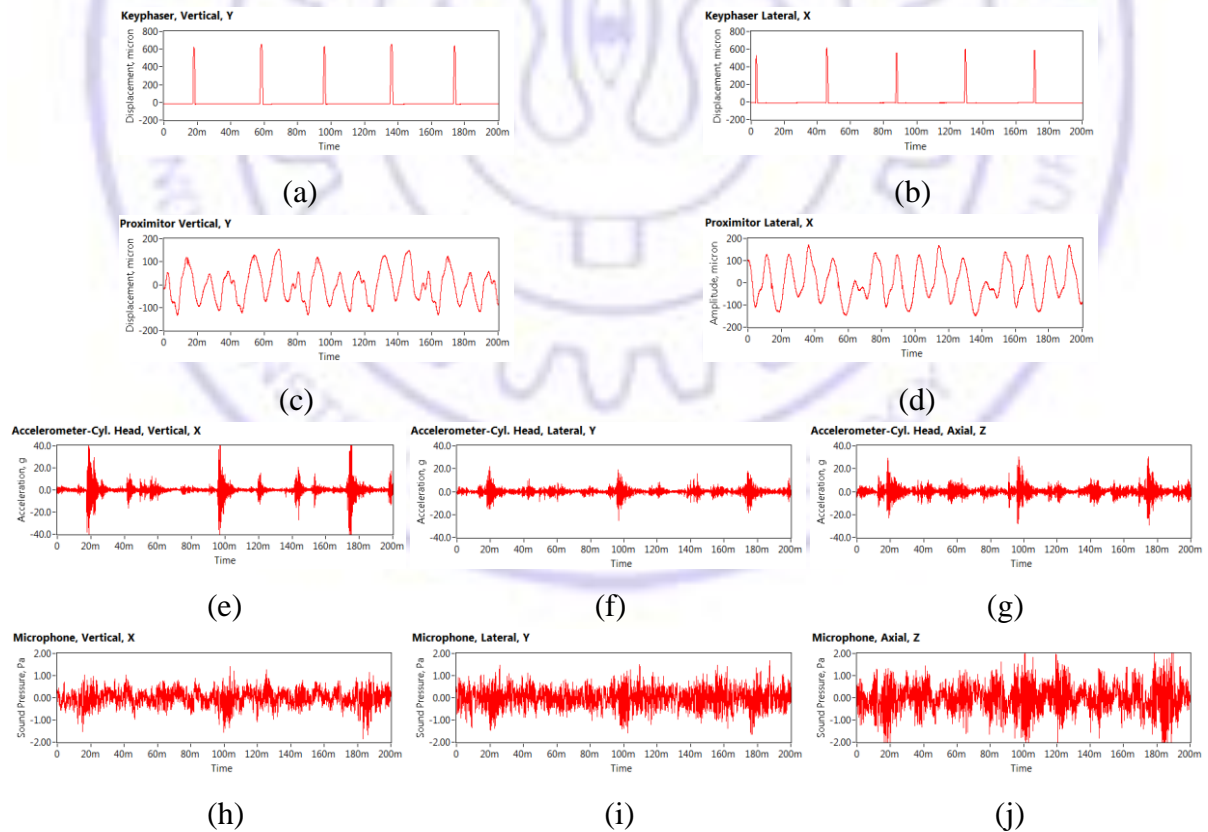


Figure 3.7: Types of Signals in Different Directions; (a, b) Keyphasor, (c, d) Proximity, (e-g) Accelerometer, (h-j) Microphone

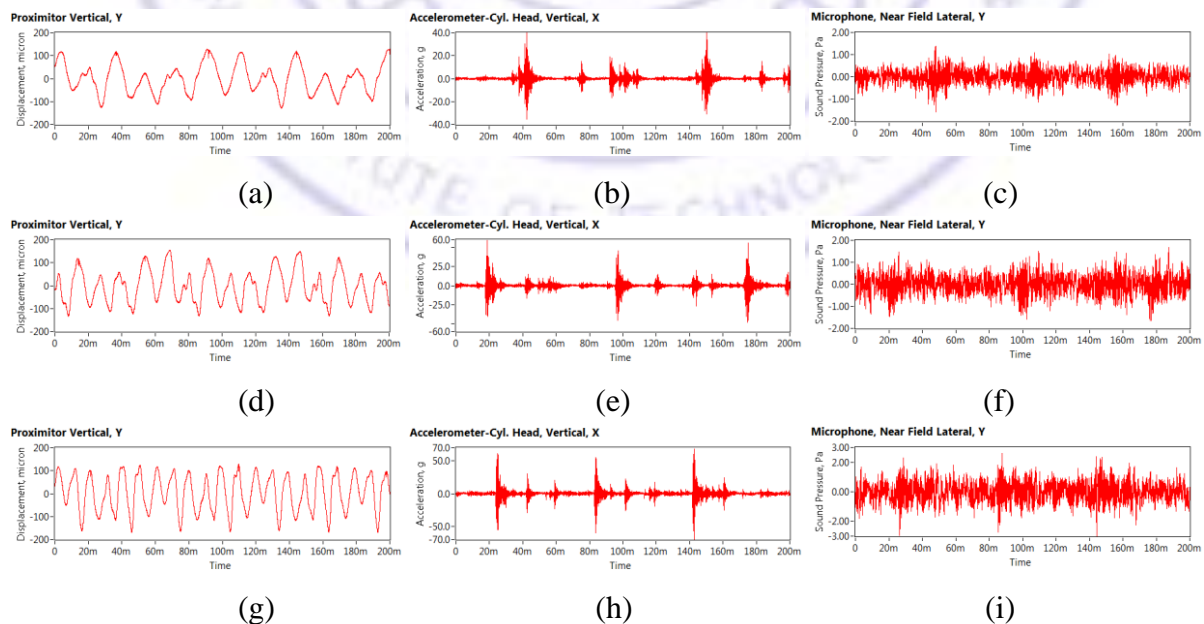
Table 3.3: Overall Levels at 1500 rpm.

Direction	Proximity, $\mu\text{m rms}$	Acceleration, g rms	Sound Pressure, Pa rms
Vertical	71.196	1.676	0.456
Lateral	76.092	1.875	0.449
Axial	-	3.126	0.700

keyphasor amplitude indicates that set-up still has minor horizontal misalignment. Proximity signal shows crankshaft has symmetric behavior. Cylinder head signal indicates that the vibration is more dominant in vertical direction and events are clearly visible. Sound pressure level shows amplitude is dominant in axial, but few events are visible in lateral direction. Table 3.3 lists rms values computed from Set No.2, it shows overall vibrations are dominant in axial direction; however realistic information requires evaluation for entire speed range.

3.3.2 Measurements with Different Speeds

This section evaluates the effect sensor and direction for entire speed range. Figure 3.8 shows vertical proximity and vibration, and lateral microphone signals at steady speed from 1000 to 3000 rpm with speed incremented in 500 rpm interval cases. Overall levels from Set No.2 data are shown in Figure 3.9. Plots indicate that both cycle peak and rms values are growing with speed, except proximity rms values. Proximity rms plot Figure 3.9 (a) shows an inverse correlation in the direction, joint direction is more effective in deciding crankshaft behavior.



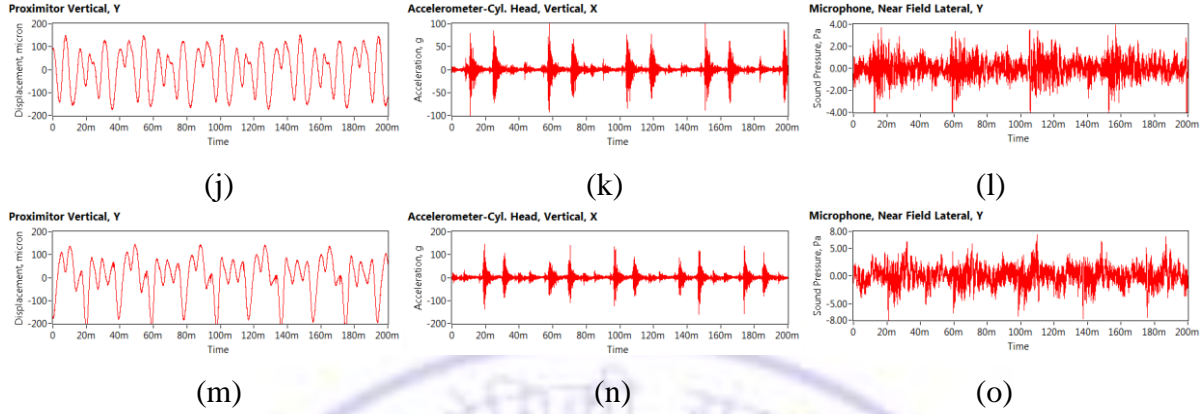


Figure 3.8: Signals for Speed Trials; (a-c) 1000 rpm, (d-f) 1500 rpm, (g-i) 2000 rpm, (j-l) 2500 rpm and (m-o) 3000 rpm

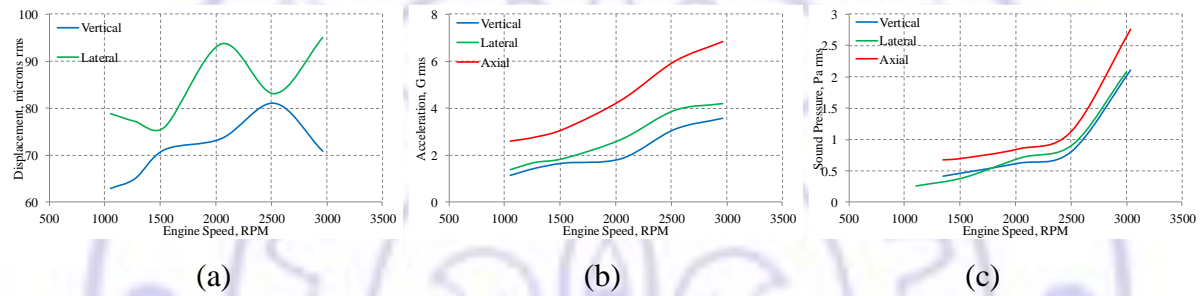


Figure 3.9: Effect of Speed and Direction; (a) Shaft Disp., (b) Vibration, (c) Sound Pr.

Vibration signals have a good correlation with sound pressure; axial direction has high amplitudes. Due to high spread, vibration signals are more effective, while sound pressure has less variation in direction so it is less contributing for health monitoring.

3.3.3 Measurements with Different Fuels

Literature (Tzeng et al. [121]) on engine fuel indicated trend is shifting to find alternative fuels to reduce the dependency but they alter performance, pollution and engine health. This section evaluates suitable fuel from cases as listed in Table 3.4 to study engine health. Figure 3.10 shows the signals that are collected at 1500 rpm. Their overall levels for entire speed

Table 3.4: Properties of the Engine Fuels

	Case No. 1, Petrol	Case No. 2, Kerosene	Case No. 3, Diesel
Flash point in °C	-43	38	52
Auto ignition in °C	250	220	210
Heating value in MJ/kg	45.8	46.20	45.50
Volatility	more	medium	less

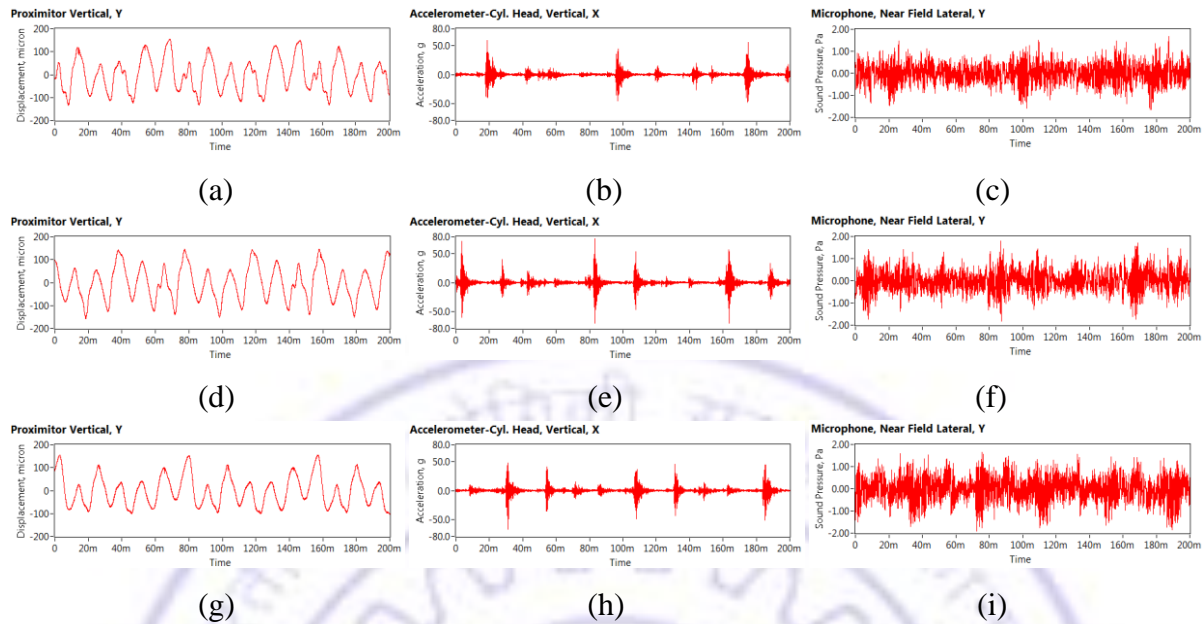


Figure 3.10: Signals for Fuel Trials; (a-c) Petrol, (d-f) Kerosene and (g-i) Diesel

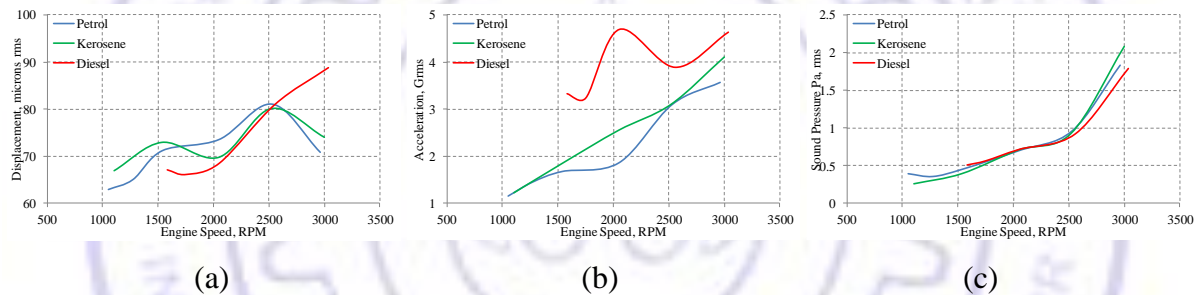


Figure 3.11: Effect of Fuel; (a) Shaft Displacement, (b) Vibration, (c) Sound Pressure

range is shown in Figure 3.11. Results indicate that the high flash point, low auto ignition and less volatile fuels give to high vibration; however they show low noise levels at high speeds. These fuels indicate high versatility in vibrations at 2000 rpm, and less versatility in shaft displacement and sound pressure. Due to higher vibrations at diesel fuel, it can provide more information; however it has high value of low idle speed, start-up issues and has shown improper correlation, so petrol fuel is selected for conducting HM study.

3.3.4 Measurements with Different Locations

Sensor locations as shown in Figure 3.12 are iterated to explore vibrations around the engine surface in its normal direction and sound pressure at different distances in lateral direction. Accelerometer is mounted on the cylinder head, inlet/exhaust, base mounting, cylinder linear,

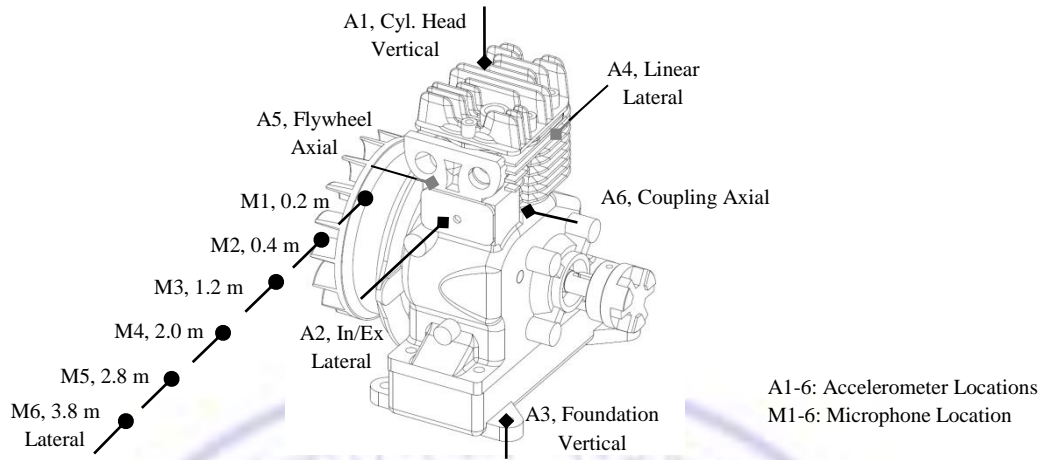


Figure 3.12: Measurement Locations and Directions for Vibration and Sound Signals

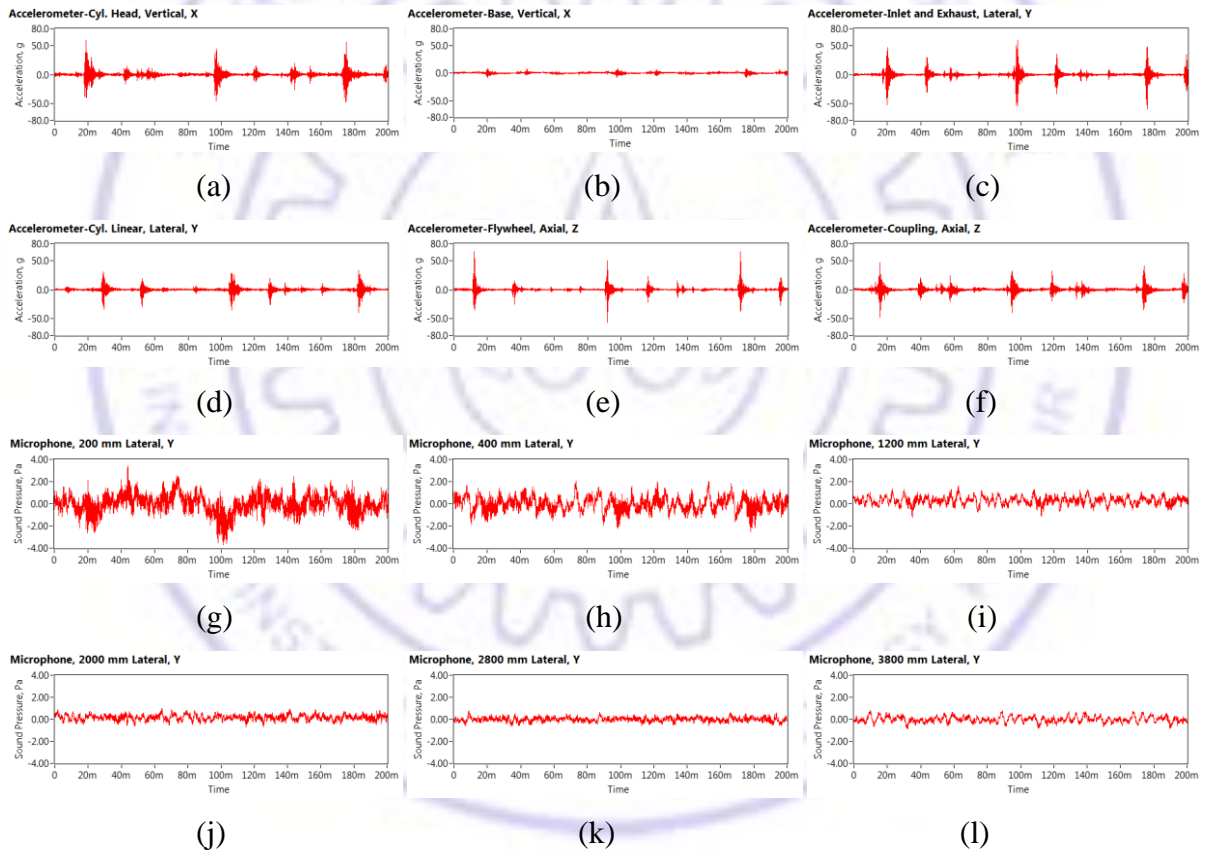


Figure 3.13: Signals for Location Trials; (a) Cyl. Head-Vertical, (b) Block Valves-Lateral, (c) Base-Vertical, (d) Linear-Lateral, (f) Block Flywheel-Axial, (e) Block Coupling-Axial, (g) Mic. 0.2 m, (h) Mic. 0.4 m, (i) Mic. 1.2 m, (j) Mic. 2.0 m, (k) Mic. 2.8 m and (l) Mic. 3.8 m

flywheel and coupling sides on block. Microphone is installed for 0.2, 0.4, 1.2, 2.0, 2.8 and 3.8 m away from the head. Signals are shown in Figure 3.13, Cyl. liner vibration plot shows

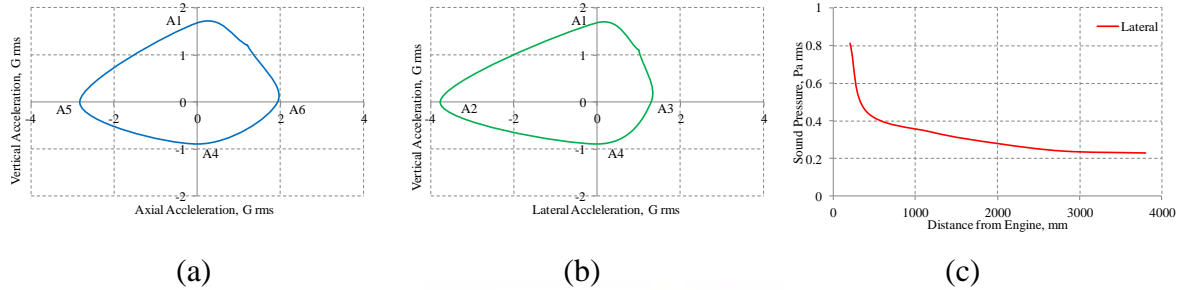


Figure 3.14: Effect of Locations; (a, b) Vibrations, (c) Sound Pressure

some additional piston slap events. Microphone at 0.2 m captured engine firing event, due to its dominance, other events are less visible and 0.4 m location has enough visualization of all the events. For a location of 1.2 m and above, the events are not visible; they are suppressed with overall levels. Polar vibration plots of measurement location is shown in Figure 3.14 (a-b), it indicates vibrations at block lateral and left side are dominant. Sound pressure is less sensitive after 2.5 m distance from the engine. Cylinder head location vibrations and microphone location between 0.4 m and 2.8 m found to be more suitable for HM study.

3.4 Dimensionality Reduction

A few multivariate statistical techniques can identify important and completely different signals, which can reduce the dimensionality of a big database. [Ballabio \[122\]](#) and [Maaten et al. \[123\]](#) reported the comparison of these techniques. They segregated signals that have strong correlation to overall process and statistically independent to each other. Principal component analysis arranges data in the order of high variability that helps to reduce data by selecting first few sensitive variables. Independent component analysis separates statistically independent sources that help to identify important sources and restrict analysis to required sources. They have been evaluated to eliminate less contributing sensors and signals.

3.4.1 Principal Components Analysis

It decomposes the signals with linear combinations of original variables and arranges them in the order of their variance, in orthogonal leading directions, called principal components. It projects data to most informative viewpoint. In doing so, dimensionality of the transformed data is reduced. Eigen-decomposition of covariance matrix of the signals is given as,

$$\Sigma = E \left[(\underline{X} - \underline{\mu})(\underline{X} - \underline{\mu})^T \right] = Q\Lambda Q^{-1} \quad 3.1$$

where $\underline{\mu} = E(x_i)$ is the mean, Λ is the diagonal matrix whose diagonal elements are the corresponding eigenvalues i.e. $\Lambda_{ii} = \lambda_i$, and Q is orthogonal transformation matrix whose i^{th} column is the eigenvector q_i of Σ corresponding to λ_i . The total variance is,

$$\sigma_v = \sum_{i=1}^n \lambda_i \quad 3.2$$

with arranging the λ_i based on their values, eigenvalue of most salient feature i.e. principal values accounting for maximum % of total variance can be retained. The transformed variables corresponding to these principal vectors are also called principal components.

$$\underline{z} = Q_{retained}^T \underline{\mu} \quad 3.3$$

where $Q_{retained}$ is the first few retained principal components. Figure 3.15 shows principal component values and their variance for the measured signals. Data consist of signals from proximity, vibration of cylinder head and engine base, and sound pressure. Results indicate sound pressure and base vibrations have high variance, while proximity and cylinder head vibrations have low variance. Signals with high variance are not suitable for comparative fault diagnosis and engine signals are highly non-stationary so proximity signals demands stationary signals. Hence, cylinder head vibrations can be selected for the study.

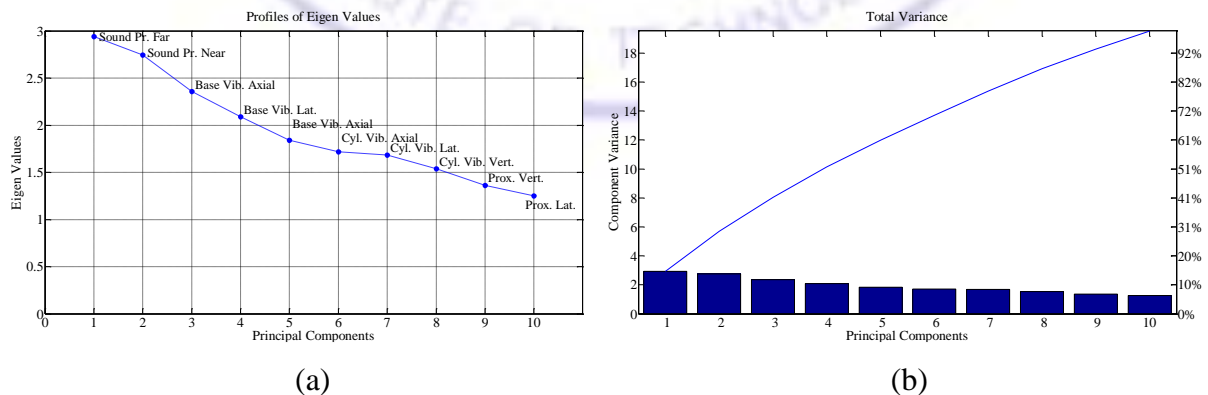


Figure 3.15: Principal Components; (a) Eigen Values, (b) Total Variance

3.4.2 Independent Component Analysis

It decomposes a multivariate signal into independent components by maximizing the statistical independent non-Gaussian source signals. It separates source signals from a mixture or background noise and repeated information from different signals with enhancing weak and corrupted features (Albarbar et al. [10]). Signal x can be represented as,

$$x = Wc + \varepsilon \quad 3.4$$

where $W = [w_1^T \ w_2^T \ \dots \ w_M^T]$ is randomly initialized weighted de-mixing matrix, c is independent source signals and ε is Gaussian noise. Updating the base vectors using,

$$w_j = E[g(w_j^T x)x] - E[g'(w_j^T x)x]w_j \quad 3.5$$

where $g(\cdot)$ is a higher order moment of the signal. Orthogonalize new W till it converges by,

$$W = W(W^T W)^{-\frac{1}{2}} \quad 3.6$$

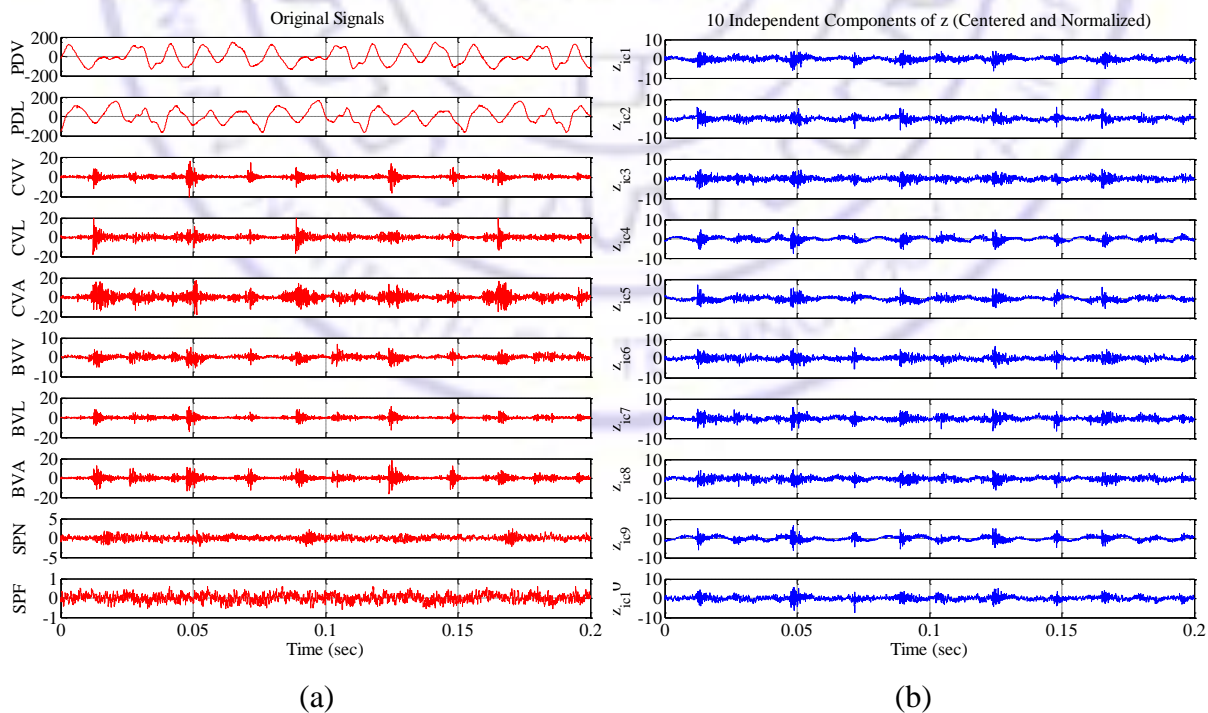


Figure 3.16: ICA of Engine Signals; (a) Original Signals, (b) Independent Components

Figure 3.16 shows original measured signals of data Set No. 2 (abbreviated as SPF to PDV for sound pressure far field to proximity displacement vertical respectively) and their independent sources identified by ICA analysis. Sources of these signals can be combustion impulsive and component collision which makes engine to shake. To reduce the computational time, the signals are analyzed for first 0.2 sec duration. Resemblance with original signals shows that they are inherently originated from vibration sources; probable due to a single vibration source that is being measured at different sensors and locations. Results confirm that cylinder head vibration signals have strong source hence they are more effective to study engine health. PCA ensured the signals with lesser variance, while ICA attempted to find the statistically independent signals.

3.5 Parameter Estimation Procedure

System identification and parameter estimation are useful in building a mathematical model, precise qualitative and quantitative physical assessment, model reduction and troubleshooting of health conditions. They have sought constant attention by several researchers [124-127]. Kerschen et al. [124] presented a review on parameter estimation in structural non-linearity. Estimation can be parametric or non-parametric; parametric searches for a few physical meaningful parameters in a parameter space. While in non-parametric, a function series is modeled by many parameters with no physical meaning and maps the domain variables to output values. Parametric estimation uses techniques such as direct approaches, linearization techniques, filtering and Markov process. In non-parametric estimation, functional series such as Chebyshev polynomials, powers, Volterra, Wiener are widely used. Tiwari and Vyas [125] estimated parameters of imbalanced non-linear rotor-bearing systems from random response. Khan and Vyas [126] used Volterra and Wiener series for estimating non-linear parameters of bearings. Chatterjee and Vyas [127] estimated parameters of non-linear Multi Degree of Freedom (MDOF) systems. Parameters can be estimated by fitting an appropriate model response on actual system response in time, frequency, orbital or time-frequency domain with ensuring minimum error.

Since engine signals are non-linear, non-stationary and have strong noise constituents, so their parameter estimation is crucial and challenging. Fourier and statistical quantification of

engine events is less significant, but time-invariant modal parameters are accurate. Frequency domain methods have difficulty in estimating damping and time domain has issues in estimating natural frequencies. Time and frequency domain methods are suitable for modal extraction of Single Degree of Freedom (1DOF), and can be extended to MDOF systems with permitting certain inaccuracy.

Recent time-frequency transforms unfold the MDOF system response into individual modal or order responses through which parameters of each mode or order can be obtained [108-109, 128-131]. Lee and Han [93] demonstrated parameters such as orbital shape and its inclination angle to indicate the engine events. These transforms can distinguish fault symptoms, but an appropriate extraction of features can quantify their characteristics. Due to structural complexity and high rotational speed of engines, events are closely placed within a cycle and each event has several closely placed modes. Estimation requires a high resolution signal and efficient transform for separating the events, modes and orders. Extracting information from these signals is tedious, so three different approaches are investigated for effective handling of crankshaft displacement, engine vibration and sound signals. In this section, theoretical backgrounds of these transforms are discussed and improvements for quantifying first few dominant parameters of the engine event signals are proposed. Linear parametric terms are identified, separated and estimated along with its associated error. Equation of motion for a linear damped vibration system is given by,

$$m\ddot{x} + c\dot{x} + kx = F \quad 3.7$$

where m , c and k are mass, damping and stiffness of the system respectively, and x , \dot{x} and \ddot{x} are system displacement, velocity and accelerations under applied excitation F . Parameters to quantify fault can be obtained from response of a MDOF system under impulsive excitation,

$$x(t) = \sum_{i=1}^n X_0^i e^{-\zeta_i p_i t} \cos(p_{di} t - \phi_i) \quad 3.8$$

where parameters p_i , and p_{di} are natural and damped natural frequencies, ζ_i is damping ratio, X_0^i is amplitude at initial conditions for i^{th} mode and n is total number of degree considered.

3.5.1 Crankshaft Displacement

A shaft centerline and orbit plot indicates its dynamic position within a bearing clearance. As shaft speeds up to a normal operation, it starts moving from bottom of the bearing clearance to a normal operating location along the shaft centerline path and continues to form an orbit around this center. Shape, orientation and location of this orbit indicate the dynamic characteristics of bearing, shaft alignment, unbalance and preload (Bachschmid et al. [132]). Orbit stability depends on its location, rotational direction and type of bearings. These plots require signals from two orthogonally mounted proximity probes on a fluid film bearing as shown in Figure 3.17 (a). At steady speed, shaft displacements of a complex harmonic signal are, $p(t)$ are $x(t) = \sum A_n \sin(n\omega t + \alpha_n)$ and $y(t) = \sum B_n \sin(n\omega t + \beta_n)$, as shown in Figure 3.17 (b). Polar form of the complex signal $p(t)$ is,

$$p(t) = x(t) + jy(t) = r^f e^{j\omega t} + r^b e^{-j\omega t} = |r^f| e^{j(\omega t + \theta^f)} + |r^b| e^{-j(\omega t - \theta^b)} \quad 3.9$$

where r^f and r^b are the forward and backward harmonic components respectively. Amplitudes of harmonic components for the direct and quadrature parts x_d , x_p , y_d and y_q of signals $x(t)$ and $y(t)$ are, $|r^f| = \frac{1}{2} \sqrt{(x_d + y_q)^2 + (y_d - x_q)^2}$; $|r^b| = \frac{1}{2} \sqrt{(x_d - y_q)^2 + (y_d + x_q)^2}$. Shape and Directivity Index (SDI) is the ratio of minor to major axis, and orientation of the ellipse i.e. angle of major axis with horizontal probe is defined as [132]:

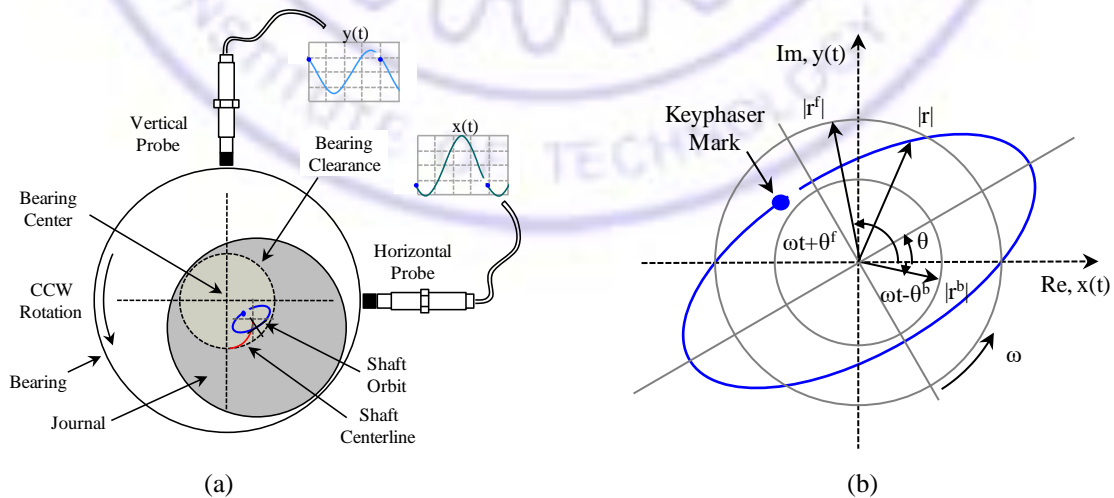


Figure 3.17: Shaft Motion; (a) Orbit and Centerline Plots, (b) Orbit in Complex Plane

$$SDI = \frac{|r^f| - |r^b|}{|r^f| + |r^b|}; \quad \theta = \frac{(\theta^f + \theta^b)}{2} \quad 3.10$$

where $\theta^f = \tan^{-1} y_d - x_q / x_d + y_q$ and $\theta^b = \tan^{-1} y_d + x_q / x_d - y_q$, sign of SDI indicates the direction of whirl with respect to the rotational direction. Normalized amplitude range of SDI indicates the degree of ellipticity i.e. 0 for straight line and 1 for circular orbit. Quantified SDI and ellipse inclination characteristics for entire speed range can distinguish faults.

3.5.2 Engine Vibration and Noise:

Parameters of vibration and sound signals can serve as fault symptoms, which can be estimated using WT, HHT and VKF. Wavelet follows convolution theory but has resolution issues, while Hilbert-Huang decomposes the signal empirically that seeks justification. Vold-Kalman filter is a state-space model that tracks orders and needs their prior knowledge. In this section, a procedure to quantify the engine signal characteristics is established.

[Daubechis \[133\]](#) gave the foundation of wavelet in 1988 and proposed its different classes. [Staszewski \[108\]](#) and [Slavič et al. \[109\]](#) enhanced wavelet for system identification with extracting its wavelet cross-section, impulse recovery, ridge and skeletons. They concluded that the wavelet ridge and skeleton methods give better accuracy. [Kijewski and Kareem \[134\]](#) studied the end effects of wavelet and suggested padding scheme for their improvements. HHT was proposed by [Huang \[78\]](#) in 1996 to decompose the signal into IMFs along with a trend in time domain, which can take care of varying frequencies, and obtains instantaneous information from the data. [Vold and Leuridan in \[129\]](#) introduced an order tracking filter from speed dependent signals based on the concepts of Kalman filter. These methods provide a new approach to estimate the parameters in a non-stationary and non-linear time series.

3.5.2.1 Wavelet based Parameter Estimation

A wavelet is a localized function with zero mean in both time and frequency domain. Wavelet coefficients, i.e. closeness or fitness of a wavelet to the signal can be obtained by translation (τ) and dilation/scaling (s) of the mother wavelet $\psi_{\tau,s}(t)$,

$$WT_x^\psi(\tau, s) = \int_{-\infty}^{\infty} x(t) \psi_{\tau,s}^*(t) dt; \quad s > 0, \tau \in \mathcal{R} \quad 3.11$$

where $\psi_{\tau,s}^*(t) = \frac{1}{s} \psi^*\left(\frac{t-\tau}{s}\right)$ is complex conjugate of base function or mother wavelet, it has to meet zero mean ($\int_{-\infty}^{\infty} \psi^*(t) dt = 0$) and finite energy ($\int_{-\infty}^{\infty} |\psi^*(t)|^2 \cdot dt < \infty$) conditions. There are many wavelets functions, but Morlet is commonly used in analysis of machinery signals. It is composed of a Gaussian window multiplied by a complex exponential carrier. A complex Morlet wavelet and its Fourier transform as discussed in [77, 135] are,

$$\psi(t) = \frac{B_{\omega_0}}{\sqrt{2\pi}} e^{-0.5 t^2} e^{j\omega_0 t}, \quad \hat{\psi}(\omega) = B_{\omega_0} e^{-0.5 (\omega - \omega_0)^2} \quad 3.12$$

where $\omega_0 = 2\pi f_0$ is central frequency, B_{ω_0} is a normalization constant, whose values are $(4\pi \sigma^2)^{1/4}$, $(4\pi)^{1/4}$, $(2\pi)^{-1/2}$, $(2)^{1/2}\pi$, 1, $(N\pi)^{-1/2}$ etc., where N is a parameter which controls the shape of a mother wavelet and σ^2 is variance that measures the spread or width and restricts time-frequency resolution. Fourier frequency is $f = f_s f_0 / s$, where f_s is sampling frequency and s is a scale. WT coefficients are computed in equilogspaced frequency bins in the form $f_k = 2^{(k-k_0)/n_v}$, $k \in \mathbb{Z}$, where n_v is called the number of voices i.e. frequency bins at each dyadic interval of frequency. Inverse Fourier transforms at each frequency f_k gives the full time evolution of the WT for this frequency bin. Wavelet transforms of a sinusoidal asymptotic signal whose amplitude envelope $X(t)$ and phase functions $\phi(t)$ are given as,

$$x(t) = X(t) \cos \phi(t) = \text{Re}[X(t) e^{j\phi(t)}] \quad 3.13$$

$$WT_x^\psi(\tau, f) = \frac{1}{2} \sqrt{f_s f_0 / f} B_{\omega_0} X(t) e^{-\left(\frac{f_s f_0}{f} \phi(t) - \omega_0\right)^2 / 2} e^{j\phi(t)\tau} \quad 3.14$$

In case of MDOF systems, total response is the superposition of all individual modal response i.e. $x(t) = \sum_{i=1}^n x_i(t)$. WT amplitude and the phase for a frequency $f = f_i$ are,

$$|WT_x^\psi(\tau, f_i)| = \frac{1}{2} \sqrt{f_s f_0 / f_i} B_{\omega_0} X(t) e^{-\left(\frac{f_s f_0}{f_i} \phi(t) - \omega_0\right)^2 / 2} \quad 3.15$$

$$\angle[WT_x^\psi(\tau, f_i)] = \phi(t) = \tan^{-1} \left(\frac{\Im[WT_x^\psi(\tau, f_i)]}{\Re[WT_x^\psi(\tau, f_i)]} \right) \quad 3.16$$

where $\Im [WT_x^\psi(\tau, f_i)]$ and $\Re [WT_x^\psi(\tau, f_i)]$ are the imaginary and real part of wavelet transform respectively. For a fixed value of f_i , its associated mode gives the most relevant contribution. The amplitude and phase for a free-decay response are,

$$X(t) = \frac{|WT_x^\psi(\tau, f_i)|}{\sqrt{f_i} e^{-(f_i \phi(t) - \omega_0)^2 / 2}} = X e^{-\xi_i p_i t} \Rightarrow \ln |WT_x^\psi(\tau, f_i)| = -\xi_i p_i t + \ln X_0 \quad 3.17$$

$$\phi(t) = p_{di} t - \phi_0 \Rightarrow \phi'(t) = p_{di} \quad 3.18$$

Modal parameters such as natural frequencies p_i and modal damping ξ_i can be obtained from WT extracted envelopes and instantaneous frequencies. WT coefficient takes maximum value at instantaneous frequency and time. Ridge is a locus in time-frequency plane where WT amplitude reaches its local maxima as defined by [Porwal \[136\]](#), i.e. when the analysis and signal frequencies are equal, which is,

$$\frac{\partial}{\partial f} \left(\frac{|WT_x^\psi(\tau, f)|^2}{f} \right) = 0 \quad 3.19$$

Ridge of WT contains maximum information. By substituting Equation 3.14 in the above equation, the locus function of the ridge $f_r(\tau)$, instantaneous frequency $f(\tau)$ and signal envelope $X(\tau)$ are determined.

$$f(\tau) = f_r(\tau) \cdot f_0 \quad 3.20$$

$$|WT_x^\psi(\tau, f_r(\tau))| = \frac{1}{2} B_{\omega_0} X(\tau) = C(\tau) X(\tau) \quad 3.21$$

Signal envelope $X(\tau)$ and frequency response $X(f)$ are computed with known correction factors $C(\tau)$ and $C(f)$. Value of normalization constant B_{ω_0} is considered as 1. Depending on the signal structure, WT coefficients are ill-defined near borders. Relative tolerance or error value for an affected portion is,

$$\epsilon_b(\tau, f) = (|WT_x^\psi(\tau, f)| - |\overline{WT}_x^\psi(\tau, f)|) / (|WT_x^\psi(\tau, f)|) \quad 3.22$$

where $|WT_x^\psi(\tau, f)|$ and $|\overline{WT}_x^\psi(\tau, f)|$ are theoretical and practical amplitude of a single tone signal. The relative boundary inaccuracies $\epsilon_b(\tau, f)$, gives time limit, i.e. width or edge effect.

$$t_{min}(\epsilon, \omega) \leq -\omega_\psi \tau_{min} / \omega, \quad t_{max}(\epsilon, \omega) \leq \omega_\psi \tau_{max} / \omega \tag{3.23}$$

where $\omega_\psi = \text{argmax}|\hat{\psi}_k(\omega)|$, researchers [137-140] employed different padding schemes for boundary effect, most appropriate is symmetric padding. In this, the edge portion is discarded and extended backward for parameter estimation. Signal is reconstructed from these parameters and compared with the original signal using correlation coefficient,

$$\rho|_{x_e, x_{recWT}} = \frac{E[(x_e - \mu_x)(x_{recWT} - \mu_{x_{recWT}})]}{\sigma_{x_e} \sigma_{x_{recWT}}} \tag{3.24}$$

where x_e and x_{recWT} are the envelopes of original and WT reconstructed signal. Figure 3.18 shows flow chart of the procedure; it uses a signal whose parameters are already known or assumed. Trails on WT resolution parameters gives clear visibility of modes, orders and events in WT amplitude plot. Parameters are estimated from separated ridge, regression of mode envelope or half power bandwidth of order. Error is computed between simulated and estimated parameters; signal reconstructed with reduced model and dependency is checked.

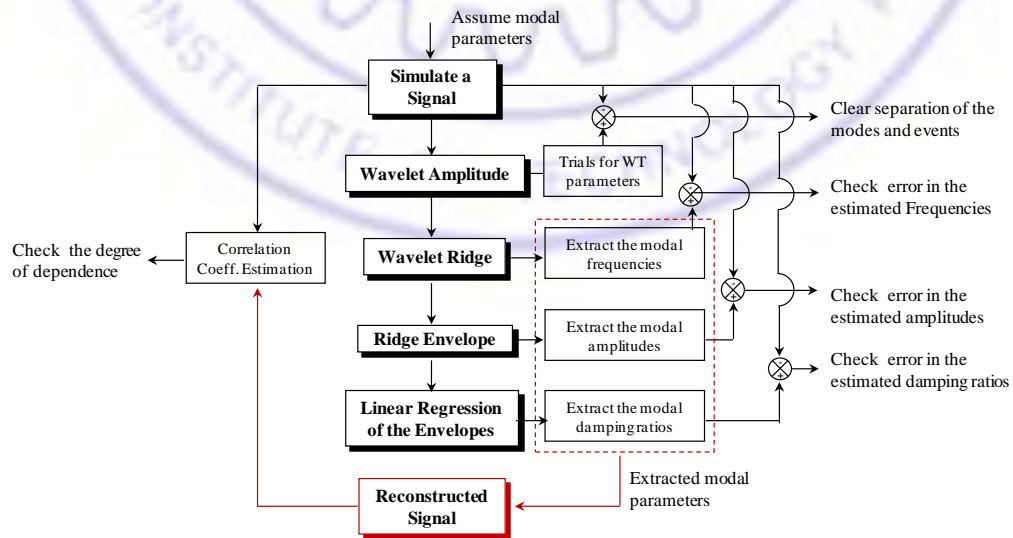


Figure 3.18: Wavelet-based Parameter Estimation Procedure

3.5.2.2 Hilbert-Huang based Parameter Estimation

HHT uses empirical mode decomposition method for decomposing the signal into its IMFs and a residue. It employs Hilbert transform (HT) on each IMF for the time-frequency information [80, 128 and 141]. An IMF is a simple oscillatory mode as a counterpart to the simple harmonic function; collectively all IMFs together can provide complete information of the object. IMF has to meet the following criteria,

1. No. of extrema and zero-crossing must be equal or differ by one from the data set.
2. Local maxima or minima envelope's mean must be zero.

Initially an IMF is iterated by subtracting the mean of upper and lower envelope within itself until it meets the criteria. Data obtained from subtracting IMFs from signal is used to calculate the residue iteratively. For first IMF, original signal $x(t)$ is considered and for the subsequent IMFs, the residue of original signal $x(t)$ and earlier IMFs are subtracted. Hence EMD decomposes the original signal $x(t)$ into total m number of IMFs and a residue, i.e.

$$x(t) = \sum_{i=1}^m c_i(t) + r_m(t) \quad 3.25$$

IMFs are extracted from a high frequency data to a low in the order. First 'n' IMFs has well correlation with the real components $x_i(t)$ and remaining IMFs have low frequency noise components. For noise free analytical signal $x(t)$, the HT of each IMF $x_i(t)$ is $y_i(t)$ and individual mode response $z_i(t)$ are,

$$x(t) = \sum_{i=1}^n x_i(t) \quad 3.26$$

$$y_i(t) = \int_{-\infty}^{\infty} \frac{x_i(\tau)}{\pi(t-\tau)} d\tau \quad 3.27$$

$$z_i(t) = x_i(t) + jy_i(t) = H_i(t)e^{-i\theta_i(t)} \quad 3.28$$

where $H_i(t) = \sqrt{x_i^2(t) + y_i^2(t)}$, $\theta_i(t) = \tan^{-1}(y_i(t)/x_i(t))$ and $\omega_i(t) = d(\theta_i(t))/dt$ are instantaneous amplitude, phase and frequency respectively. Hilbert spectral analysis constitutes time, frequency and amplitude $\{t, f_i(t), H_i(t)\}$ in time-frequency representation. Residue is a monotonic function, so it is not considered in HT. The HT of all IMFs is,

$$x(t) = \text{Re} \sum_{i=1}^n H_i(t) e^{j \omega_i(t)t} \quad 3.29$$

Original signal can be expanded in a Fourier representation with H_i and ω_i that are treated as constants,

$$x(t) = \text{Re} \sum_{i=1}^n H_i e^{j \omega_i t} \quad 3.30$$

An IMF represents a generalized Fourier expansion, improves the H_i and ω_i , and accommodates non-linear and non-stationary effects. Number of IMFs depends on the type of the signal; they affect computational efficiency of Hilbert spectral analysis. Literature [88, 142-143] reports an improved HHT based on IMF amplitude thresholds and mono-components. Amplitude threshold does not work well for non-stationary impulsive signals, whose amplitude continuously changes as it does not contain any frequency or resemblance criteria for the removal of IMFs. In practical cases, mono-component IMFs rarely exist. A Pearson product-moment correlation coefficient based criteria is proposed for the elimination of IMFs, statistical hypothesis with p value equal or less than 0.1 is used to eliminate the irrelevant IMFs which are added to the residue. Most authors prefer $p < 0.05$, i.e. less than 1 in a 20 chance of being wrong.

$$\rho|_{x, x_{i=1 \dots n}} = \frac{E[(x - \mu_x)(x_i - \mu_{x_i})]}{\sigma_x \sigma_{x_i}} \quad \text{for statistical hypothesis } p \text{ value} \leq 0.1 \quad 3.31$$

Similar to WT coefficients, HHT parameters are ill-treated at time borders, due to interpolation error. Literature [139-140] suggests a few methods to overcoming this issue. Similar to WT process, edge portion of an IMF modal response is discarded with the time-width. In Equation 3.22, instead of WT amplitudes, the HHT amplitudes i.e. modal response amplitude H_i of each IMF is used. Signal is reconstructed from the HHT estimated parameters $\{t, f_i(t), H_i(t)\}$, and compared with original signal. HHT correlation coefficient is computed using Equation 3.24 with replacing the x_{recWT} by HHT reconstructed envelope x_{recHHT} .

3.5.2.3 Vold-Kalman Filter based Parameter Estimation

It extracts the orders in time signals of a rotating machine that are in phase consistent with shaft speed. It works on the principle that time signal $y(t)$ is sum of deterministic harmonic and non-correlated signal. Time signal is,

$$y(t) = x(t) + v(t) \quad 3.32$$

where $x(t)$ is correlated to speed and $v(t)$ is non-correlated broadband signal. Deterministic signal is the sum of individual time histories, $x_k(t)$ of each order,

$$x(t) = \sum_1^k x_k(t) = \sum_1^k a_k(t) p_k(t) \quad 3.33$$

VKF uses linear estimation technique in decomposing the correlated signal $x(t)$ into the product of a complex envelope $a_k(t)$ and a complex phasor $p_k(t) = e^{2\pi i k \int_0^t \omega(u) du}$ that is provided by the keyphasor signal. Where $\omega(u)$ is the instantaneous speed of the shaft and $\int_0^t \omega(u) du$ is elapsed instantaneous position of the shaft in revolutions. The discrete form of the complex phasor can be expressed as $p_k(N) = e^{2\pi i k \sum_{m=0}^N \omega(m)\Delta T}$. Instantaneous position can be used to define the state and measurement equations of the Kalman filter. A least square technique is used to smooth the unknown complex envelope $a_k(t)$ and relate the tracked orders to the measured signal. Structural and data equations of VKF of the orders are equivalent to state and measurement prediction of Kalman filter as,

$$\bar{a}_k(t) = M a_k(t-1) + v_{p_k}(t) \Rightarrow \bar{\mathbf{A}}(t) = \mathbf{M} \mathbf{A}(t-1) + \mathbf{V}(t) \quad 3.34$$

$$\bar{y}_k(t) = \sum_1^k \bar{a}_k(t) p_k(t) + v_y(t) \Rightarrow \bar{\mathbf{y}}(t) = \mathbf{B}(t) \bar{\mathbf{A}}(t) + \mathbf{Z}(t) \quad 3.35$$

where $\mathbf{B}(t)$ and \mathbf{M} are known position measurement and state transition matrices respectively. Amplitude envelope can be smoothen by number of poles. Final state i.e. envelope is estimated using,

$$a_{k_{est}} = \bar{a}_k(t) + K (y(t) - \bar{y}_k(t)) \Rightarrow \mathbf{A}(t) = \bar{\mathbf{A}}(t) + K (y(t) - \bar{\mathbf{y}}(t)) \quad 3.36$$

where K is Kalman gain estimated based on variance in the state and measurement noise, $y(t)$ is actual signal, and $\bar{y}(t)$ is measurement predicted signal. It separates the order with known instantaneous frequency, prior information on resonance frequency and damping that can be obtained from STFT analysis (Herlufsen et al. [144]) or roughly assumed values. They influence the selection of filter and bandwidth. Constant or frequency dependent bandwidth separates various components of the signal. A 3dB bandwidth for resonance and minimum filter bandwidth for each order as given in [144] are,

$$\Delta f_{3dB} = 2\zeta f_n \quad 3.37$$

$$B_{3dB} \geq \frac{k SR_{RPM}}{30\Delta f_{3dB}} \quad 3.38$$

where f_n is natural frequency, ζ is damping ratio and SR_{RPM} is the sweep rate in RPM/s , Selection of a filter improves with increasing number of pole count and pass band flat frequency response. Modal parameters can be estimated based on employing a half power bandwidth method on the separated orders. A recent third generation of VKF discussed in Brandt [145] and Wilkens [146] tracks and separates multi orders, crossed orders and multi shaft responses.

3.6 Estimation of Engine Signal Parameters

Procedures discussed in the previous section are validated on numerically simulated signals and then implemented on the signals measured on the actual engine.

3.6.1 Numerical Simulation

This section deals with numerical simulation of signals that resemble typical IC engine shaft motion i.e. displacement, vibration and sound pressure. It estimates their parameters.

3.6.1.1 Estimation of Shaft Orbit Parameters

In orbit based parameter estimation, parameter of signals that resemble typical proximity for horizontal and vertical shaft displacements are simulated. Shaft speed is ramped at constant acceleration rate from 1000 - 4000 rpm for a period of 4 sec.

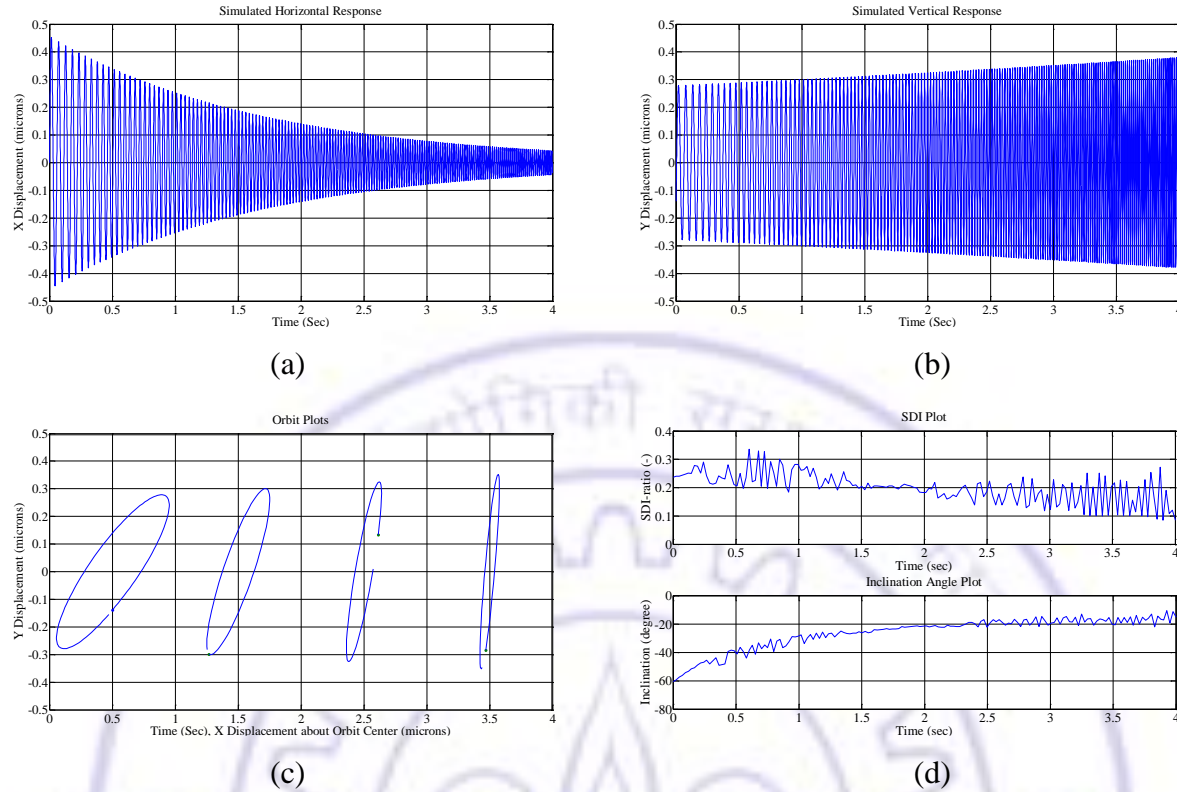


Figure 3.19: Shaft Motion Parameters; (a) Horizontal Displacements, (b) Vertical Displacements, (c) Orbit and (d) SDI and Inclination Plot

The complex harmonic signal $p(t)$ is simulated as,

$$p(t) = 1e^{-0.0075 \cdot (104.72 + 78.54t)} \sin(104.72t + 78.54t^2/2) + j0.25e^{0.001 \cdot (104.72 + 78.54t)} \sin((104.72t + 78.54t^2/2) - 0.524) \quad 3.39$$

A 30° phase delay is added to the vertical signal. Simulated vertical and horizontal signals are shown in Figure 3.19 (a-b). Its orbit plots are constructed as shown in Figure 3.19 (c). Procedure discussed in Section 3.5.1 is used to compute instantaneous 'SDI' and inclination angle ' θ ' as shown in Figure 3.19 (d). Positive sign of SDI indicates whirl is in forward direction, however decrease in its amplitude indicates that orbit is getting flatten with simultaneous increase in inclination angle. The resonance condition i.e. change in direction of the whirl is not observed in this simulated signal, so it is not sufficient to extract modal parameters.

3.6.1.2 Estimation of Engine Event Parameters

In this section, signals that resemble typical engine cycle vibration and sound pressure are generated with the assumed parameters and impact conditions for the first two modes. Transient response of two individual 1DOF is coupled for vibration signal construction. Typical sound signal is generated by adding noise to the above vibration signal. Total response is then unfolded into individual modes using WT and HHT methods. Modal parameters are estimated using linear regression of the individual modes and signal is reconstructed. Relative errors between assumed and estimated parameters are reported.

Case 1: Signal resembling engine cycle vibration

A signal with four events to represent four strokes, two modes in each event is considered, whose modal parameters resemble typical vibration signal of Figure 3.5 (a₃) engine cycle. Mathematical expression for this signal is,

$$x(t) = \sum_{i=1}^4 \sum_{j=1}^2 X_{ij} e^{-\zeta_{ij} \omega_{ij} t} \sin(\omega_{ij} t) \quad t_{i-1} \leq t < t_i \quad 3.40$$

Where i is event number, j is mode number and $t_i - t_{i-1}$ is the event duration, and other notations are as per Equation 3.8. Simulated parameters for this signal are tabulated along with the constructed signal in Figure 3.20. Time and frequency spacing are varied to explore superiority of the WT and HHT for parameter estimation. Simulated signal is sampled at 25 kHz, and Morlet wavelet with a resolution parameter of 10, 323 numbers of voices, 500-3000 Hz, analysis frequency range, 2503 time bins and 361 frequency bins are used. Relative

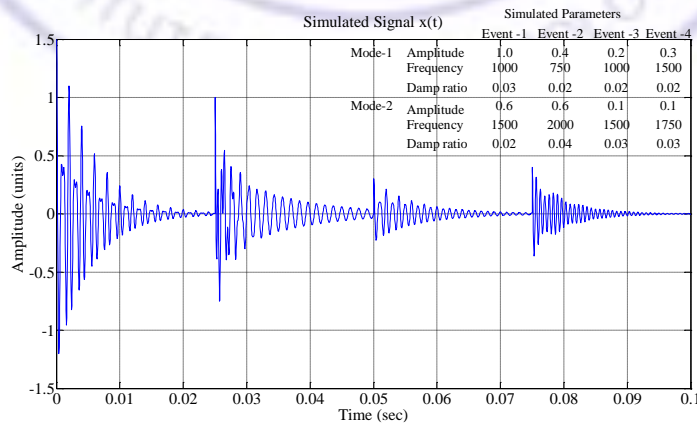


Figure 3.20: Simulated Engine Cycle Vibration Signal

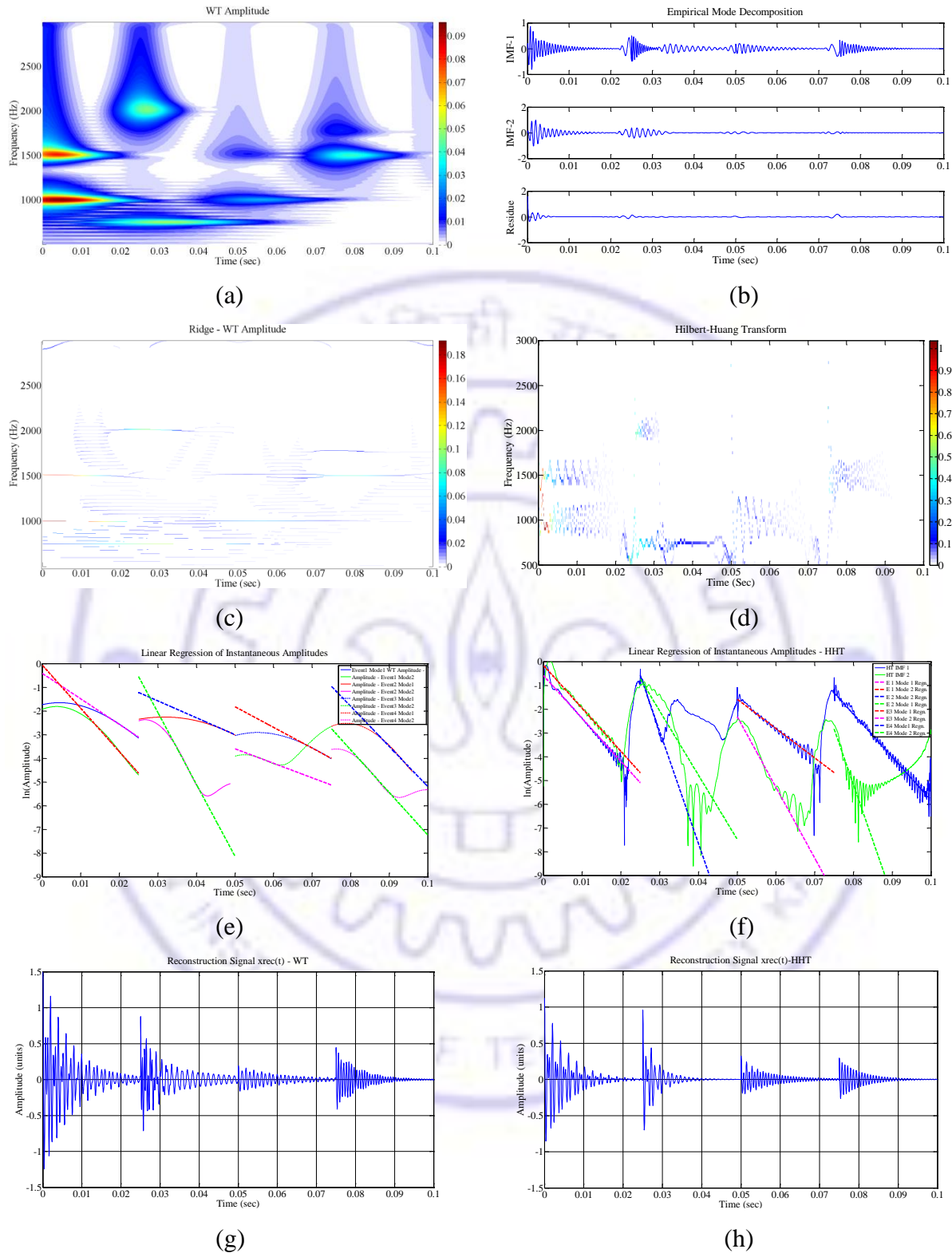


Figure 3.21: Transforms of Simulated Engine Cycle Vibration Signal; (a, b) WT and IMF Amplitudes, (c, d) Ridge -WT and HT, (e, f) Linear Regression – Envelopes and (g, h) Reconstructed Signals

tolerance of 1% is used for eliminating the HHT and WT edge affected length. Transforms of the simulated signal is shown in Figure 3.21 (a-h) and estimated parameters are listed in Table 3.5. Figure 3.21 (a) shows that the wavelet resolution parameters are sufficiently good enough to separate the events and modes. Figure 3.21 (c, d) demonstrate that processing of ridge extracted from WT and IMFs can provide instantaneous frequency, amplitude and damping. Linear regression of envelope of the modal amplitudes is shown in Figure 3.21 (e, f). Figure 3.21 (g, h) shows the reconstructed signals based on WT and HHT estimates. Both methods are capable of separating the modes and estimating parameters. In no-padding, the amplitude estimate has an error up to 75%, however the errors are significantly reduced in linear regression case. First event, second mode has a cutting portion length of 0.0256 sec for 1% relative tolerance value, since length of event is 0.025 sec, so the edge length is reconsidered by increasing relative tolerance value with 10%. Frequencies are well estimated and damping values have some error. Un-improved EMD has 11 IMFs, while in improved

Table 3.5: WT and HHT based System Parameters of Simulated Noise Free Signal

Parameters	WT (% Error)		HHT (% Error)	
	Mode-1	Mode-2	Mode-1	Mode-2
Event No. 1:				
Amplitude	0.66 (-33.60)	0.94 (-57.33)	0.57 (-42.60)	0.55 (-8.17)
Frequency	1001.80 (0.18)	1516.20 (1.08)	978.90 (-2.114)	1466.50 (-2.23)
Damping ratio	0.0171 (-43.00)	0.0192 (-4.00)	0.0300 (0.00)	0.0194 (-3.00)
Time - width	0.0166	0.0115		
Band - width	2.15	3.23		
Event No. 2:				
Amplitude	0.29 (-50.67)	0.58 (44.75)	0.40 (-33.17)	0.56 (39)
Frequency	749.50 (-0.07)	2012.80 (0.64)	934.00 (-53.29)	1361.70 (-1.08)
Damping ratio	0.0151 (-24.50)	0.024 (-94.00)	0.0386 (-3.50)	0.0543 (-6.00)
Time - width	0.0219	0.0080		
Band - width	1.61	4.27		
Event No. 3:				
Amplitude	0.16 (-19.00)	0.03 (-72.63)	0.12 (-40.50)	0.20 (103.00)
Frequency	1005.80 (0.58)	1488.40 (-0.77)	682.43 (-31.75)	1421.20 (81.56)
Damping ratio	0.0138 (-31.00)	0.0065 (-78.33)	0.0799 (299.50)	0.0137 (-54.33)
Time - width	0.0166	0.0115		
Band - width	2.15	3.23		
Event No. 4:				
Amplitude	0.38 (27.11)	0.06 (-36.41)	0.32 (5.33)	0.27 (170.00)
Frequency	1502.30 (0.15)	1778.40 (1.63)	933.37 (-37.77)	1382.00 (-21.03)
Damping ratio	0.0180 (-10.00)	0.0161 (-46.33)	0.0948 (374.00)	0.0208 (-30.67)
Time - width	0.0115	0.0092		
Band - width	3.23	3.75		
<u>Reconstructed Signal</u>				
Corr. Coeff.	0.9694		0.9184	

EMD case, they have reduced to only 2. Correlation coefficient of WT and HHT based reconstructed signals are 0.97 and 0.92 respectively, which indicates that WT has better reconstruction capability. Due to non-linearity in HHT, separation of closely placed modes is difficult and IMF contains the mixed information of nearby modes.

Case 2: Signal resembling engine cycle sound pressure.

A Gaussian noise of signal-to-noise ratio (SNR) 6.02 dB [108-109], i.e. 25% of the amplitude is added to the signal of the previous case. Figure 3.22 resembles engine sound pressure signal as seen in Figure 3.5 (a₄). SNR is computed with the following expression,

$$SNR = 10 \log_{10} \left(\frac{X_{signal}}{X_{noise}} \right) \quad 3.41$$

where X_{signal} and X_{noise} are amplitudes of signal and noise respectively. MATLAB inbuilt function `awgn()` is used to add an additive Gaussian white noise on the previous signal. The

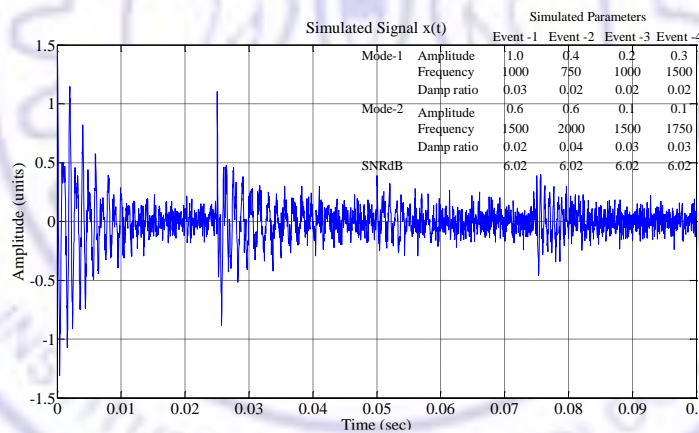
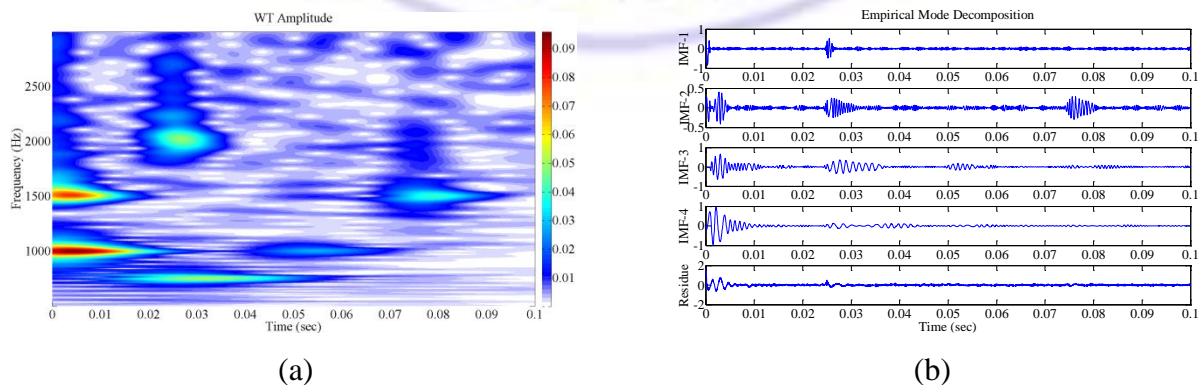


Figure 3.22: Simulated Engine Cycle Sound Pressure Signal



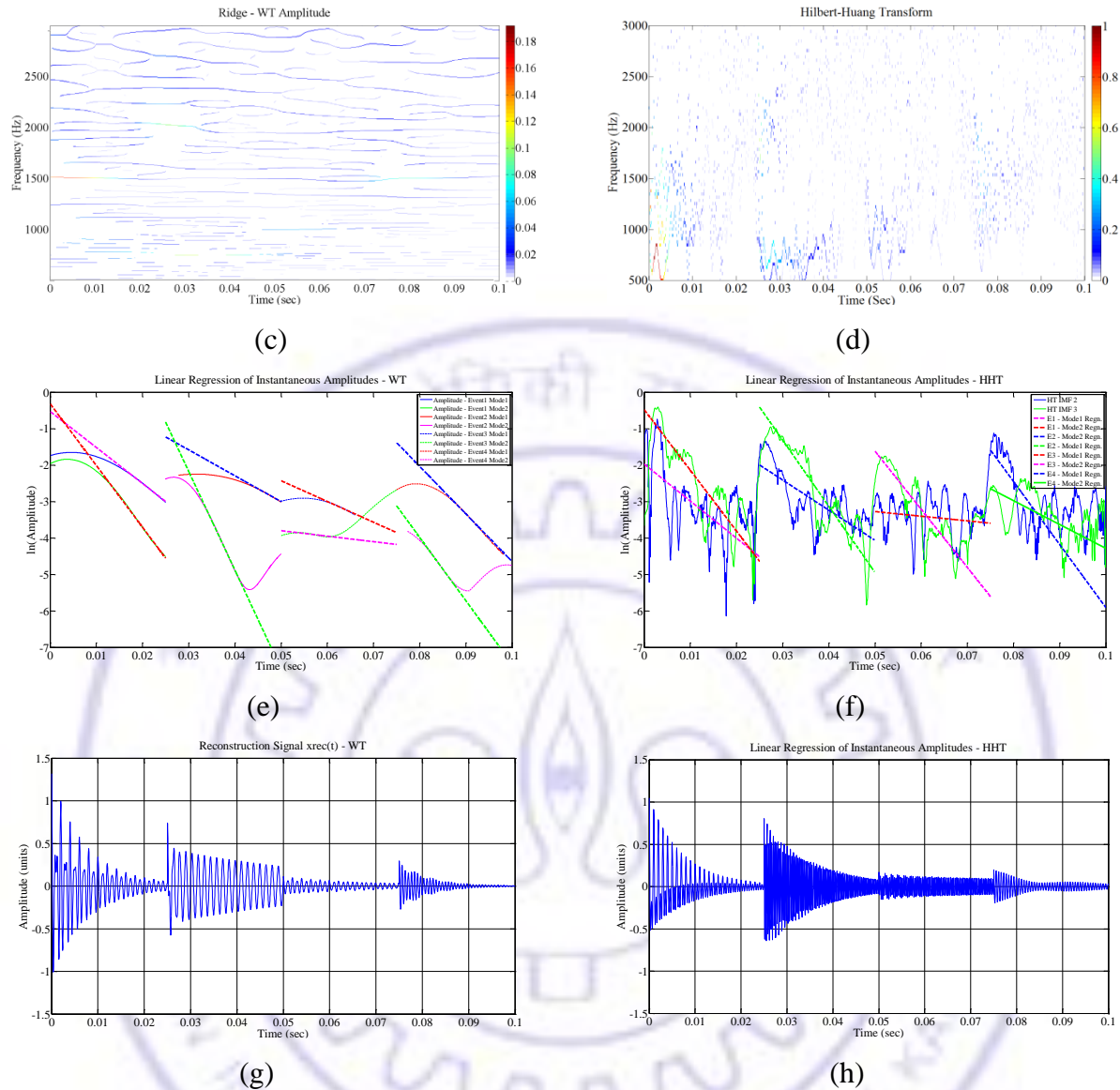


Figure 3.23: Transforms of Simulated Engine Cycle Sound Pressure Signal; (a, b) WT and IMF Amplitudes, (c, d) Ridge -WT and HT, (e, f) Linear Regression – Envelopes and (g, h) Reconstructed Signals

transforms of this signal are shown in Figure 3.23 (a-f). Table 3.6 lists the parameters estimated based on WT and HHT. Despite significant noise, procedure is capable of estimating modal parameters for required accuracy. Un-improved EMD has created 17 IMFs, which have reduced to only 4 IMFs. First IMF have almost constant amplitude and events are appearing in IMF 2 and 3, since noise is a random signal of highest frequency, so first IMF is used to estimate the noise, while IMF 2 and 3 are used to estimate first two modes.

Table 3.6: WT and HHT based System Parameters of Simulated Noisy Signal

Parameters	WT (% Error)		HHT (% Error)	
	Mode-1	Mode-2	Mode-1	Mode-2
Event No. 1:				
Amplitude	0.73 (-27.12)	0.59 (-1.67)	0.62 (-37.80)	0.14 (-76.83)
Frequency	996.80 (-0.32)	1497.50 (-0.17)	998.05 (-0.195)	1997.40 (33.16)
Damping ratio	0.0172 (-42.67)	0.0194 (-3.00)	0.0266 (-11.33)	0.0081 (-59.50)
Time - width	0.0166	0.0112		
Band - width	2.15	3.23		
Event No. 2:				
Amplitude	0.44 (-26.50)	0.29 (-26.50)	0.14 (66)	0.66 (10.83)
Frequency	751.78 (0.24)	2013.14 (0.66)	1388.40 (85.12)	2959.30 (47.96)
Damping ratio	0.0055 (-86.25)	0.0641 (-220.50)	0.0208 (4.00)	0.0045 (-88.75)
Time - width	0.0219	0.0080		
Band - width	1.61	4.27		
Event No. 3:				
Amplitude	0.09 (-56.00)	0.02 (-77.60)	0.04 (-81.10)	0.13 (125.00)
Frequency	1003.30 (0.33)	1518.20 (-1.21)	705.00 (-29.50)	2941.60 (22.98)
Damping ratio	0.0070 (-65.00)	0.0064 (-78.67)	0.0360 (94.50)	0.0007 (-78.67)
Time - width	0.0166	0.0112		
Band - width	2.15	3.23		
Event No. 4:				
Amplitude	0.25 (-17.00)	0.04 (-56.20)	0.13 (-56.67)	0.07 (-32.00)
Frequency	1502.00 (0.13)	1777.50 (1.57)	1802.00 (20.13)	2466.10 (40.92)
Damping ratio	0.0166 (-17.00)	0.0161 (-46.33)	0.0053 (-73.50)	0.0112 (-62.67)
Time - width	0.0112	0.0094		
Band - width	3.23	3.75		
SNR dB	-	-	7.62 (23.00)	
		<u>Reconstructed Signal</u>		
Corr. Coeff.	0.8855		0.6100	

Due to large fluctuation of amplitudes, linear regression is fitted about the mean fluctuation. Correlation coefficients for WT and HHT are 0.89 and 0.61 respectively; this indicates that the reconstructed signal is well correlated to the original signal. Added noise has less effect on WT parameter estimation, while in HHT, it affects considerably. Despite of complex signal with noise, WT is efficient, but unable to estimate the noise constituent, while 1st IMF of the HHT directly helps to predict noise present in the signal.

3.6.1.3 Estimation of Engine Ramp Parameters

To study the identification capability of WT and HHT on non-steady state process, a possible single degree of freedom (1DOF) mathematical expression for run-up and coast-down are simulated in this section. During run-up, the noise and vibration levels increases and decreases during coast down, it is assumed that the engine also passes through the structural resonances.

Case 1: Engine ramp-up signal for inertia loading

Time-invariant model parameters are clearly observable at critical speed. Engines can operate above the critical speeds and get resonate during start and shut-downs. Parameters of accelerated cranktrain system through critical speed are estimated using WT, HHT and VKF transforms. A cranktrain mounted on the bearings is simulated for engine run-up condition. Inertia force is swept through a significant resonance and the simulated parameters are listed in Table 3.7. Run up signal has an increase in the vibration level and at structural resonances as shown in the Figure 3.24. Engine is modeled as 1DOF system with cranktrain as a lumped mass on the bearing whose lowest stiffness and damping are estimated using bearing dynamics approach as listed in [Friswell et al. \[18\]](#). Equation of viscous damped system with inertia loading is given by,

$$m\ddot{x} + c\dot{x} + kx = m_r\omega_r^2 r \sin[\omega_0 t + \alpha t^2/2] \quad 0 \leq t < 10 \quad 3.42$$

where x is response, $m_r\omega_r^2 r$ is crankshaft unbalance amplitude and $\alpha = (\omega_l - \omega_0)/t_l$ is speed ramp rate. In this chapter, the simulation is carried out to generate signals; detailed simulation to study faults is attempted in Chapter 4. System has a critical speed around 6,816 rpm and maximum speed recorded in test is 6,000 rpm, to pass the critical speed, it is simulated up to 10,000 rpm. Solution is numerically integrated by 4th order Runge-Kutta for simulated response. Response transforms are shown in Figure 3.25. Results are listed in Table 3.8, it indicates that transforms are able to separate mode and estimate modal parameters. WT captures theoretical intent; helps to quantify and report accurately. HHT captured actual variation, which is difficult to interpret and requires smoothing techniques so,

Table 3.7: Simulated Parameters for Inertia Ramp-up

Parameters and units	Symbols	Values
Crank radius [m]	r	0.025
Net rotating mass [kg]	m_r	0.0449
Crank shaft mass [kg]	m	3.525
Bearing Damping coefficient [Ns/m]	c	3.378×10^3
Bearing stiffness [N/m]	k	1.796×10^6
Ramp speeds [rpm]	N_0 to N_f	1000 to 10000
Ramp duration [s]	t_0 to t_f	0 to 10

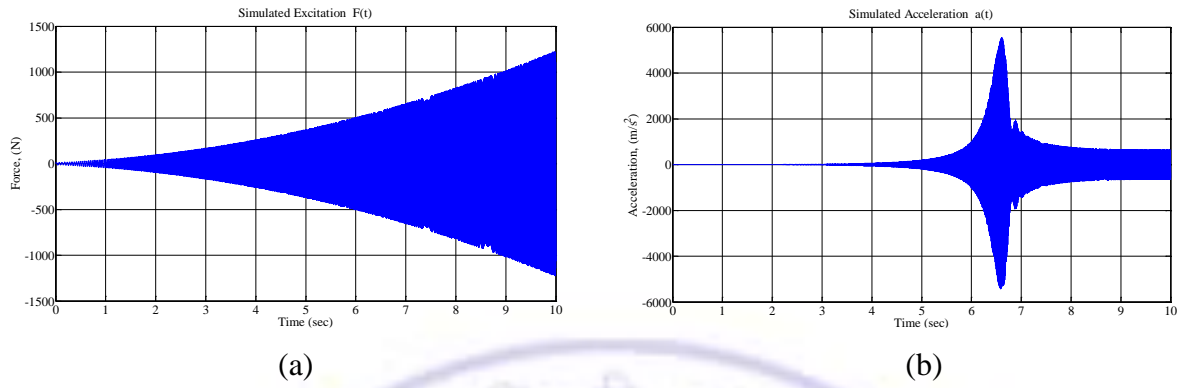
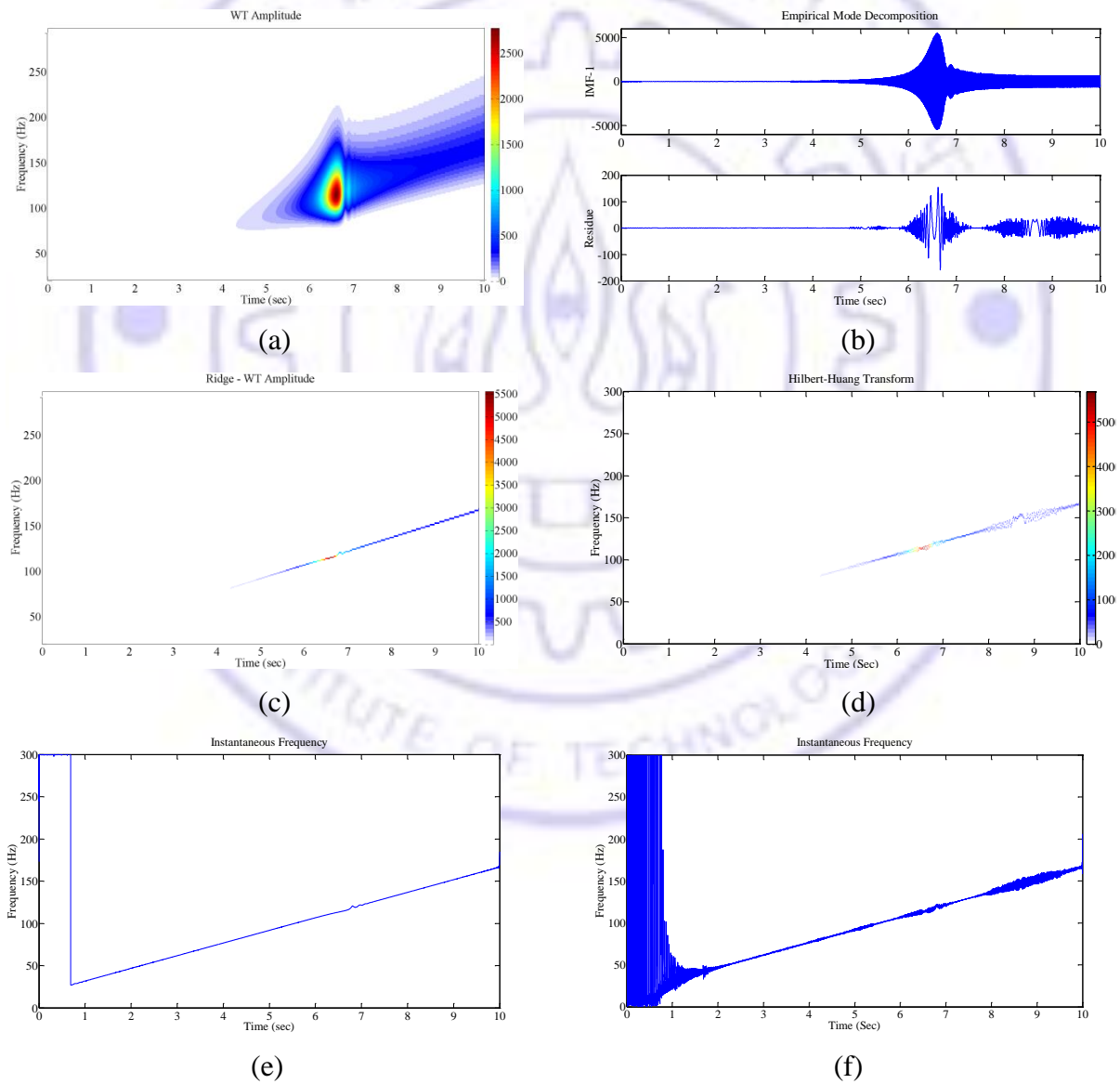


Figure 3.24: Simulated Ramp-up Signal; (a) Excitation, (b) Response



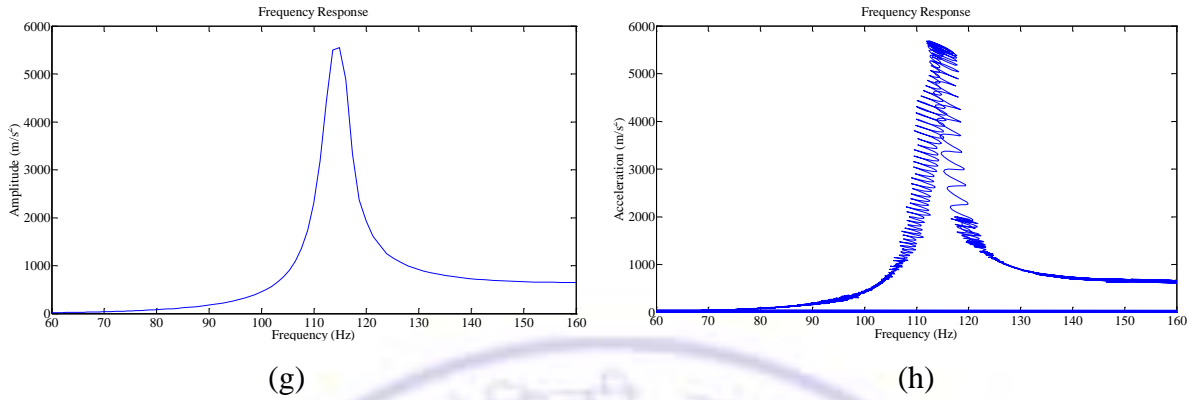


Figure 3.25: Transforms of Simulated Ramp-up Signal; (a, b) WT and IMF Amplitudes, (c, d) Ridge-WT and HHT, (e, f) Inst. Frequency and (g, h) Frequency Response

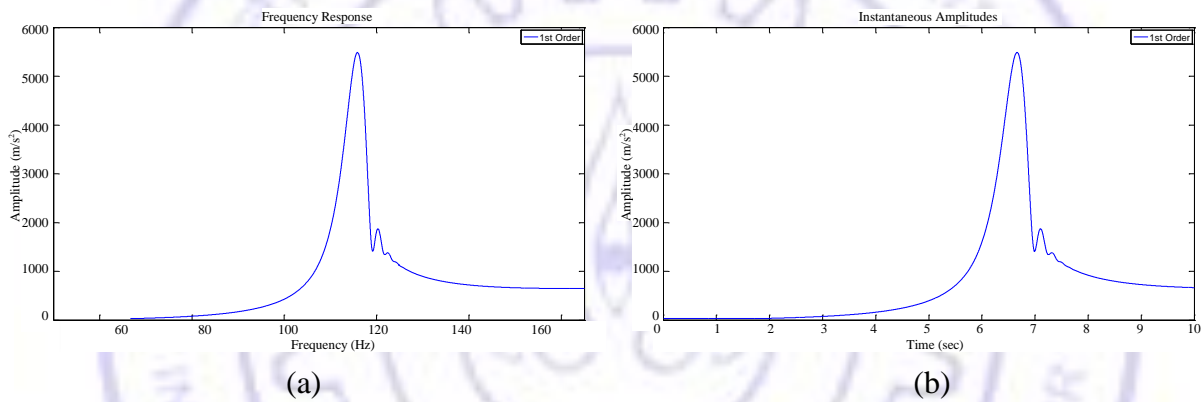


Figure 3.26: Vold-Kalman Filter Order; (a) Frequency Response, (b) Inst. amplitudes

Table 3.8 System Parameters from Inertia Ramp-up Analysis

Parameters	Simulated	WT(% Error)	HHT(% Error)	VKF(% Error)
Resonance Amplitude, m/s^2	5545.70	5548.70 (0.054)	5564.10(0.332)	5490.80 (-0.989)
Natural Frequency, Hz	113.60	114.86 (1.107)	115.11 (1.221)	115.86 (-1.984)
Damping Ratio, -	0.013	0.0218 (62.59)	0.0164 (-24.67)	(39.29)
WT Time - width	-	0.0347	-	-
WT Band - width	-	1.2373	-	-
VKF 3dB bandwidth, Hz	-	-	-	15
VKF No. poles -	-	-	-	2

frequency response parameters are estimated from mean values. Un-improved EMD created 19 IMFs, which have reduced to only 1. Figure 3.26 shows the orders that are extracted using VKF. It indicated that the extraction is accurate; however it used a roughly assumed bandwidth and number of pole information.

Case: 2 Engine ramp-up signal for engine shaking load

In this case, along with crankshaft inertia, the engine slider inertia, gas and friction forces are estimated based on the operating characteristics given in Heywood [120] and Cho et al. [147] and employed. Engine speed is ramped up to 6,000 rpm. Total shaking force excitation at steady speed along horizontal and slider axis is,

$$F = m_r r \omega^2 \sin(\omega_0 t + \alpha t^2 / 2) + m_s r \omega^2 \left[\cos(\omega_0 t + \alpha t^2 / 2) + \frac{r}{l} \cos(2\omega_0 t + \alpha t^2) \right] - pA \left[1 + \frac{1}{3} \sin \left(\frac{1}{2} \omega_0 t + \alpha t^2 / 4 \right) \right] + \mu \frac{\pi D r_w}{h} r \omega \left[\sin(\omega_0 t + \alpha t^2 / 2) + \frac{r}{2l} \sin(2\omega_0 t + \alpha t^2) \right] \quad 3.43$$

where the notations and their values of the equation are given in the Table 3.9. Excitation contains half, first and second order loading. The transforms are being used to separate these orders. Figure 3.27 shows the excitation and its simulated response.

Figure 3.28 shows WT and HHT separated orders. Each IMF contains information of multiple orders. Figure 3.29 (a-b) shows the orders extracted using VKF. Improved EMD has reduced from 23 IMFs to only 3 IMFs. EMD is unable to completely separate the individual orders. Lower order amplitudes of an IMF are being replaced with a higher amplitude portion of lower orders in other higher IMFs. Due to high non-linearity, estimation becomes difficult and non-conclusive, so HHT is less efficient. Table 3.10 shows the extracted parameters from these transforms; transforms are able to estimate the natural frequency,

Table 3.9: Simulated Parameters for Shaking Force Ramp-up

Parameters and units	Symbols	Values
Slider mass [kg]	m_s	0.192
Connecting rod length [m]	l	0.098
Connecting rod damping [Ns/m]	c	20.758
Connecting rod stiffness [N/m ²]	k	86185714.286
Cylinder diameter [m]	D	0.055
Peak Cyl. Pressure [N/m ²]	P_0	1.5×10^6
Ring Width [mm]	r_w	3×10^{-3}
Film thickness [mm]	h	$3 \times 10^{-3}, 5 \times 10^{-6}$
Friction constant [-]	μ	0.2
Ramp rate [rpm/s]	\dot{N}	1200
Ramp duration [s]	t_f	10

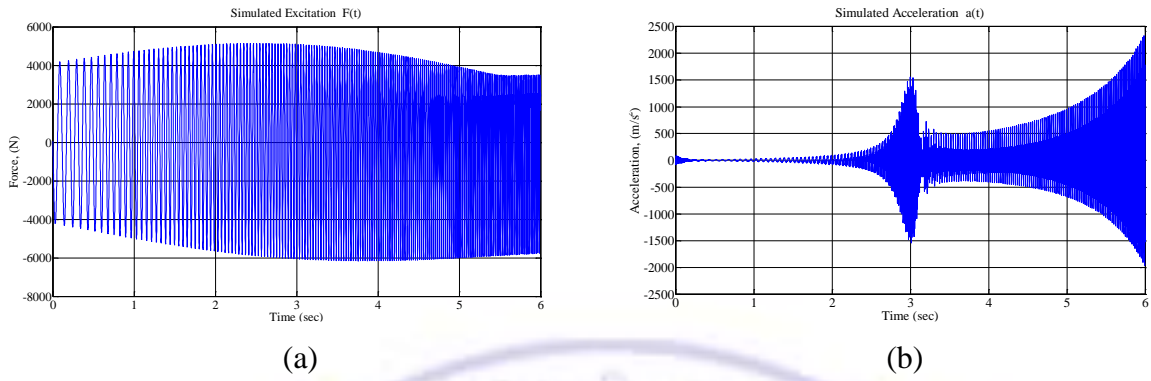
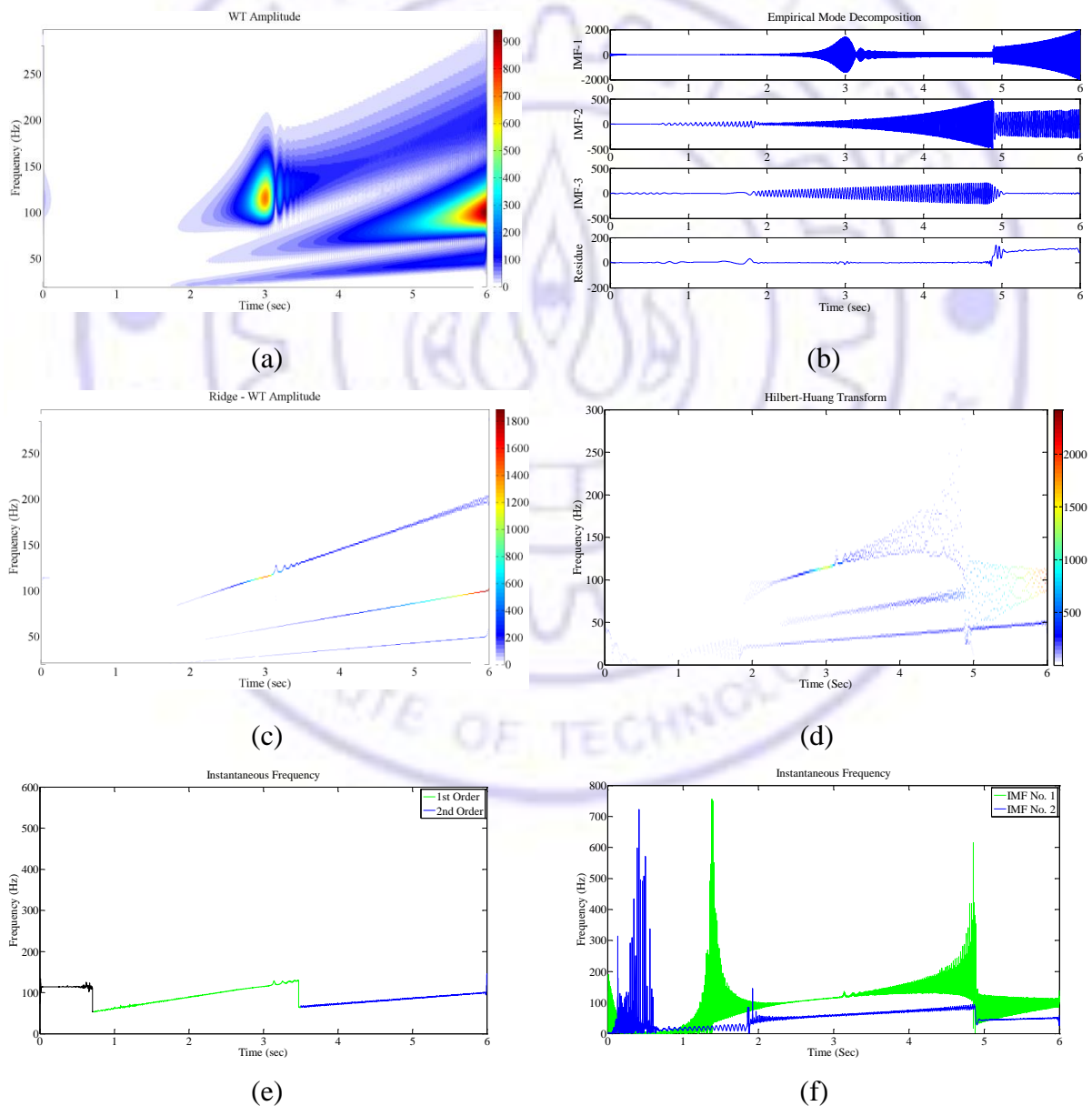


Figure 3.27: Simulated Ramp-up Signal for Engine Shaking; (a) Excitation, (b) Response



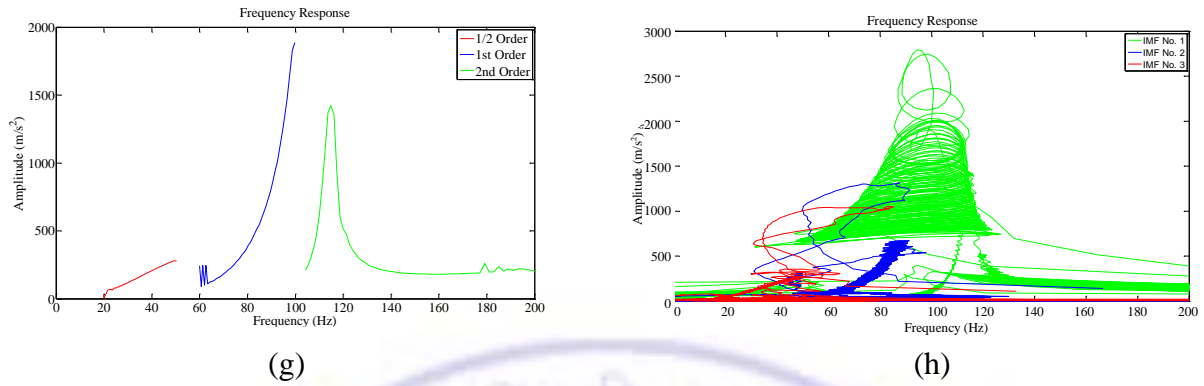


Figure 3.28: Transforms of Engine Ramp-up Signal for Engine Shaking Load; (a, b) WT and IMF Amplitudes, (c, d) Ridges, (e, f) Inst. Frequency and (g, h) Frequency Response

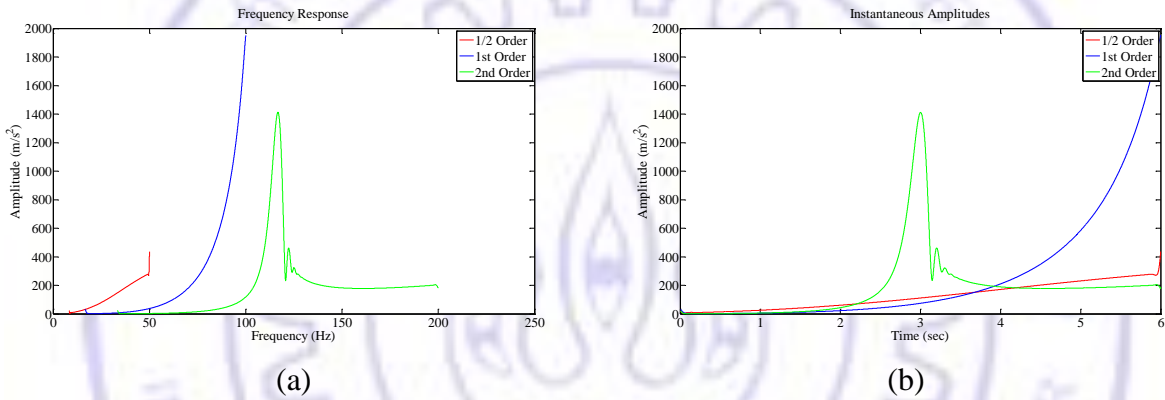


Figure 3.29: Vold-Kalman Filter Orders; (a) Frequency Response, (b) Inst. Amplitudes

Table 3.10 System Parameters from Shaking Force Ramp-up Analysis

Parameters	Simulated	WT(% Error)	HHT(% Error)	VKF(% Error)
$\frac{1}{2}$ Order Amplitude, m/s^2	-	279.70	319.9	282.10
1 st Order Amplitude, m/s^2	-	1886.30	660.9	1971.90
2 nd Order Amplitude, m/s^2	-	200.50	373.6	208.80
Resonance Amplitude, m/s^2	-	1721.50	2741.40	1427.40
Natural Frequency, Hz	113.60	114.86 (1.11)	98.89 (-12.87)	117.019(3.01)
Damping Ratio, -	0.0130	0.0224 (62.59)	0.1351 (9.06)	0.0217(61.63)
WT Time - width	-	0.0112	-	-
WT Band - width	-	3.23	-	-
VKF 1 st 3dB bandwidth, Hz	-	-	-	20
VKF No. poles -	-	-	-	2

while IMFs have exchanged order amplitudes. WT separated orders accurately; due to band pass filter it has an issue of suppressing low amplitude ridge information. VKF found to be simple and easy tool, but uses rough information of instantaneous frequency of the orders.

3.6.2 Implementation on Engine Signals

Signals collected in Section 3.2.4 are further processed as per the procedure discussed in Section 3.6.1 and the parameters of events and orders are estimated.

3.6.2.1 Crank Shaft Displacement Parameters

Figure 3.30 (a-b) shows crankshaft displacement signals filtered from Figure 3.5 (c₂) with eliminating asymmetry issue by taking conjugate for first 2 seconds. Orbits at 1500 rpm are shown in Figure 3.31, they indicate that third order is dominant and its behavior for different speed is shown in Figure 3.32 (a-e). Computed SDI and inclination angle are shown in Figure 3.33. In the selected speed range, whirl is in forward direction and no shaft resonance is observed. It indicates that SDI values are decreasing with increase in speed that represents a dominant preload or shaking force in the direction of inclination angle.

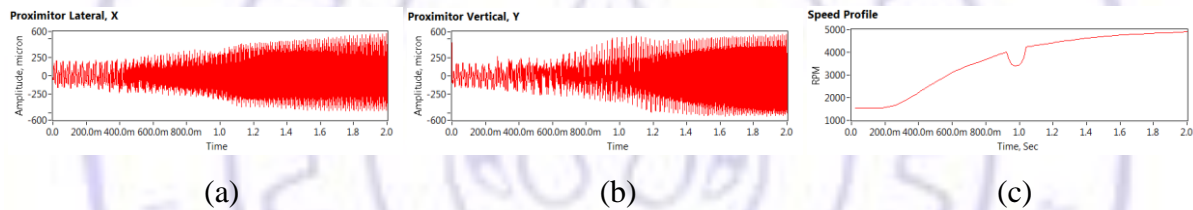


Figure 3.30: Crankshaft Displacements; (a) Lateral, (b) Vertical, (c) Speed Profile

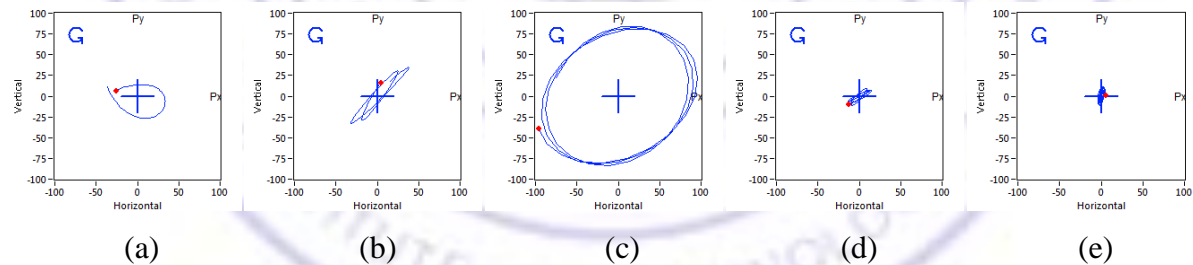


Figure 3.31: Crankshaft Orbits for Orders at 1500 rpm; (a) 1st, (b) 2nd, (c) 3rd, (d) 4th (e) 5th

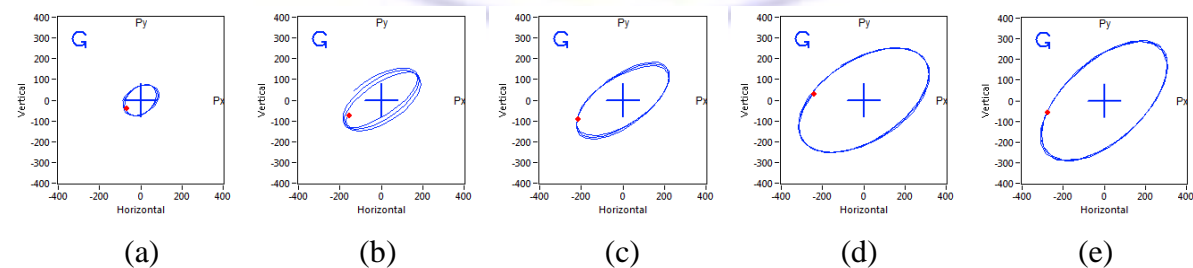


Figure 3.32: Crankshaft 3rd Order Orbits at Engine Speed; (a) 1000 rpm, (b) 2000 rpm, (c) 3000 rpm, (d) 4000 rpm and (e) 5000 rpm

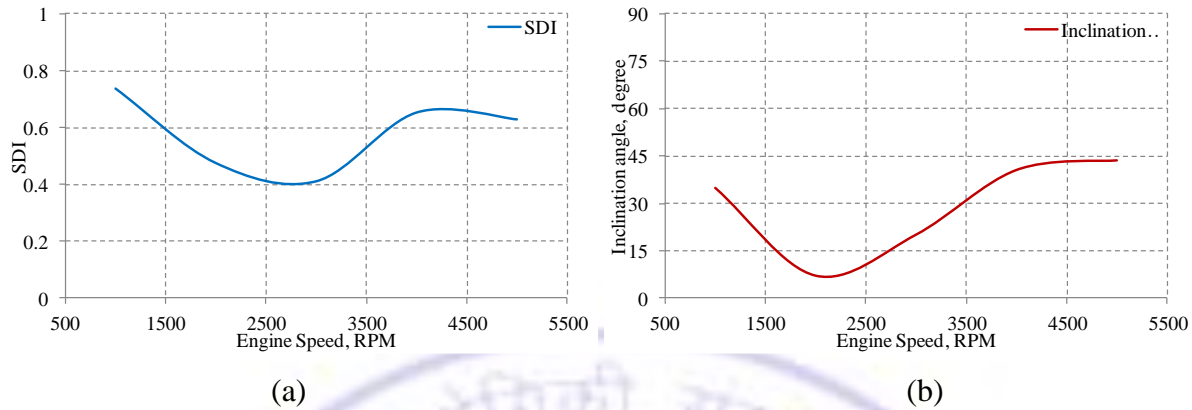


Figure 3.33: System Parameters from Orbit Plots; (a) SDI, (b) Inclination angle

3.6.2.2 Vibration Parameters of Engine Events

Figure 3.34 is a cylinder head vibration signal plot of Figure 3.6, which is filtered from Figure 3.5 (a₃) for a complete engine cycle with the steps discussed in section 3.2.5. Its WT and HHT based decomposition, parameter estimation and reconstructed are shown in Figure 3.35. WT coefficients are computed for the frequency range 1 kHz - 10 kHz with 877 frequencies bins and 4096 time bins (n_v 264 and f_0 7.5). IMFs for two revolutions of crank are shown in Figure 3.35 (a, b). Fundamental modes of majority engine components that consume high energy lie within the selected frequency range. EVO event of vibration signal is around 15° crank angle ahead of its simulated lift; kinematic simulation of EVO has slight error. EVC shows high amplitude and low damping that indicates valve is likely to fail much earlier than remaining components. SO event has both lowest damping and amplitude, hence it is less harmful. WT and HHT ridges are shown in Figure 3.35 (c, d), from which several ridges are observed in each event, linear regression of first two dominant modes and IMFs are shown in Figure 3.35 (e, f). Modal parameters are obtained by fitting a curve on skeleton of each mode separately and they are listed for all selected events in Table 3.11. Figure 3.35 (g, h) shows reconstructed signal; it has a good correlation for the individual events, while overall correlation coefficient of WT and HHT are 0.44 and 0.36 respectively. This indicates WT has a better reconstruction capability for engine vibration signals. In the measured signal, amplitude of combustion event is dominant, while in selected frequency range, WT estimated that the EVC event is dominant. In EMD, it shows only first few IMFs that are significant in capturing the information. Un-improved EMD has constructed 12 IMFs which have reduced to only 6 IMFs that have good correlation with the signal.

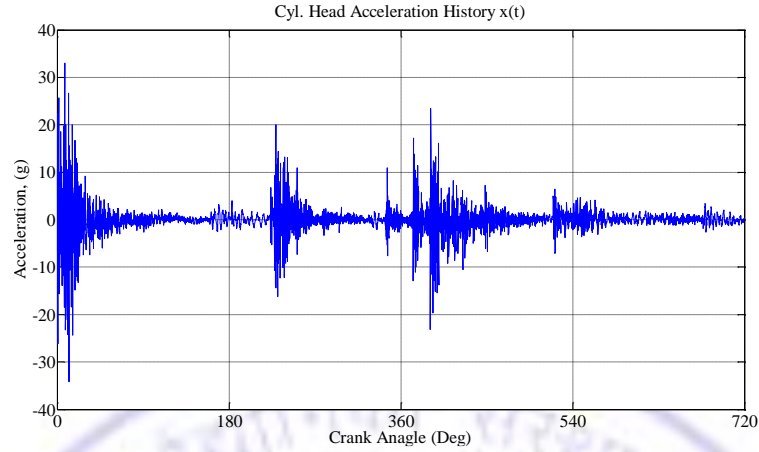
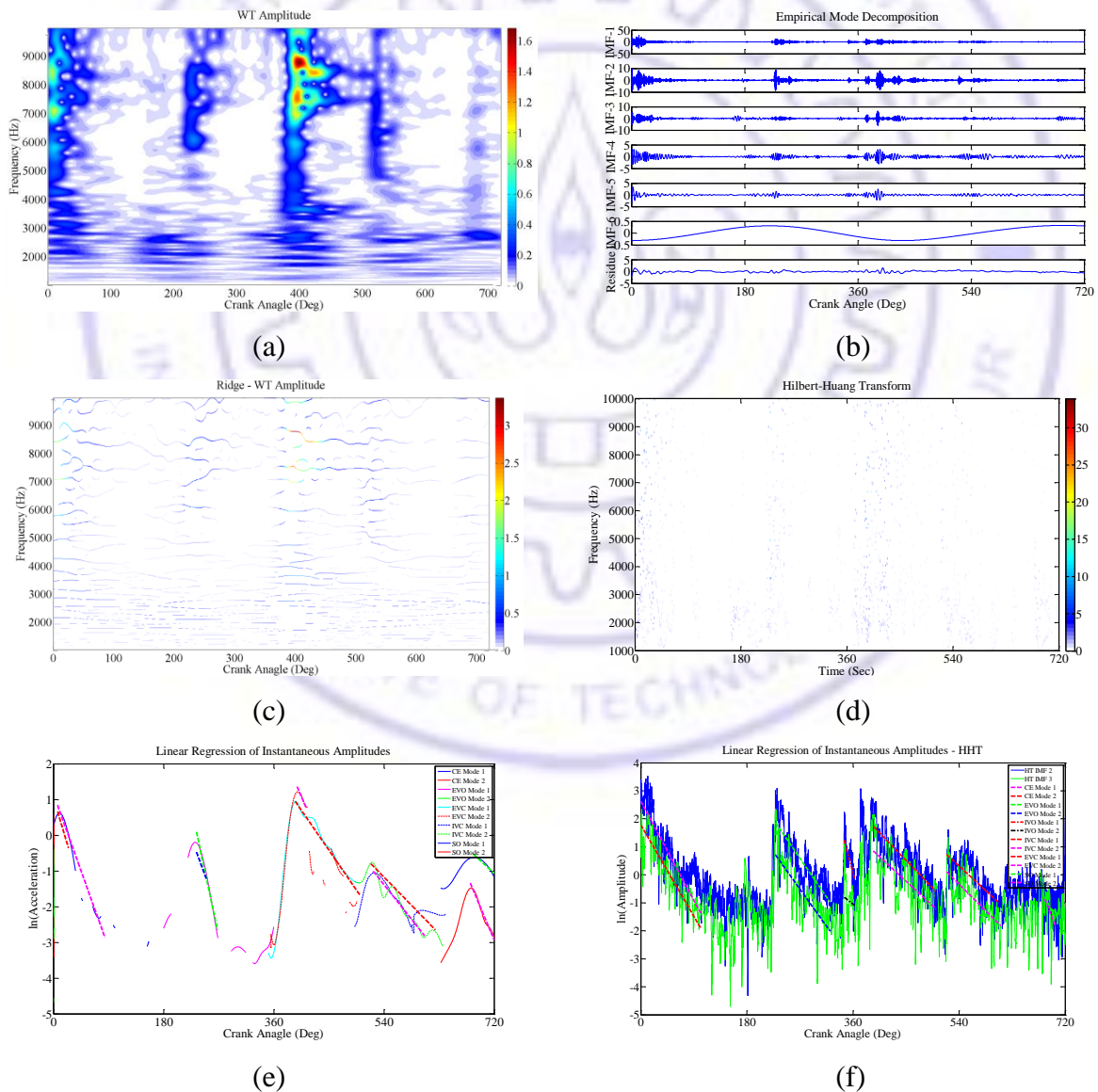


Figure 3.34: Cylinder Head Vibration Signal for a Full Cycle



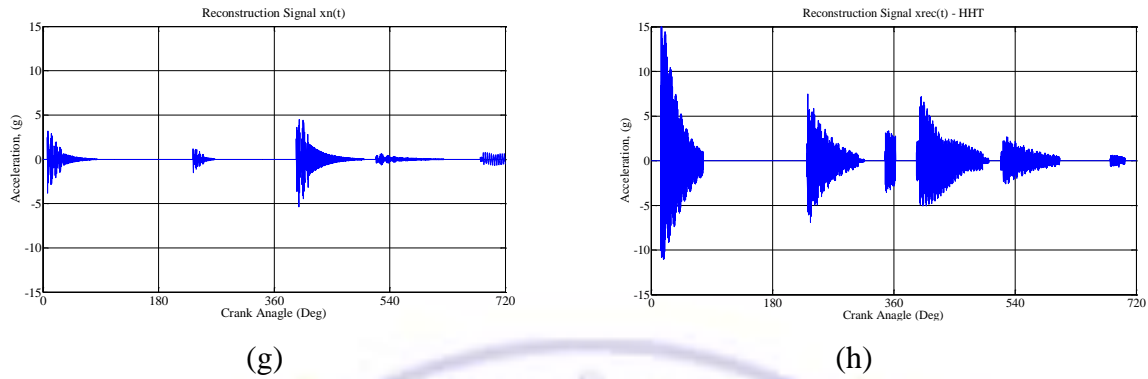


Figure 3.35: Transforms of Cyl. Head Vibration Signal; (a, b) WT and IMF Amplitudes; (c, d) Ridge -WT and HT; (e, f) Linear Regression - Envelopes and (g, h) Reconstructed

Table 3.11: Engine System Parameters of Vibration Signals at Cylinder Head

Parameters	Event: CE		Event: EVO		Event: IVO		Event: EVC		Event: IVC		Event: SO	
	Mode-1	Mode-2	Mode-1	Mode-2	Mode-1	Mode-2	Mode-1	Mode-2	Mode-1	Mode-2	Mode-1	Mode-2
WT of vibration signal												
Amplitude	2.31	1.94	1.10	0.62	-	-	3.89	2.61	0.44	0.37	0.59	0.26
Frequency	7090.90	8426.60	6082.70	7797.60	-	-	7591.00	8708.20	6560.60	7456.00	2730.90	5781.90
Damping	0.0097	0.0098	0.0189	0.0085	-	-	0.0072	0.0064	0.0045	0.0126	3.42e-5	0.0101
Angle - width	25.20	22.50	30.60	24.30			24.30	20.70	27.90	24.30	66.60	32.40
Band -	18.64	22.11	15.96	20.49			19.90	19.59	17.23	19.59	7.17	15.19
Reconstructed Signal Corr.	0.4402											
HHT of vibration signal												
Amplitude	5.95	13.86	2.03	5.99	3.46	0.45	2.35	5.59	1.13	2.08	0.64	0.49
Frequency	9107.00	17093.00	9728.60	16736.00	9661.20	17576.00	9569.90	17109.00	9408.90	16585.00	9734.80	16951.00
Damping	0.0057	0.0033	0.0043	0.0026	0.0025	0.0064	0.0029	0.0018	0.0032	0.0017	0.0021	0.0022
Reconstructed Signal Corr.	0.3571											

The procedure is capable of estimating the model parameter despite close modes and events of measured vibration signals. HHT predicted higher frequencies and amplitudes, since IMFs contain full information, while selected frequency range of WT has eliminated high frequency information. IMFs have strong non-linear composition, though the HHT is efficient in computation, parameter estimation from its IMF is difficult. At high frequency, HHT ridges are discontinued and highly scattered about their mean. HHT retains the major information of the signals, while WT give partial information due to resolution and filtration of only interested range of frequencies.

3.6.2.3 Noise Parameters of Engine Events

Near field sound signal for a full cycle at 1500 rpm is shown in Figure 3.36. It is a sound pressure plot of Figure 3.6, filtered from Figure 3.5 (a₄) for a complete engine cycle with the

steps discussed in Section 3.2.5. Due to large background noise, only firing events are visible. Sound signals at lower speed (1000 rpm in Figure 3.8) indicated they are similar to engine vibration signals with other noticeable events. With engine speed, noise level increased and events dissolved rapidly, so events get less visible. Figure 3.37 shows WT and HHT plots used in parameter estimation. Figure 3.37 (a, b) shows coefficients that are computed with same wavelet parameters as discussed in previous section. Events are fitted with linear regression and modal parameters are estimated for first two dominant modes of WT and first two IMFs of HHT shown in Figure 3.37 (c, d) respectively. CE and EVC events show highest amplitudes. Figure 3.37 (e, f) shows linear regression of first two dominant modes. From the estimated parameters, sound pressure signal is reconstructed in Figure 3.37 (g, h) and correlated with its original signal. Un-improved EMD has 11 IMFs, which has been reduced to 10 IMFs. First two dominant modes within selected frequency range of WT and IMFs in HHT are filtered and their event parameters are estimated. Modal parameters for all selected events are listed in Table 3.12. Correlation coefficient of WT and HHT reconstructed signals with measured sound pressure signal are 0.067 and 0.16 respectively. This indicates that the reconstructed signals of HHT have a high correlation with original signal due to consideration of estimated noise, while WT has a very low correlation. Selected frequency range of WT is sufficient, since dominant events are observed in this range. HHT estimation shows higher frequencies in comparison to WT. Despite high noise in measured signal, HHT estimated background noise and showed a good correlation, however improved EMD is unable to reduce the number of IMFs. Estimation from highly non-linear IMFs is

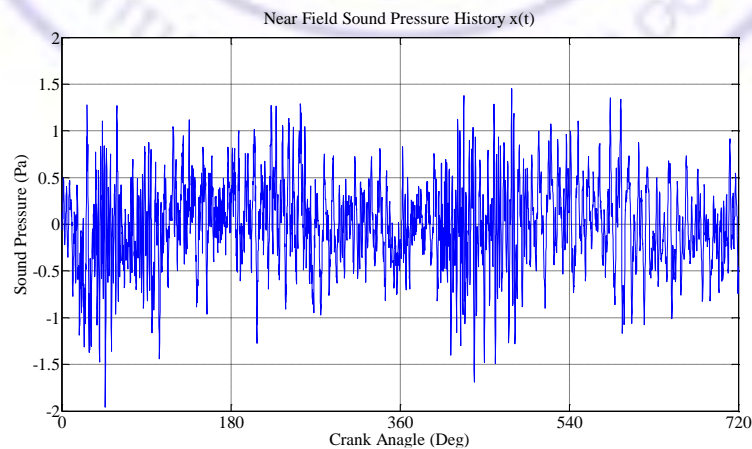


Figure 3.36: Near Field Sound Pressure Signal for a Full Cycle

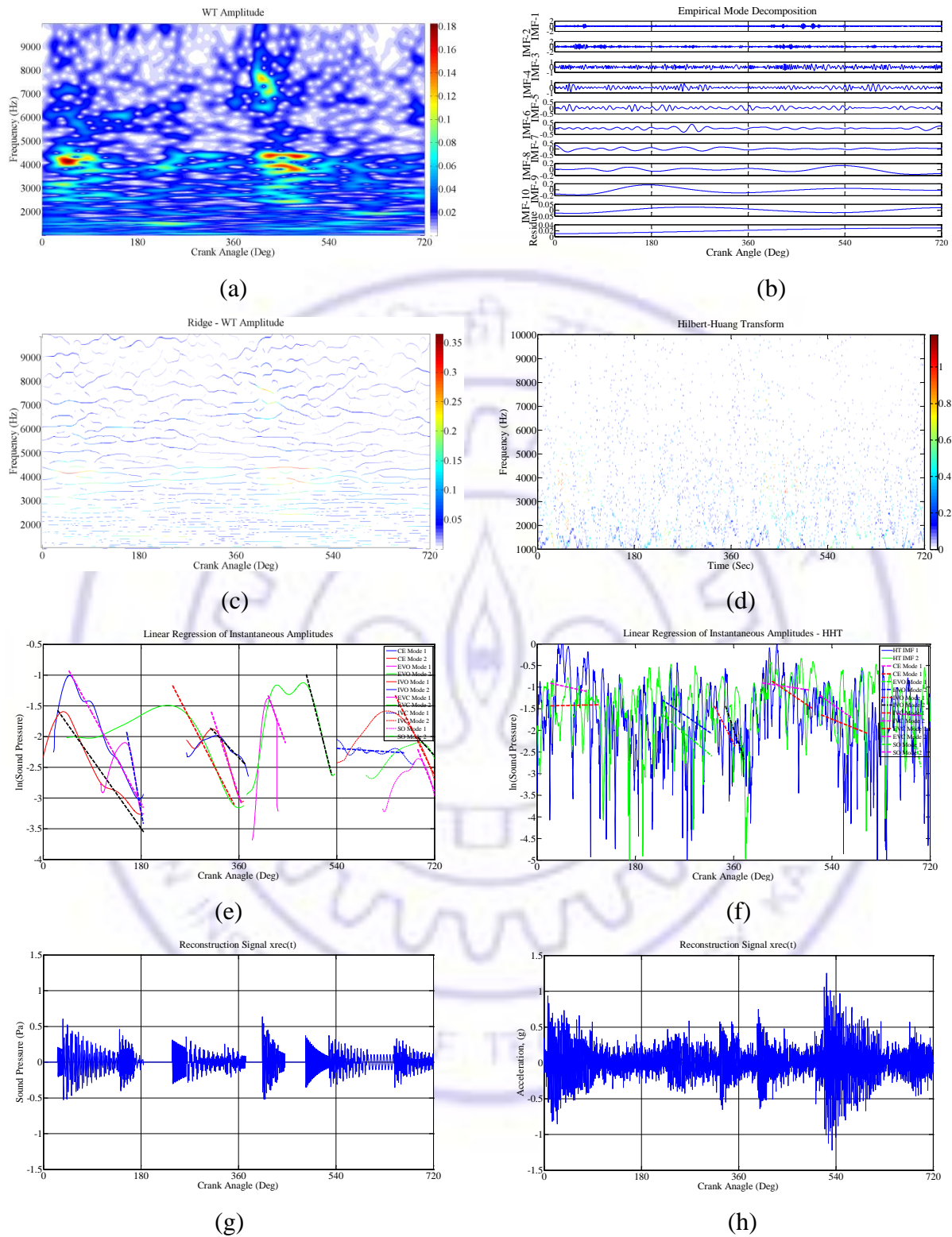


Figure 3.37: Transforms of Near Field Sound Pressure Signal; (a, b) WT and IMF Amplitudes, (c, d) Ridge -WT and HT, (e, f) Linear Regression - Envelopes and (g, h) Reconstructed Signals

Table 3.12: Engine System Parameters of Near Field Sound Signal

Parameters	Event: CE		Event: EVO		Event: IVO		Event: EVC		Event: IVC		Event: SO	
	Mode-1	Mode -2	Mode-1	Mode -2	Mode-1	Mode -2	Mode-1	Mode -2	Mode-1	Mode -2	Mode-1	Mode -
WT of sound pressure signal												
Amplitude	0.40	0.21	0.15	0.31	0.20	0.15	0.26	0.37	0.11	0.26	0.11	0.13
Frequency	3111.60	4218.20	1571.40	5952.30	1092.20	4229.60	4320.90	7777.80	1537.10	3967.20	2757.90	4035.70
Damping	0.0075	0.0043	0.0443	0.0041	0.0353	0.0031	0.0081	0.0065	5.37e-4	0.0065	0.0115	0.0035
Angle - width	56.70	43.20	117.00	30.60	159.30	42.30	42.30	24.30	115.20	45.90	65.70	46.80
Band -	8.13	11.08	4.13	15.63	2.86	11.11	11.35	20.43	16.19	10.44	7.25	10.60
Reconstructed Signal Corr.	0.0670											
HHT of sound pressure signal												
Amplitude	0.3702	0.4401	0.2964	0.1148	0.5580	0.1872	0.3412	0.8147	0.2815	0.1371	0.2047	0.0577
Frequency	3878.1	8054.1	3799.4	15486	4521.0	8659.7	4036.2	6519.7	3639.6	9313.8	4405.2	9243.0
Damping	0.0027	0.0028	0.0048	0.0017	0.0139	0.0059	0.0020	0.0031	0.0112	7.651e-4	0.0015	0.0095
SNR dB	4.9598											
Reconstructed Signal Corr.	0.1615											

tedious due to the structural complexity. A careful attempt has made to locate events and separate end effects in both WT and HHT. Even though signal has 30% noise, HHT allows estimation of its parameters, while WT is unable to give any information. Assessment of modal parameters on the structural health indicates that EVO and EVC events has relatively low damping and high amplitude, this shows the valve is likely to fail much earlier than remaining components.

3.6.2.4 Noise and Vibration Parameters from Ramp-up Analysis

In this section, measured vibration and sound pressure transient signals of Set No. 3 shown in Figure 3.5 are analyzed to extract the engine order and critical speed information. Data is extracted for the first 2 sec duration of ramp as shown in Figure 3.38. Speed profile shows a maximum speed of 5,100 rpm .i.e. 85 Hz is observed in the 1st running order. WT coefficients are computed for the frequency range of 1 kHz - 10 kHz with 877 frequencies bins and 4096 time bins (n_v 16 and f_0 1). WT amplitude plot shown in Figure 3.39 indicates that vibration signal has $\frac{1}{2}$, 1st and 2nd orders, while sound pressure signal has $\frac{1}{2}$, 1st and 1.5 orders. Parameters of dominant resonance are estimated using half power bandwidth method

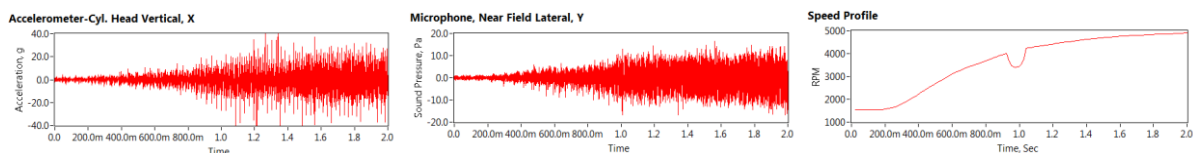


Figure 3.38: Engine Ramp-up Signals; (a) Cyl. Head Vibration, (b) Near Field Sound pressure and (c) Speed Profile

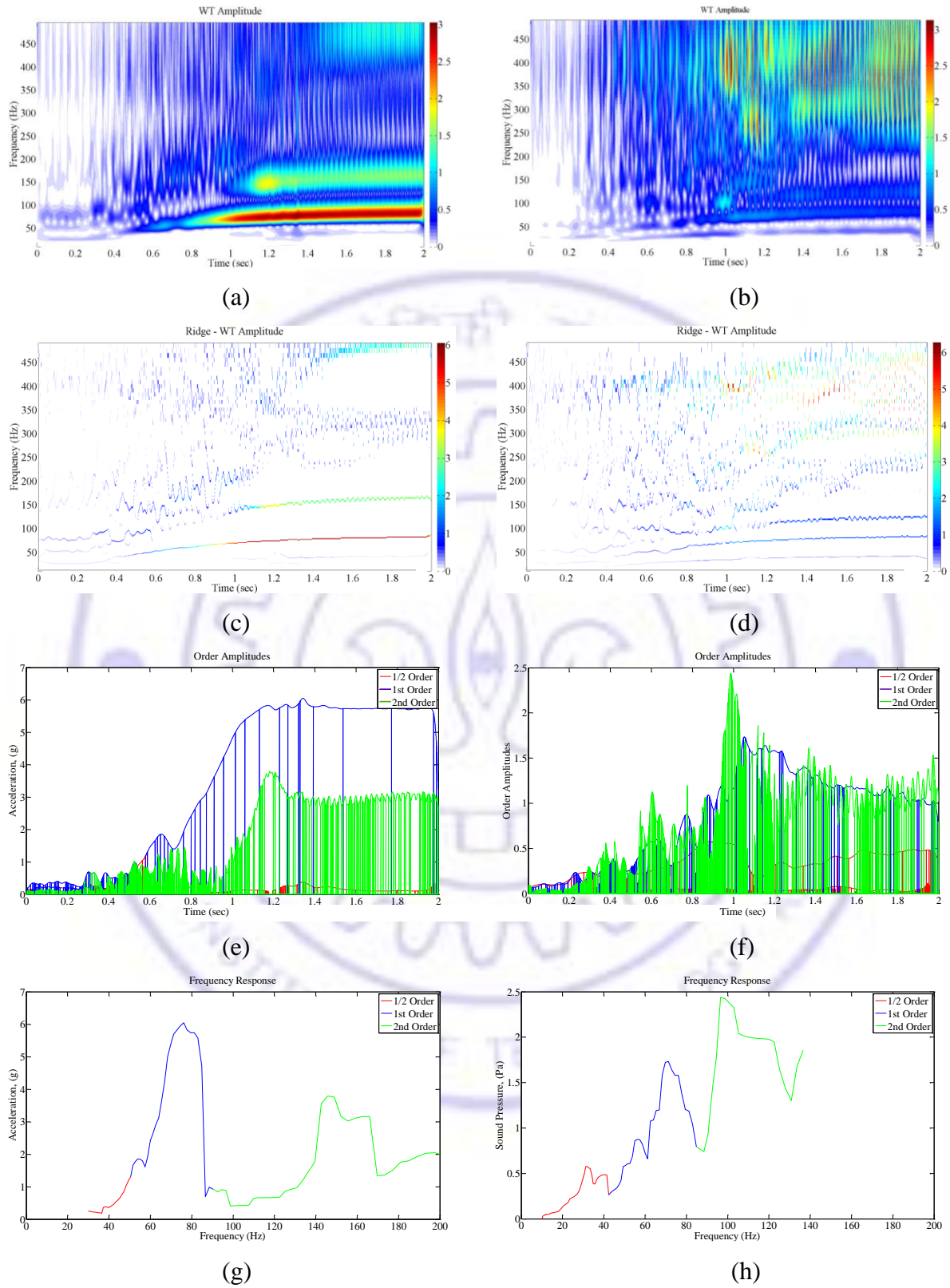


Figure 3.39: Transforms of Cyl. Head Vibration and Near Field Sound Signal: (a, b) WT Amplitudes; (c, d) Ridge, (e, f) Inst. Frequency and (g, h) Frequency Response

Table 3.13 Engine System Parameters from Ramp Signal Analysis

Parameters	Vibration m/s ²	Sound Pressure, Pa
$\frac{1}{2}$ Order Amplitude, at 5100 rpm	0.115	0.489
1 st Order Amplitude, at 5100 rpm	5.731	1.036
1.5 Order Amplitude, at 5100 rpm	-	1.195
2 nd Order Amplitude, at 5100 rpm	3.013	-
Resonance Amplitude,	6.047, 3.765	1.737
Natural Frequency, Hz	76.145, 145.766	69.910
Damping Ratio, -	0.129, 0.095	0.108

on WT identified orders. WT plot of vibration signal has two dominant critical speeds at 4569 rpm and 8746 rpm, while in sound pressure, only one dominant resonance at 4195 rpm is observed. Maximum amplitude extraction method for 1.5 order sound pressure signal is not efficient. The band pass filter technique used in extracting order amplitude is not sufficient, several zero values are observed in the second order amplitude envelope. Table 3.13 lists the estimated parameters. They represent inherent condition of the study engine.

3.7 Conclusions

In this chapter, an experimental set-up is built, instrumented and calibrated. It is evaluated to select most sensitive operating condition for an effective EHM. Set-up is capable to simulate emulated structural fault and failure conditions, measure vibration, noise and shaft motion signals. A parameter estimation procedure is formulated and transforms are evaluated.

After the set-up was built, it was tested for healthy condition by justifying the occurrence of features of the acquired signals in time and FFT domain. Initially, it was identified with few inherent faults, such as unbalance and coupling misalignment, however their amplitudes were consistent. Prior to start the experimentation, a calibration process with common practices was adopted to set the set-up as a standard reference i.e. Normal healthy. Calibration trials were made by adjusting the engine foundation levels, positions and pre-tensions to eliminate fault orders and minimise their amplitudes. For the entire set of experiments, above finalised adjustments of foundation were retained constant. In the acquired signal, repeatability over events in the signal and repeatability of data sets has been checked. The signals are collected for five times for every change in each condition.

Speed, shaft displacement and vibro-acoustic signals are acquired with sufficient resolution in different sets for an entire operating range. Events and running orders in the signals are identified, and most critical one are selected for the study. Signals are then assessed for effectiveness with different sensors, their mounting locations and directions, fuels and speed conditions. Signals are collected and cycle events are identified. It can be concluded that the cylinder head vertical vibration signal is more sensitive in picking engine events and are more effective around 2000 rpm with diesel fuel.

The dimensionality of engine database is reduced by using multivariate principal and independent component methods. It also confirms that cylinder head vibrations in vertical direction are more suitable for the health management study.

A parameter estimation procedure is established using Orbit, Wavelet transform, Hilbert-Huang transform and Vold-Kalman filter. Numerically simulated signals that resemble events, modes and noise nature of the measured crankshaft, and vibro-acoustic signals are used. HHT demonstrated a simple method that does not require any resolution criteria and estimates the background noise effectively. But it is tedious process; amplitude of IMFs fluctuates, which increases error in the parameter estimation. Low frequency IMF gives several monotonic high amplitude modes, which are less useful. Improved HHT shows a few significant IMFs that are sufficient for signal representation and enables better computational efficiency. High amplitude IMF superimpose with nearby mode, so it is difficult to interpret and separate the mode segments. HHT ridges are not continuous, so tracking a high frequency ridge is difficult due to its poor representation and intersection of several IMF ridges. WT proves to be more robust and efficient method in parameter estimation and separates the nearby modes. However it is computationally less efficient as it takes exponentially high time for increased resolution in signal and window resolution parameters.

Transient response of proximity and vibration are simulated with known parameters under constant acceleration rate with detailed engine loading for realistic parameter estimation. Orbit parameters and whirl are estimated from the simulated proximity signals. System parameters are estimated from WT, HHT and VKF. WT has separated the orders effectively,

while HHT is unable to separate the orders. VKF has tracked the orders, but uses rough information of instantaneous frequency. Numerically constructed signals that can resemble measured signals demand the detailed physics-based modeling for the accurate representation and need for fault and failure study.

Procedure is implemented on measured engine signals that have both structural complexity and background noise. Despite practical situation, procedure is capable of identifying, separating, and quantifying the dominant event features and noise level. Vibro-acoustic parameters provide capabilities in monitoring the critical health of an engine. WT and HHT confirm that combustion and exhaust valve opening events are dominant. Events in acoustic signals are less clear due to noise level. Higher modes provide poor estimation due to certain overlap of events and modes. Estimated parameters give exclusive criteria in separating engine events, ability to reconstruct signal and quantify the health condition. Signal reconstruction indicated that the first two dominant modes and IMFs are sufficient to represent each event with the calculated correlation coefficient. Results indicated that the proposed parameter monitoring procedure is useful in quantifying the events and health of an engine. This study concludes that WT is a superior tool and its parameter estimation of cylinder head vibrations is a most sensitive approach for EHM. WT based engine ramp-up analysis has separated the orders and identifies some critical speeds.

Evaluation of set-up provided most sensitive conditions and reduced the database that can help for quick fault diagnosis. However fault diagnosis only at selected conditions and data sets can compromise certain accuracy in the prediction process. Though parameter estimation from non-stationary signals is highly accurate, precisely quantify structural health conditions of the engine, but it is tedious and time consuming. Since engines have infinite events, modes and orders so it still has practical issues in implementing for fault diagnosis from entire engine database. It requires development of algorithms for automatic identification and extraction of parameters from important events, modes and orders. With this limitation, engine fault diagnosis from stationary signals using statistical and fast Fourier transform still seems to be a viable option. Though achieving stationary conditions for data acquisition is quite difficult but estimation of their parameters is easy, which supports the database with

increased verity by different conditions and speeds. In Chapter 5, fault diagnosis with cylinder head vertical and near field sound pressure signals of Data Set No. 1 at 1500 rpm is carried-out using FFT and WT plots. A manual fault diagnosis using statistical and fast Fourier transform feature database of Data Set 2 signals from all ten sensors and all five speeds have been also carried-out.



CHAPTER 4

PHYSICS-BASED HEALTH MANAGEMENT

*This elegant generalization is mathematically very appealing;
but physics means facing facts. You should take up case by case.*

- Kariamanickam Srinivasa Krishnan (1898 - 1961)

4.1 Introduction

In Chapter 3, an experimental set-up is built to study emulated field faults and failures, it is evaluated to select sensitive conditions, reduce database and estimate few parameters. Experimental models consume huge time and expense, and provide scant information, while physics-based models offer a virtual environment and high fidelity results with few governing equations to gain ideal insight, compare designs and generate inputs. A modern engine houses thousands of components and several devices, they interact simultaneously with chemical, thermal, fluid and structural environments. Its cycles have significant variations caused uneven admissions and highly stochastic operations. Due to large uncertainty, they are too complex for physical reasoning. Actual structural faults of a machine are minute geometric and material defects that grow with time and lead dysfunction or failure. Physics-based analytical, numerical and software models are inadequate to predict real faults and failures: 1. Analytical models form a close-form solution with primitive geometry and load functions, which predict system gross response. Highly approximated model are inadequate to include tiny local defects. 2. Discrete models predict certain level response, has fairly good control on governing equations but inefficient to capture local effect due to large numerical error. 3. Commercial software supports accurate geometry modeling and few routine environments, but unavailability of source code, methodology, and provision to include advanced dynamics and stochasticity poses a challenge. So they are being solved by computational intelligence (CI) [148-149] as attempted in Chapter 5 and 6.

Faults and failures can be observed by change in structural responses such as shaft motion, vibration, noise and fatigue. Researchers have attempted to predict them using lumped mass discretized (LMD) models. [Markert et al. \[17\]](#) formulated an unbalance and rub. [Bachschmid et al. \[101\]](#), [Sinha et al. \[150\]](#) and [Sekhar and Prabhu \[151\]](#) studied an unbalance, misalignment and bow. [Darpe et al. \[100\]](#) investigated crack. Studies have been restricted to investigate few basic faults. They introduced faults in a shaft by modeling it as a beam under steady speed. [Vyas and Rao \[152\]](#) demonstrated life estimation in simple components. Such approximations are insufficient to study real faults and failures, but detailed dynamics, geometry and cumulative effect of interdisciplinary loads has a potential to respond for added defects. Advances in rotor such as gyroscopic effect, cross coupling, speed dependent stiffness and time dependent properties, Rayleigh damping, hydrodynamic, asperity contact friction and operational environments can increase realistic prediction. Software supports certain properties that are useful to validate and enhance discrete models. Integrating component flexibility and properties in multibody models is being attracted by researchers [\[153-158\]](#), as it assess cumulative effects accurately and has potential to indicate faults at gross response. With imposed conditions, it is challenging to formulate and evaluate physics-based models for predicting machine health conditions. Purpose of this chapter is to,

1. Build physics-based models of an engine to simulate realistic defects and failures.
2. Extract sensitive features from its vibration, noise and fatigue responses.
3. Evaluate and explore these models under initiated faults and failures.
4. Build a database of fault and failure symptoms to support an efficient EHM.

Section 4.2 describes engine mechanism, its actual faults and catastrophic failures. A simulation methodology is developed in Section 4.3 using LMD and FMBD models by idealizing powertrain and estimating operational properties. Section 4.4 discusses solution methods for fault diagnosis. Section 4.5 evaluates the models with performing reduction using vibration analysis. Responses of selected physics-based models are compared with experimental results. In Section 4.6, they are investigated for fault diagnosis and compared for an experimental fault case. Section 4.7 discusses solution methods for failure prognosis. In Section 4.8, fatigue analysis is employed to estimate RUL of the failing component by computing life for crack initiation and propagation. Last section lists the conclusions.

4.2 Engine Mechanism and its Actual Failures

Specifications of the selected engine are listed in Section 3.2. Engine is a portable, single cylinder, vertical, offset head valve, air cooled and spark ignition type. The current section discusses their functionality. Engine has a fuel ignition, governor, silencer and carburettor systems. It doesn't include auxiliary systems such as turbo or super charger, exhaust gas recirculation, radiator and electronic control units that are common in a modern automotive engine. Figure 4.1 show its cut section and schematic diagram of the mechanism. Cylinder block houses powertrain (crank, valve and gear trains) components, cylinder head at upper side and oil sump at bottom end. Crankshaft is supported by two main ball bearings, located at asymmetric distance from the central vertical plane. Left portion of crankshaft carries a flywheel and pinion gear, while other end carries a coupling to deliver output power. Pinion transmits power to the centrifugal governor via camshaft gear. Camshaft drives valve-train components, while governor regulates engine speed by controlling throttle position. Speed ramp can be obtained by adjusting governor flyweight against the retainer spring. Crank and piston pin journals are operated with hydrodynamic lubrication. Flash type lubrication supplies oil into the journals and main bearings. Flywheel houses ignition coil and starter assembly to generate electricity required for the spark plug. Solid model of the powertrain is shown in Figure 4.2; it consists of crank, gear and valvetrains. Asymmetricity of crankshaft is due to the counter, crank pin and reciprocating masses that causes variable elasticity and

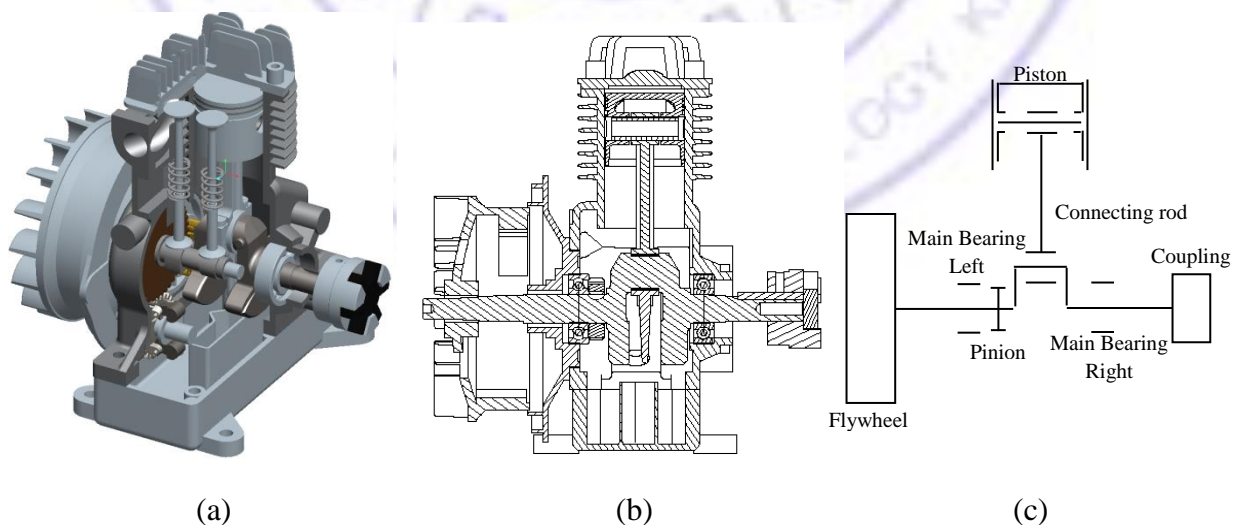


Figure 4.1: Engine Models; (a) Cutaway, (b) Sectional Drawing, (c) Functional Diagram

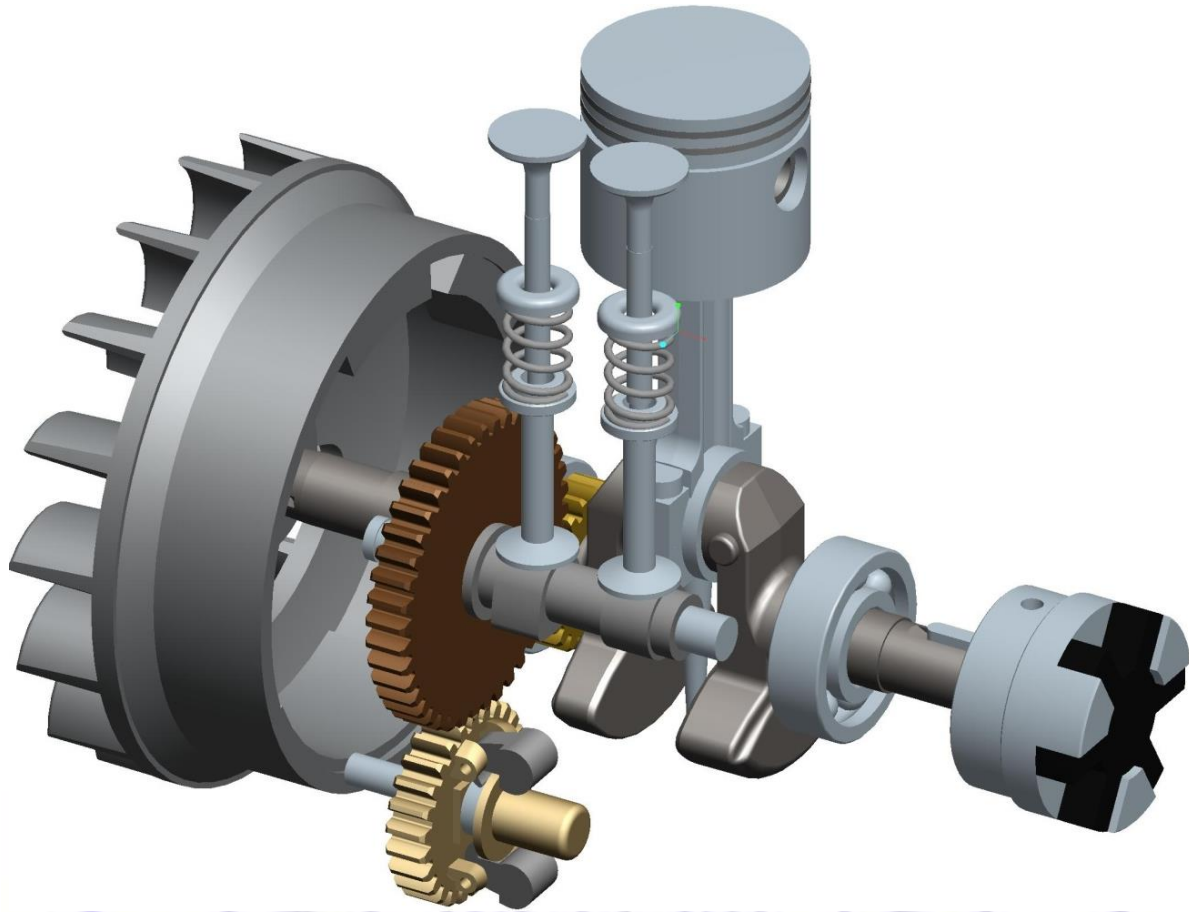


Figure 4.2: Solid Model of the Powertrain

instability. Connecting rod oscillates between crankshaft and piston assembly, so its elastic properties are varying significantly for crank angle. Loads are also asymmetric due to unbalanced reciprocating masses and strong firing force. Components operate at different speeds and loads; they cause irregular operations and intermittent collisions that can result non-linear and non-stationary signals. Fault can occur in any of these components and any location in a component, so careful modelling of dynamics with recent developments and giving equal attention to each component can potentially predict their faults and failures.

Figure 4.3 shows few typical catastrophic field failures in cranktrain components of different engines. Figure 4.3 (a) shows bend in connecting rod due to heavy load that result from hydrostatic lock, abnormal increase in cylinder pressure, over heating or low lubrication. Steel connecting rod usually gets bend, while aluminium rod has a low cycle brittle fracture, as shown in Figure 4.3 (b). Figure 4.3 (c) indicates crankpin wear, which is

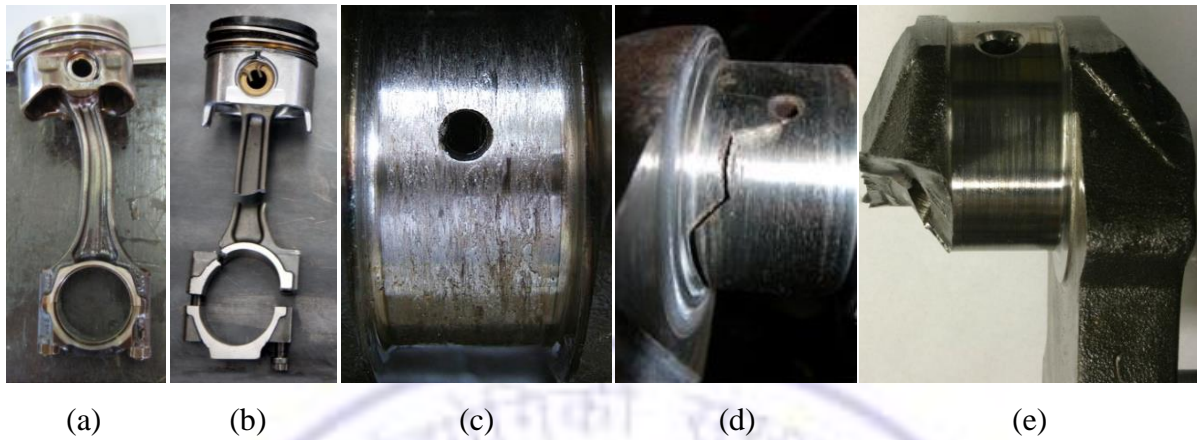


Figure 4.3: Typical Catastrophic Failures in Cranktrain: (a) Connecting Rod Bend [159], (b) Connecting Rod and Big End Fracture [160], (c) Crank Pin Worn [161], (d) Crank Pin Crack [162] and (e) Crank Web Fracture [163]

caused by an increased clearance or lack of lubrication. Fracture in a crankpin and crankshaft web as shown in Figure 4.3 (d and e), occurs due to material defect and repetitive loading. Zima and Greuter [43] surveyed percentage failures of engine components. They reported that the crankshaft failures are about 20%, while connecting rod and piston are about 25% of the total failures. Such failures have serious consequences on engine health. Physics-based models can simulate certain conditions to mimic real field faults and failures. Faults that resembles above field defects are introduced in the geometry of respective component and then forced to propagate into failure. The actual size of initiated faults is a micron level and usual numerical error is much larger than the local fault response. For a larger fault dimensions, physics-based models can easily give a recognisable change in the response. So a procedure is proposed in this chapter to model detailed dynamics and geometry with including loads from multiple domains to simulate abovementioned fault and failures.

4.3 Engine Physics-based Models

Physics-based models are in use for predicting dynamics and gross vibrations of vehicle [164-170], and powertrain [14-16, 92, 171-189]. They mainly focus on increasing functionality of LMD [14-16] to eliminate dependence of commercial software or test and to formulate a routine procedure in commercial software for design development. Gross

motions of a vehicle are governed by suspension, which have low frequency and few modes that can have better correlation with experiments. But large number of different stiffness components in engine system requires consideration of several modes and a wider frequency range; they have difficulty in modelling and correlation with system level experiments. Literature [174-189] indicates modeling flexible dynamics of engine system with including recent developments can predict accurate response. Increased geometry and flexibility (Ricci [16] and Ricci et al. [92]) can permit modelling of minute geometrical defects. Due to large error in idealization and computational time, prior to investigate them for faults and failures it is necessary to evaluate. LMD models need to be evaluated for increasing details and size to accommodate complexity and FMBD models for optimally reduced size.

LMD models discretize the system by idealizing geometry into a fewer DOFs and predicts gross response numerically. They are easy to iterate, can accommodate recent developments and couple multiple domains. They are capable to model certain operating characteristics of the fault. A large fault can easily change the response. Unbalance occurs due to process variation; mass of component either increases due to continuous wear of manufacturing die or decrease by wear loss that can be modeled as inertia force. Lack of lubrication, either due to overheating or blow-by can be modeled as frictional force. Due to simplified geometry, flaws such as crack and bend are difficult to model, which demands detailed geometry.

Some commercial MBD software permits modelling of detailed geometry, component flexibility and routine environments. Local flaws such as crack, wear and bend can be modeled by deviating geometry of flexible component locally at the fault location. They also provide common platform with other software; outputs such as stiffness, mass, damping, loads and response information can enhance LMD modelling. They are solve by numerical integration in time domain using predefined initial conditions that integrates responses of previous step to obtain system response in subsequent steps. MBD software simulates the system as a group of rigid or flexible bodies that are linked by kinematic joints at their interfaces to transfer the forces and movements. It computes response as generalised coordinate, in which rigid body motion is combined with component deformation respect to rigid body motion. Component rigid body motions are computed either using coordinate

partitioning or appended constraining method, while component deformations due to flexibility are computed using finite element (FE) method. They employ a model reduction technique to reduce model size and avoid consideration of very small displacements or rotations of the component. Model reductions techniques such as Guyan and Craig - Bampton (CB) represent the component fundamental deformations with lower number of coordinate i.e. model deformations (Wagner et al. [91] and Qu [190]). In Guyan reduction [191], model size is statically condensed by eliminating the interior DOFs with minimum loss of accuracy, which may lose some local dynamic effects depending on the selection of set points. CB method combines motion of boundary points with modes of structure, assuming the boundary points are held fixed. It reduces large FE models into lower size mass, stiffness for a frequency range, and retains fundamental mode shape with response information. It allows different boundary conditions at interface. In the current approach, CB model reduction is used. Equation of motions (EOM) for a free-free, un-damped structure is,

$$\mathbf{M}\ddot{\mathbf{u}} + \mathbf{K}\mathbf{u} = \mathbf{F} \quad 4.1$$

where \mathbf{M} and \mathbf{K} are FE mass and stiffness matrix respectively, \mathbf{F} is a external load vector. CB partitions [16, 91-92, 192-195] the physical DOFs into boundary \mathbf{u}_b and interior \mathbf{u}_i DOFs.

$$\begin{bmatrix} \mathbf{M}_{bb} & \mathbf{M}_{bi} \\ \mathbf{M}_{ib} & \mathbf{M}_{ii} \end{bmatrix} \begin{Bmatrix} \ddot{\mathbf{u}}_b \\ \ddot{\mathbf{u}}_i \end{Bmatrix} + \begin{bmatrix} \mathbf{K}_{bb} & \mathbf{K}_{bi} \\ \mathbf{K}_{ib} & \mathbf{K}_{ii} \end{bmatrix} \begin{Bmatrix} \mathbf{u}_b \\ \mathbf{u}_i \end{Bmatrix} = \begin{Bmatrix} \mathbf{F}_b \\ \mathbf{F}_i \end{Bmatrix} \quad 4.2$$

Externally applied interior forces are zero i.e. $\mathbf{F}_i = \mathbf{0}$. Physical displacements \mathbf{u} can be obtained from modal displacements \mathbf{q} using CB coordinate transformation as,

$$\mathbf{u} = \begin{Bmatrix} \mathbf{u}_b \\ \mathbf{u}_i \end{Bmatrix} = \begin{bmatrix} \mathbf{I} & \mathbf{0} \\ \boldsymbol{\phi}_{ib} & \boldsymbol{\phi}_{iq} \end{bmatrix} \begin{Bmatrix} \mathbf{u}_b \\ \mathbf{q} \end{Bmatrix} \quad 4.3$$

where $\boldsymbol{\phi}_{ib}$ is a matrix of shapes that represents details of rigid body motions, which is obtained by considering lower partition of the static portion of Equation 4.2 and solving for the i -set displacements, $\boldsymbol{\phi}_{iq}$ is a matrix that satisfies i -set eigen problem i.e. fixed base mode shapes. Boundary DOFs of the transformation matrix are termed as constraint modes, which

$$\mathbf{u}_i = -\mathbf{K}_{ii}\mathbf{K}_{ib}\mathbf{u}_b = \boldsymbol{\phi}_{ib}\mathbf{u}_b \quad 4.4$$

$$\mathbf{K}_{ii}\boldsymbol{\phi}_{iq} = \mathbf{M}_{ii}\boldsymbol{\phi}_{iq}\boldsymbol{\lambda} \quad 4.5$$

are static deformation shapes of the component when subjected to unit displacements at each of the b -set DOFs; the remaining being restrained. Last column of the transformation matrix represents fixed interface normal modes, i.e., eigenvectors representing dynamics of interior substructure relative to the interface. Corresponding eigenvalues are used in the diagonal matrix $\boldsymbol{\lambda}$. Hence a generalized coordinate vector consists of both physical \mathbf{u}_b and modal \mathbf{q} displacements. Interface DOFs are retained in the reduced representation to facilitate component coupling. Combining Equations 4.2, 4.3 and pre-multiplying by $\boldsymbol{\phi}_{cb}^T$,

$$\begin{bmatrix} \mathbf{M}_s & -\mathbf{P}^T \\ -\mathbf{P} & \mathbf{I} \end{bmatrix} \begin{Bmatrix} \ddot{\mathbf{u}}_b \\ \ddot{\mathbf{q}} \end{Bmatrix} + \begin{bmatrix} \mathbf{K}_s & \mathbf{0} \\ \mathbf{0} & \boldsymbol{\lambda} \end{bmatrix} \begin{Bmatrix} \mathbf{u}_b \\ \mathbf{q} \end{Bmatrix} = \begin{Bmatrix} \mathbf{F}_b \\ \mathbf{0} \end{Bmatrix} \quad 4.6$$

CB substructure representation is obtained by defining the CB mass and stiffness matrices. $\mathbf{M}_s = \mathbf{M}_{bb} + \mathbf{M}_{bi}\boldsymbol{\phi}_{ib} + \boldsymbol{\phi}_{ib}^T\mathbf{M}_{ib} + \boldsymbol{\phi}_{ib}^T\mathbf{M}_{ib}\boldsymbol{\phi}_{ib}$ and $\mathbf{K}_s = \mathbf{K}_{bb} + \mathbf{K}_{bi}\boldsymbol{\phi}_{ib}$ are the statically reduced mass and stiffness matrices respectively. $\mathbf{P} = -\boldsymbol{\phi}_{iq}^T(\mathbf{M}_{bb}\boldsymbol{\phi}_{ib} + \mathbf{M}_{ib})$ is the modal participation factor matrix that contains multiplication factors for the acceleration inputs at interface DOFs,

$$\ddot{\mathbf{q}} + \boldsymbol{\lambda}\mathbf{q} = \mathbf{P}\ddot{\mathbf{u}}_b \quad 4.7$$

An optimal reduction would result in minimal set of component modes that ensures acceptable accuracy in the simulation results. Singular perturbation and importance analysis [196-197] reduces the response variables. In this work, instead selecting component modes, models are selected based on the flexible effect and less effective components are made as rigid. Model reduction can be carried out in commercial FE software. Software such as ADAMS, COMSOL, SIMPACK, ANSYS, HYPERWORKS offers a general MBD platform, while specialized tools such as ENGDYN and EXCITE performs engine MBD simulation. They permit modeling of geometrical defects in the normal flexible component. Model reduction is carried out in NASTRAN and flexible MBD modelling in ADAMS/flex.

Information about threshold limit and remaining survivability can be predicted using wear and fatigue models. Engine failures depend on cumulative effect of cyclic temperature, cylinder pressure variations and sound level fluctuations. Repeated thermal reversals that occur due to combustion can cause thermo-mechanical fatigue. Fluctuation of cylinder pressure, inertia, friction, increased joint clearance and repeated collision adds stress reversals that induce structural fatigue. Repeated extreme high noise level due to cylinder firing can also induce vibrations in the engine components that cause acoustic fatigue. In the fatigue analysis, the loads and stress from the FE or flexible multibody software can be imported into the commercial fatigue software such as FATIGUE, FE-SAFE, nCode, NASGRO and AFGROW. Fatigue software uses cyclic material, service load and compensated geometry database to predict the durable life, crack growth and RUL.

4.3.1 Simulation Methodology

This section proposes different idealization of LMD and FMBD models for studying the engine fault and failure symptoms. Engine geometry is approximated; load profiles are estimated by performing associated thermodynamic, hydrodynamic and engine dynamics analysis. These loads are verified at selected conditions with test, referred literature and commercial rigid MBD tools respectively. Rayleigh damping is used to estimate component material damping. Model reduction is studied and optimised model is used to introduce the structural faults and failures. Kinematic and structural dynamic (free, forced fatigue and fracture) analysis is carried out to extract vibrations, stresses, life cycles and crack growth response characteristics. Features from time and time-frequency domain are explored to quantify symptoms of different faults and failures.

In LMD, four different models of powertrain with increasing DOFs are built and simulated to predict cranktrain and valvetrain vibrations. These models are enhanced by rotor dynamic developments (gyroscopic, friction, Rayleigh damping and speed dependent properties). A simple speed dependent hydrodynamic and asperity contact friction force at the piston ring and liner is proposed. Rayleigh coefficients are used to define material damping. Combustion force for the complete speed range is added by computing pressure history from a calibrated thermodynamic engine model. Component unbalance forces are estimated using mass and

COG properties from CAD model. Its finite element assembly mass and stiffness are estimated using geometrical properties. EOMs are numerically solved in MATLAB using inbuilt function ODE45 and ODE15s as soft and stiff differential equation solvers respectively under estimated impacts and steady speed excitations. Proposed model is used to investigate the effects of added unbalance and friction faults, which are in common due to manufacture and operational defects.

In FMBD approach, a rigid cranktrain is built and converted into complete flexible by replacing individually its rigid components with flexible components. Effect of component flexibility is studied by comparing modal characteristics and vibration response. Solid modeling is carried out in PRO/ENGINEER, FE models are built in MSC/PATRAN and component modal information i.e. modal neutral files (MNFs) are generated in MSC/NASTRAN. Fatigue cycles and crack growth are estimated using strain-life approach in MSC/FATIGUE. Crack and bend faults that resemble field defects discussed in Section 4.2 are introduced in the proposed flexible model. Symptoms of faults in the flexible connecting rod are compared with normal-healthy system. Models are further used to study crack growth in connecting rod and estimate its RUL.

Solid models are meshed with TET10 elements and meshed models are interfaced with RBE2 elements. MNF for the first 26 modes is created using CB model reduction technique. In MBD, crankshaft main bearing, crank pin - connecting rod journal, connecting rod - piston pin journal, piston pin - piston and piston - liner joints are modelled as revolute or slider joint. In MBD tool, a rigid cranktrain is built and converted into complete flexible cranktrain by replacing the rigid components with its MNF components. The generalised coordinates due to rigid MBD motions are subtracted from generalised coordinates of FMBD to obtain crankshaft and piston vibrations.

Engine base and cylinder head vibrations are computed from crank and cam shaft, and piston and valve vibrations. Responses from LMD and FMBD models are compared with a set of experimental results. Following section discusses the powertrain model idealisation, force estimation and solution. Figure 4.4 shows its framework.

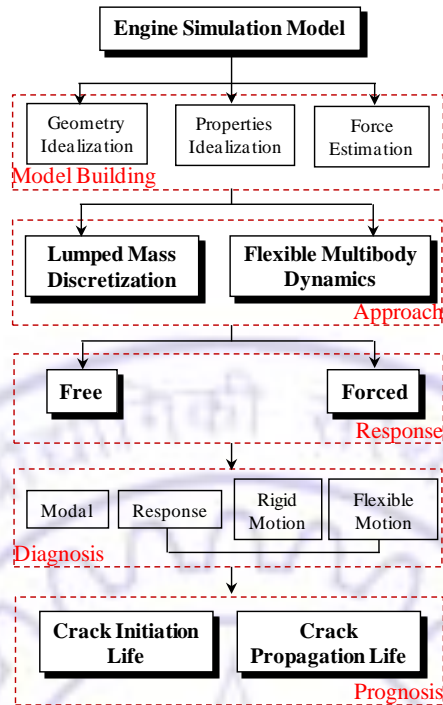


Figure 4.4: Framework for Physics-based Engine Health Management

4.3.2 Model Idealisation

Effect of powertrain idealisation, flexibility and model reduction are studied using LMD and MBD in MATLAB and ADAMS respectively. In LMD, models are built with different support and excitation conditions. Rotor dynamic effects are included in accordance with [Friswell et al. \[18\]](#) and [Rao \[198\]](#). In FMBD, models are built by converting rigid components into flexible using the procedure discussed in [\[199-200\]](#). Engine base and cylinder head vibrations of these models are studied.

In LMD modelling,

Model No. 1: 4 DOF Crankshaft, Camshaft, 2DOF Conn. Rod and 1DOF Valvetrain

Model No. 2: Base Excitation on Crankshaft and Connecting Rod

Model No. 3: Base Excitation on 20 DOF Crankshaft and Connecting Rod

Model No. 4: 24 DOF Coupled Cranktrain (Flexible Crankshaft and Connecting Rod)

In MBD modelling,

Model No. 5: Complete Rigid Cranktrain

Model No. 6: 1,28,925 DOF Flexible Crankshaft

Model No. 7: 12,054 DOF Flexible Connecting Rod

Model No. 8: 3,699 DOF Flexible Piston Pin

Model No. 9: 27,675 DOF Flexible Piston

Model No. 10: 1,72,353 DOF Complete Flexible Cranktrain

Model No. 11: Complete Rigid Valvetrain

Model No. 12: 65,085 DOF Complete Flexible Valvetrain

Model No. 1: 4 DOF Crankshaft, 2DOF Conn. Rod and 1DOF Valvetrain

In this model, a 4 DOF $(x, y, \varphi_x, \varphi_y)$ crankshaft, 2 DOF (y, φ_z) connecting rod and 1DOF (y) valvetrain are treated as separate models on rigid support as shown in Figure 4.5 (b) and Figure 4.6 (b, d) respectively. Crankshaft and rotating mass of connecting rod are lumped with flywheel mass located at the intersection point of slider and crankshaft axis. Sliding mass (reciprocating mass of connecting rod and piston assembly) is modelled at the slider. EOMs of crankshaft are modelled using rotor dynamics as discussed in [18],

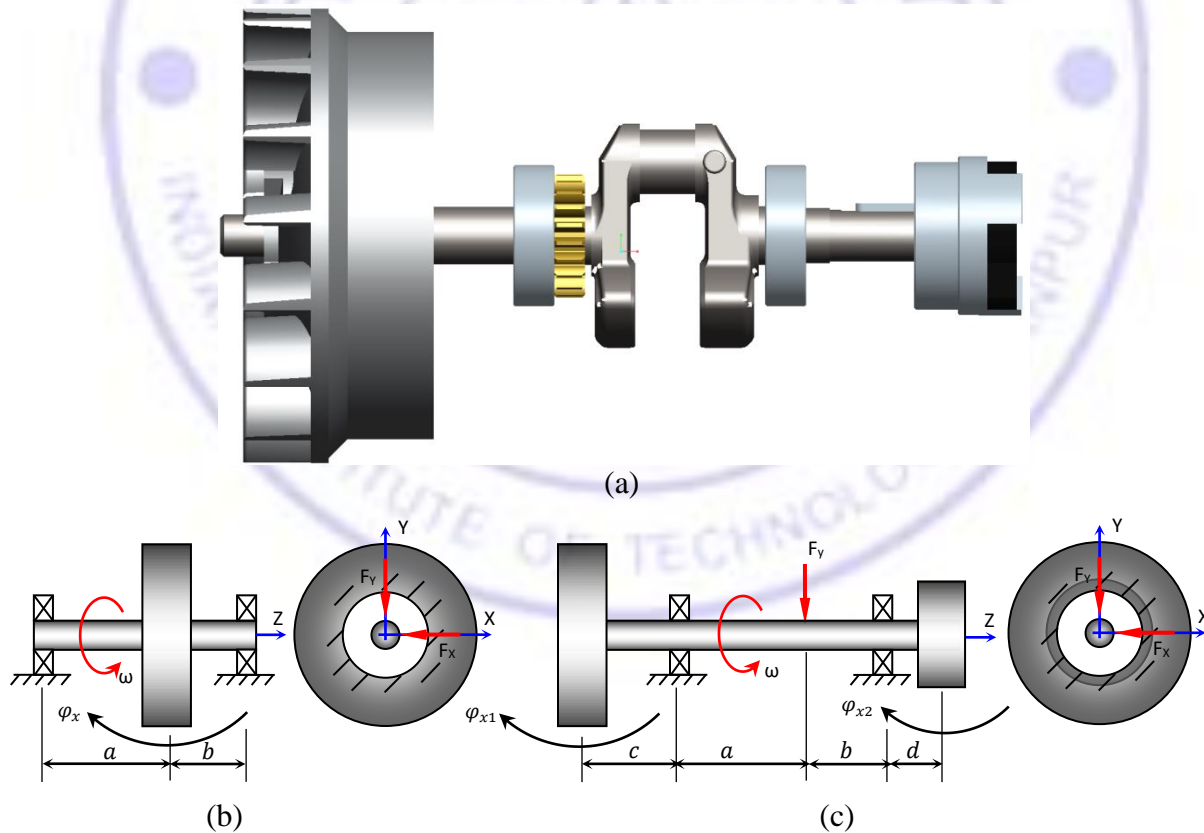


Figure 4.5: Crankshaft Solid Model and its LMD; (a) Solid Model, (b) Masses Lumped at Axis Centre, (c) Masses Lumped at Flywheel and Coupling Centres

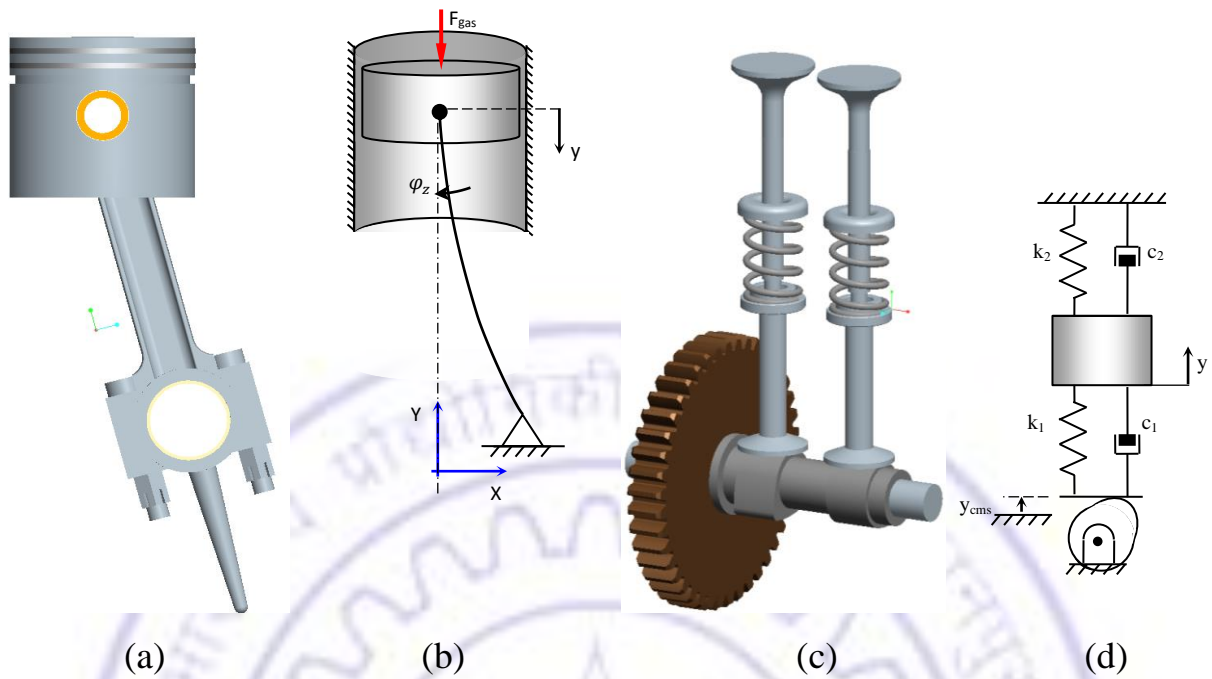


Figure 4.6: Conn.Rod and Valvetrain Solid Models and LMD; (a, b) Conn. Rod Solid Model and its Lumped Mass Model, (c, d) Valvetrain Solid Model and its Lumped Mass Model

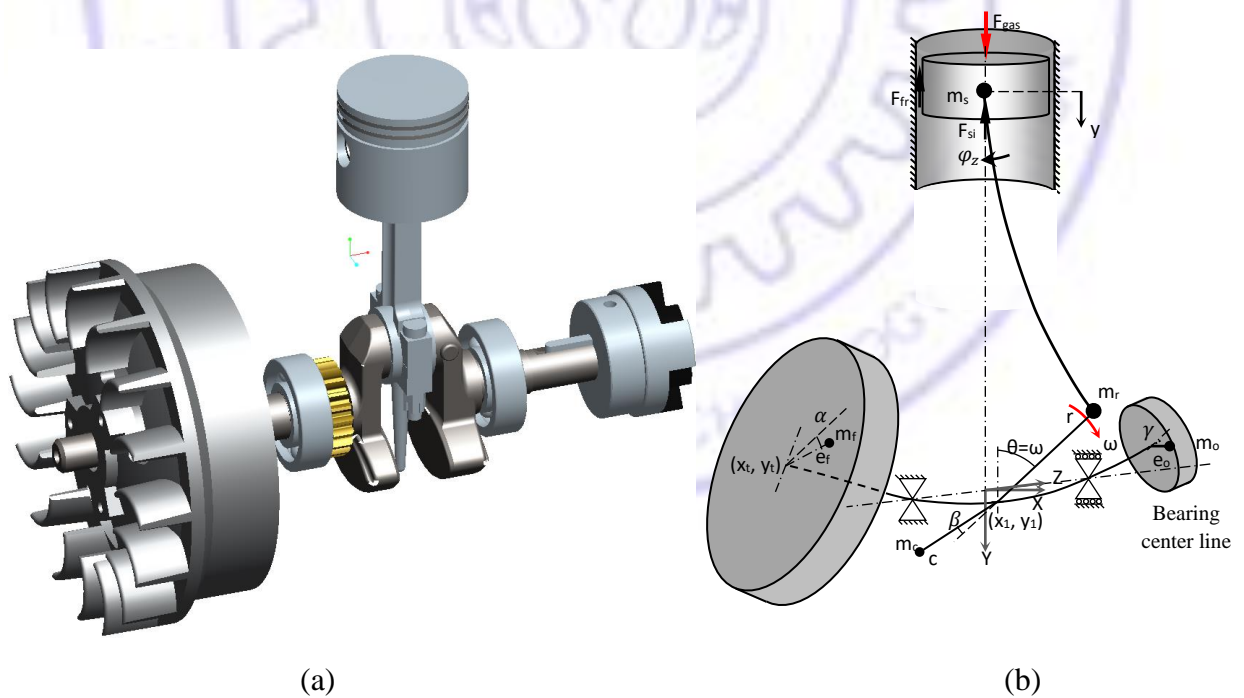


Figure 4.7: Cranktrain Solid Model and its LMD; (a) Solid Model, (b) Kinetostatic Condition of Flexible Cranktrain

$$m\ddot{x} + c_{xx}\dot{x} + k_{xx}x + c_{x\varphi_y}\dot{\varphi}_y + k_{x\varphi_y}\varphi_y = F_{riX}(\omega t) + F_{ciX}(\omega t) + F_{fiX}(\omega t) + F_{oiX}(\omega t) \quad 4.8$$

$$m\ddot{y} + c_{yy}\dot{y} + k_{yy}y + c_{yx}\dot{\varphi}_x + k_{y\varphi_x}\varphi_x = F_{riY}(\omega t) + F_{ciY}(\omega t) + F_{fiY}(\omega t) + F_{oiY}(\omega t) + F_{siY}(\omega t) + F_{gas}(\omega t) + F_{fr}(\omega t) + F_{rg} + F_{cg} + F_{fg} + F_{og} + F_{sg} \quad 4.9$$

$$I_d\ddot{\varphi}_x + I_p\Omega\dot{\varphi}_y + c_{\varphi_{xy}}\dot{y} + k_{\varphi_{xy}}y + c_{\varphi_x\varphi_x}\dot{\varphi}_x + k_{\varphi_x\varphi_x}\varphi_x = 0 \quad 4.10$$

$$I_d\ddot{\varphi}_y - I_p\Omega\dot{\varphi}_x + c_{\varphi_{yx}}\dot{x} + k_{\varphi_{yx}}x + c_{\varphi_y\varphi_y}\dot{\varphi}_y + k_{\varphi_y\varphi_y}\varphi_y = 0 \quad 4.11$$

where, suffix r, c, f, o and s denotes the rotating, counter, flywheel, coupling and slider masses respectively. Notations X and Y represents horizontal and vertical directions, i and g are inertia and gravity terms. F_{gas} is gas force and F_{fr} is friction force. I_d, I_p and Ω are the diametral and polar moment of inertia, and angular velocity of flywheel respectively. By retaining same notations used in Equation 4.8-4.11, the EOM for connecting rod are,

$$m\ddot{y} + c_{yy}(\omega t)\dot{y} + k_{yy}(\omega t)y + c_{yz}(\omega t)\dot{\varphi}_z + k_{y\varphi_z}(\omega t)\varphi_z = F_{gas}(\omega t) + F_{siY}(\omega t) + F_{fr}(\omega t) + F_{sg} \quad 4.12$$

$$I_d\ddot{\varphi}_z + c_{\varphi_{zy}}(\omega t)\dot{y} + k_{\varphi_{zy}}(\omega t)y + c_{\varphi_z\varphi_z}(\omega t)\dot{\varphi}_z + k_{\varphi_z\varphi_z}(\omega t)\varphi_z = 0 \quad 4.13$$

In the above equations, moments ($f_y e \cos \omega t \varphi_x$ and $f_x e \sin \omega t \varphi_y$, where e and φ are eccentricity of load and angular displacement respectively, f_x and f_y are internal elastic forces) due to internal elastic and damping forces that have quadratic angular displacement terms, which are very small and can be neglected. Crankshaft stiffness values are adopted from pinned - pinned beam theory given in [Friswell et al. \[18\]](#) as: $k_{xx} = k_{yy} = 3EI(a^3 + b^3)(ab)^{-3}$, $k_{x\varphi_y} = -k_{y\varphi_x} = 3EI(a^3 - b^3)(ab)^{-2}$, $k_{\varphi_y\varphi_y} = k_{\varphi_x\varphi_x} = 3EI(a + b)(ab)^{-1}$, while for connecting rod: $k_{yy}(\omega t) = EAl^{-1} + (3EI l^{-3} - EAl^{-1}) \lambda^2 \sin^2 \omega t$, $k_{\varphi_z\varphi_z}(\omega t) = EAl/3 + EI/l$ and $k_{y\varphi_z}(\omega t) = -0.5EA\sqrt{1 - \lambda^2 \sin^2 \omega t} - 1.5EI l^{-2} \lambda \sin \omega t$ are estimated from frame theory. $\lambda = r/l$ is crank to connecting rod length ratio. Notations are shown in Figure 4.7 (b) and the parameter values are listed in Table 4.1. To avoid geometric non-linearity, the fluctuation of λ and ωt for deformed conditions are ignored, since connecting rod deformations are very small in comparison to its length. Material damping of the components are estimated using Rayleigh damping expression: $C = \alpha_1 M + \alpha_2 K$, where damping matrix is a linear combination of mass M and stiffness K matrices. Real scalars α_1 and α_2 are damping ratios assumed as 3% and 5%, for crankshaft at 200 Hz and 1000 Hz respectively, and for connecting rod at 500 Hz and 1000 Hz respectively. In valvetrain, cam jumps-in the

valve system, drives the valve and jumps-out, so it induces free and forced vibrations. Initially, cam makes an impact on the follower and get in contact with valve spring by closing the valve clearance. At the end of the valve lift, cam separates, so valve hits the valve seat due to the stretching of spring. EOM of cam dynamics as discussed in Norton [201] is used to model the valvetrain. EOM for jump-in and jump-out conditions of the cam is,

$$m\ddot{y} + c_2\dot{y} + k_2y = 0 \quad 4.14$$

For contact condition of the cam,

$$m\ddot{y} + c_2\dot{y} + k_2y = c_1(\dot{y}_{cms} - \dot{y}) + k_1(y_{cms} - y) \quad 4.15$$

where m indicates the entire mass of the follower train, k_2 and c_2 are valve spring stiffness and damping, k_1 and c_1 are follower stiffness and damping respectively. y_{cms} is the cam lift.

Equations 4.8-4.15 are solved numerically for every crank angle with ODE45 and ODE15s as discussed in Section 4.3.1 simulation methodology. Powertrain vibrations are being transmitted to the engine base through crankshaft and camshaft bearings, slider and valve joints. Valve vibrations are combined with slider to predict cylinder head vibrations. Crankshaft and camshaft vibrations are combined for engine base vibrations. The measured vibrations at cylinder head and engine base are reported in Chapter 3. The measured and predicted vibrations of the selected models are compared in Section 4.5.2.

Table 4.1: System Parameters of the Engine

Parameters and units	Symbols	Values
Cylinder diameter [m]	D	0.055
Crankshaft rotating mass [kg] and crank length [m]	m_r and r	0.071 and 0.025
Counter mass [kg], length [m] and inclination [°]	m_c , c and β	0.116, 0.025 and 0
Conn. rod length and elastic properties [N, Nm ²]	l and EA , EI	0.098 and 8446200, 217.581
Flywheel, Coupling and Slider mass [kg]	m , m_o and m_s	2.935, 0.805 and 0.192
Crankshaft length dimensions [m]	a , b , c , d	0.0456, 0.0403, 0.060, 0.0513
Crankshaft dia. [m] and elastic property [Nm ²]	d_{cs} and EI	0.020 and 1649.336
Flywheel center [m] and inclination [°]	r_f and θ_f	9.245e-3, -19.890
Coupling center [m] and inclination [°]	r_o and θ_o	9.993e-5, 180
Conn. rod length and elastic properties [N, Nm ²]	l and EA , EI	0.098 and 8446200, 217.581

Model No. 2: Base Excited Crankshaft and Connecting Rod

In this model, the crankshaft of Figure 4.5 (b) receives motion excitation from Model No. 1 connecting rod and Figure 4.6 (b) is subjected to base excitation from Model No. 1 crankshaft motion. Elastic forces of other components are included in the Equations 4.8-4.13; Connecting rod forces in Equations 4.9 are replaced by its elastic forces, while Equations 4.12 - 4.13 accommodate elastic forces from crankshaft displacement y_{cs} and velocity \dot{y}_{cs} as,

$$m\ddot{y} + c_{yy}(\dot{y} - \dot{y}_{cs}) + k_{yy}(y - y_{cs}) + c_{yz}\dot{\varphi}_z + k_{y\varphi_z}\varphi_z = F_{gas} + F_{siY} + F_{fr} + F_{sg} \quad 4.16$$

$$I_d\ddot{\varphi}_z + c_{\varphi zy}(\dot{y} - \dot{y}_{cs}) + k_{\varphi zy}(y - y_{cs}) + c_{\varphi z\varphi_z}\dot{\varphi}_z + k_{\varphi z\varphi_z}\varphi_z = 0 \quad 4.17$$

Model No. 3: 20 DOF Crankshaft and 2 DOF Connecting Rod with Support Motion

It revises the Model No. 2 by a detailed crankshaft as shown in Figure 4.5 (c) with 20 DOF systems, where flywheel and coupling are modelled at their exact locations. Crankshaft mass and stiffness are obtained using FE approach. Inertia, gas and friction force on the respective nodes are assembled in \mathbf{f} force vector.

$$\mathbf{M}\ddot{\mathbf{z}} + (\mathbf{C} + \Omega\mathbf{G})\dot{\mathbf{z}} + \mathbf{K}\mathbf{z} = \mathbf{f}_{inertia} + \mathbf{f}_{gas} + \mathbf{f}_{friction} + \mathbf{f}_{gravity} \quad 4.18$$

Model No. 4: 24 DOF Coupled Cranktrain (Flexible Crankshaft and Connecting Rod)

In this model, the complete cranktrain is modelled with connecting rod that is linked to the crankshaft of Model No. 3. Global matrices are formed using FE assembly approach. The kinetostatics condition for every crank angle as shown in Figure 4.7 (b) is simulated.

Model No. 5: Complete Rigid Multibody Cranktrain

In MBD tool, the kinematic joints are modelled between the solid model components as shown in Figure 4.8 (a), EOM for rigid MBD given in [Shabana \[202\]](#) is,

$$\mathbf{M}\ddot{\mathbf{q}} + \Phi_{\mathbf{q}}^T\lambda = \mathbf{f}_{inertia} + \mathbf{f}_{gas} + \mathbf{f}_{friction} + \mathbf{f}_{gravity} + \mathbf{f}_v \quad 4.19$$

where λ is Lagrange multiplier vector and $\Phi_{\mathbf{q}}$ is constraint Jacobian matrix with initial condition $\Phi(\mathbf{q}, t) = \mathbf{0}$, such that $\Phi_{\mathbf{q}}\dot{\mathbf{q}} = \nu$, $\Phi_{\mathbf{q}}\ddot{\mathbf{q}} = \gamma$ and \mathbf{f}_v contains gyroscopic and Coriolis force components. Here generalized coordinates are due to pure rigid body motions.

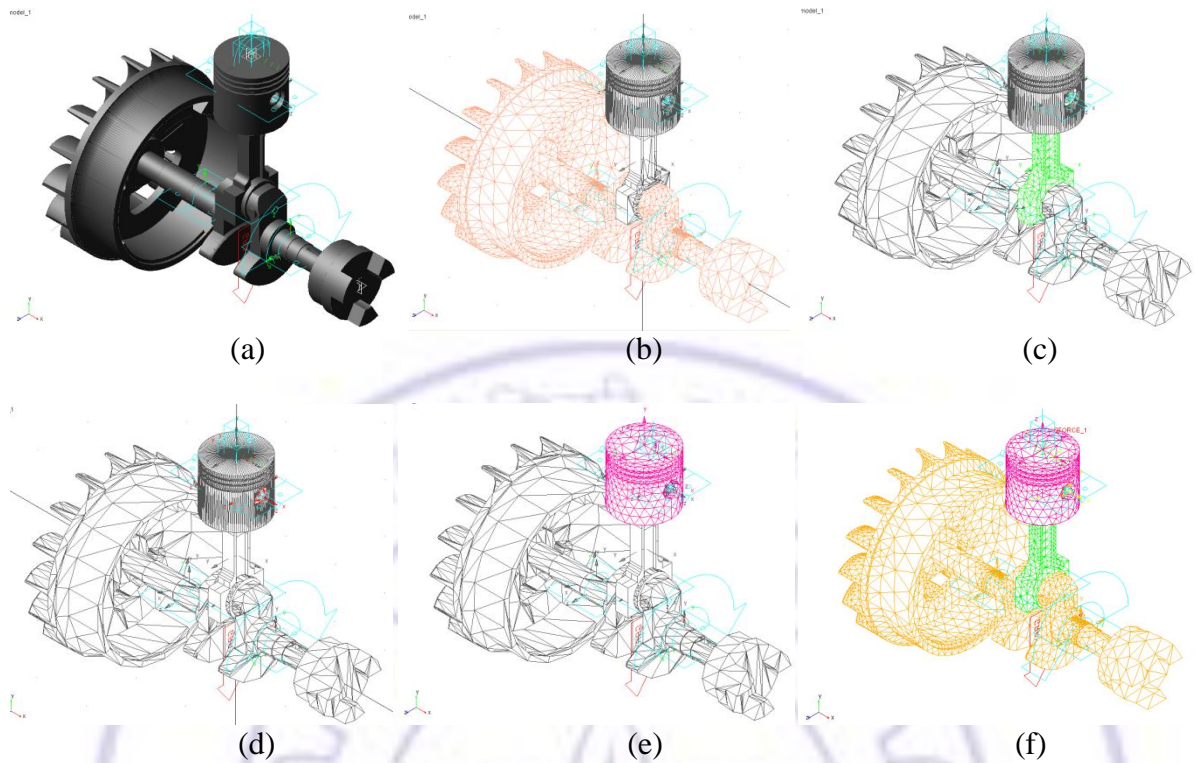


Figure 4.8: Cranktrain MBD Models: (a) Rigid Cranktrain, (b) Flex. Crankshaft, (c) Flex. Connecting Rod, (d) Flex. Piston Pin, (e) Flex. Piston, (d) Flex. Cranktrain

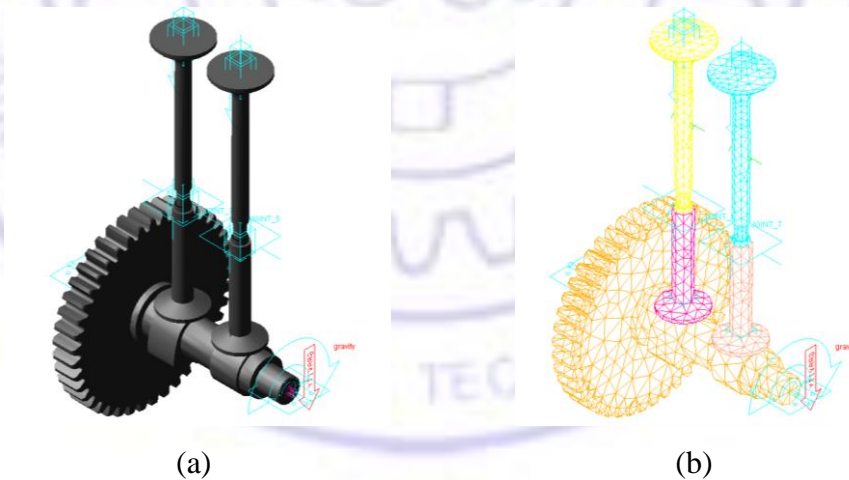


Figure 4.9: Valvetrain MBD Models: (a) Rigid Valvetrain, (b) Flex. Valvetrain

Model No. 6: Flexible Crankshaft

Rigid crankshaft of Model No. 5 is replaced by a flexible MNF of crankshaft with 1, 28, 925 DOFs. MNF is created with total 26 modes in NASTRAN and imported to ADAMS/Flex as

shown in Figure 4.8 (b). EOM of flexible MBD model is formulated in accordance with [Shabana \[202\]](#) and [Drab et al. \[203\]](#). The component vibrations can be obtained by subtracting rigid body generalized coordinates from flexible body.

$$M\ddot{q} + (C + \Omega G)\dot{q} + Kq + \Phi_q^T \lambda = f_{inertia} + f_{gas} + f_{friction} + f_{gravity} + f_v \quad 4.20$$

Model No. 7: Flexible Connecting Rod

This model is prepared by replacing the rigid connecting rod of Model No. 5 with flexible connecting rod MNF of 12, 054 DOFs as shown in Figure 4.8 (c).

Model No. 8: Flexible Piston Pin

In this model, the rigid piston pin of Model No. 5 is replaced by flexible piston pin MNF with 3,699 DOFs as shown in Figure 4.8 (d).

Model No. 9: Flexible Piston

Rigid piston of Model No. 5 is replaced by a flexible piston MNF with 27, 675 DOFs and the model is prepared as shown in Figure 4.8 (e).

Model No. 10: Complete Flexible Cranktrain

Flexible cranktrain (Figure 4.8 (f) with total 1, 72, 353 DOFs) is modelled by replacing components of Model No. 5 with respective flexible models that are used in Model No. 6-9.

Model No. 11: Complete Rigid Multibody Valvetrain

Similar to Model No. 5, a MBD model of valvetrain is built with rigid components; the kinematic joints are modelled between the solid model components as shown in Figure 4.9 (a). The valve spring is modelled by spring element.

Model No. 12: Complete Flexible Valvetrain

The flexible valvetrain (Figure 4.9 (b) with total 65,085 DOFs) is built by replacing rigid components of Model No. 11 with respective flexible MNFs.

4.3.3 Material Description

This section estimates material properties required for the engine physics-based modelling. Materials are issued by publications of ASM, SAE and Yamagata [204]. Cylinder block consist of heavy load carrying members that experiences high compressive strength, so in most cases it is a single piece with low carbon steel. Block of small engines is usually low carbon steel or liner is casted in aluminium block. Cylinder head is usually made of aluminium. Piston requires light and sufficiently strong material to handle the gas pressure generated by combustion; hence the piston is made of aluminium alloy. Piston rings have high elastic material made of fine grain cast iron or alloy spring steel that is not affected by working heat. Usually for larger engines, connecting rods are made of nickel, chrome, and chrome vanadium steels by forging, special types of cast-iron or nickel alloy castings that have good service life. In this study, engine has an aluminium connecting rod. Typical bearings are made of steel or bronze to which a lining of relatively soft bearing material is applied. Table 4.2 provides the materials; their structural properties that are used in the current physics-based modelling.

4.3.4 Load Estimation

Forces required for dynamic analysis are estimated and employed in the model. Major forces such as cranktrain inertia, gas, friction and gravitational forces are considered. While aerodynamic, magnetic, electrical forces etc. are neglected.

Table 4.2: Materials of the Engine Components

Components	Materials
Cylinder block	30C8, Low carbon steel
Cylinder head	Aluminum alloys
Piston	Aluminum alloy 4652, Al-Si-Cu-Mg alloy
Piston ring	Fine Grain or Silicon Cast Iron, Spring steel and stainless steel
Tappet valve	Heat resistive steel, Alloy steel
Valve spring	Spring steel, music wire
Push rod	Medium carbon steel
Crankshaft, Camshaft, Piston pin	Plain carbon steel 10C4, Co-Mo steel, 37C15 Alloy steel
Exhaust manifold	High-Si cast iron, Stainless steel tube and sheet
Flywheel	Cast iron
Gears	Mild steel
Journal bearings	Al-Si-Sn and Cu-Pb alloys
Main bearings	SKF 6043-C3, white metal, leaded bronze
Lubricant	SAE 20W40

Gravitational Forces: Due to considerable self weight of the engine, the gravitational effects are employed in physics-based model. In LMD model, these forces are computed separately and added to the net vertical force. In MBD, acceleration due to gravity, ‘ g ’ is activated in vertical direction of the model.

Gas Force: It is estimated from cylinder pressure data for the entire speed range. Cylinder pressure history can be obtained either from experimental or simulation approach. Experimental approach requires a pressure transducer, additional instrumentation and a setup, while simulation uses thermodynamic model tuned to its test performance. Simulation model is useful to obtain gas pressure history, temperature profiles and friction forces for entire speed range. In this work, gas force is estimated by building a thermodynamic model and correlating it its measured power and torque curves. The load profiles at various speeds are generated and fed to a simulation model.

Thermodynamic model uses 1D gas dynamics to simulate combustion and flow in pipes. Engine geometry, valve and ignition timings are iterated for optimal power, torque, fuel consumption and noise. It solves conservation and thermodynamic laws for calculating pressure, temperature, fluid velocity along the flow by employing mixing model, work heat transfer model, mass transport and gas properties at elevated conditions. Charge is divided into un-burnt and burnt gas zones under chemical equilibrium. Fuel burn rate controls the mixing zone. Mass and energy conservation relations are established based on first law of thermodynamics. For IC engine, it can be formulated as “change of internal energy in the cylinder is the sum of fuel heat input, wall heat losses, piston work, enthalpy flow due to charge, blow-by, exit and evaporation energies”, represented in equation form as [205],

$$\frac{d(m_c u)}{d(\omega t)} = \frac{dQ_F}{d(\omega t)} - \sum \frac{dQ_w}{d(\omega t)} - p_c \frac{dV}{d(\omega t)} + \sum h_i \frac{dm_i}{d(\omega t)} - h_{bb} \frac{dm_{bb}}{d(\omega t)} - \sum h_e \frac{dm_e}{d(\omega t)} - q_{ev} f \frac{dm_{ev}}{d(\omega t)} \quad 4.21$$

where u , Q_F , Q_w , q_{ev} are internal, fuel, wall heat and evaporating fuel energies respectively. m_c , m_i , m_{bb} , m_e and m_{ev} are cylinder, charge, blow-by, exhaust and evaporating fuel masses respectively. h_i , h_{bb} and h_e are enthalpies corresponding to charge, blow-by and exhaust respectively. Cylinder volume V is obtained using displacement and compression ratio

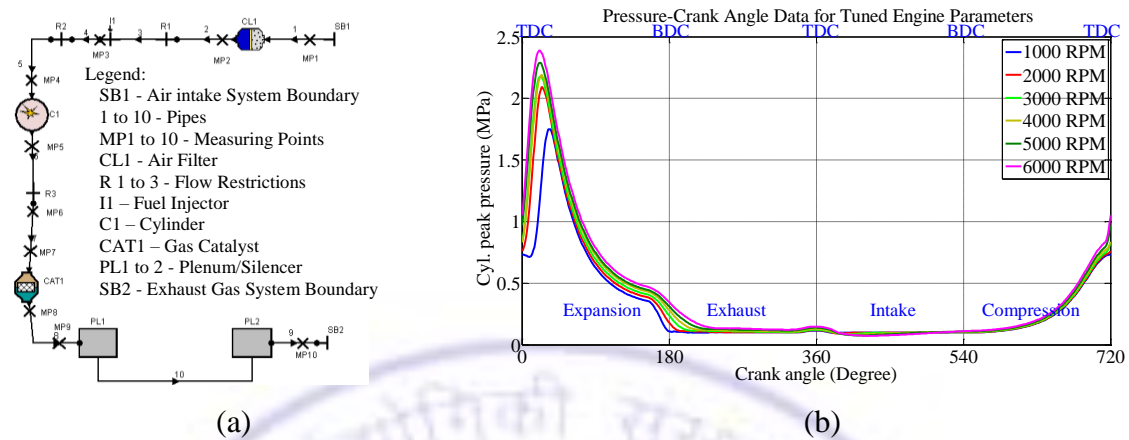


Figure 4.10: Engine Cycle Simulation; (a) Layout, (b) Cyl. Pressure-Crank Angle Results

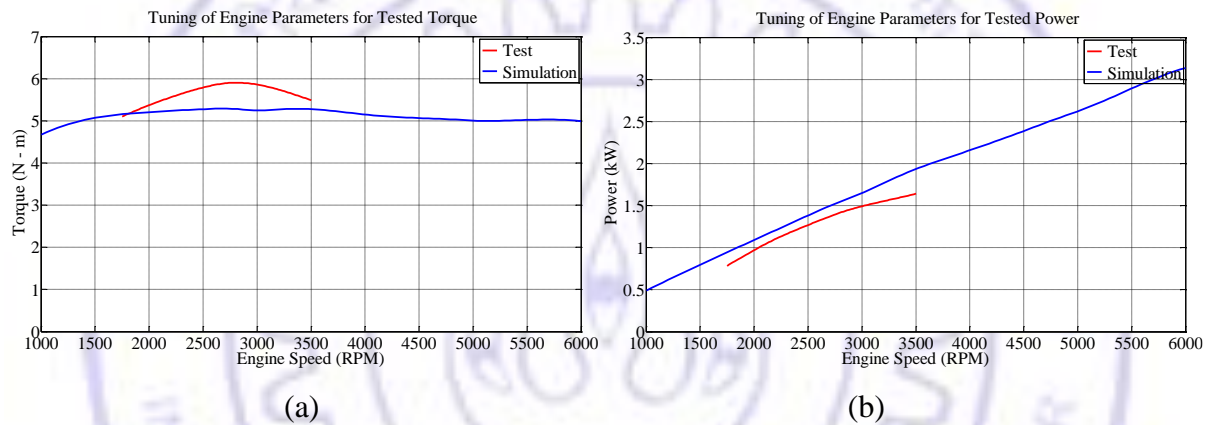


Figure 4.11: Tuned Parameters-Simulated v/s Test; (a) Torque, (b) Power

information, and p_c denotes cylinder pressure. Thermodynamic state is solved for in-cylinder temperature and cylinder pressure can be obtained from gas equation. Heat transfer to walls of the combustion chamber is calculated using heat transfer models. Rate of heat release at a specific operating point is determined from generic cylinder pressure history and combustion models. Air and combustion product rate are calculated from the un-burnt and burnt mixture zones separately. Mole fractions burnt are computed from the chemical equilibrium. Simulation can be carried-out using discretized approach (Ramachandran [206]) or commercial engine cycle software such as WAVE, BOOST and POWER. In this work, BOOST has been used; it simulates a wide variety of IC engines by modelling cylinder, plenum, pipe and system boundaries with 1D element. It computes mean values of pressures, temperatures and flow velocities over cross-section of the pipes using gas dynamic equations.

Flow losses and heat release are modelled by flow coefficients and combustion models respectively. Figure 4.10 (a) shows thermodynamic layout of study engine; it is constructed with measured geometrical dimensions and test data from manufacturer. It is tuned with varying effective length of pipes to optimally match test performance curves. Figure 4.11(a and b) shows comparison of tuned torque and power curves respectively with test. Attempts to further reduce simulation error in a torque curve of Figure 4.11(a) have shown an increased error in power curve of Figure 4.11(b). However trend of simulated curves have a close match with test. Tuned model is explored for speed where no test data is available. Tuned model is further used to compute cylinder pressure for varying speeds as shown in Figure 4.10 (b). At full-load condition, cylinder pressure - crank angle data is converted into gas load F_{gas} and normal force F_n as discussed in [Kolchin and Demidov \[207\]](#) as,

$$F_{gas} = (p_g - p_0)A \quad 4.22$$

$$F_n(\omega t) = (-F_{gas} + F_{siY}) / \sqrt{\frac{1}{\lambda^2 \sin^2(\omega t)} - 1} \quad 4.23$$

where A , p_g and p_0 are bore area, cylinder pressure and ambient pressure respectively. These loads are applied as input loads to the physics-based models.

Inertia Forces: Counter, rotating and reciprocating masses of crankshaft, connecting rod, and piston slider masses are estimated using engine dynamics ([Rangwala \[208\]](#)). Crankshaft counter mass is estimated from CAD model by a trial mass at crankpin and iterated until COG aligns to origin, connecting rod masses are estimated based on COG of the connecting rod. Mass and COG of flywheel and coupling are extracted from CAD model. Counter, rotating and slider mass are modelled at their respective centres and forces are computed for every instantaneous crank angle ωt . Slider inertia force F_{siY} in vertical direction is $m_s r \omega^2 [\cos(\omega t) + \lambda \cos(2\omega t)]$. Rotating, counter, flywheel and coupling inertia forces are F_{riY} , F_{ciY} , F_{fiY} and F_{oiY} in vertical direction with expressions $m_r r \omega^2 \cos(\omega t)$, $m_c c \omega^2 \cos(\omega t + \pi + \beta)$, $m_f e_f \omega^2 \cos(\omega t + \alpha)$ and $m_o e_o \omega^2 \cos(\omega t + \gamma)$ respectively. While in horizontal direction, forces are represented as F_{riX} , F_{ciX} , F_{fiX} and F_{oiX} with expressions $m_r r \omega^2 \sin(\omega t)$, $m_c c \omega^2 \sin(\omega t + \pi + \beta)$, $m_f e_f \omega^2 \sin(\omega t + \alpha)$ and $m_o e_o \omega^2 \sin(\omega t + \gamma)$ respectively. These notations are described in Figure 4.7 (b) and values are listed in Table 4.1.

LMD modelling practice in MATLAB is verified with commercial tools (Pro/ Mechanism and ADAMS) for net vertical and horizontal loads on bearing at 3000 rpm. Gravitational, gas, and inertia force are considered on the respective component. Component masses are obtained from the measurement and COG is extracted from CAD model. LMD forces for every crank angle as shown in Figure 4.12 (a). They are modelled as,

$$F_X(\omega t) = F_n(\omega t) + F_{riX}(\omega t) + F_{ciX}(\omega t) + F_{fiX}(\omega t) + F_{oiX}(\omega t) \tag{4.24}$$

$$F_Y(\omega t) = F_{gas}(\omega t) + F_{riY}(\omega t) + F_{ciY}(\omega t) + F_{fiY}(\omega t) + F_{oiY}(\omega t) + F_{siY}(\omega t) + F_{rg} + F_{cg} + F_{fg} + F_{og} + F_{sg} \tag{4.25}$$

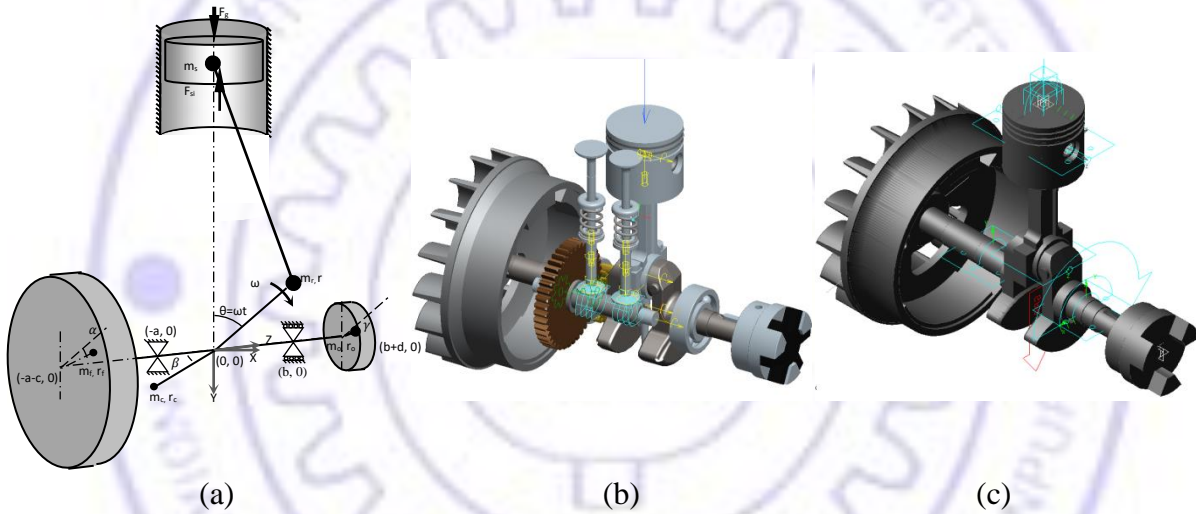


Figure 4.12: Powertrain Dynamic Models; (a) MATLAB, (b) Pro/Mechanism, (c) ADAMS

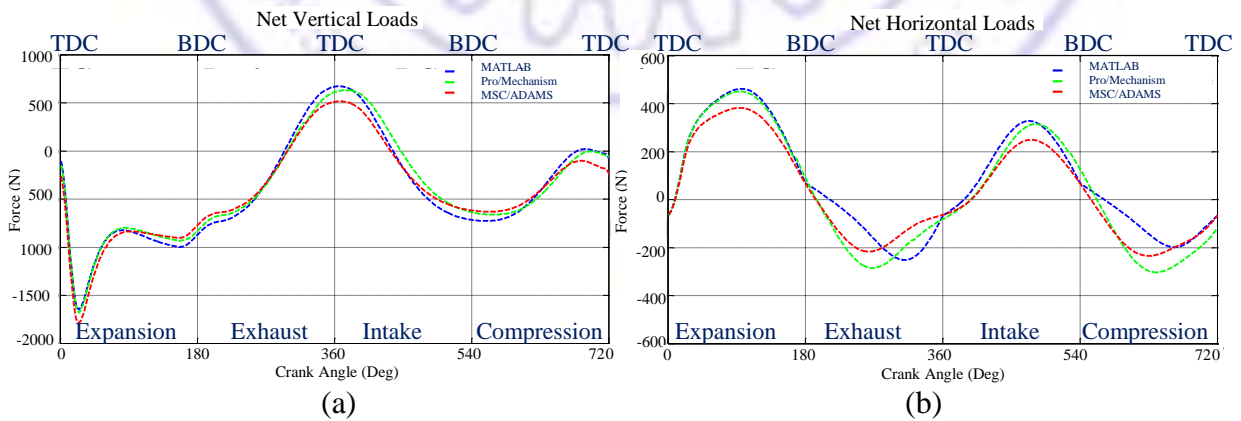


Figure 4.13: Net Forces on Crankshaft-MATLAB v/s Commercial Tools; (a) Vertical Loads, (b) Horizontal Loads

In Pro/ENGINEER and ADAMS, kinematic joints are established between the components and net load on the joints are computed by performing rigid body dynamic analysis. Figure 4.12 (b) shows the detailed rigid body powertrain model as simulated in Pro/Mechanism module. In ADAMS, rigid body cranktrain model is built by removing small geometrical features as shown in Figure 4.12 (c). Figure 4.13 indicates the net vertical and horizontal loads on the crankshaft. Dashed blue line indicates load estimated from the MATLAB, while dashed green and red indicates values from Pro/Mechanism and ADAMS. Plots show detailed geometry has contributed to higher balancing by reducing vertical forces and increasing horizontal forces to bring them closer to each other.

Frictional Force: Mistry [209] estimated that about 40-50% of mechanical frictional losses are due to friction between piston ring and cylinder wall interface that can significantly change engine performance. Frictional force is estimated and included in the LMD model. ADAMS has an option to include both static and dynamic friction coefficients. Reynolds equation derived by Patir and Cheng [210] for hydrodynamic lubrication is,

$$\frac{\partial}{\partial x} \left(\frac{\varphi_x h^3}{\mu} \frac{\partial \bar{p}}{\partial x} \right) = 6u \frac{\partial \bar{h}_T}{\partial x} + 6u\sigma \frac{\partial \varphi_s}{\partial x} + 12 \frac{\partial \bar{h}_T}{\partial t} \quad 4.26$$

where u is sliding velocity, σ is surface roughness, μ is dynamic viscosity, φ_x and φ_s are flow and share factors, h is nominal film thickness, \bar{p} is mean hydrodynamic pressure and \bar{h}_T is average gap. It is solved numerically for pressure distribution; friction force is estimated using oil film pressure in conjunction with asperity contact pressure. Cho et al. [211]

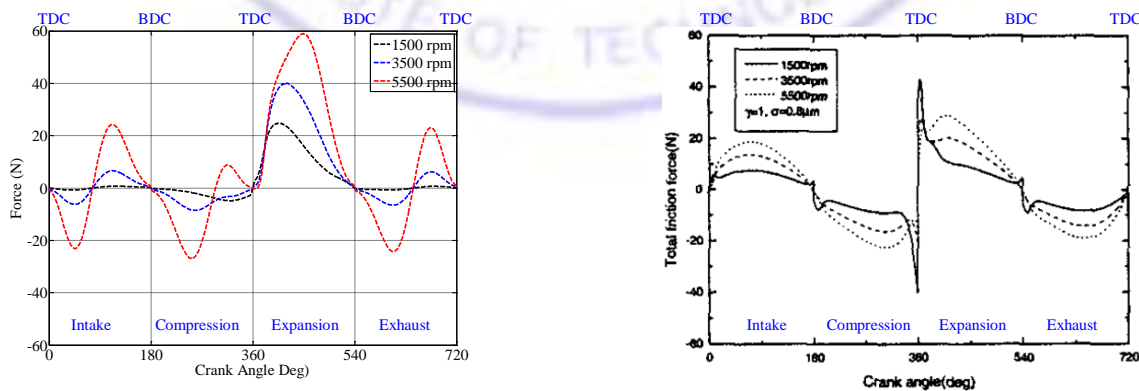


Figure 4.14: Total Ring Frictional Force: (a) Estimated, (b) From literature [211]

solved friction for a similar engine and reported the total friction force. It is the sum of viscous and boundary friction. This approach is accurate, but it is tedious to solve as it demands several numerical integrations. Stribeck speed dependent model is a simple empirical expression that takes less computational time and it is expressed by,

$$F_f(\omega t) = F_n f \left(\frac{v}{Av^2 + B|v| + C} + Dv \right) \quad 4.27$$

where f is a overall scaling factor, A, B, C and D are friction parameters, for medium speed engines they are 1.5, 57m/s, 0, 1.5m/s and 3.6×10^{-3} respectively. Ring friction force for three different speeds from the simulation estimated and literature [210] are shown in Figure 4.14 (a) and Figure 4.14 (b) respectively. Literature solves Equation 4.26 for minimum oil film thickness. Viscous friction force is obtained from viscous shear stress caused by hydrodynamic lubrication and boundary friction force due to asperity contact. Simulation has not captured friction force at both TDC and BDC properly, while overall amplitudes and nature are well matched with the published literature. In firing stroke, both have reported high friction force. Stribeck friction force is included in the analysis of LMD models. MBD model has an option to include static and dynamic friction coefficients. Friction force is measured for similar engine in Takiguchi et al. [212] and Mufti et al. [213]; a comparison indicates that the computed amplitudes have a close match and similar trend.

4.4 Model Solution for Fault Diagnosis

This section reviews solution approach for LMD and MBD models. Cranktrain LMD model is formulated using rotor dynamics by using MATLAB scripts given in [18]. In MBD approach, Rigid and flexible models of the cranktrain are constructed in ADAMS. These models are solved for free and forced vibration characteristics.

4.4.1 Free Vibration Response

Free vibration results (natural frequencies and mode shapes) points the permissible range of operation, which can be obtained by ignoring external applied force terms in Equation 4.8-4.20. Free vibrations due to the impact are computed by solving,

$$\begin{Bmatrix} \dot{x} \\ \dot{\ddot{x}} \end{Bmatrix} = \begin{bmatrix} 0 & I \\ -M^{-1}K & -M^{-1}C \end{bmatrix} \begin{Bmatrix} x \\ \dot{x} \end{Bmatrix} \quad 4.28$$

Free vibration solution of crankshaft using Model No. 1, 3 and 6 indicates that the first mode is 400, 250 and 317 Hz while second bending is 1700, 750 and 754 Hz respectively. This indicates different idealization leads to different characteristics. Crankshaft excitation frequency has 15-100 Hz range so it does not experience the resonance conditions, which makes extraction of modal characteristics from operating deflection shape is difficult. Minute variations of the actual defects occur at the surfaces so the global mass and stiffness matrices remain unaltered, and modal characteristics do not change significantly. Hence forced vibration is required to be explored for studying the engine fault diagnosis.

4.4.2 Forced Vibration Response

Change in amplitudes of vibration and stress information during motion can be used to detect defect. In LMD approach, powertrain forced response is proposed to detect the added defects. Consideration of crank angle dependent stiffness and damping of connecting rod, gyroscopic effects, speed dependent stiffness and damping properties of crankshaft can help to represent its accurate dynamics. Forces estimated in Section 4.3.4 at 1500 rpm are employed. Vibration solutions of discrete crankshaft, slider and camshaft under rigid support are obtained from,

$$\begin{Bmatrix} \dot{x} \\ \dot{\ddot{x}} \end{Bmatrix} = \begin{bmatrix} 0 & I \\ -M^{-1}K & -M^{-1}C \end{bmatrix} \begin{Bmatrix} x \\ \dot{x} \end{Bmatrix} + \begin{Bmatrix} 0 \\ M^{-1}F \end{Bmatrix} \quad 4.29$$

In case of camshaft, inertia and valve spring-damper elastic forces are included in the force term.

$$\begin{Bmatrix} \dot{x} \\ \dot{\ddot{x}} \end{Bmatrix} = \begin{bmatrix} 0 & I \\ -M^{-1}K & -M^{-1}C \end{bmatrix} \begin{Bmatrix} x \\ \dot{x} \end{Bmatrix} + \begin{Bmatrix} 0 \\ M^{-1}Kx + M^{-1}C\dot{x} + M^{-1}F \end{Bmatrix} \quad 4.30$$

Valvetrain vibrations under cam lift condition, support motion excited by cam are included,

$$\begin{Bmatrix} \dot{x} \\ \dot{\ddot{x}} \end{Bmatrix} = \begin{bmatrix} 0 & I \\ -m^{-1}(k_1 + k_2) & -m^{-1}(c_1 + c_2) \end{bmatrix} \begin{Bmatrix} x \\ \dot{x} \end{Bmatrix} + \begin{Bmatrix} 0 \\ m^{-1}k_1x_{cms} + m^{-1}c_1\dot{x}_{cms} \end{Bmatrix} \quad 4.31$$

From the initial condition at $t = 0$, $z_0 = \begin{Bmatrix} x_0 \\ \dot{x}_0 \end{Bmatrix}$ and $\dot{z}_0 = \begin{Bmatrix} \dot{x}_0 \\ \ddot{x}_0 \end{Bmatrix}$, solution is obtained through integration schemes. A fourth order Runge-Kutta (ODE45, ODE15s) method is used to iterate for every crank angle. Time dependent solutions are obtained as, $z_t = z_{t-1} + \dot{z}_{t-1}\Delta t$. In case of MBD model, cranktrain and valvetrain vibrations are estimated using rigid and flexible MBD with FE modelling approach. Rigid MBD solution is obtained from,

$$\begin{Bmatrix} \ddot{\mathbf{q}} \\ \boldsymbol{\lambda} \end{Bmatrix} = \begin{bmatrix} \mathbf{M} & \boldsymbol{\Phi}_q^T \\ \boldsymbol{\Phi}_q & \mathbf{0} \end{bmatrix}^{-1} \begin{Bmatrix} \mathbf{f} \\ \gamma \end{Bmatrix} = \ddot{\mathbf{q}}_i \begin{Bmatrix} \mathbf{q}_0 \\ \dot{\mathbf{q}}_0 \end{Bmatrix} \quad 4.32$$

Flexible MBD, the solution is obtained from,

$$\begin{Bmatrix} \ddot{\mathbf{q}} \\ \boldsymbol{\lambda} \end{Bmatrix} = \begin{bmatrix} \mathbf{M} & \boldsymbol{\Phi}_q^T \\ \boldsymbol{\Phi}_q & \mathbf{0} \end{bmatrix}^{-1} \begin{Bmatrix} \mathbf{f} - (\mathbf{C} + \Omega\mathbf{G})\dot{\mathbf{q}} - \mathbf{K}\mathbf{q} \\ \gamma \end{Bmatrix} = \ddot{\mathbf{q}}_i \begin{Bmatrix} \mathbf{q}_0 \\ \dot{\mathbf{q}}_0 \end{Bmatrix} \quad 4.33$$

From initial condition at $t = 0$, $z_0 = \begin{Bmatrix} \mathbf{q}_0 \\ \dot{\mathbf{q}}_0 \end{Bmatrix}$ and $\dot{z}_0 = \begin{Bmatrix} \dot{\mathbf{q}}_0 \\ \ddot{\mathbf{q}}_0 \end{Bmatrix}$, accelerations and Lagrange multipliers can be integrated to obtain velocities and generalized coordinates. Time dependent solutions are then obtained. Component responses of the different models are compared and selected model is used to study fault symptom in time domain and their wavelet plots.

4.5 Model Evaluation, Reduction and Selection

This section reviews the most appropriate idealisation of above discussed models. Responses of different idealisation are compared and a set of computed response are compared with the experimental results for an identical case. Well correlated models are selected and further used for fault diagnosis and failure prognosis with initiating the defects.

4.5.1 Comparison of Model Responses

Figure 4.15 shows vertical vibrations of crankshaft at flywheel and slider mass that are computed from LMD Model No. 1-4. Figure 4.15 (a-b) indicates that the slider has high amplitude of vibrations in comparison to crankshaft. In Model No. 2, individual flexible effect of crankshaft and connecting rod are considered. Crankshaft and connecting rod

vibrations of Model No. 1 are fed to each other as base excitation and additional elastic forces. Figure 4.15 (c-d) specifies vibrations of crankshaft are not contributed significantly to the connecting rod, while connecting rod vibrations have increased the amplitude of crankshaft vibrations. It indicates that this idealization is not accurate and conforms crankshaft supports connecting rod while connecting rod does not support crankshaft. Figure 4.15 (e-f) shows vibrations of Model No. 3 (detailed crankshaft and slider). It indicates the detailed mass distribution and larger flexibility of crankshaft lowers vibration amplitudes. In Model No.1 and 2, masses are lumped at a single node that makes approximation crude and results in high amplitudes. In Model No. 4, cranktrain solution is obtained by solving kinetostatics condition for every crank angle, without considering multibody effects. Figure 4.15 (g-h) shows crankshaft has similar amplitudes but slider has showed lower amplitudes due to increased flexibility. It can be summarised that different idealisations give flexibility to include the details that give different responses. Appropriate idealization can be selected based on test correlation and model reduction. However Model No. 3 has sufficient details and has a realistic approximation, so it is selected to study fault diagnosis. It can incorporate unbalance and friction defects, but they have difficulty in modelling the crack and wear defects which requires detailed geometry, so FMBD models have been explored.

Figure 4.16 (a-b) shows vertical vibrations computed from camshaft and valve LMD models as discussed in Section 4.3.2. Vibrations due to collision of cam-tappet and valve-seat are computed for each event by including the collision conditions. It can be seen that the camshaft vibrations have two events, while valve has four events. Camshaft events have high frequency oscillations, while valves have low frequency vibrations. Engine base and cylinder head vibrations are computed by adding the camshaft and valve vibrations to the above simulated crankshaft and slider vibrations respectively. Figure 4.17 shows crankshaft and slider accelerations from MBD models (Models No. 5-10) in vertical direction, computed at centre of mass of the component. Figure 4.17 (a-b) shows acceleration plot computed from Model No. 5 rigid MBD, they represent pure rigid body motion. Due to large inertia force, they show high amplitude acceleration around TDC and BDC. Figure 4.17 (c-l) shows the acceleration plot of FMBD due to individual flexibility of crankshaft, connecting rod, piston pin, piston and complete cranktrain model respectively.

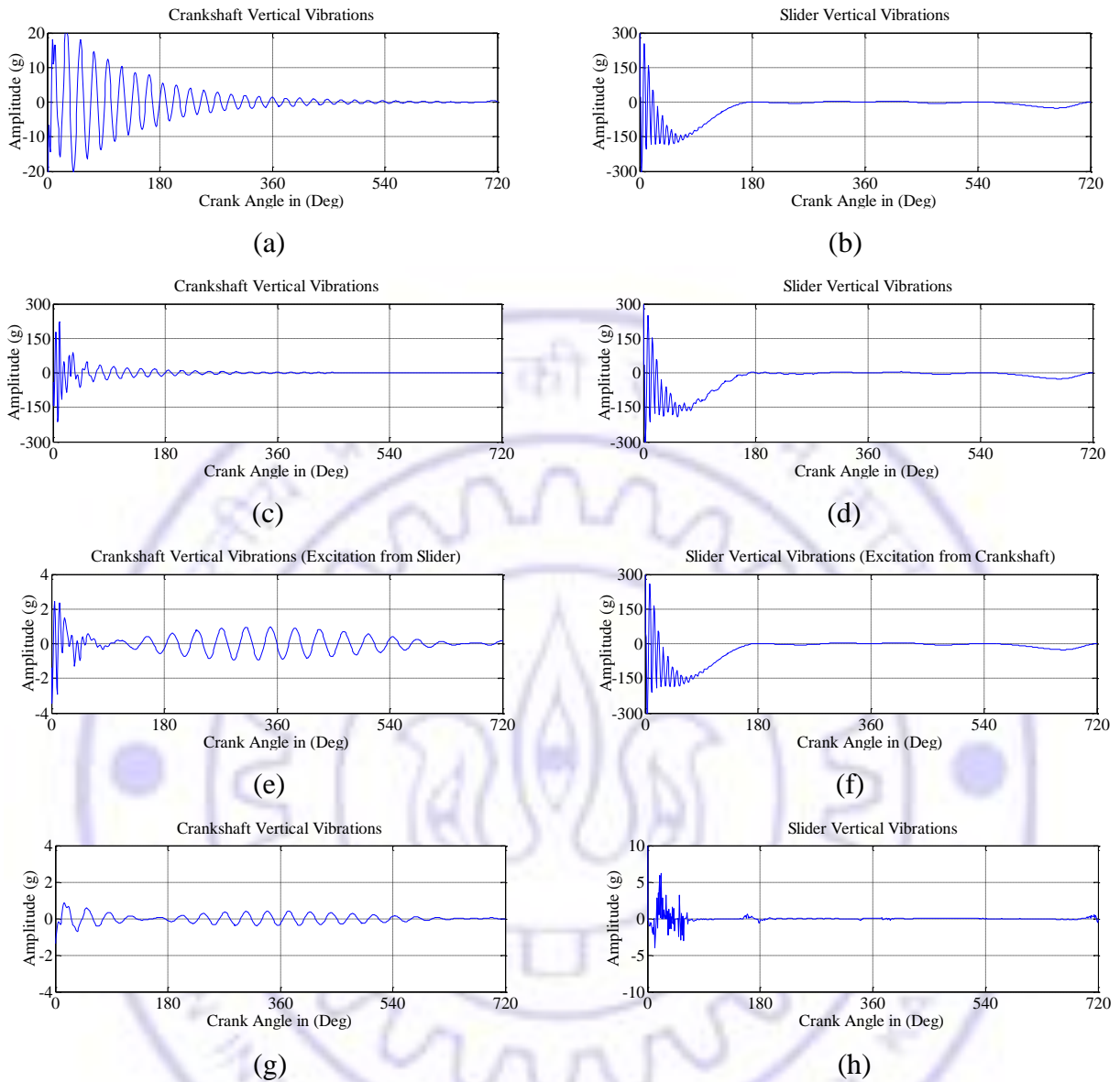


Figure 4.15: Crankshaft and Slider Vibrations of LMD Model; (a, b) Model No. 1, (c, d) Model No. 2, (e, f) Model No. 3 and (g, h) Model No. 4

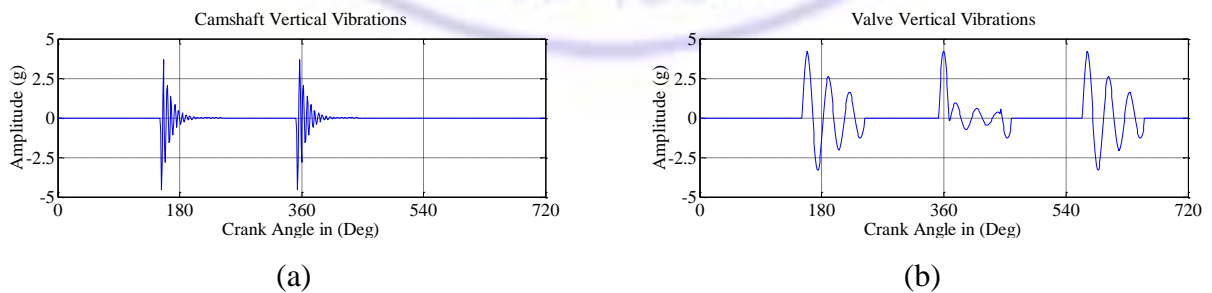


Figure 4.16: Camshaft and Valve Vibrations of LMD Model; (a, b) Model No. 1-4

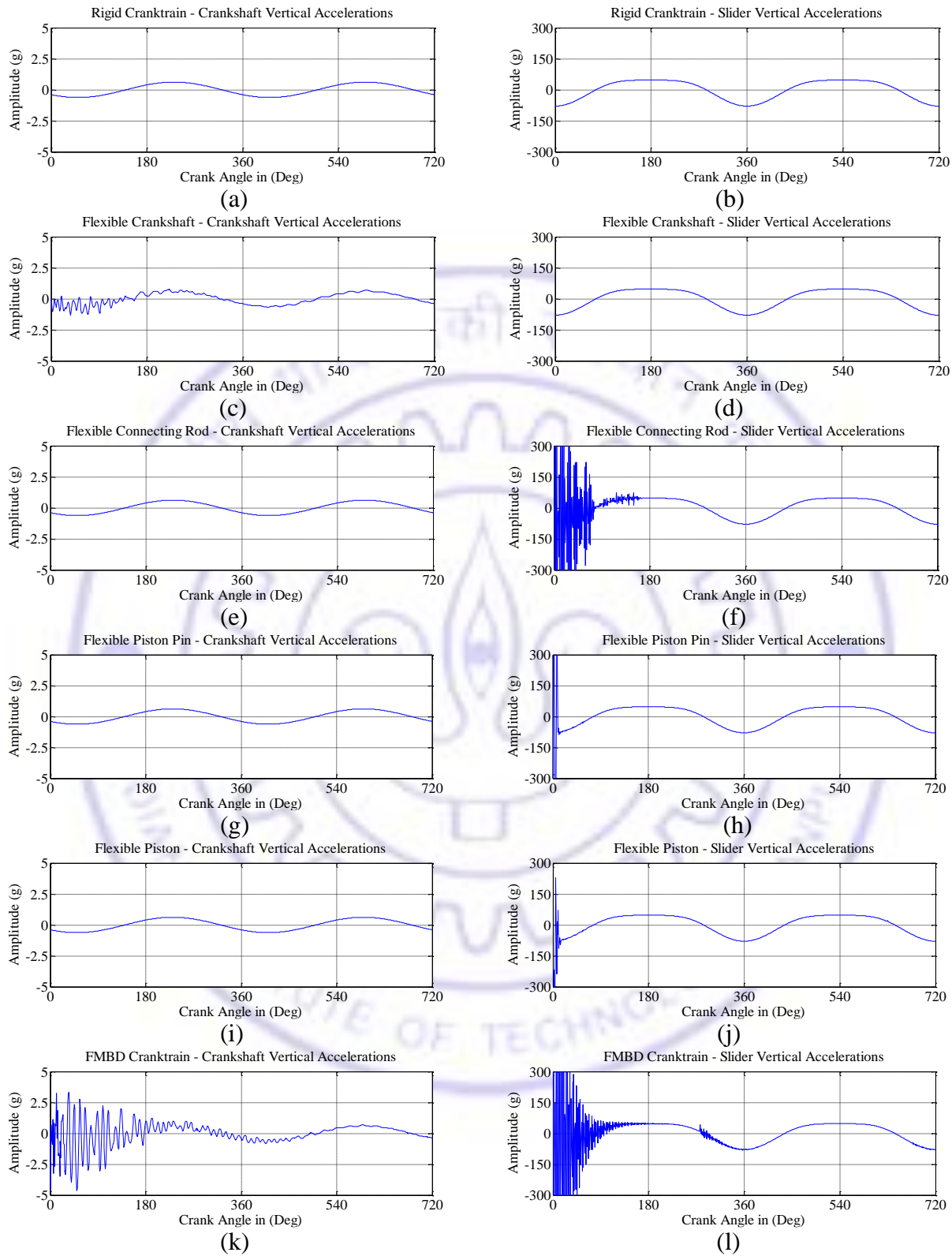


Figure 4.17: Accelerations of Crankshaft and Slider MBD Model; (a, b) Model No. 5, (c, d) Model No. 6, (e, f) Model No. 7, (g, h) Model No. 8, (i, j) Model No. 9, (k, l) Model No. 10

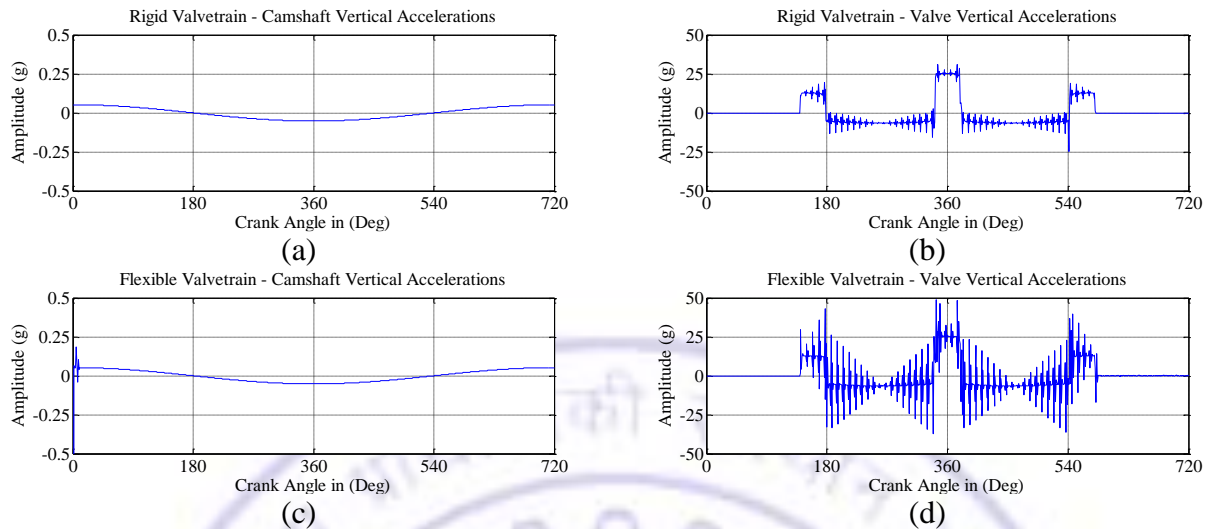


Figure 4.18: Accelerations of Camshaft and Valve MBD Model; (a, b) Model No. 11, (c, d) Model No. 12

Due to the added flexibility, components undergo rigid motion along with bouncing oscillation about the rigid motion to compensate internal elastic loads. It is evident that only crankshaft and connecting rod plays major contribution in cranktrain flexibility.

Camshaft and valve accelerations from MBD models (Models No. 11) in vertical direction are shown in Figure 4.18 (a-b), their accelerations due to flexibility of entire valvetrain (Models No. 12) are shown in Figure 4.18 (c-d). Valves have bouncing effect during their opening and closing. The camshaft has transient phenomena during the firing event.

Ricci [16] employed a model reduction by studying modal participation factor, model order and accuracy of selected models. A reduced model has a response with acceptable accuracy and a minimum number of component modes. Lowest number of modes used in CB modeling without losing the highest accuracy can be considered as reduced model. In this work, instead of selecting best order of a model, models that are more appropriate and have sufficient DOFs to study faults and failures are selected as reduced model. Model No.3 of LMD and Model No. 10 of FMBD are selected as reduced model and used to compare with experiments, and then used in diagnosis and prognosis study.

4.5.2 Comparison with Experiments

Vibrations measured from the study engine are discussed in Section 3.2.4 of Chapter 3. Engine base and cylinder head vibrations at 1500 rpm for a normal case are plotted in Figure 4.19. Signal has several events; they are mainly engine firing, opening and closing of valves, piston slap, and start of ignition. Signal also contains other events due to clearances, misalignment and unbalance in gear, shaft and bearings; however they are inconsiderable at the selected measurement locations. Valve and geartrains have intermittent contact joints that induce impact during their contacts. Powertrain vibrations get transmit to engine block through the combustion chamber, valve seats, crankshaft bearings and camshaft bearings. Engine base is near to the bearings of crankshaft and camshaft, so it contains vibrations transmitted by these shafts. Vibrations at cylinder head are prominently influenced by combustion and valve operations, so slider and valve vibrations are its key constituents.

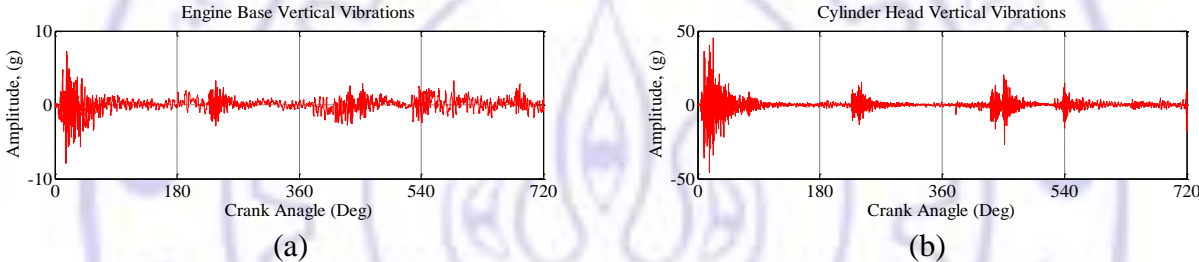


Figure 4.19: Measured Vertical Vibrations; (a) Engine base, (b) Cylinder head

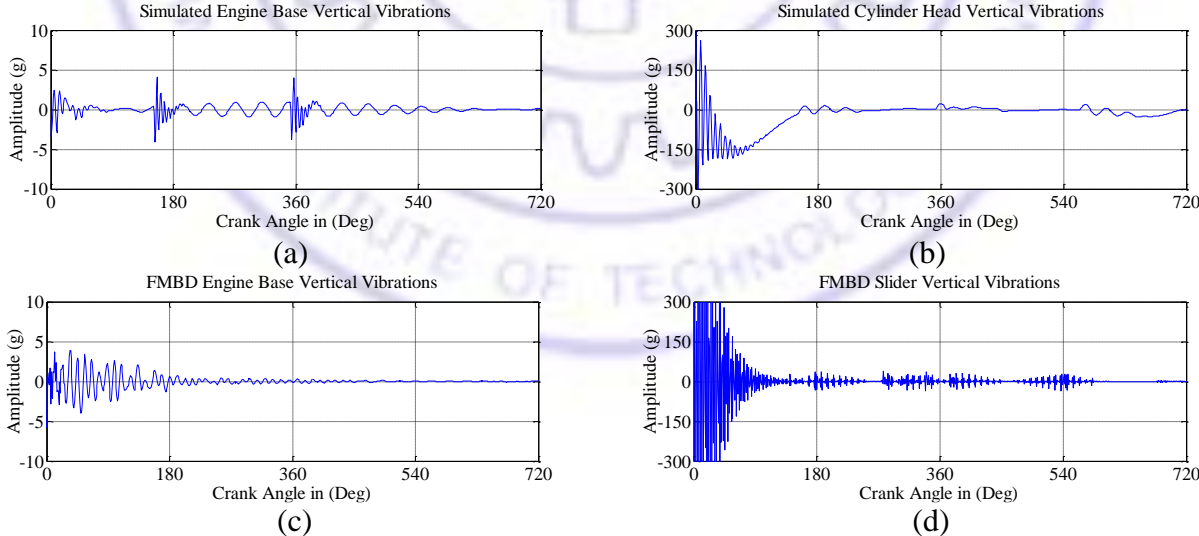


Figure 4.20: Simulated Vertical Vibrations; (a, b) LMD and (c, d) FMBD

In LMD model, engine base vibrations are computed by adding crankshaft (Figure 4.15 (e)) and camshaft (Figure 4.16 (a)) vibrations. Cylinder head vibrations are obtained by adding slider (Figure 4.15 (f)) and valve (Figure 4.16 (b)) vibrations. In case of FMBD models, component vibrations are computed by subtracting the generalized coordinates due to pure rigid body motions (Figure 4.17 (a-b)) from their flexibility body motions (Figure 4.17 (k-l)). Then similar to LMD model, engine base and cylinder head vibrations are computed from FMBD crankshaft, camshaft, valve and slider vibrations. Computed vibrations of LMD and FMBD models at engine base and cylinder head are shown in Figure 4.20 (a-b) and Figure 4.20 (c-d) respectively. Despite complexity, simulated responses are comparable to the measured vibrations. Amplitude of vibrations at cylinder head is more than the engine base, it is due to the fact that cylinder head is subjected to large pulsation loadings and base is clamped to the mounting table. Amplitudes of simulated vibrations at base are smaller than the measured values, while in case of cylinder head they are larger. Vibrations at crankshaft lasted for longer duration, while they died quickly in slider. Firing and valve events have a similarity in the occurrence and amplitudes, and matched with the measurement. Firing event clearly seen but piston-linear, gear and bearing dynamics are not considered, so vibrations due to events such as piston slap, gear tooth meshing and bearing defects are not appearing in the simulated vibrations.

4.6 Engine Fault Diagnosis

Fault diagnosis of rotor LMD models have been successfully studied by [99-101, 151] and Dimarogonas et al. [214]. In this section, powertrain models of LMD and FMBD models that are built in the previous section are used to introduce the defects such as unbalance, crack and wear, and study their behaviour. Time domain responses and their wavelet domain symptoms are being investigated for different faults.

4.6.1 Fault Cases

Powertrain faults are selected based on most common occurrence and possibility to include them in the physics-based model. Physical nature of these faults has been discussed in the Section 4.2. In LMD model, the unbalance and lack of lubrication are investigated, while in FMBD, crack and bend faults are studied. Following fault cases are formed,

In LMD modelling,

Fault No. 1: Normal i.e. Healthy Engine (NOR)

Fault No. 2: Mass Unbalance Fault (MUF)

Fault No. 3: Worn Piston Ring (WPR)

In FMBD modelling,

Fault No. 4: Normal i.e. Healthy Engine (NOR)

Fault No. 5: Cracked Connecting Rod (CCR)

Fault No. 6: Bent Connecting Rod (BCR)

Fault No. 1: Normal i.e. Healthy Engine

A flexible cranktrain of Model No. 3 is considered as a healthy state. It can simulate the faults that are resulting from variation of gas, inertia due to manufacturing defect and effect of friction due to lack of lubrication faults. Friction and unbalance fault are modelled as additional forces and employed on this model.

Fault No. 2: Mass Unbalance Fault

Variation in the inertia force occurs due to the manufacturing process and wear related geometric deviations. Over the period manufacturing dies and molds get worn resulting in production of oversize components that increase or decrease of mass that consequently changes the inertia force. Components are subjected to wear and tear which reduces the weight and results in the reduction of inertia force. To simulate such effects, mass of the powertrain is increased by 25% and added in the geometrical centres in the Model No. 3.

Fault No. 3: Lack of Lubrication Fault

Due to the lack of lubrication or no lubrication, the friction between the components increases with increase in the force magnitude. Lack of lubrication increase the friction and wear between the piston ring and liner that leads to engine seizer. In the slider joint of Model No. 3, frictional forces on the slider are increased from 60 N to 600 N.

Fault No. 4: Normal i.e. Healthy Engine

A flexible cranktrain of Model No. 10 is considered as a healthy state and connecting rod faults are investigated. The bend and crack modelled as cut faults are being introduced in flexible components of FMBD with deviating the geometry locally. Faults shown in Figure 4.21 are added in this model. The bend and cracks are modelled in the FE components by deviating geometry. Procedure adopted for creation of MNF and replacement of normal healthy components with defective MNF models is discussed in Model No-7. Flexible effects of the valvetrain are not included in these studies.

Fault No. 5: Cracked Connecting Rod

A thin cut of 0.5 mm wide and half the depth at mid way in connecting rod is modelled as crack opening in the FE model as shown in Figure 4.21 (b). It replaces the connecting rod of Model No. 10 i.e. Figure 4.21 (a). It indicates the prior situation of connecting rod fracture.

Fault No. 6: Bent Connecting Rod

The connecting rod is bent in the rotation direction and the FE model at this configuration as shown in Figure 4.21 (c). It is replaced by connecting rod of the Model No. 10. The condition indicates the prior situation of hydrostatic lock.

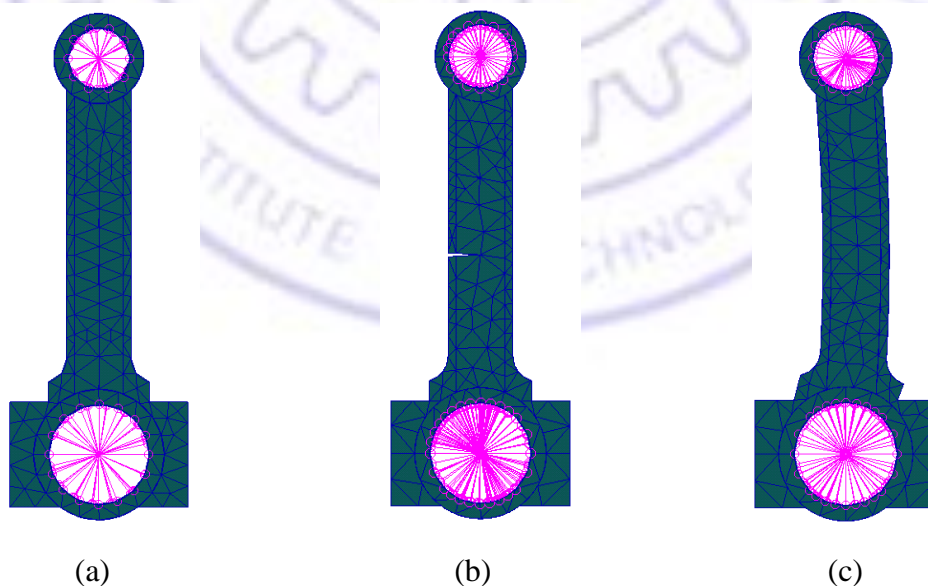


Figure 4.21: Added Fault in Connecting Rod FE Models; (a) Normal, (b) Crack, (c) Bent

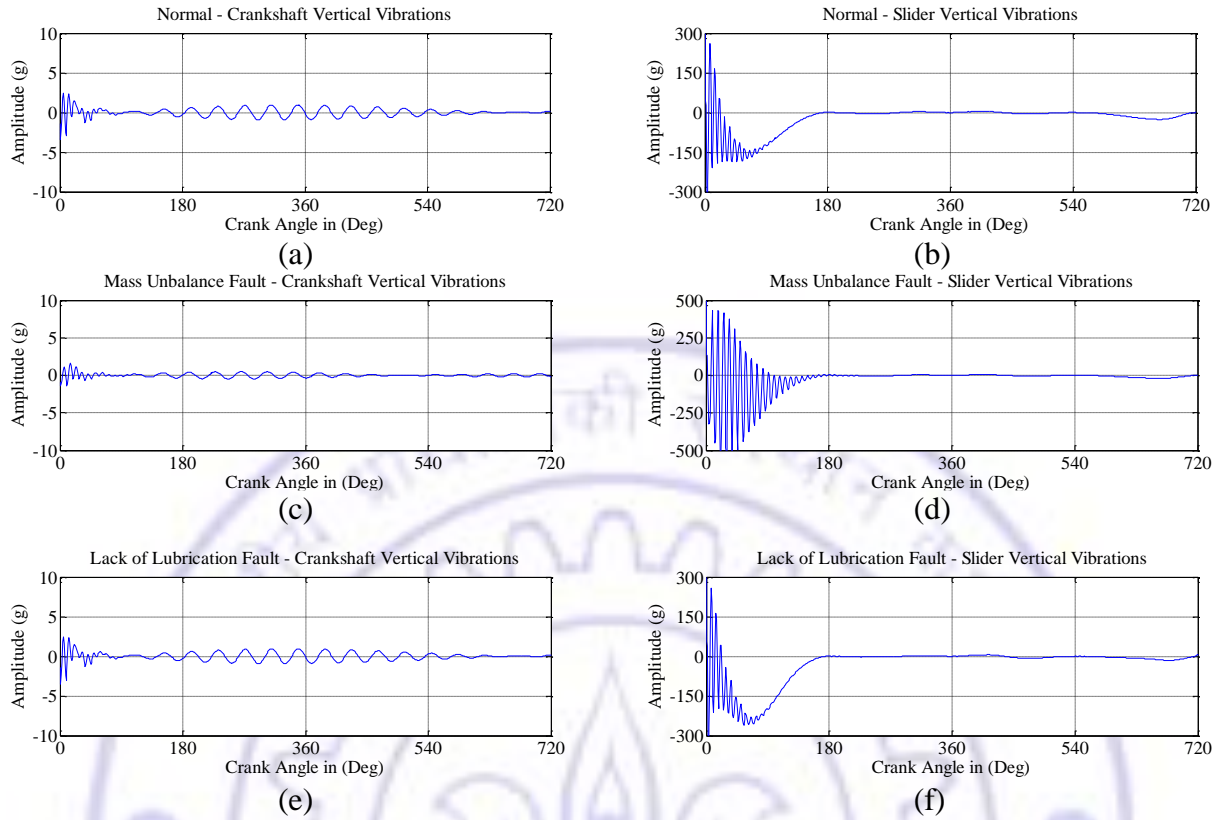


Figure 4.22: Fault Response from LMD; (a, b) Normal, (c, d) Unbalance, (e, f) Friction Fault

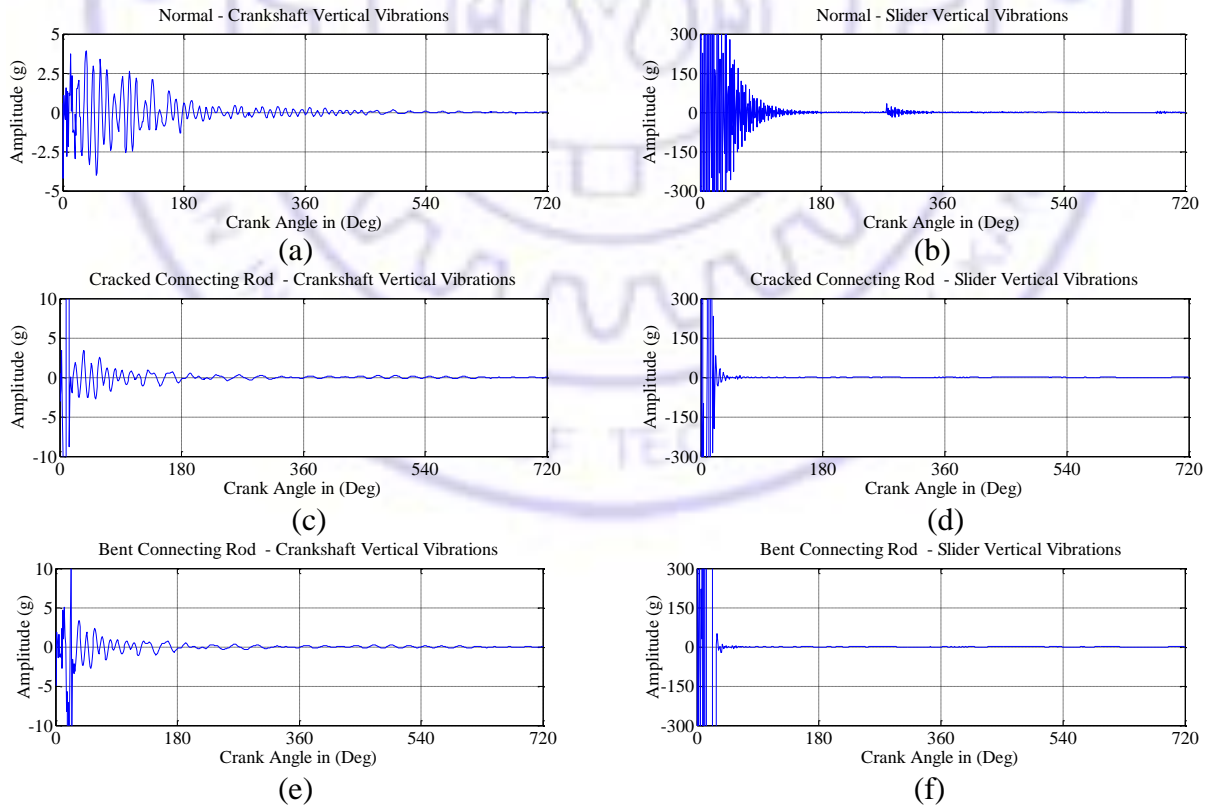


Figure 4.23: Con. Rod Fault Response from FMBD; (a, b) Normal, (c, d) Crack, (e, f) Bend

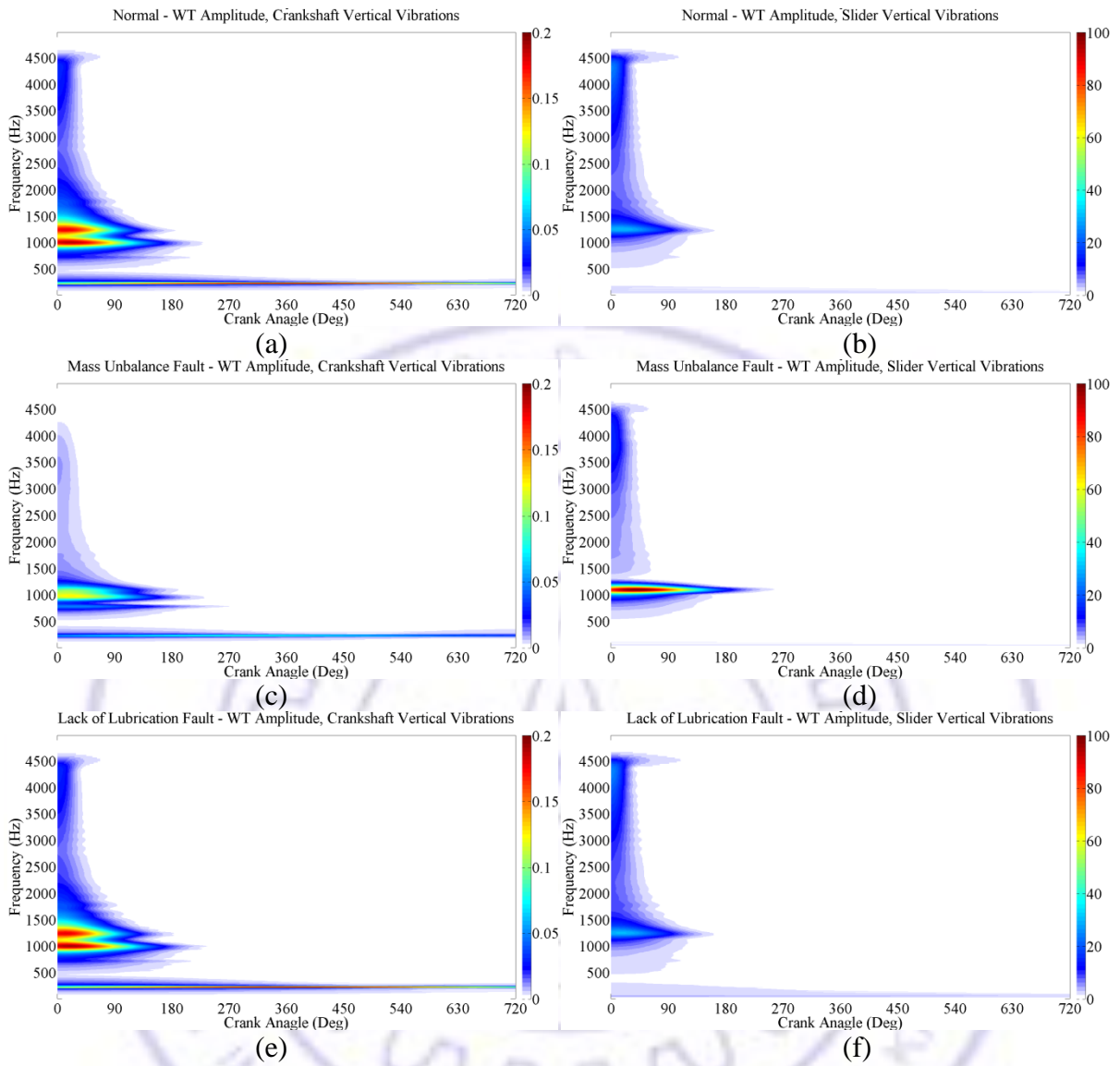
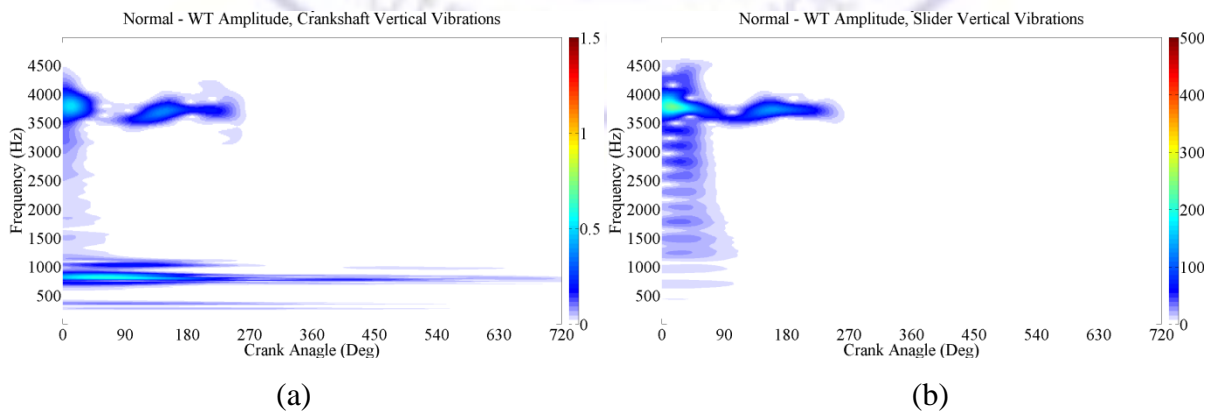


Figure 4.24: WT Plots of LMD Faults; (a, b) Normal, (c, d) Unbalance and (e, f) Friction



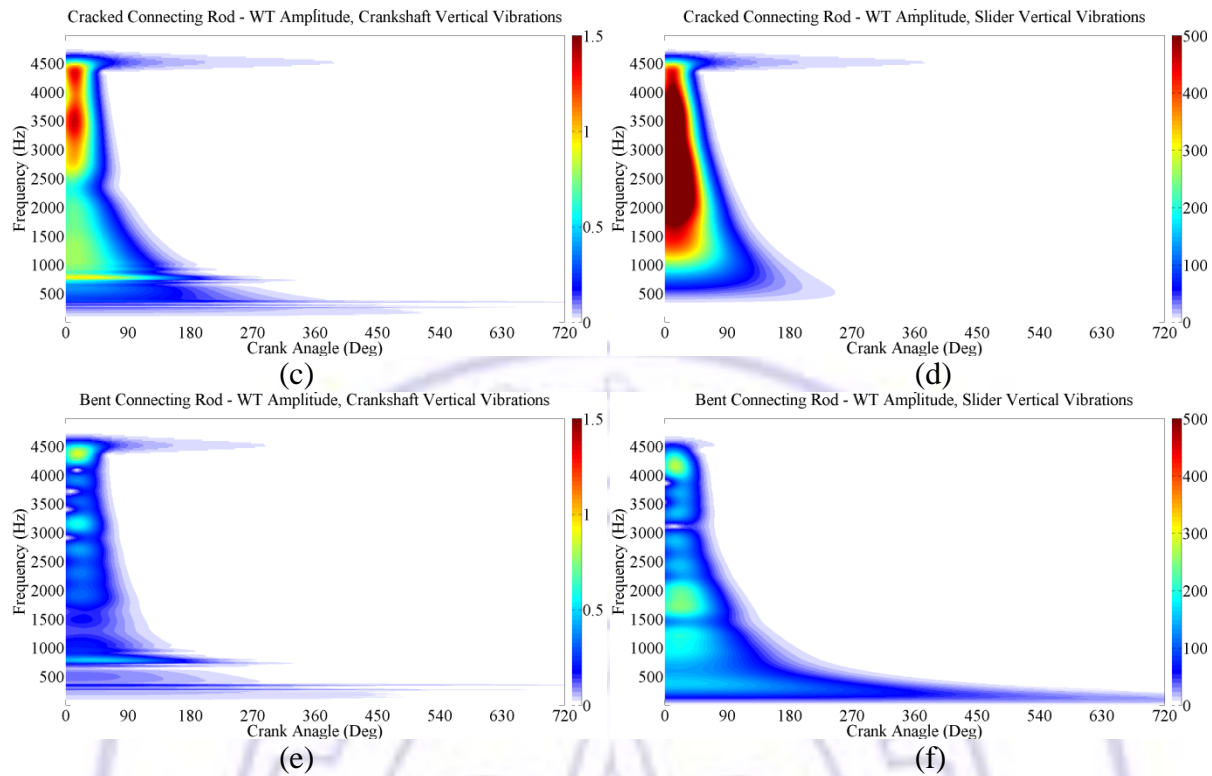


Figure 4.25: WT Plots of FMBD Faults; (a, b) Normal, (c, d) Cracked and (e, f) Bent Fault

4.6.2 Fault Response Comparison

Figure 4.22 shows comparison of vibration responses under initiated unbalance and friction faults. Engine base plots indicated a small variation in the responses, while the cylinder head shows significant changes. Under unbalance, the cylinder head has shown with increase in the amplitude of vibrations and these vibrations lasted for longer duration, while in case of engine base the amplitudes are reduced. Hence it can be concluded that the increased unbalance increases vibrations in cylinder head and reduces in crankshaft. In the case lack of lubrication, the slider vibrations are slightly increased. Wavelet plot of these signals for faults are shown in Figure 4.24. The engine base plot indicated 1000 Hz and 1200 Hz clear modes for normal and friction fault plots, but a single mode at 1000 Hz is seen in case of unbalance with lowering second mode value. Wavelet showed not much changes in friction fault case.

Figure 4.23 shows FMBD response of healthy cranktrain, fault with half cut and bend at middle of connecting rod in the inward direction of motion. Vibration amplitudes at engine

base are lowered due to crack, while at cylinder head they died quickly. Marginal variations are observed in the results of bent connecting rod as compared to cracked connecting rod. Wavelet transform of FMBD faulty signals are shown in Figure 4.25. It shows faults are clearly visible. For normal condition, engine base indicated modes at 900 Hz and 3700 Hz respectively. In case of cracked connecting rod, they are observed at 800 Hz and 3500 Hz with large spread amplitude in frequency domain. Cylinder head plot shows high amplitude of vibration in frequency axis, which is also widely spread in the frequency domain. Bent connecting rod indicates several modes, which lasted for a small duration and showed similar but smaller amplitude response of the cracked connecting rod. WT analysis indicates that it is sufficiently good enough to identify and distinguish fault symptoms.

4.6.3 Fault Diagnosis Comparison with Experiments

To evaluate physics-based fault diagnosis approach, WT plots of a normal and cracked case i.e. Figure 4.25 (a, c) are compared with experimental WT plots. i.e. Figure 5.7 (a, c). Connecting rod State No. 1 cut length 0 mm and State No. 5 cut length 4 mm discussed in Section 5.2.2 are considered as experimental normal and cracked cases respectively. Signal generated by these states Figure 5.3 (b, h) i.e. vibration responses under normal and initiated cracked connecting rod are transformed to WT plots Figure 5.7 (a, c). They are re-plotted in Figure 4.26 to ensure identical comparison for one full cycle duration. Figure 4.26 (a, c) is diagnosis by physics-based approach, while Figure 4.26 (b, d) is experimental.

Both of the above approaches are successful in differentiating the faults and a few similarities can be seen in the WT plots. Plot amplitudes are not well matched, and several events and modes that present in experimental WT plots are missing in physics-based WT plots. Cylinder head vibrations mainly contain the vibrations from combustion firing, valve collision and piston slap vibrations. Simulated physics-based plots represent pure combustion firing vibrations. So, vibrations due to other events and components are missing. Real system contains infinite modes of all components, so physics-based plots showed only connecting rod modes while experimental plots showed the modes all components that are involved. Despite simplification of dynamics, physics-based approach is capable of easily classifying the fault.

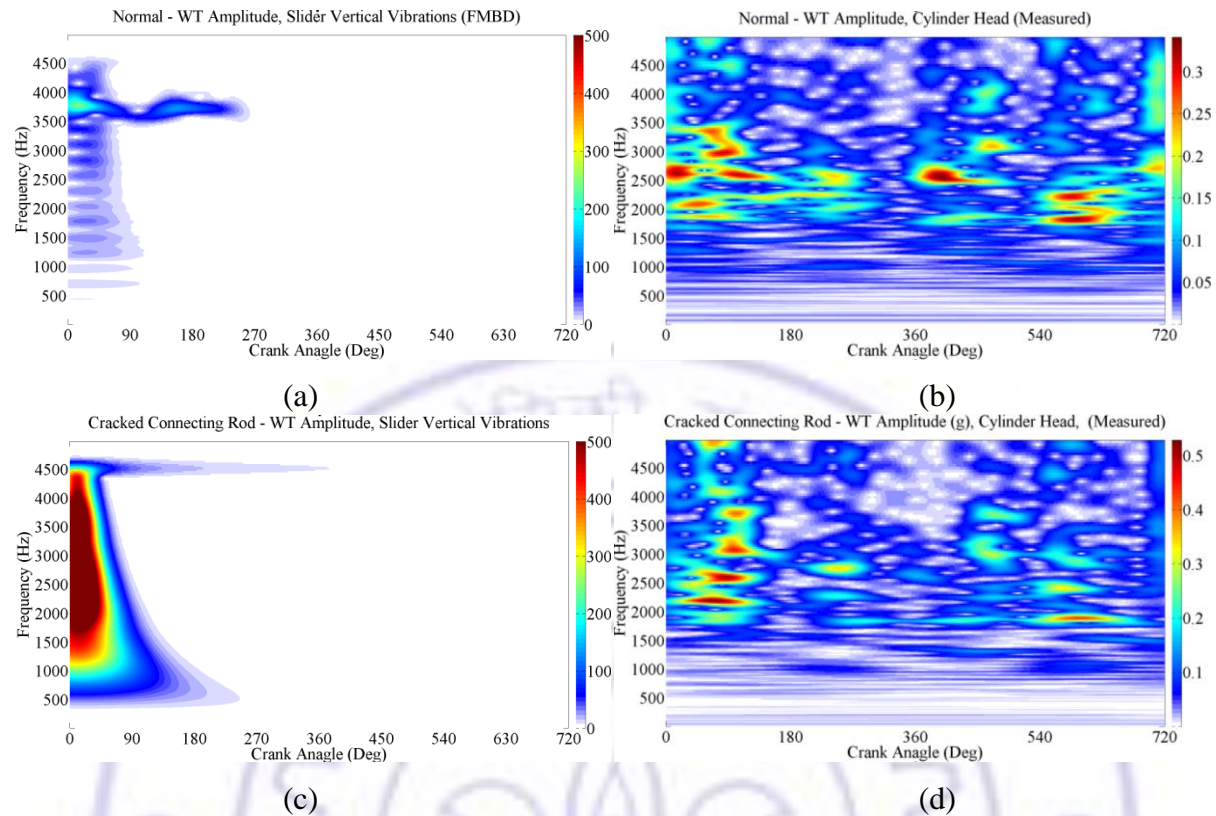


Figure 4.26: WT Plots of FMBD and Experiments; (a, b) Normal, (c, d) Cracked Conn. Rod

4.7 Model Solution for Failure Prognosis

This section formulates a procedure to predict engine survivability due to repeated, fluctuating and rapidly applied loads. [Vyas and Rao \[152\]](#) proposed different fatigue and crack models under uniaxial tension for predicting the life of a turbine blade. Mixed-mode cracks are investigated by [Wang et al. \[215\]](#) under uniaxial tension. [Agrawal and Kishore \[216\]](#) estimated stress intensities at crack front using surface information, which can be used to predict life. Current study employs these models for predicting life in engine components.

4.7.1. Fatigue Life

Fatigue is a failure under a repeated load which never reaches a level sufficient to cause failure in a single application. A fracture is rapid growth of a crack once it has been initiated to complete breakage in two. Analysis involves estimation of total life for fracture, or life for crack initiation or growth of an initiated crack to a critical size for fracture. First two uses cyclic material properties, service load and stress distribution, while third one uses additional

geometry compliance function to define stress state at the crack tip. Survival life can be predicted using durability analysis, which accumulates all aspects (loading conditions, environmental concerns, material characterizations etc.) that affect the life of a product.

Stress-life approach estimates total life (due to crack ignition and growth) with assuming nominal stresses below the tensile elastic limit and component has long lives i.e. above 10^5 cycles. Stress amplitude is extracted from Goodman $\left(\frac{\sigma_a}{\sigma_e} + \frac{\sigma_m}{\sigma_u} = 1\right)$ or Gerber $\left(\frac{\sigma_a}{\sigma_e} + \left(\frac{\sigma_m}{\sigma_u}\right)^2 = 1\right)$ curves and life is estimated from Figure 4.27 (a), where σ_e , σ_u , σ_a and σ_m are endurance, ultimate, amplitude and mean stresses respectively. Transient loads can be converted into a set of equivalent constant amplitude cycles and damage in each cycle can be accumulated using Miner's rule, $(\sum_{i=1}^k n_i/N_i = 1)$, where k is the number of stress levels, n_i and N_i are number of cycles accumulated and required for a failure at stress σ_i respectively. It does not account local plasticity that causes some fatigue, so this approach is less in use.

High loads and stress concentration causes plastic deformation around the notches that continue to make material either strong or weak by forming hysteresis loop. Cracks are initiated at these regions and leads to a relatively short life. It is studied using strain-life approach. In hysteresis tests, strain is controlled and stress range is stabilized with recording cycles to failure, which can be converted into reversals to failure, i.e. $2N_f$ to compensate two reversals in a cycle. Cycles to failure are shown in Figure 4.27 (b) obtained by fitting test data and material constants. In the simulation, elastic strain is obtained from stress range and elastic modulus, while plastic is determined by elastic-plastic conversion using Neuber's rule $(\varepsilon_t = \sigma_f'(2N_f)^b/E + \varepsilon_f'(2N_f)^c)$, where σ_f' and ε_f' are strength and ductility coefficients, b and c

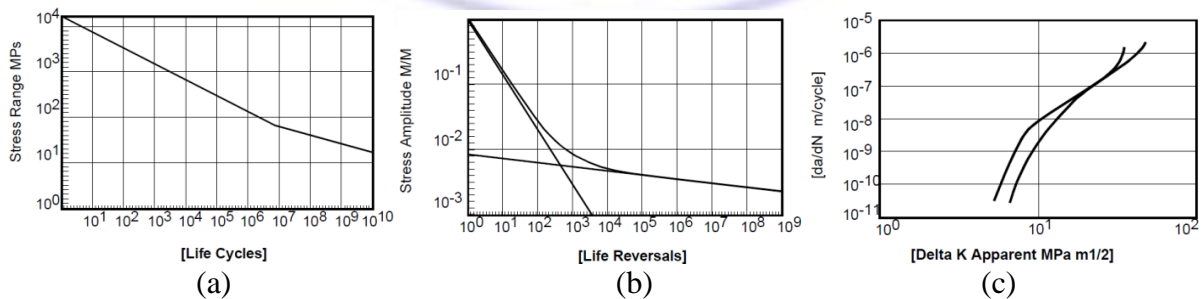


Figure 4.27: Fatigue Life Curves [217]: (a) S-N Curve, (b) ε -N Curve, (c) Fracture Curve

are their exponents respectively. Cycles to total strain are estimated from Figure 4.27 (b). In case of strain levels, damage is assessed in each cycle and accumulated using Miner's rule. Software such as FATIGUE, FE-SAFE, nCode, COMSOL and ANSYS estimates fatigue life for crack initiation. Durability is investigated under various service loads.

4.7.2 Fracture Life

Voids, flaws and metallurgical discontinuities are inherently exists that initiate the crack, once initiated it grows rapidly towards complete fracture. Plot of its growth rate verses stress intensity show three regions; first and last unstable growth, and stable follows Paris law as,

$$\frac{da}{dN} = C(\Delta K)^m \quad 4.34$$

where da/dN represents crack growth rate as shown in Figure 4.26 (c) for two different load ratio, In stable growth period, crack growth rate is proportional to applied stress intensity ΔK at the crack tip, which is a function of crack length, geometry and stress level. C and m are material constants that are ordinate intercept and slope respectively. Their values for different materials can be obtained from [Kumar \[218\]](#) and [Ellyin \[219\]](#). Crack growth life gives RUL. For stable range, it is studied using linear elastic fracture mechanics (LEFM) for calculating stress field near the crack tip i.e. crack front. Cracks are propagated when stress intensity exceeds the material fracture toughness. A fracture can occur by opening (I), sliding (II) or tearing (III) modes depending on the displacements with respect to crack front. In practical cases, crack occurs with the combination of these modes and usually the mode I is dominant. If plastic deformations at crack-tip are high, then it is studied using Elasto-plastic Fracture Mechanics (EPFM). For a given crack length, number of cycles to fracture can be estimated using Equation 4.34. Stress intensity factor (SIF) can be computed using two different approaches. In first approach, overall stress field is estimated for an un-cracked model and local stresses at the crack location are taken to a standalone fracture tool such as FATIGUE or ANSYS, where a suitable crack model is employed to estimate K using the relation,

$$K = Y\sigma\sqrt{\pi a} \quad 4.35$$

where Y is compliance function that embodies global geometry of the component, crack size, shape and location. FATIGUE has a library of compliance functions that supports a variety of standard geometric cases such as holes, plates, corners, cylinders, weld joints and a user defined non-dimensional function. It relates crack size with total possible crack size based on test, analysis or standard expressions. In second approach, crack is actually included in FE model. By evaluating the initial crack, software such as MARC, NASGROW or AFGROW extends its length and re-analyses iteratively for instantaneous K . It is accurate, but it requires knowledge of crack paths well ahead of time due to redistribution of stresses.

4.8 Engine Failure Prognosis

In this section, life for crack initiation and crack propagation are investigated in the engine powertrain components. A procedure is formulated, different failure models are considered and component survivability in terms of RUL is predicted.

Stresses and deformations are computed from Model No. 10 in ADAMS/Durability that computes stresses and export them to fatigue life prediction programs. Typical stresses and deformations at engine firing condition are shown in Figure 4.28 and their peak values are listed in Table 4.3. Plots indicate that the deformations in piston are high while stresses are high in piston pin. In comparison to the yield limits (276 MPa for Aluminum and 370 MPa for Plain carbon steel) and allowable displacement requirements, the stresses and displacements are within the safe limit and will not cause static failure.

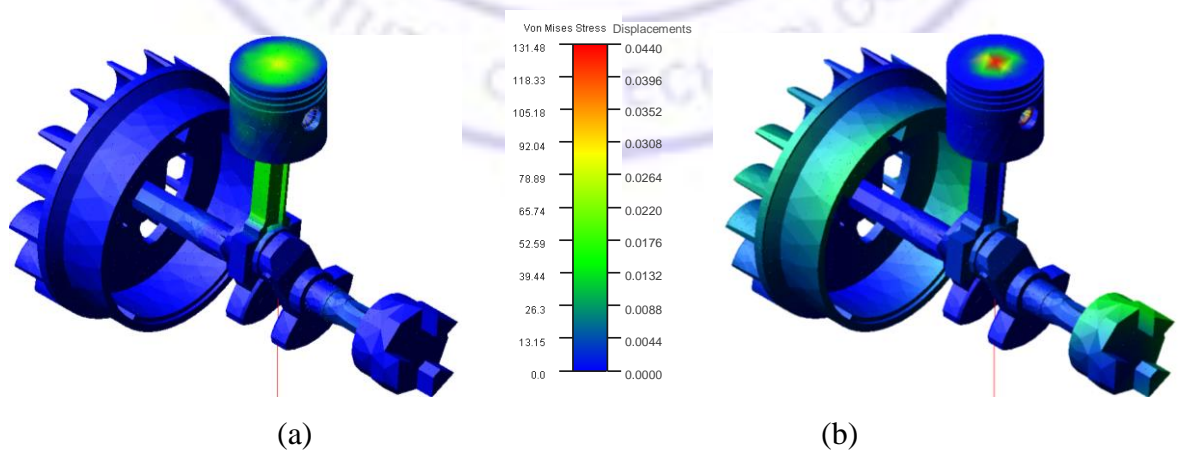


Figure 4.28: Cranktrain Responses at 26° CA; (a) von Misses Stresses, (b) Deformations

Table 4.3: Summary of the Cranktrain Responses

Response	Crankshaft	Connecting Rod	Piston Pin	Piston
Deformation, mm	0.008	0.023	0.0015	0.044
von Misses Stresses, MPa	21.58	56.51	131.48	99.61
Factor of Safety	17.14	4.88	2.82	2.77

4.8.1 Failure Cases

In estimating powertrain life, component stresses from NASTRAN and load history from ADAMS of Model No. 10 are taken to FATIGUE, where strain–life is analysed with assigning fatigue material properties. Lowest number of cycles for crack initiation and a location in a component are considered as minimum life of the powertrain and location of failure respectively. Crack progression life is predicted in the connecting rod of Model No. 10 using LEFM theory. Connecting rod is usually either cracks or bends at heavy loaded locations along mid way, transitions to crank pin or piston pin as seen in Figure 4.3. A crack at midway location of the connecting rod is investigated using FATIGUE crack models. A single edge crack in tension (SENT) and bending (SENB) models as shown in Figure 4.29 are incorporated. The crack progression parameters and RUL at 1500 RPM are tabulated for these models.

In crack initiation life study,

Failure No. 1: Crankshaft Life

Failure No. 2: Connecting Rod Life

Failure No. 3: Piston Pin Life

Failure No. 4: Piston Life

In crack progression life study,

Failure No. 5: Connecting Rod using SENT Model

Failure No. 6: Connecting Rod using SENB Model

Failure No. 1: Crankshaft Life

The geometry of crankshaft and ADAMS modal stress results are taken to FATIGUE, where Neuber plasticity correction and material stress concentration factors, reversal loading information are included in estimating its crack initiation life.

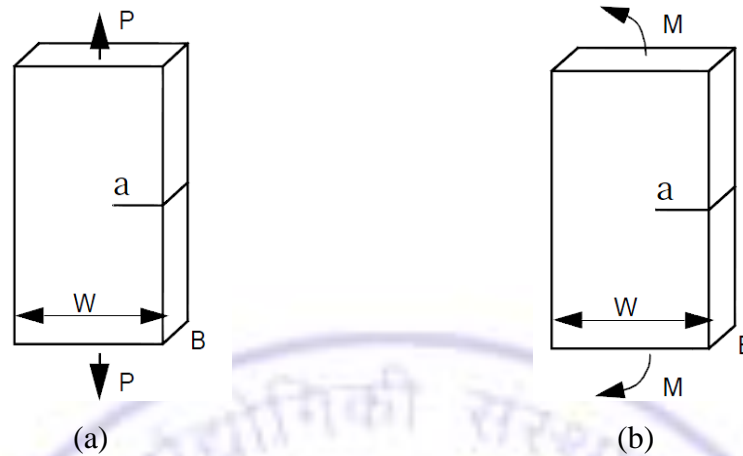


Figure 4.29: Crack Progression Models [217] for the Connecting Rod: (a) SENT, (b) SENB

Failure No. 2: Connecting Rod Life

In this model, similar to Failure No. 1, the crack initiation life is estimated for connecting rod.

Failure No. 3: Piston Pin Life

The procedure of Failure No. 1 is adopted for piston pin and the crack initiation life is estimated in the piston pin.

Failure No. 4: Piston Life

The procedure of Failure No. 1 is adopted for piston and the crack initiation life is estimated.

Failure No. 5: Connecting Rod using SENT Model

In this case, far field distribution is taken from the Model No. 10 un-cracked connecting rod at mid portion location. The compliance function is defined in FATIGUE for single edge crack in tension as shown in Figure 4.29 (a). Connecting rod fatigue material is defined as Aluminium 2219-T851[218] with stress ratio 0.5.

Failure No. 6: Connecting Rod using SENB Model

In this model, compliance function of model of Failure No. 5 is replaced by is single edge crack in pure bending shown in Figure 4.29 (b).

4.8.2 Failure Life Comparison

Comparison of crack initiation life responses in the crankshaft, connecting rod, piston pin and piston are shown in Figure 4.30. Minimum lives can be reported as $10^{8.55}$, $10^{7.33}$, $10^{7.30}$ and $10^{8.26}$ log of life respectively by omitting life due to discretization error at sharp edge/corner in these components. So, minimum lives for crack initiation in these components

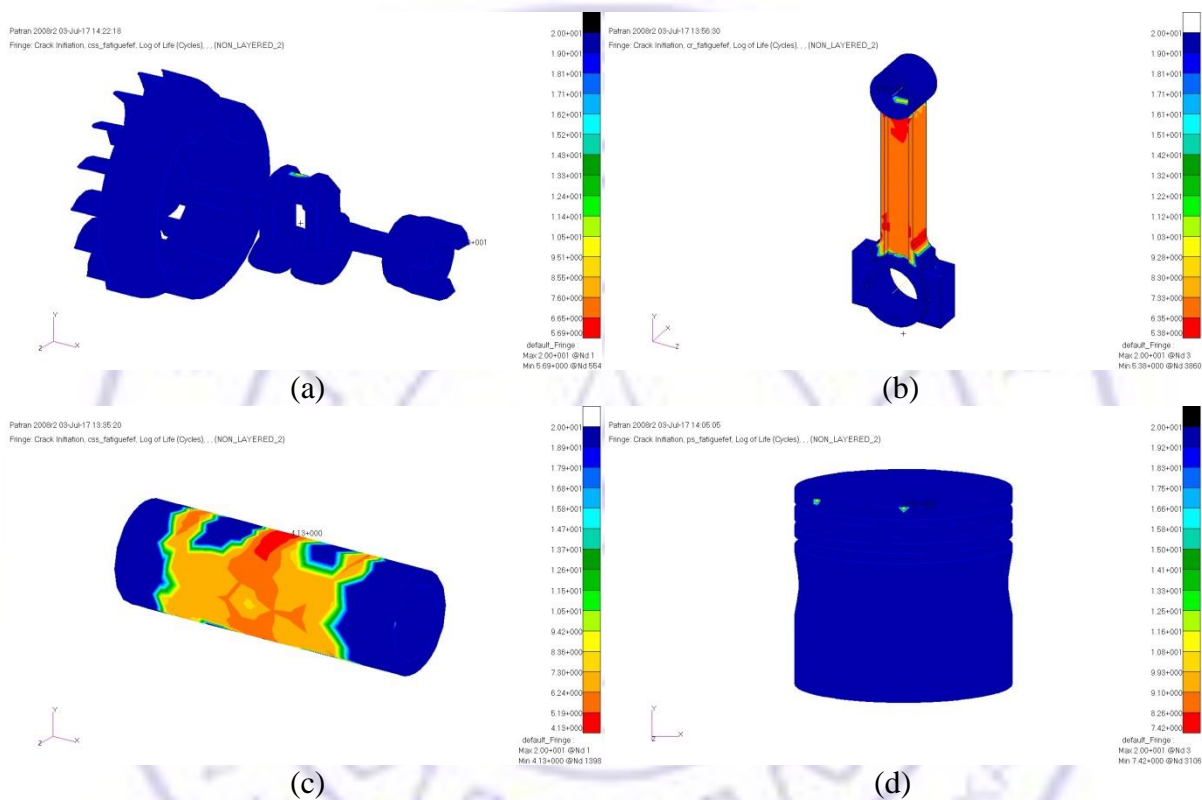


Figure 4.30: Engine Fatigue Life; (a) Crankshaft, (b) Conn. Rod, (c) Piston Pin, (d) Piston

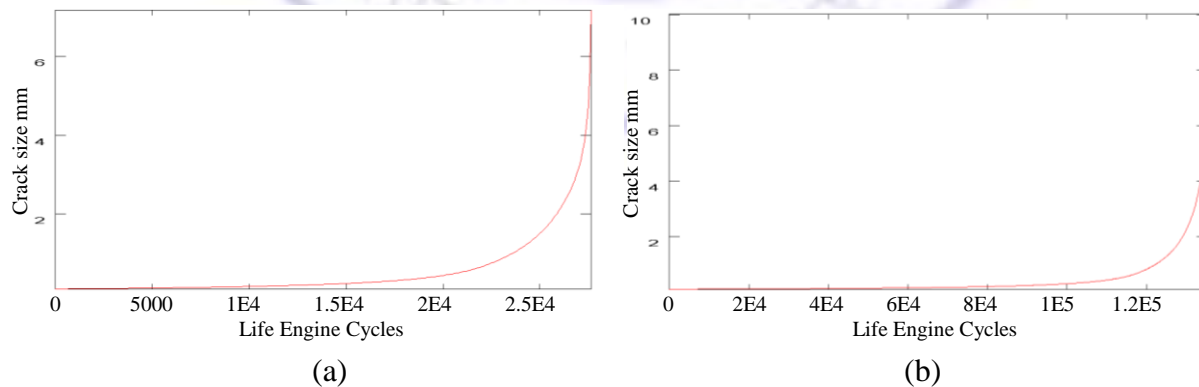


Figure 4.31: Crack Growth Curve of Connecting Rod; (a) SENT, (b) SENB

Table 4.4: Connecting Rod Crack Progression Model Results

Parameters	SENT Model	SENB Model
Life (engine cycles)	2.765e4	1.353e5
Original crack size (mm)	0.100	0.100
Crack size (mm)	7.176	10.025
DLKAPP	62.943	63.163
DLKEFF	65.874	66.295
da/dN	6.345E-5	6.475E-5

are 354813389, 21379621, 19952623 and 181970086 engine cycles respectively, i.e. 7885, 475, 443 and 4044 hours life at 1500 rpm respectively. So, crack first initiates in piston pin and then in connecting rod, piston and crankshaft in a sequence. It contradicts Table 4.3 results that sequence failures are piston, piston pin, connecting rod and crankshaft. The differences are due to consideration of approximations in static and fatigue failure.

Crack propagation curves shown in Figure 4.31 indicate different growth rates for connecting rod when modeled using Failure No. 5 and 6 i.e. SENT and SENB. In SENT model, crack grew over 7 mm before fracture with consuming around 30000 constant amplitude engine cycles at 1500 rpm i.e. 40 minutes. Though it took 475 hours (equivalent to years of operation) to get crack initiated, once initiated, it grow very rapidly and fractures as stress intensity condition exceeds the fracture toughness. In actual experiment, connecting rod has suddenly fractured in the trial of 6 mm cut length step. Differences are due to error in operating load estimation and unaccounted thermo mechanical fatigue. Engine accumulated some cumulative damage during data acquisition at other speeds, so actual connecting rod has fractured much earlier. Comparison of SENT and SENB approach results are listed in Table 4.4. They report that life in SENT is small; the total lives are 214,07,271 and 215,14,921 engine cycles in SENT and SENB respectively, it indicates connecting rod last slightly longer if undergo pure bending mode. SENT has high degradation rate, so crack can take less number of cycles to propagate for the fracture. DLKAPP and DLKEFF of SENT are small that indicate both the apparent and actual driving force for all the regions of the da/dN curve are less despite of same initial crack length. SENT has smaller region for crack growth that rises the concern regarding the stability of crack growth. Major load on connecting rod is due to engine firing that occurs at TDC so pure bending effects are much smaller; hence SENT model can be considered as realistic for computing the RUL of connecting rod.

4.9 Conclusions

In this chapter, a physics-based diagnosis and prognosis framework for powertrain is proposed and evaluated. Simple lumped mass discrete models and detailed flexible multibody models are explored for free, forced, fatigue and fracture responses. Models are studied for effective idealisation, and faults and failures are investigated in selected models.

In LMD, different idealizations are studied by enhancing engine structural dynamics with the help of advanced rotor dynamics. In multibody approach, a detailed rigid multibody model is developed in a commercial MBD tool and is converted into flexible for an optimal model reduction. Loads required for these analyses are estimated by performing thermodynamic, hydrodynamic, and engine dynamic analysis. These loads are validated by comparing with test, literature and commercial tool respectively. Rayleigh damping is used to estimate the material damping. Comparative study of LMD and FMBD results with experiment indicates that certain models have good correlation with experiment and superior in predicting the engine vibration responses. The selected LMD and FMBD models are further used to investigate fault diagnosis and failure prognosis by introducing the defect.

Common faults such as unbalance and friction defects are modelled as change in forces in LMD models, while crack and bend are introduced by deviating geometry locally in FMBD models. Wavelet transform indicates models are successful in giving fault characteristics. Comparison of FMBD fault diagnosis approach with experiments indicates some similarity between results. Considering the complexity of real system they are reasonable.

Crack initiation and propagation models are proposed for to predict powertrain failure and predict engine survivability. A strain-based fatigue and fracture mechanics approach is used to extract life for crack initiation and propagation. Component survivability in terms of RUL is predicted. Predicted fracture lives are compared with experiment and observations are reported. Low life in piston pin indicated the need for an earliest logistic support. Simulation results have a close match with the experimental results. This indicates that some of the proposed physics based models are sufficiently good enough to predict faults and failures.

CHAPTER 5

DATA-DRIVEN AND MODEL-BASED HEALTH MANAGEMENT

An approximate answer to the right problem is worth a good deal more than an exact answer to an approximate problem.

- John Tukey (1915-2000)

5.1 Introduction

Chapter 3 reported an experimental set-up, its sensitive conditions for measurements and few parameters for data analytics to facilitate effective health management. In Chapter 4, physics-based approach is explored to study few selected faults and failures. It conforms that studying real faults and failures using physics-based models is still a challenge ([Wang et al. \[220\]](#), [Achenbach \[221\]](#) and [Peng et al. \[222\]](#)) due to structural complexity and highly uncertain processes. However, demand to enhance and use them for managing the health is continuously growing. Health management is realistic when actual faults and environments are considered. Increased surveillance and big multivariate data are rigorously forcing to automate their handling process. Data-driven, model-based and hybrid methods ([Srivastava and Han \[13\]](#)) have proven success in managing the health of rotating machinery using stationary signals, but to deal non-stationary signals and reciprocating machinery they need enhancements. Data-driven techniques use statistical reasoner to test inter-relationship within the data, and intelligent models to review true nature of relationships by learning weights to adapt for changes. Model-based approaches use physics, priori belief or knowledge models and uncertainty of the variables to deal imprecision and uncertainty. A hybrid model combines above techniques to increase flexibility and to handle the complex systems.

This chapter evaluates the capabilities of data learning and rule based techniques to enhance EHM system. A manual fault diagnosis method is attempted to compare statistical and Fourier plots of the signals collected at steady speed for a larger duration, and variation in a engine cycle by WT plots. It is then automated using data-driven and model-based techniques with statistical and Fourier features for entire speed range. Statistical classifiers such as hypothesis testing, clustering and Multiple Discriminant Analysis (MDA) classifies the data based on fault symptoms. They form a parametric expression or distribution to detect fault using null against alternative or checks similarity in the features to groups them into categories or discriminates the group by a discriminant function. Intelligent models such as ANN and SVM learns the weight from data and classify faults, by either minimizing error functions or maximizing boundary margins. Model-based approaches such as Fuzzy and rough set classify based on rules from experience, knowledge or physics. A series of tests at increasing fault amplitudes can track degradation and failure; the information can be used to estimate RUL. A model-based filter such as Kalman, particle or a time series can predict general degradation states from prior information with certain actions. Kalman uses Gaussian distribution and linear actions, while particle filter uses non-Gaussian distribution and non-linear actions. In this chapter, MDA, ANN and fuzzy models are built to diagnose engine faults, and particle filter is formulated to predict states. In Chapter 6, above techniques are combined into hybrid models for classify the engine faults. Purpose of this chapter is to,

1. Compare engine fault signals and their transforms for a manual fault diagnosis.
2. Extract the features, and automate statistical and intelligent-based fault diagnosis.
3. Propose and evaluate model-based models for engine failure prognosis.
4. Select most effective models and assess engine health.

Section 5.2 describes the fault and failure samples, subsequent section discusses the signals measured from these samples, compares statistical, Fourier and wavelet plots. Further, the features are extracted from these transforms. In Section 5.4, statistical and intelligent models are proposed to detect fault symptoms based on the extracted features. In Section 5.5, failure characteristics are assessed with run-to-fail experiments. In later section, a model-based approach is employed to predict connecting rod failures and degradation symptoms from the measured signals. Last section of this chapter summarizes the conclusion.

5.2 Fault and Failure Samples

To investigate realistic faults and failures, physical components that are rejected either due to deterioration or breakage as listed in Section 3.2 are used. Sample size of the components is varying based on their availability. From the literature (Bloch and Geitner [39], Zima and Greuter [43] and Denton [44]) and survey conducted at the service stations, a sample with most common and dominant features is finalized. It is re-used directly or used to intend a defect in a fresh component. Common failures of an IC engine as listed in literature [43] by component percentage are: piston rings-25%, crank-20%, engine bearings-16%, valve leakage-8%, cam, gears and other fasteners contributes for remaining amounts. Survey indicated that common and long term chronic defects that lead to failure are: worn valves, worn piston rings and bearings.

5.2.1 Fault Cases

Rejected samples have been identified with different defect features in combination and mixed mode failures. A partially damaged sample that has single dominant defect as in worn valve, high clearance in main bearing and worn piston rings are selected for re-use. Specifications of the broken and worn samples are used as reference to replicate crack, wear and chop-out material in fresh components. Lobe of exhaust cam is grinded to lower its height by 3 mm. Connecting rod liner thickness is grinded to reduce its thickness from 1.25 mm to 0.75 mm. A tooth in primary gear is chopped off and a thin 4 mm deep cut is made in connecting rod at halfway of its length. They are listed as below cases. Normal/healthy components are replaced by respective faulty sample in the test engine to acquire signals,

Fault No. 1: Normal i.e. Healthy Engine (NOR)

Fault No. 2: Main Bearing Fault (MBF)

Fault No. 3: Cracked Connecting Rod (CCR)

Fault No. 4: Worn Exhaust Valve (WEV)

Fault No. 5: Tooth Missing or Chipped Primary Gear (TMG)

Fault No. 6: Worn Cam Lobe (WCL)

Fault No. 7: Worn Crank Journal (WCJ)

Fault No. 8: Worn Piston Ring (WPR)

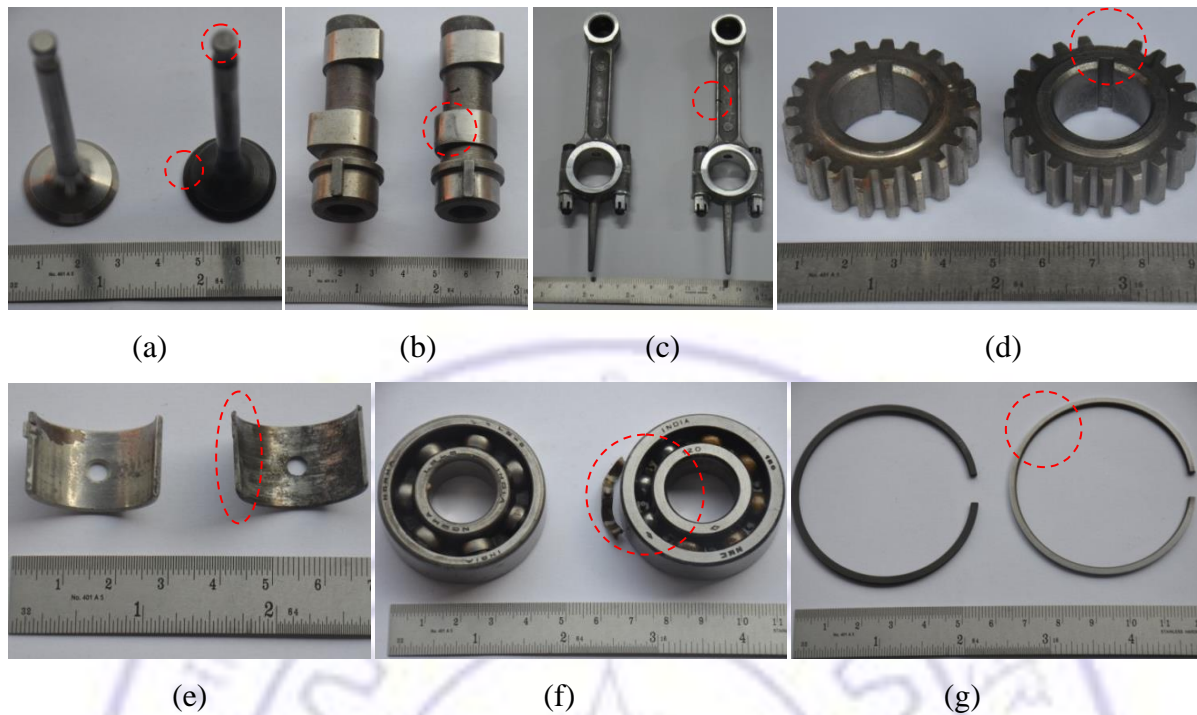


Figure 5.1: Healthy and Defective Components; (a) Worn Exhaust Valve, (b) Worn Cam, (c) Cracked Connecting Rod, (d) Tooth Missing Primary Gear, (e) Worn Crank Journal, (f) Defective Main Bearing and (g) Worn Piston Ring

Figure 5.1 shows the healthy and defective engine components. They represent deteriorated condition of the components for a healthy engine. In each figure, defective component is placed right to its healthy component with defects highlighted in dotted circles. Figure 5.1 (a) shows the healthy and deteriorated exhaust valve having worn at width of valve seat and valve tappet land. Worn seat has change in contact area that leads to fluid leakage, while worn tappet land increases the valve clearance. Low compression, change in contact area and increased gaps alter the noise and vibration characteristics. In Figure 5.1 (b), lobe of exhaust cam has a worn that represents insufficient lubrication or arises from manufacturing defect. Figure 5.1 (c) shows a healthy connecting rod with pre-defined cut at midway of the rod; the cut indicates a possible situation of crack before its fracture. Figure 5.1 (d) shows a primary gear with a tooth chopped off, which signifies a gear with tooth missing condition. Figure 5.1 (e) represents journals of the crank pin worn, which increases clearance between connecting rod and crank pin. Main bearing shown in Figure 5.1 (f) has worn in raceways, balls and has broken cage. They occur due to lack of lubrication or excessive loading.

5.2.2 Failure States

Normally crack initiation in an engine occurs after years of regular operation, which takes months to propagate into fracture. In experimental simulation, to accelerate crack propagation into fracture, a 0.5 mm wide cut is introduced at halfway of a fresh connecting rod and depth of cut length is increased with a step of 1.0 mm till it fractures in the engine during data acquisition. Connecting rod has finally fractured for 6.0 mm depth of cut state and 2500 rpm stage. Figure 5.2 shows a few degradation states of connecting rod; first one has 0 to 8 mm marks at 1 mm step, second has a 4 mm cut while third one is after complete fractured. Engine signals are collected for the following states.

State No. 1: Cut Length 0.0 mm

State No. 2: Cut Length 1.0 mm

State No. 3: Cut Length 2.0 mm

State No. 4: Cut Length 3.0 mm

State No. 5: Cut Length 4.0 mm

State No. 6: Cut Length 5.0 mm

State No. 7: Cut Length 6.0 mm

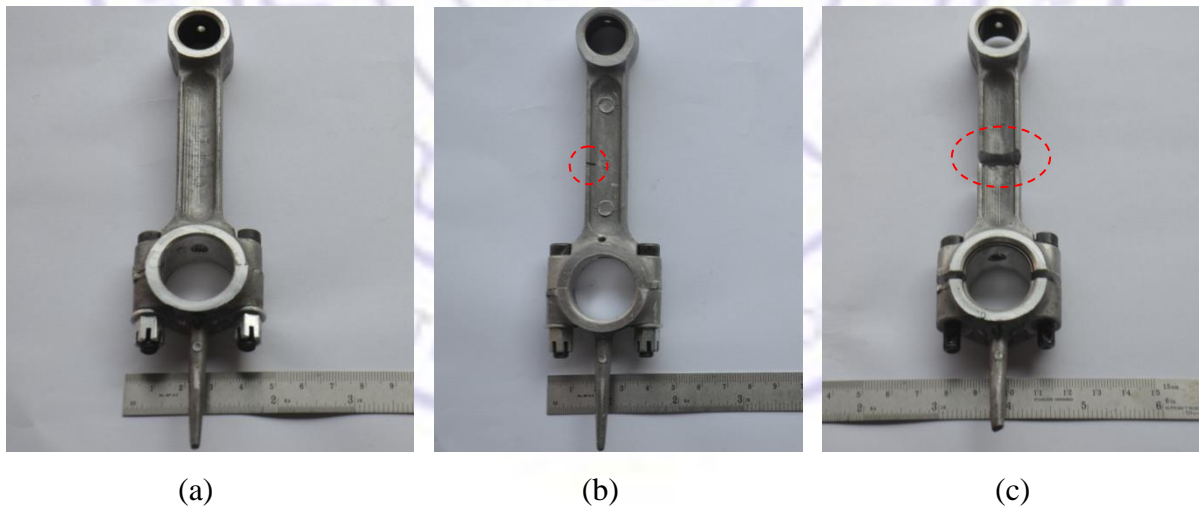


Figure 5.2: Connecting Rod Cut Length States; (a) 0.0 mm, (b) 4.0 mm and (c) Fractured

5.3 Signals from Faulty Samples

Fault samples selected in Section 5.2.1 are introduced in the engine by replacing their healthy components, re-assembling and conducting data acquisition. Engine signal Data Set No. 1 to

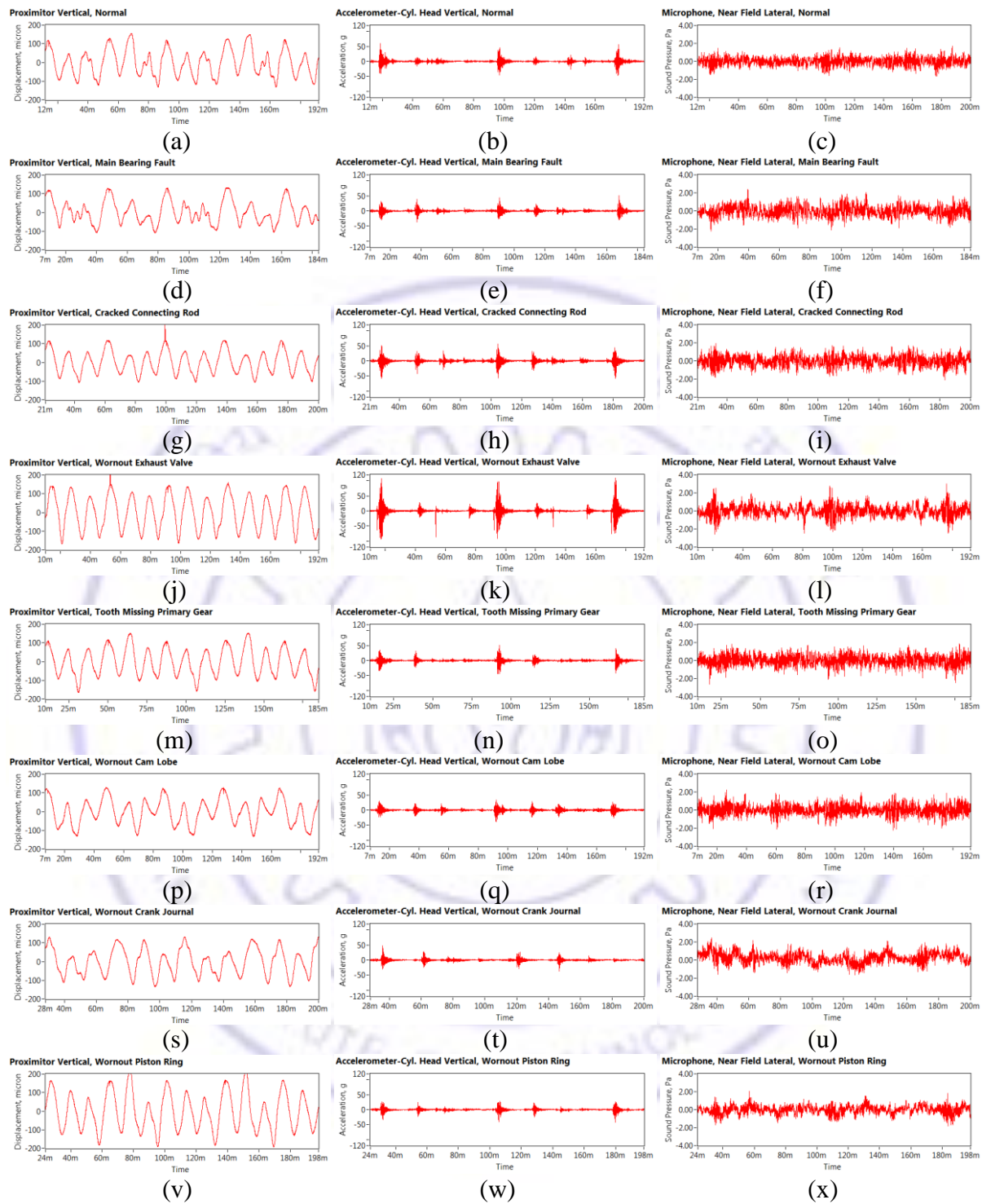


Figure 5.3: Proximity, Vibration and Sound Pressure Signals: (a-c) Healthy, (d-f) Main Bearing Fault, (g-i) Cracked Connecting Rod, (j-l) Worn Exhaust Valve, (m-o) Tooth Chipped Primary Gear, (p-r) Worn Cam Lobe, (s-u) Worn Crank Journal and (v-x) Worn Piston Ring

3 is collected as discussed in Section 3.2.4. Figure 5.3 shows the signals of Data Set No. 1 at 1500 rpm case for two full crankshaft revolutions.

Proximity signal shows crankshaft has irregular oscillations; they increased for main bearing fault, smoothed for a valve worn fault and its amplitudes increased for piston ring worn. Vibration signals show amplitude of cylinder firing event is high for valve worn defect and low for piston ring worn. Presence of large number of events in vibration signals of connecting rod fault indicates probable piston slap events. Its peak amplitudes at all events are considerably high so events are clearly visible, while for other faults they are less visible. Superimposing the engine information identifies them as valve opening and closing events. Tooth missing of primary gear has lowered the amplitudes of inlet valve events. Sound pressure signal shows presence of almost constant amplitude noise throughout the time, a clear and high amplitude sound pressure is seen in valve worn condition. In general, plots also indicate that there is a cycle-to-cycle variation in the amplitudes, which are useful for extraction of time invariant modal features. Cycle-to-cycle variation can be eliminated with averaging a large number of cycles at steady speed. Plots of statistical moments, fast Fourier and wavelet transforms are manually compared in the next few sections.

5.3.1 Comparison of Statistical Moments

Statistical moments measure the expected values and distribution of the signal. They have been widely used for machinery fault classification (Vyas and Satishkumar [223]). This section compares them manually for the selected faults obtained from Data Set No. 2 signal at steady 1500 rpm engine speed.

Moments of the proximity vertical, cylinder and base vibration vertical and near field sound pressure lateral signals are computed from the expressions listed in Table 5.1. They are plotted in Figure 5.4 for all the faulty cases. The moments are randomly distributed and few are overlapping that makes manual classification difficult, and demands for an automatic classifier. Classification with few moments can lead to misclassification error. In general, added defect has lowered some features and increased other features. Cracked connecting rod presented lower amplitude moments, but worn exhaust valve indicated higher amplitudes.

Table 5.1: Statistical Moments for Fault Comparison

No.	Moments	Expression	Measures
1	Absolute Mean (M ₁)	$\mu_x = E(x_i) = \frac{1}{n} \sum_{i=1}^n x_i$	Expected value
2	Maximum Peak (M ₂)	$x_{max} = \max(x_i)$	Highest amplitude
3	Minimum Peak (M ₃)	$x_{min} = \min(x_i)$	Lowest amplitude
4	Standard Deviation (M ₄)	$\sigma = \left(\frac{1}{n} \sum (x_i - \mu_x)^2\right)^{0.5}$	Amount of dispersion, spread
5	Coefficient of Variation (M ₅)	$V = \sigma/\mu_x$	Standardized dispersion
6	Variance (M ₆)	$s = \sigma^2 = \frac{1}{n} \sum (x_i - \mu_x)^2 = \frac{1}{2} E(x_i - \mu_x)^2$	Mean square error
7	Root Mean Square (M ₇)	$x_{RMS} = \left(\frac{1}{n} \sum (x_i)^2\right)^{0.5}$	Power content
8	Crest Factor (M ₈)	$C_f = \frac{x_{max}}{x_{RMS}}$	Extremeness of the peaks
9	Shape Factor (M ₉)	$S_f = \frac{x_{RMS}}{\mu_x}$	Affected by an object's shape
10	Median (M ₁₀)	$x_{0.5(n+1)}$ n odd, $\frac{1}{2}(x_{0.5n} + x_{0.5n+1})$ n even	Middle value
11	Mode (M ₁₁)	$x _{p(x)=max}$	Most frequent value
12	Range (M ₁₂)	$R = x_{max} - x_{min}$	Interval that indicate dispersion
13	Inter-Quartile Range (M ₁₃)	$IQR = x_{0.75} - x_{0.25}$	Quartile variability
14	Mid Range (M ₁₄)	$MR = (x_{max} + x_{min})/2$	Mean Interval
15	Mean Absolute Dev. (M ₁₅)	$MAD = \frac{1}{n} \sum (x_i - \mu_x)$	Average distance from mean
16	Geometric Mean (M ₁₆)	$G_m = (x_1 x_2 x_3 \dots x_n)^{1/n}$	Central tendency
17	Harmonic Mean (M ₁₇)	$H_m = \left(\frac{1}{n} \sum_{i=0}^n \frac{1}{x_i}\right)^{1/n}$	Average of rates
18	Skewness (M ₁₈)	$S_k = \frac{1}{x_{RMS}^3} E(x_i - \mu_x)^3$	Symmetry
19	Kurtosis (M ₁₉)	$K_r = \frac{1}{x_{RMS}^4} E(x_i - \mu_x)^4$	Flatness
20	Fifth Moment (M ₂₀)	$F_r = \frac{1}{x_{RMS}^5} E(x_i - \mu_x)^5$	Mode and tail movements

M₁₋₂₀ Moments, n – No. of sample, p(x) – Probability, **max** – maximum of the data, **min** – minimum of the data

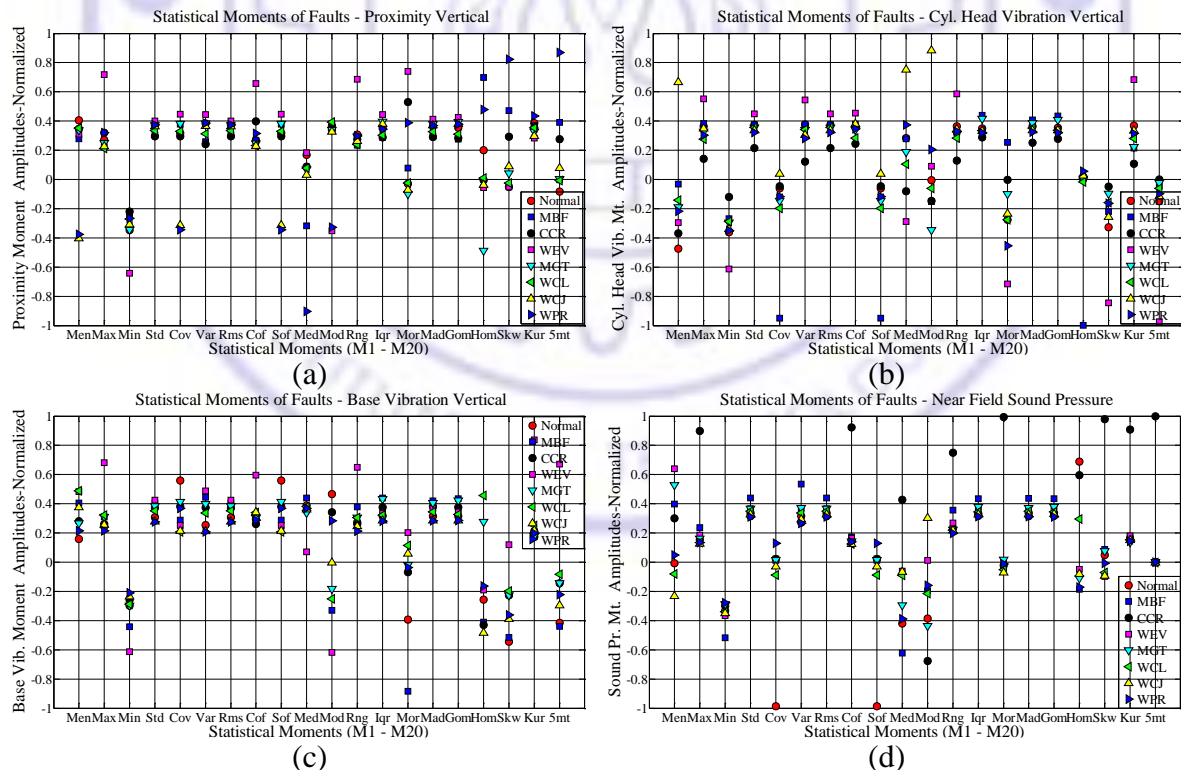


Figure 5.4: Statistical Moment Plots; (a) Crank Shaft Displacement, (b) Cyl. Head Vibration, (c) Base Vibration, (d) Near Field Sound Pressure

5.3.2 Comparison of Fourier Spectrums

Fourier features can distinguish harmonic characteristics of the faults. They are well suited for steady speed signals of rotating machinery. A few references [7, 52] and [6, 55] find their application on IC engines. In this section, FFT of cylinder head vibration and near field sound pressure are compared for all faulty cases at 1500 rpm.

FFT of Set No. 2 vibration and sound pressure signals are shown in Figure 5.5 and 5.6 respectively. Vibration signals indicated low amplitude for normal case, while exhaust valve and main bearing faults display higher values. Faults of crank journal, cracked connecting rod and cam lobe worn have shown much lower vibration. Chipped off gear, main bearing and piston ring worn shows the presence of higher order vibration harmonics. Table 5.2 lists fault salient features whose amplitudes are above 0.05g. Sound signals show high amplitude 1st order for main bearing, exhaust valve and piston ring worn fault. The 8th and 9th order amplitudes of normal case sound signals drastically increased or decreased for all the fault cases, which makes easy for fault classification. Crank journal, cracked connecting rod and cam lobe worn fault resulted into much lower sound pressure. Presence of several harmonics in main bearing and crank journal demonstrated signals are highly non-stationary. FFT salient features of each fault, whose amplitudes are above 0.04 Pa are listed in Table 5.2.

Table 5.2: Vibration and Sound Pressure Symptoms of the Engine Faults

Fault	Vibration							Sound							
	H _{2.5}	H _{3.0}	H _{5.0}	H _{6.5}	H _{7.0}	H _{>8.0}	H _{1<2}	H _{2.0}	H _{3.5}	H _{4.5}	H _{5.0}	H _{6.0}	H _{8.0}	H _{1<2}	H _∞
NOR	✓	✓	-	-	-	-	-	✓	✓	-	✓	-	-	-	-
MBF	✓	✓	✓	✓	-	-	-	✓	✓	-	✓	✓	✓	-	✓
CCR	-	-	-	-	-	-	-	✓	-	-	-	✓	-	-	-
WEV	-	✓	-	-	-	-	-	✓	✓	✓	✓	✓	✓	-	-
TMG	✓	✓	-	-	✓	✓	✓	✓	-	✓	-	-	✓	✓	-
WCL	-	✓	-	-	-	-	-	✓	-	✓	✓	✓	-	-	-
WCJ	-	✓	-	-	-	-	-	-	✓	-	✓	-	-	-	✓
WPR	✓	✓	-	-	✓	-	-	✓	✓	✓	✓	-	✓	-	-

H_{0.5-10} Harmonic Orders, ✓ Order Present, - Order Absent, H_∞ High Frequency Noise.

5.3.3 Comparison of Wavelet Contours

WT amplitude plots of Set No. 1 cylinder head vibration and near field sound pressure signals of all the faults at 1500 are computed as per the procedure discussed in

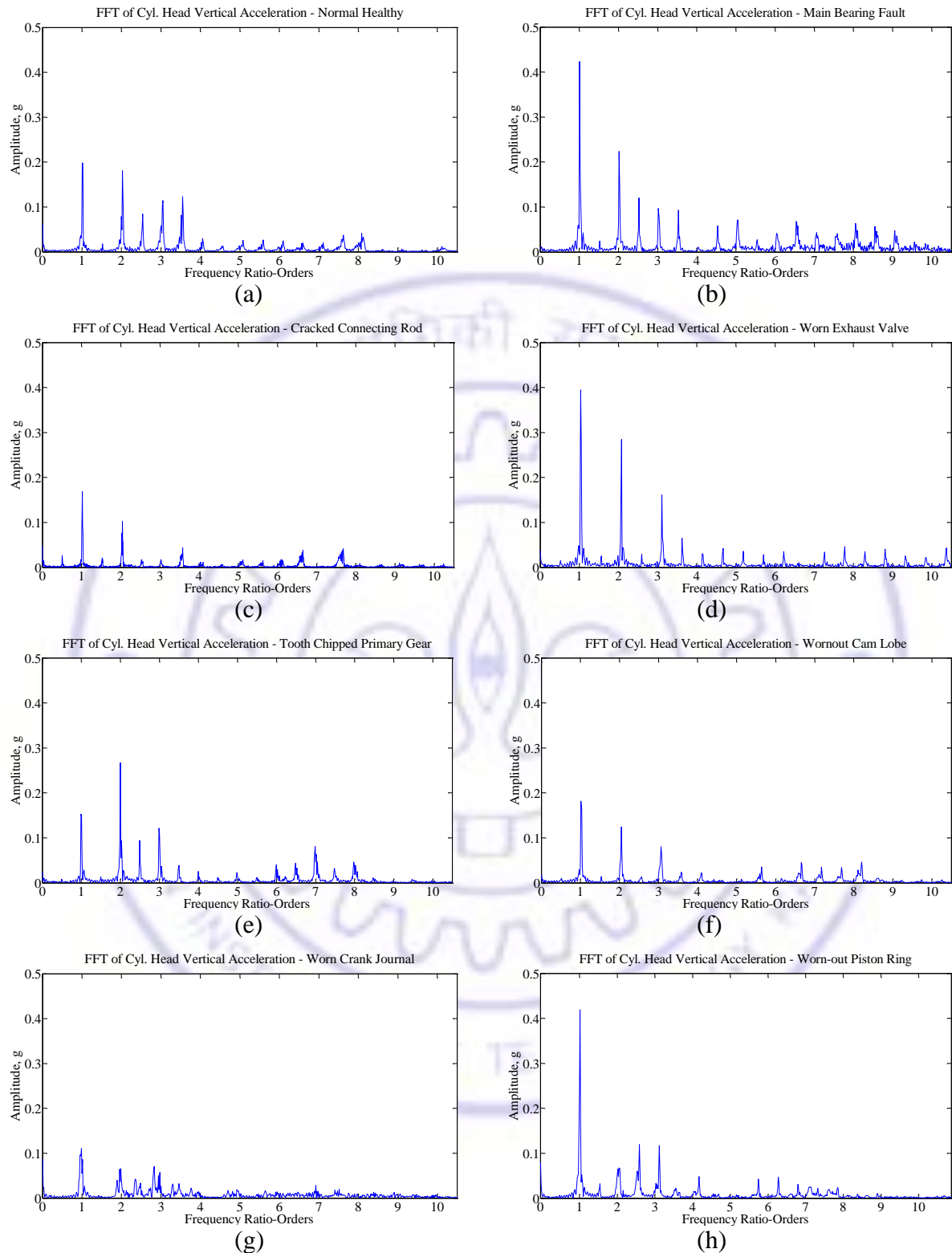


Figure 5.5: Cyl. Head Vertical Vibration FFT Plots; (a) Normal, (b) Main Bearing Fault, (c) Cracked Con. Rod, (d)Worn Ex. Valve, (e)Tooth Missing Gear, (f) Worn Cam Lobe, (g) Worn Crank Journal and (h) Worn Piston Ring

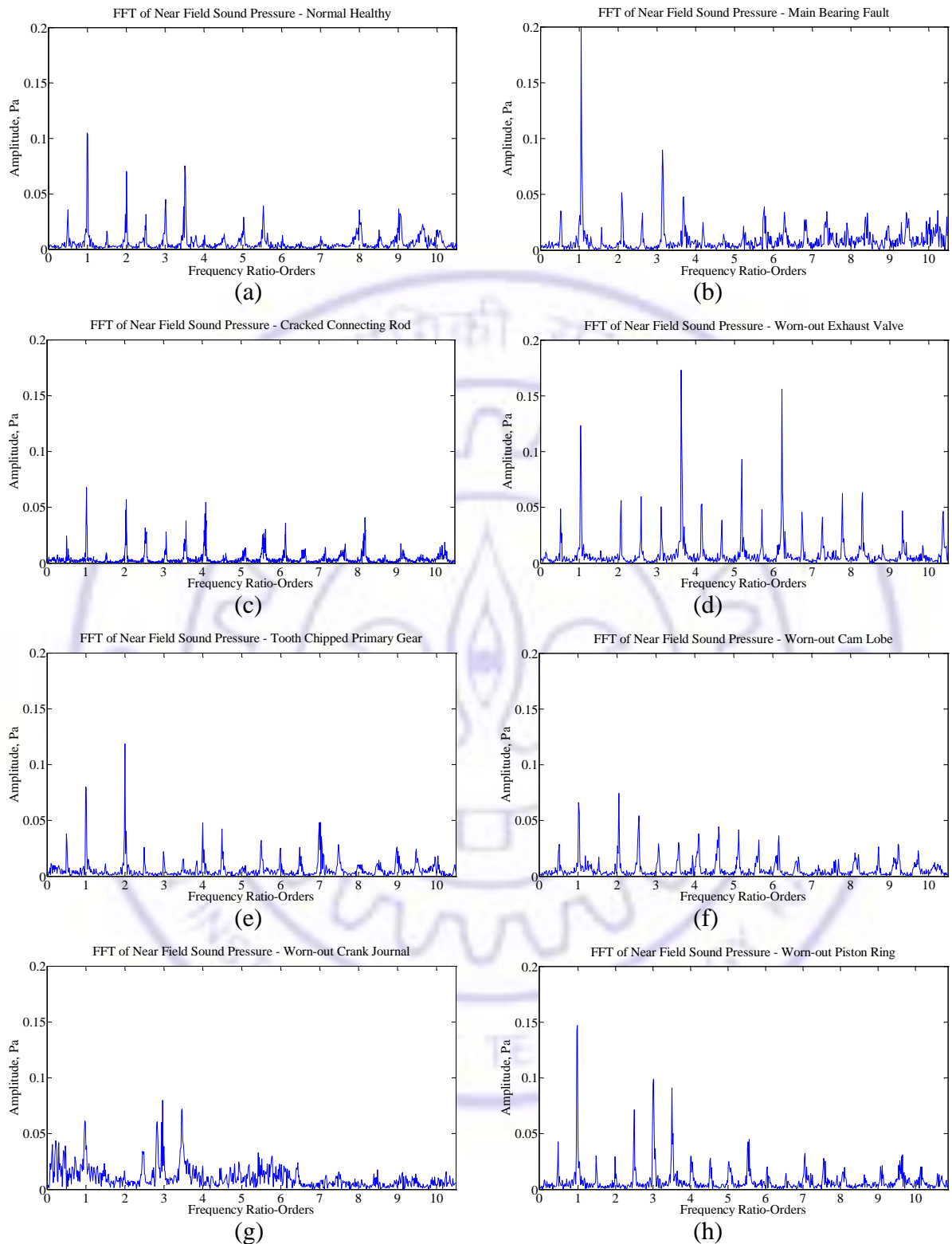


Figure 5.6: Near Field. Sound Pressure FFT Plots; (a) Normal, (b) Main Bearing Fault, (c) Cracked Con. Rod, (d)Worn Ex. Valve, (e)Tooth Missing Gear, (f) Worn Cam Lobe, (g) Worn Crank Journal and (h) Worn Piston Ring

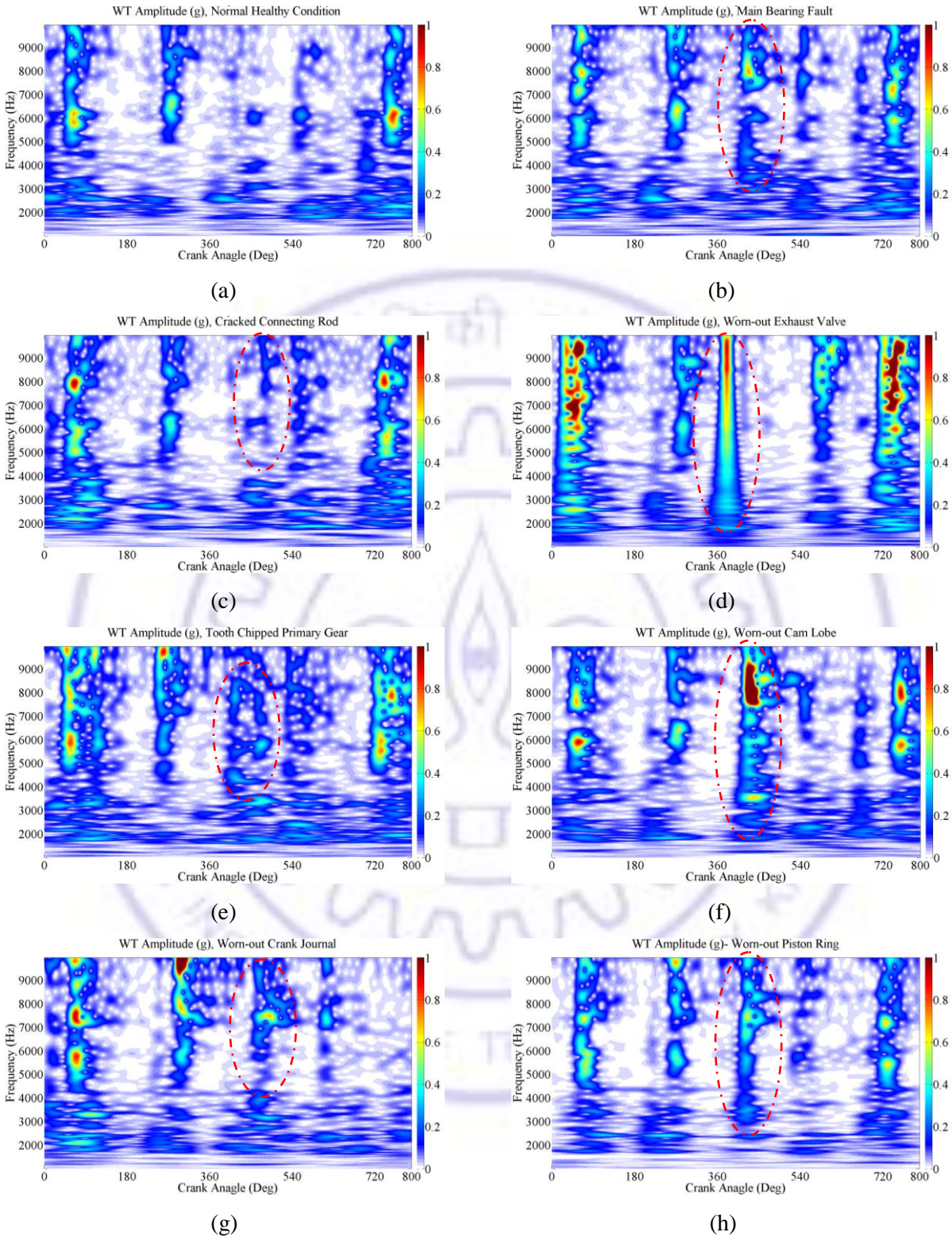


Figure 5.7: WT Plots for Cyl. Head Vibration Signal: (a) Normal, (b) Main Bearing Fault, (c) Cracked Con. Rod, (d)Worn Ex. Valve, (e)Tooth Missing Gear, (f) Worn Cam Lobe, (g) Worn Crank Journal and (h) Worn Piston Ring

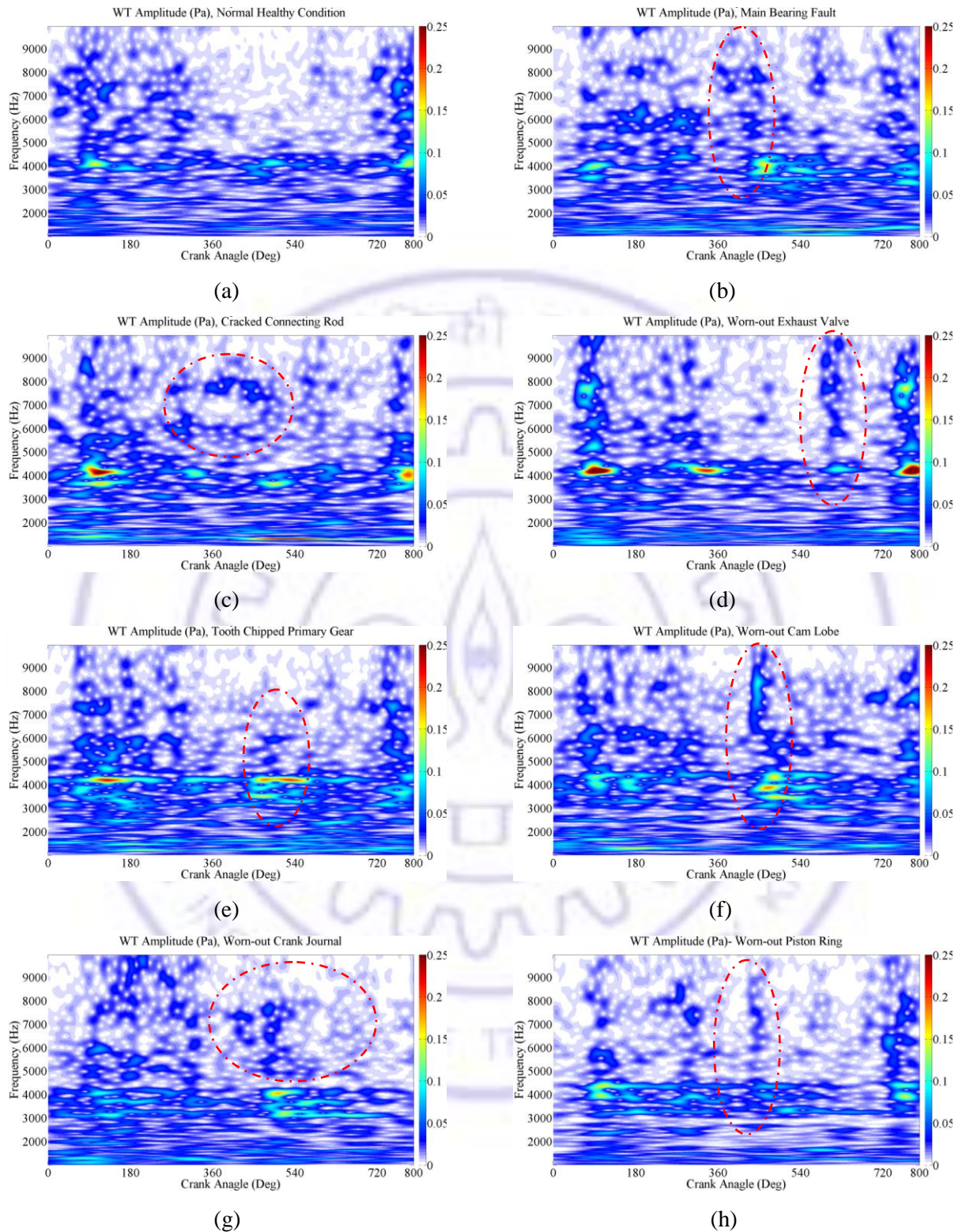


Figure 5.8: WT Plots for Near Field Sound Pressure Signal: (a) Normal, (b) Main Bearing Fault, (c) Cracked Con. Rod, (d) Worn Ex. Valve, (e) Tooth Missing Gear, (f) Worn Cam Lobe, (g) Worn Crank Journal and (h) Worn Piston Ring

Section 3.6.2.2 and 3.6.2.3. FFT of vibration and sound signals are shown in Figure 5.5-5.6. Plots are computed for 1.11 cycles i.e. 2.22 revolutions, 800° crank angle for 1-10 kHz range. All the plots have aligned for identical cycle with firing, exhaust, intake and compression strokes. Dominant salient features of each fault are highlighted in the respective plots.

Figure 5.7 (a) shows the WT amplitude of vibration signal at normal-healthy condition; it has a few high amplitude resonances. Firing and exhaust valve have dominant resonances around 6 kHz. Figure 5.7 (b-h) displays the WT amplitude at faulty conditions. WT plot of main bearing fault has additional dominant resonances at 450° CA, and 8 kHz at 500° CA. Cracked connecting rod shows high frequency resonances in 360° - 540° CA range. Exhaust valve has frequency dependent amplitude at 380° CA. Chipped gear exhibits medium frequency resonances in 360° - 540° CA range. Cam worn fault has dominant resonances at 8 kHz at 450° CA, worn journal and worn piston ring indicated resonances around 7 kHz at 400° CA. In general, all faults have dominant salient features in 360° - 540° CA range.

Figure 5.8 (a) demonstrates WT amplitude of sound signal at normal healthy condition with low amplitudes and high frequency (4 kHz) resonance for firing event. Main bearing and cracked connecting rod reveals some resonances around 7 kHz. Worn cam lobe and piston ring has a constant frequency response for a particular 360° - 540° CA range.

5.3.4 Feature Selection and Extraction

Features required to train the fault classifier are extracted from the transformed signals of Set No. 2. Statistical moments and harmonic orders are extracted for time domain signals from all the ten sensors and five speed stages using statistical analysis and fast Fourier transform. For all healthy and faulty conditions, a fault feature set is formed by extracting twenty features from each signal at each speed stage. Feature sets are fed to the classifier as inputs. To classify each fault, a target vector of element size 8 is assigned with binary values, where 1 and 0 indicates the presence and absence of a particular fault. Fault feature sets are formed from the inputs as,

Feature Set No. 1: Statistical moments

Feature Set No. 2: Harmonic orders

Feature Set No. 1: Statistical moments are computed from Table 5.1. Table 5.3 describes the training scheme with twenty moment's data for a normal case at 1500 rpm stage (Figure 3.7: c-j). To accompany all eight faults, one hundred and sixty moment's data are used to train the network. Data from other stage: 1000 rpm, 2000 rpm, 2500 rpm and 3000 rpm have been also used for the training.

Feature Set No. 2: Table 5.4 lists first ten harmonic and sub harmonic order peak amplitudes extracted from FFT spectra such as Figure 5.5 (a) cylinder head vertical and Figure 5.6 (a) sound pressure near field signals for normal case at 1500 rpm stage. Extraction process is repeated for all other signals, speed stages and fault cases.

Table 5.3: Statistical Moment Training Data

No.	Input Vector: Moments				Output Vector							
	M_1	M_2	...	M_{20}	NOR	MBF	CCR	WEV	TMG	WCL	WCJ	WPR
1	0.26	151.00	...	0.48	1	0	0	0	0	0	0	0
2	1.76	168.00	...	-0.38	1	0	0	0	0	0	0	0
3	-0.03	18.78	...	-42.58	1	0	0	0	0	0	0	0
4	-0.01	25.19	...	26.89	1	0	0	0	0	0	0	0
5	-0.02	23.62	...	3.81	1	0	0	0	0	0	0	0
6	0.01	6.73	...	-16.06	1	0	0	0	0	0	0	0
7	0.01	16.92	...	-18.76	1	0	0	0	0	0	0	0
8	0.02	18.79	...	-3.33	1	0	0	0	0	0	0	0
9	0.00	2.39	...	-0.01	1	0	0	0	0	0	0	0
10	0.00	0.753	...	-0.46	1	0	0	0	0	0	0	0

M_{1-4} Moments, **NOR** - Healthy or Normal, **MBF** - Defective main bearing, **CCR** - Cracked connecting rod, **WEV** - Worn out exhaust valve, **TMG** - Tooth missing primary gear, **WCL** - Worn cam lobe, **WCJ** - Crank Journal worn and **WPR** - Piston ring worn.

Table 5.4: Harmonic Order Training Data

No.	Input Vector: Harmonics				Output Vector							
	$H_{0.5}$	H_1	...	H_{10}	NOR	MBF	CCR	WEV	TMG	WCL	WCJ	WPR
1	15.94	25.51	...	1.75	1	0	0	0	0	0	0	0
2	23.70	18.79	...	4.36	1	0	0	0	0	0	0	0
3	0.00	0.20	...	0.01	1	0	0	0	0	0	0	0
4	0.01	0.02	...	0.02	1	0	0	0	0	0	0	0
5	0.00	0.25	...	0.03	1	0	0	0	0	0	0	0
6	0.01	0.28	...	0.02	1	0	0	0	0	0	0	0
7	0.01	0.05	...	0.01	1	0	0	0	0	0	0	0
8	0.00	0.03	...	0.01	1	0	0	0	0	0	0	0
9	0.04	0.10	...	0.02	1	0	0	0	0	0	0	0
10	0.02	0.05	...	0.02	1	0	0	0	0	0	0	0

$H_{0.5-10}$ Harmonic Orders.

5.4 Engine Fault Classification

This section builds statistical and intelligent classifiers that classify the engine signal features extracted in Section 5.3.4. A classifier is built, trained and tested for both statistical moment and harmonic order features. Performances of the classifier are compared in terms of optimal resources, efficient combinations and robustness to classify all eight faults.

5.4.1 Statistical Classification

Statistical techniques such as hypothesis testing, Multiple Discriminant Analysis (MDA), Multivariate Analysis of Variance (MANOVA) and cluster analysis can separate the various multivariate populations in an optimal way. Hypothesis tests compare the mean or variances of two or more sample data sets for the presence of a feature against alternative hypothesis in which they are absent. Discriminant analysis distinguishes the groups by a function. MANOVA sorts the available features according to their relevance. Cluster analysis segregates the features among groups and similar features within a group. [Jardine et al. \[1\]](#) reviewed the techniques that are being used for classification of the rotating machinery faults. Due to the non-stationary nature of IC engine signals, these methods are rarely used. In this work, a MDA is proposed for classifying engine faults.

Multiple Discriminant Analysis: Fisher Discriminant Analysis (FDA) is a powerful method for classification and dimensionality reduction of two-class problem ([Fisher \[224\]](#)). Similar to PCA, it projects a high-dimensional data onto a low-dimensional space, where the data achieves maximum class separation based on their Gaussian distributions. Separation boundary line is called as a discriminant function, which can be expressed as a linear combination of each observation. MDA is an extension of FDA for C -class problem. Discriminant function of a n number of samples $\mathbf{x} = \{x_1 \ x_2 \ \dots \ x_n\}$ with m number of observations in each sample and each observation belongs to one of C classes $\{X_1 \ \dots \ X_c \ \dots \ X_C\}$ of heterogeneous means and identical covariance can be expressed as,

$$\mathbf{y} = w^0 + \mathbf{w}'\mathbf{x} \tag{5.1}$$

where w^0 is a constant term, and w' is a vector, that affects the variables x , which represents probability of getting into the fault. It projects a higher dimensional data onto a line, where samples of different classes are being separated and same classes are being clustered together. An optimal transform maximizes the ratio of class scatter B to the scatter within the class W ,

$$B = \sum_{c=1}^C n_c (\bar{x}_c - \bar{x})(\bar{x}_c - \bar{x})^T \quad 5.2$$

$$W = \sum_{c=1}^C \sum_{x \in X_c} (x - \bar{x}_c)(x - \bar{x}_c)^T \quad 5.3$$

where n_c is number of training samples for each class, $\bar{x}_c = \frac{1}{n_c} \sum_{x \in X_c} x$ is sample mean from class c and $\bar{x} = \frac{1}{n} \sum_{c=1}^C n_c \bar{x}_c$ is the mean of all samples. Maximization of Fisher criterion is,

$$J(w) = \frac{w' B w}{w' W w} \quad 5.4$$

where w is the Fisher optimal discriminant direction. For non-singular W , the above equation can be transformed into eigenvalue problem as,

$$W^{-1} B w = \lambda w \quad 5.5$$

where $\lambda = \lambda_1, \lambda_2 \dots \lambda_r$ are the eigenvalues and corresponding eigenvectors can be denoted as $w = w_1, w_2 \dots w_r$. MDA uses $C - 1$ discriminant functions to discriminate among C -classes. Classes in Quadratic Discriminant Analysis (QDA) possess heterogeneous means and covariance; the discriminating function is given by [Duta et al. \[225\]](#),

$$y = w^0 + w' x + x' w'' x \quad 5.6$$

MATLAB inbuilt function *fitcdiscr()* is used to create the classifier. Misclassification cost per class in the existing data is checked and expected misclassification cost per observation in the new class is predicted. A cost matrix with 0 cost represents correct classification of an observation into its true class and 1 for incorrect classification.

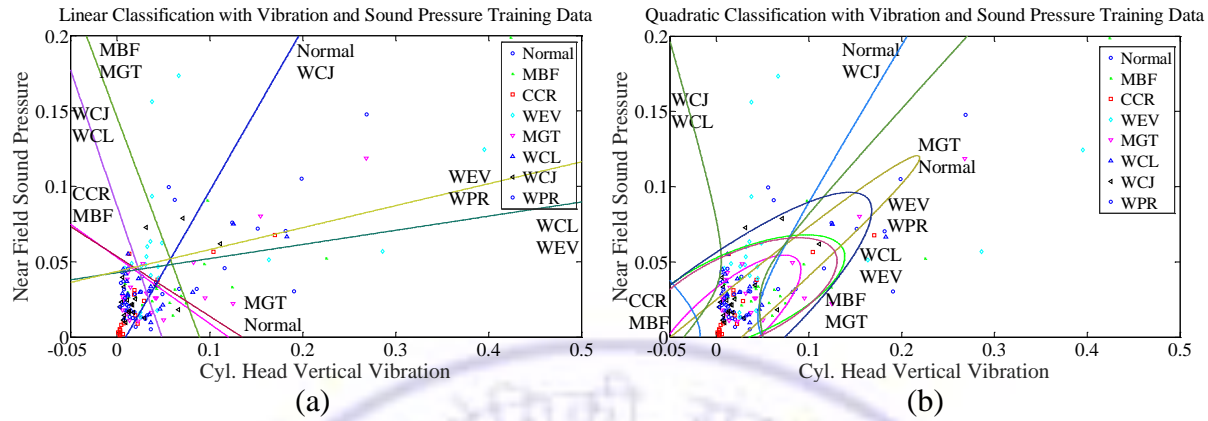


Figure 5.9: Discrimination of Faults from Vib. and Sound Pr. Data; (a) Linear, (b) Quadratic

Figure 5.9 (a) indicates that data has significant overlap, so they are not linearly separable. QDA in Figure 5.9 (b) denotes that it partially failed to separate the data. Performances of these classifiers are evaluated by computing the cost of misclassification. Data set used for training has 8 faults and 20 numbers of observations for each fault and speed case. Table 5.5 lists the desired percentage share of observations, a 100% share indicates that data does not contains other faults, i.e. 0% cross share represents the presence of a respective fault. Table 5.6 shows percentage of a fault being misclassified to other faults for 1500 rpm case.

Table 5.5: Fault Share (%) for MDA Training

No.	Fault	NOR	MBF	CCR	WEV	MGT	WCL	WCJ	WPR
1	NOR	100	0	0	0	0	0	0	0
2	MBF	0	100	0	0	0	0	0	0
3	CCR	0	0	100	0	0	0	0	0
4	WEV	0	0	0	100	0	0	0	0
5	MGT	0	0	0	0	100	0	0	0
6	WCL	0	0	0	0	0	100	0	0
7	WCJ	0	0	0	0	0	0	100	0
8	WPR	0	0	0	0	0	0	0	100

Table 5.6: MDA Classification Performance (%) at 1500 rpm

Fault	LDA								QDA							
	Data	NOR	MBF	CCR	WEV	MGT	WCL	WCJ	WPR	NOR	MBF	CCR	WEV	MGT	WCL	WCJ
NOR	40	10	0	5	5	5	5	30	55	5	5	0	0	20	0	15
MBF	10	25	10	10	10	15	15	5	0	55	15	10	5	10	5	0
CCR	10	5	15	25	25	5	10	5	0	5	75	5	0	10	5	0
WEV	0	0	5	35	40	0	5	15	0	0	0	100	0	0	0	0
MGT	5	10	0	10	65	0	5	5	0	0	0	0	100	0	0	0
WCL	5	15	20	10	25	10	15	0	0	0	5	10	0	75	0	10
WCJ	10	5	15	15	20	20	15	0	0	10	15	5	0	10	50	10
WPR	10	5	10	20	15	10	5	25	0	5	10	15	0	5	5	60

Table 5.7: MDA Classification Performance (%) for Sensor Cases

No.	Inputs Sensor, Architecture	Statistical LDA	FFT LDA
1	Proximity, Horizontal	25.00	50.00
2	Proximity, Vertical	100.00	62.50
3	Cyl. Head Vibration, Vertical	100.00	75.00
4	Cyl. Head Vibration, Lateral	87.50	50.00
5	Cyl. Head Vibration, Axial	87.50	62.50
6	Base Vibration, Vertical	100.00	100.00
7	Base Vibration, Lateral	100.00	100.00
8	Base Vibration, Axial	87.50	50.00
9	Near Field, Sound Pressure	62.50	87.50
10	Far Field, Sound Pressure	37.50	37.50

Table 5.8: Overall MDA Classification Performance (%) for Speed Cases

No.	Inputs	Discriminant	1000	1500	2000	2500	3000	All
1	Statistical	Linear	23.75	23.12	26.25	30.00	24.37	25.50
2	FFT	„	46.25	28.75	21.87	38.12	39.37	34.87
3	Statistical	Quadratic	70.62	73.12	71.87	73.12	73.75	72.49
4	FFT	„	70.00	71.25	55.00	63.75	55.62	63.12

QDA has reported high efficiency of the classification. Table 5.7 lists the capability of each sensor that correctly classifies the fault. It shows vertically mounted sensors are more capable to differentiate the faults. Table 5.8 shows the classification performance for each speed case and overall performance for all speed case combined under statistical and FFT inputs. The best classification is achieved at 3000 rpm case with QDA.

5.4.2 Intelligent Classification

Intelligent models have an ability to perceive information, reason, retain knowledge and adapt to the changing environments. In this section, a neural model is proposed and evaluated its capabilities in diagnosing the engine faults.

Artificial Neural Networks: ANN is widely used for rotating machinery (Vyas and Satishkumar [223]) and a few cases IC engine ([111-112] and [119]) fault classification. This section reviews its theoretical background, builds an engine ANN model and performs fault diagnosis. Figure 5.10 shows perceptron model of a biological neuron that is fed to a Multi-Layer Perceptron Network (MLPN). Output of an i^{th} perceptron after the activation function is,

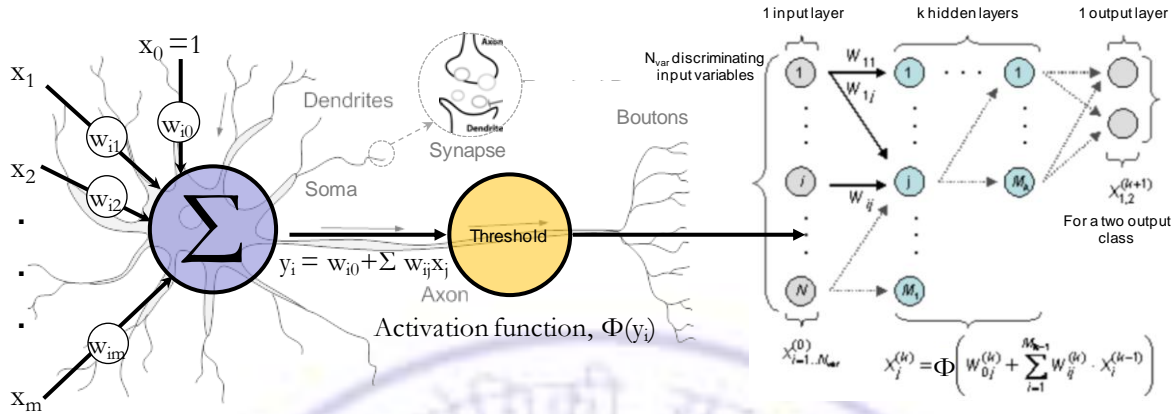


Figure 5.10: Perceptron Model Mapped to Biological Neuron and Fed to Multi Layers

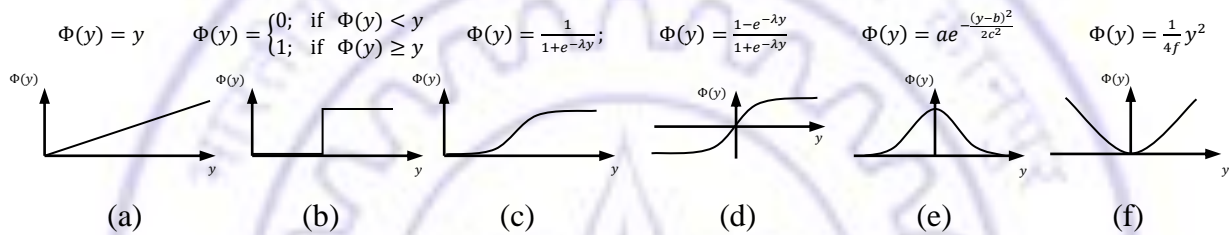


Figure 5.11: Activation Functions; (a) Linear, (b) Step (c) Sigmoid (d) Bipolar Sigmoid (e) Gaussian and (f) Parabolic

$$o_i = \Phi(y_i) = \Phi(w_{i0} + \sum_{j=1}^m w_{ij}x_j) \tag{5.7}$$

where $\Phi(\cdot)$ is an activation function, different types of activations are shown in Figure 5.11 that assigns response based on input activity level. Sigmoid and Gaussian functions are most commonly used activation functions. Parameter λ indicates a slope, while a, b and c are height, centre and width of the Gaussian function respectively. Information is flowing without forming a cycle; hence they are also called feed forward networks. A MLPN is used to train with the below mentioned learning rules,

Hebbian: $\Delta w_{ij} = \eta \cdot [o_i] \cdot x_j$ 5.8

Widrow- Hoff: $\Delta w_{ij} = \eta \cdot [d_i - o_i] \cdot x_j$ 5.9

Extended Delta: $\Delta w_{ij} = \eta \cdot [d_i - o_i] \cdot o'_i \cdot x_j$ 5.10

Co-relation: $\Delta w_{ij} = \eta \cdot [d_i] \cdot x_j$ 5.11

Covariance: $\Delta w_{ij} = \eta \cdot [y_i - \mu_y] \cdot [x_j - \mu_x]$ 5.12

where η is learning rate, d is desired or target value, o is actual output and $[d - o]$ is an error. x_j and y_i are the elemental inputs and outputs with their respective means μ_x and μ_y . Delta rule leads to a solution that is closer to the optimum, since it incorporates derivative of the activation function that reduces error more sharply; hence it is used in this work.

Gradient Descent Algorithm: Perceptron training rule may not converge if points are not linearly separable. In such case, weights are adjusted for all the training points to converge for best fit and reducing the total error. A gradient descent approach minimizes error by deciding the direction of error and continues to iterate till error becomes less than or equal to the specified value.

$$\Delta w_{ij} = -\eta \left(\frac{\delta E}{\delta w_{ij}} \right) \quad \text{where } E = \frac{1}{2} \sum_{j=1}^n (d_i - o_i)^2 \quad 5.13$$

Back Propagation Algorithm: A feed forward network is constructed with l , m and n as number of inputs (x_j), neurons (y_i) in hidden layer and outputs (o_k) respectively. Random weights (set between -0.05 and 0.05) are assigned and iterations are carried out until the termination condition (i.e. error limit or number of iterations) is met,

1. Forward propagate the inputs through network to generate the outputs.

$$y_i = \Phi(w_{i0} + \sum_{j=1}^l w_{ij}x_j) \quad j = 1 \dots l \quad 5.14$$

$$o_k = \Phi(w_{k0} + \sum_{j=1}^n w_{kj}y_j) \quad k = 1 \dots n \quad 5.15$$

2. Backward propagate the errors using propagated outputs and targets in order to generate deltas for all output and hidden neurons.

$$e_k = \sum_{k=1}^n (d_k - o_k) o_k \quad j = 1 \dots m \quad 5.16$$

$$e_i = \sum_{k=1}^n e_i w_{ij} y_i \quad j = 1 \dots m \quad 5.17$$

3. Gradient of the weight is obtained from output delta and input activation. Weight and basis are iterated in opposite direction by subtracting a ratio from the weight.

$$w_{kj}^{new} = w_{kj}^{old} + \eta e_k y_j; \quad w_{k0}^{new} = w_{k0}^{old} + \eta e_k \quad k = 1 \cdots n \text{ \& } j = 1 \cdots m \quad 5.18$$

$$w_{ij}^{new} = w_{ij}^{old} + \eta e_i x_j; \quad w_{i0}^{new} = w_{i0}^{old} + \eta e_i \quad j = 1 \cdots m \text{ \& } i = 1 \cdots l \quad 5.19$$

Generally, it requires $2n + 1$ number of neurons in a hidden layer. Error e_j is calculated for each hidden layer by feeding back the total error in each layer. Weight change in backward propagation can be combined to current and previous gradients.

$$w_{kj}(t + 1) = w_{kj}(t) + \eta e_k y_j + \mu [w_{kj}(t) - w_{kj}(t - 1)] \quad 5.20$$

where μ is the moment factor, whose value lies between 0 and 1. Feed-forward back propagation architecture is used by taking statistical moments and harmonic orders as listed in Table 5.3 and 5.4 as input features. Architecture consists of 20 input nodes and 8 nodes corresponding to the specific fault in the output layer. Cases are formed with varying the number of hidden layers and number of neurons in each hidden layer. In the first case, a hidden layer with 20 neurons is studied (Network architecture 20-20-8), while in the second case, 2 hidden layer with 20 neurons in each hidden layer is studied (Network architecture 20-20-20-8).

Network training process is started with total 1600 samples i.e. 20 features, 10 sensor signals and 8 faults. Initial weights are randomly assigned and during the learning process weights are automatically adjusted to minimize mean square error (MSE). A MSE is the difference between target output value (0 or 1) and network predicted output. Minimum error ensures correct fault identification. Training parameters such as number of iterations (1000) and learning rate (0.01) are arbitrarily chosen, and retained constant between the cases. Trained network is tested with unknown class. Network performance in terms of fault misclassification, effect of speed cases and sensor capability are reported. Figure 5.12 shows training performance and output classification for FFT input features. A MSE value of 11.5 is achieved within 1000 iterations for a 1500 rpm and output classification. Training has a success of 31%, which is low but considering the database that consist of features form all sensors and speed cases is large and complex so there is a chance of significant overlap of the features.

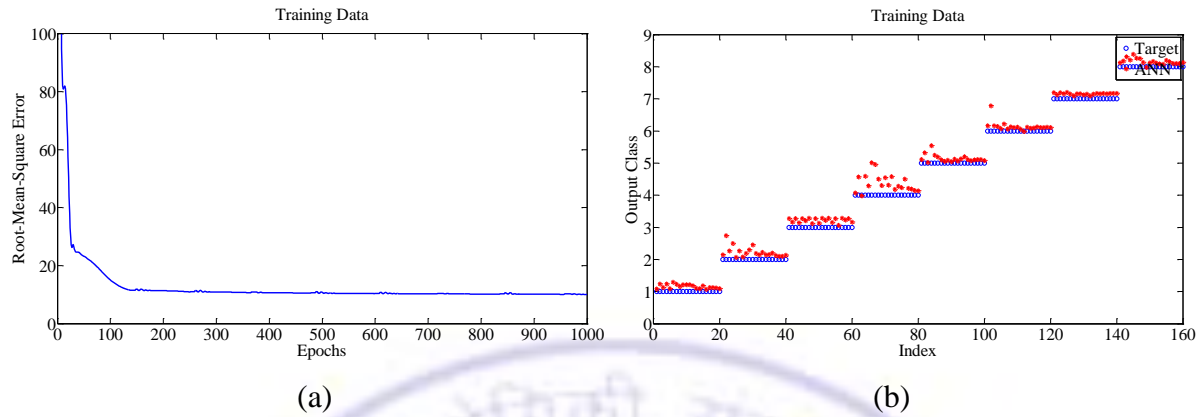


Figure 5.12: ANN Performance Plots; (a) RMSE, (b) Correct Output Classification

Table 5.9: ANN Classification Performance (%) at 1500 rpm

Set	Architecture 20-20-8								Architecture 20-20-20-8							
	Nor	MBF	CCR	WEV	MGT	WCL	WCJ	WPR	Nor	MBF	CCR	WEV	MGT	WCL	WCJ	WPR
Nor	27	11	8	10	10	11	12	11	37	13	6	10	1	14	14	20
MBF	9	30	7	10	11	11	11	11	19	33	5	10	2	12	14	19
CCR	10	10	28	10	11	11	11	11	17	13	26	10	2	13	13	20
WEV	9	10	7	30	9	11	12	11	17	13	6	31	1	12	13	20
MGT	7	12	8	8	31	9	11	12	16	14	6	9	21	13	12	21
WCL	9	10	7	10	10	31	11	11	18	13	5	9	1	32	13	21
WCJ	10	9	7	10	11	11	31	12	18	14	5	10	2	14	32	21
WPR	9	10	7	10	11	12	12	31	17	14	6	10	1	14	14	35

Table 5.10: ANN Classification Performance (%) for Sensor Cases

No.	Inputs Sensor	Statistical		FFT	
		20-20-8	20-20-8	20-20-8	20-20-8
1	Proximity, Horizontal	41.38	96.43	42.36	94.36
2	Proximity, Vertical	46.98	97.84	38.00	94.69
3	Cyl. Head Accelerometer, Vertical	24.25	13.16	21.83	15.00
4	Cyl. Head Accelerometer, Lateral	19.08	13.47	17.71	15.30
5	Cyl. Head Accelerometer, Axial	23.38	14.21	17.83	15.83
6	Base Accelerometer, Vertical	19.44	13.06	17.52	14.91
7	Base Accelerometer, Lateral	21.63	12.70	19.29	14.67
8	Base Accelerometer, Axial	15.74	12.89	15.79	14.77
9	Near Field, Microphone	28.01	12.97	29.75	14.78
10	Far Field, Microphone	14.86	12.60	11.56	14.65

Table 5.11: Overall ANN Classification Performance (%) for Speed Cases

No.	Inputs	Architecture	1000	1500	2000	2500	3000	All
1	Statistical	20-20-8	27.77	25.47	26.17	31.66	18.28	25.87
2	FFT	„	30.12	29.93	32.24	33.64	35.31	32.25
3	Statistical	20-20-20-8	23.04	23.16	23.20	25.00	19.64	22.81
4	FFT	„	28.08	30.89	30.75	33.88	24.80	29.68

Table 5.9 shows the percentage of fault being correctly classified (blue bold) and misclassified (un-bold) for 1500 rpm case. It indicates that the network has classified the data correctly by a major percentage, but there are some chances that it classifies into other faults due their overlap. Table 5.10 shows the correct classification percentage by each sensor. In most of the cases, FFT features of vertical proximity have shown highest capability by picking up variation in fault features. Near field microphone has shown some capability, while accelerometer has low capability in separating the faults. Correct classification performance for a particular speed case is obtained by averaging the individual percentages. Table 5.11 shows their values for all other speed cases. In case of 2500 rpm, the network has shown highest performance.

5.4.3 Model-based Classification

ANN is a data-driven classifier that uses huge data sets, consumes time and attempts to match exact patterns. It can't take knowledge, imprecision and experience information. Engine signals have a background noise that carry information from different fault modes, so fault symptoms are imprecise and unclear. Model-based classifier such as fuzzy and rough sets uses rule-based models that can represent the symptoms accurate with less iteration. In this section, a fuzzy logic system is proposed to diagnose the engine faults.

Fuzzy Logic System: Fuzzy uses knowledge based information to describe uncertain and ambiguous behaviors of the system. The variables are fuzzified as low, high, fast and slow membership functions. They are operated with rules to get the output variables and a decision from the outputs through the output membership functions. [Mechefske \[103\]](#) and [Ogaji et al. \[226\]](#) applied fuzzy logic for machinery fault diagnosis; they determined certain shape and limits of membership functions effectively to classify the fault. Fuzzy measure and fuzzy integral identifies certain interactions among the features that can increase diagnostic capability. It aggregates the worth of each feature and their supporting evidence that can be number, fuzzy set or interval information. [Liu \[227\]](#) used them for machinery fault detection; he presented an effective feature level fuzzy data fusion method. [Wu et al. \[21\]](#), and [Celik and Bayir \[114\]](#) employed fuzzy logic for IC engine fault diagnosis. They tracked order and performance amplitudes to classify fault. This section briefs the fuzzy logic and employs it

Fuzzy set can be empty, equivalent, subset or complement based on the membership, which can have union and intersection operations with the membership functions. Fuzzy inference system (FIS) is shown in Figure 5.14; the input variables are fuzzified by membership functions to determine a degree of input variable. Fuzzy rule with operator AND or OR i.e. minimum or maximum limit of the membership values is used to decide a degree of output variable. A single number from the degree of output variable is defuzzified. Inference rule generated using AND or OR operations is a logical form that consist of a function, which takes premises, analyzes their syntax and returns to a conclusion with de-fuzzification. It is constructed with relational, compositional and logic methods, while defuzzification uses centroid and maxima methods. Fuzzy inference can be Mamdani or Sugeno type as discussed in [Jang et al. \[228\]](#) based on way the crisp output is generated from the fuzzy inputs. In Mamdani inference, the output is defuzzified while in Sugeno it is either linear or constant computed by weighted average of the inputs.

This section discusses the methodology to build fuzzy system using statistical moment and harmonic order features that are listed in Table 5.3 and 5.4 respectively. Table has 10 variables, 20 features for a fault and speed case. There exist 5 speed cases and 8 fault classes. It requires 5000 membership functions for a 5 membership feature. Let X be the feature set,

$$X = \{x_1, x_2, x_3, \dots, x_{20}\} \quad 5.23$$

A rule can be formed by an interaction of membership function among the features of a variable i.e. $\mu(x_1) \cdots \mu(x_{20})$ to classify each fault. It requires minimum 8 inference rules. There are more than 80 rules for a speed case to account misclassification and inability to find clear trend. Hence a fuzzy inference rule is,

$$((\mu_1 \cap \mu_2 \cap \cdots \mu_{20})(x) = \min\{\mu_1(x), \mu_2(x) \cdots \mu_{20}(x)\}; \text{ for all } x \in X \quad 5.24$$

In order to reduce problem size, logic is evaluated for 1500 rpm case with first 10 FFT features. Fuzzy rules with desired memberships for each fault are shown in Table 5.12.

Table 5.12: Fuzzy Rules for Inference and True Memberships for Each Fault

Rule No.	If				Then								
	$\mu(x_1)$	$\mu(x_2)$...	$\mu(x_{10})$	NOR	MBF	CCR	WEV	TMG	WCL	WCJ	WPR	
1	L	VL	...	M	1	0	0	0	0	0	0	0	
2	VH	M	...	L	0	1	0	0	0	0	0	0	
3	0	0	1	0	0	0	0	0	
4	0	0	0	1	0	0	0	0	
5	0	0	0	0	1	0	0	0	
6	0	0	0	0	0	1	0	0	
7	0	0	0	0	0	0	1	0	
8	0	0	0	0	0	0	0	1	

$\mu(x_{1...10})$ are the membership functions of the features

True membership values can be represented by the fault matrix with diagonal cell value as 1 and remaining cell values as 0, where 1 and 0 corresponds to true and false condition of the fault. Shape and limits of membership function can decide tolerance of the fault. Limits are chosen based on mean (μ) and multiple of standard deviation (σ) from a five trial set of signals of Data set No. 2 on each feature. Limits of fuzzy membership domain are,

$$\text{Lower Limit} = \mu - n \sigma \tag{5.25}$$

$$\text{Higher Limit} = \mu + n \sigma \tag{5.26}$$

where n is accuracy factor of classification, which is investigated with 1 to 10 for the membership function. Optimal value of n is determined by a value for which highest correct

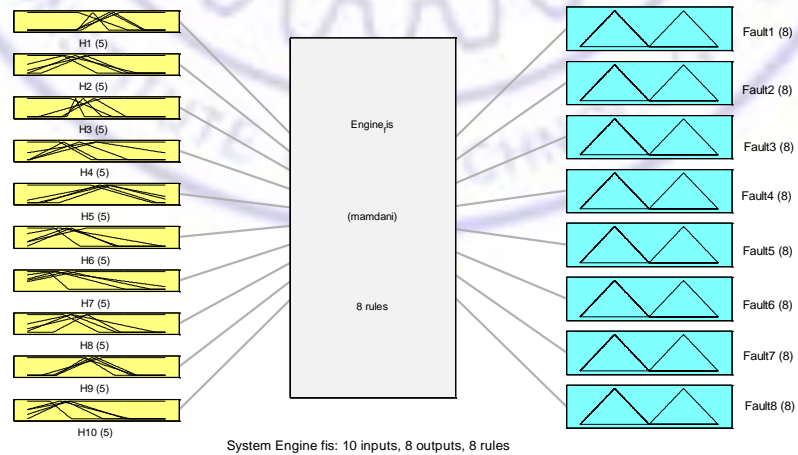


Figure 5.15: Engine Fuzzy Logic System

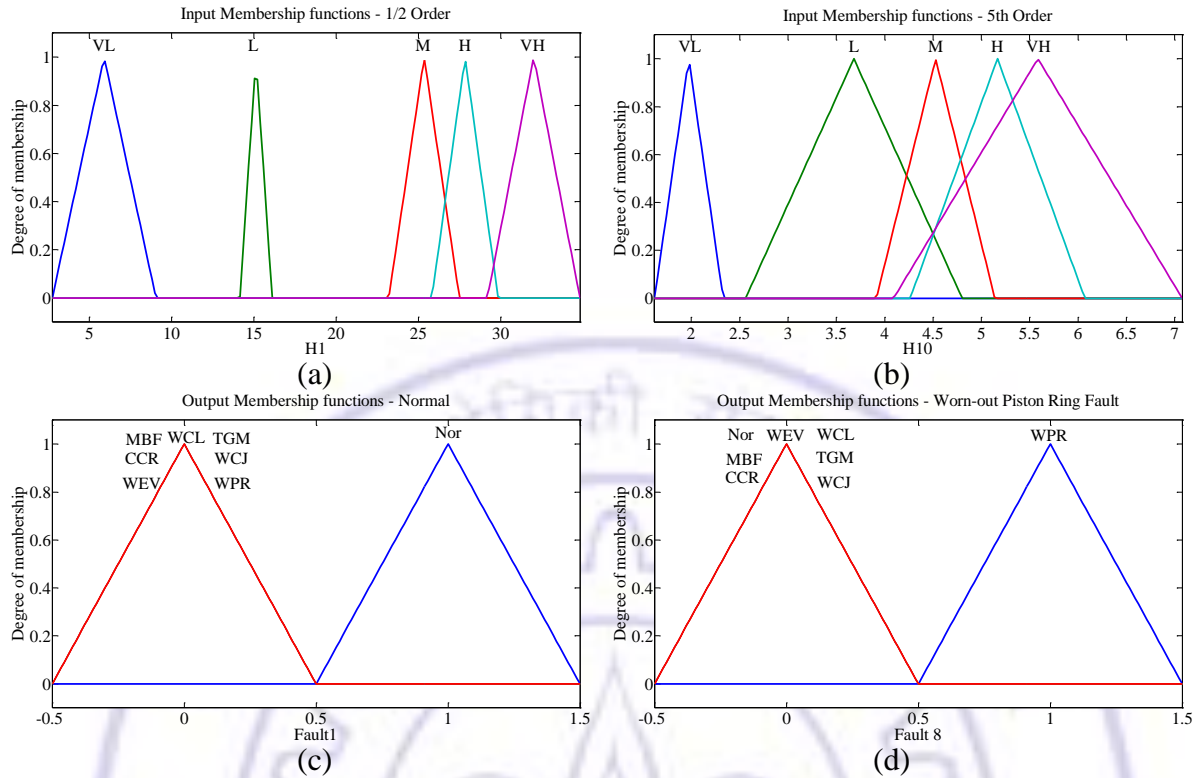


Figure 5.16: Membership Functions: (a) $H_{0.5}$ (b) $H_{5.0}$, (c) Fault No. 1 and (d) Fault No. 8

Table 5.13: Membership Values for CCR Data at 1500 rpm with Triangular Function

Set	n (multiples of S. D)							
	1	2	3	4	6	8	9	10
Nor	0.000	0.000	0.000	0.000	0.000	0.000	0.000	0.062
MBF	0.500	0.000	0.000	0.000	0.000	0.199	0.290	0.343
CCR	0.500	1.000	1.000	1.000	1.000	1.000	1.000	0.844
WEV	0.500	0.500	0.000	0.000	0.000	0.000	0.000	0.000
MGT	0.500	0.500	0.500	0.000	0.000	0.339	0.386	0.414
WCL	0.000	0.000	0.000	0.000	0.000	0.284	0.344	0.381
WCJ	0.000	0.000	0.000	0.000	0.000	0.282	0.343	0.380
WPR	0.500	0.500	0.500	0.000	0.000	0.000	0.102	0.231

0.000-0.499: Faults misclassified, 0.500: No clear trend for classification, 0.501-1.000: Correctly classified

Table 5.14: Fuzzy Classification Performance (%) at 1500 rpm

Set	Triangular								Gaussian							
	Nor	MBF	CCR	WEV	MGT	WCL	WCJ	WPR	Nor	MBF	CCR	WEV	MGT	WCL	WCJ	WPR
Nor	77	19	16	10	12	10	14	15	78	22	22	22	22	22	22	22
MBF	7	83	5	7	5	10	6	11	18	77	18	18	18	23	18	18
CCR	8	7	89	0	7	4	0	3	8	8	92	8	8	8	8	8
WEV	7	13	5	87	5	5	5	9	16	16	16	84	16	16	16	16
MGT	8	11	14	5	76	7	6	19	23	23	23	23	77	23	23	23
WCL	12	11	6	1	1	75	0	7	7	7	7	7	7	90	7	10
WCJ	11	8	24	5	5	5	70	12	15	15	21	15	15	15	79	15
WPR	8	23	5	5	5	5	5	77	12	12	12	12	12	12	12	88

Table 5.15: Fuzzy Classification Performance (%) for Sensor Cases

No.	Inputs Sensor, Membership	FFT	
		Triangular	Gaussian
1	Proximity, Horizontal	72.87	64.38
2	Proximity, Vertical	100.00	87.69
3	Cyl. Head Vibration, Vertical	75.00	74.08
4	Cyl. Head Vibration, Lateral	79.32	78.48
5	Cyl. Head Vibration, Axial	83.35	77.35
6	Base Vibration, Vertical	68.69	77.74
7	Base Vibration, Lateral	91.99	89.83
8	Base Vibration, Axial	87.59	89.73
9	Near Field, Sound Pressure	72.65	93.33
10	Far Field, Sound Pressure	61.72	99.19

classification is achieved between true membership and predicted membership. Cases are formed by varying the membership function shapes. In first case, input variables are constructed with triangle membership functions while in second case, Gaussian membership functions are considered. Figure 5.15 shows the fuzzy logic system constructed for engine; it shows input-output membership functions and inference system. Figure 5.16 (a-b) shows the membership domain constructed for first ($H_{0.5}$) and fifth order ($H_{5.0}$) of a horizontal proximity signal. Input variable membership functions are defined as very low (VL), low (L), medium (M), high (H) and very high (VH) respectively. Figure 5.16 (c-d) shows the output variable membership functions for first (Nor) and last (WPR) faults.

Table 5.13 listed the membership values computed by varying accuracy factor n for CCR fault data. Its optimal value is found 4 and 0.5 respectively for triangular and Gaussian membership functions. Triangular memberships give exact information, while Gaussian memberships shared the fault information. Table 5.14 shows the percentage of fault being correctly classified (blue bold) and misclassified (un-bold) into other faults. It is evident that by a major percentage, the logic is capable of classifying faults correctly. Table 5.15 shows correct classification percentage by sensor. In most of the cases, vertical proximity and microphone is capable of picking up the variation in fault features and logic has an ability to separate the faults. Due to the representation of entire set of samples by their generic form i.e. mean and standard deviations, only few rules are sufficient to classify the data. Fuzzy systems have less computational time, rules are generated manually and fuzzy system does not have learning capability so it is tedious to generate rules for a large set of variables.

Study of overall fuzzy classification performance for all speed cases and statistical moment feature requires significant time for fuzzification of variables and rule generation. Fuzzy is well suited for systems with only few variables.

5.5 Signals from Failure Samples

Connecting rod samples with different fault amplitudes that have been discussed in Section 5.2.2 are used to collect fault propagation signals. In the new samples, a cut of length 1.0-6.0 mm (Figure 5.2: a-c) is introduced in the step of 1.0 mm. Healthy connecting rod of engine is replaced by its cut length samples and Set No. 1 to 3 data are collected. Figure 5.17 shows vertical proximity and cylinder head vibration, and near field sound pressure of data Set No. 1 for all cut length samples. Proximity signals for a healthy condition shows irregularity that is reduced initially and increased with increased cut length. Engine vibrations also have shown similar trend as proximity signal. Sound pressure signals are not able to show a clear sign, except for a cut-length corresponding to fracture condition state.

5.5.1 Features Correlation

During the data acquisition for 2500 rpm stage with cut length 6.0 mm step; the connecting rod has suddenly fractured into two major pieces as shown in Figure 5.2 (c). Figure 5.18 shows rms amplitudes of these signals extracted for all cut lengths and speeds. Cylinder head vibration signals have shown growing amplitudes, proximity signals have shown decreasing trend and sound pressure has very small variation over the increased cut length.

Above series of increasing cut length steps are treated as crack length in crack propagation model. The critical length and cycles for unstable rapid fracture is estimated by fracture mechanics theory. In machineries, both component motion and fracture are dynamic, so crack length is not visible and it is not suitable for direct measurement. Information from the signals such as proximity, vibration and sound for cut or notch length can be combined with fracture mechanics model of same crack length. Thus, number of cycles to fracture and RUL can be estimated directly from engine signals. Information from prior signals and state-space representation of crack can be used to build a prognostic model and forecast the fracture. Paris law of crack length as a function of load cycle is given by,

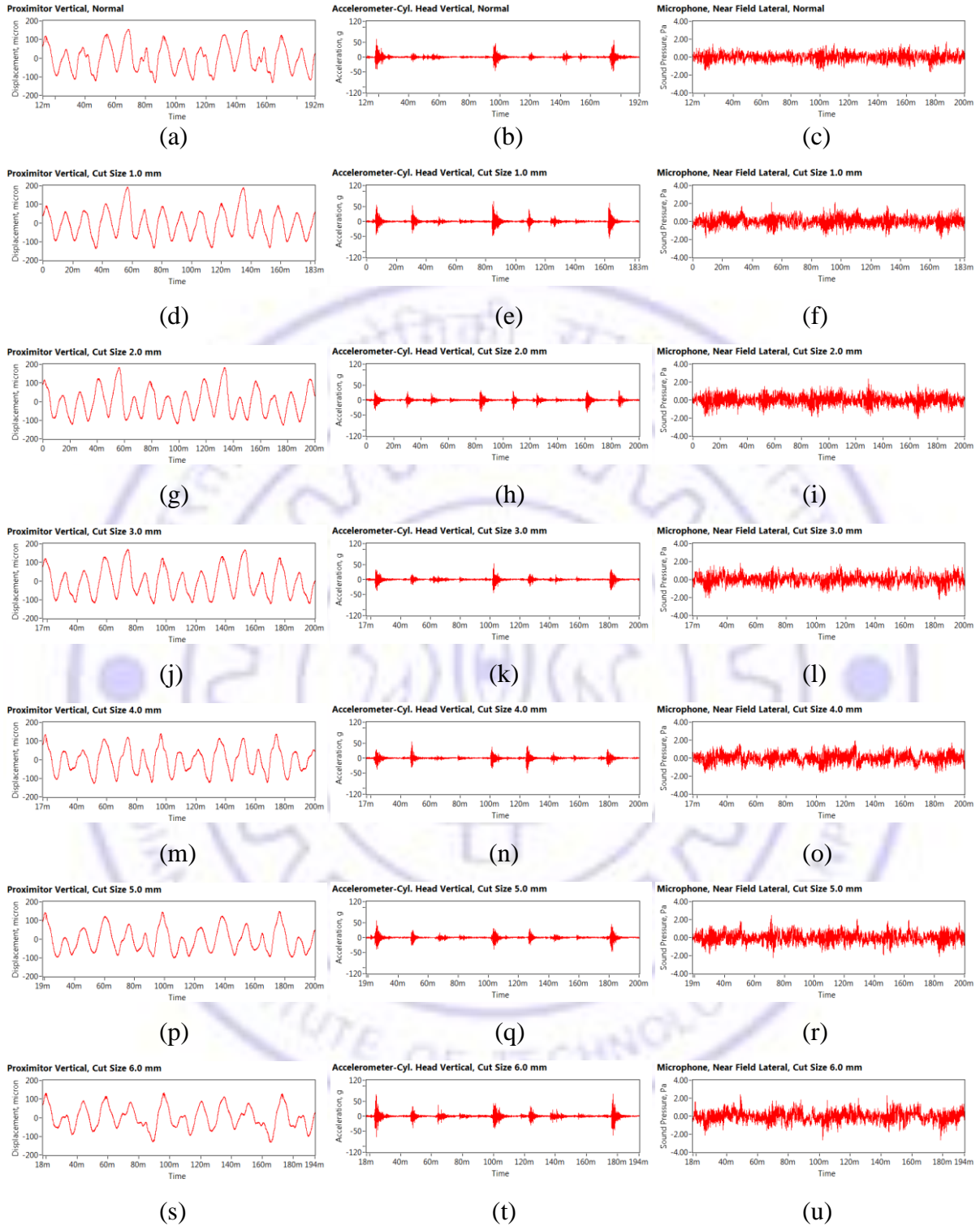


Figure 5.17: Proximity, Vibration and Sound Pressure Signals for Cut Length: (a-c) Healthy; (d-f) Cut length 1.0 mm, (g-i) Cut length 2.0 mm, (j-l) Cut length 3.0 mm, (m-o) Cut length 4.0 mm, (p-r) Cut length 5.0 mm, and (s-u) Cut length 6.0 mm

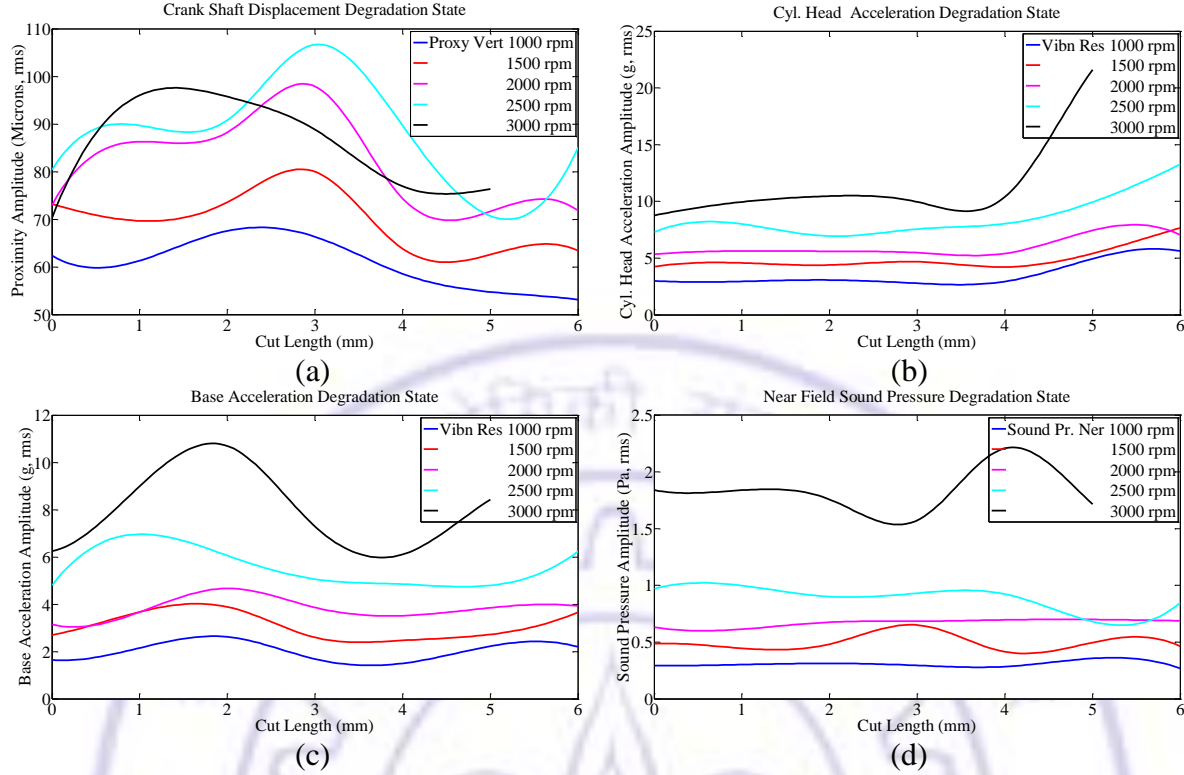


Figure 5.18: Signals Features v/s Cut lengths: (a) Shaft Displacements; (b) Head Vibrations, (c) Base Vibrations and (d) Near and Far Field Sound Pressures

$$\frac{da}{dN} = C(\Delta K)^m \quad 5.27$$

where $\Delta K = f(a/W)\Delta\sigma\sqrt{\pi a}$ is the stress intensity factor, $\Delta\sigma$ is stress range, a is crack length, $f(a/W)$ is geometric factor for a width W . C and m are material constants and their values for Aluminum alloy (7075-T6) are 1.1×10^{-11} and 3.89 respectively. Geometric factor for single edge crack is $f(a/W) = 1.12 - 0.23(a/W) + 10.6(a/W)^2 - 21.7(a/W)^3 + 30.4(a/W)^4$. By substituting ΔK expression in above equation and integrating gives the expression of crack propagation life [218] in cycles as,

$$N_f = \frac{a_0^{(-m/2+1)} - a_f^{(-m/2+1)}}{(m/2-1)Cf^m(a_0/W)(\Delta\sigma)^m\pi^{m/2}} \quad 5.28$$

where a_0 and a_f are initial and final crack lengths, and their values are taken as 0.1 mm and 6.0 mm respectively. Figure 5.19 (a) and (b) shows crack growth rate estimated for constant amplitude reversals and its *RUL* plots for different speeds using Equation 5.30, respectively.

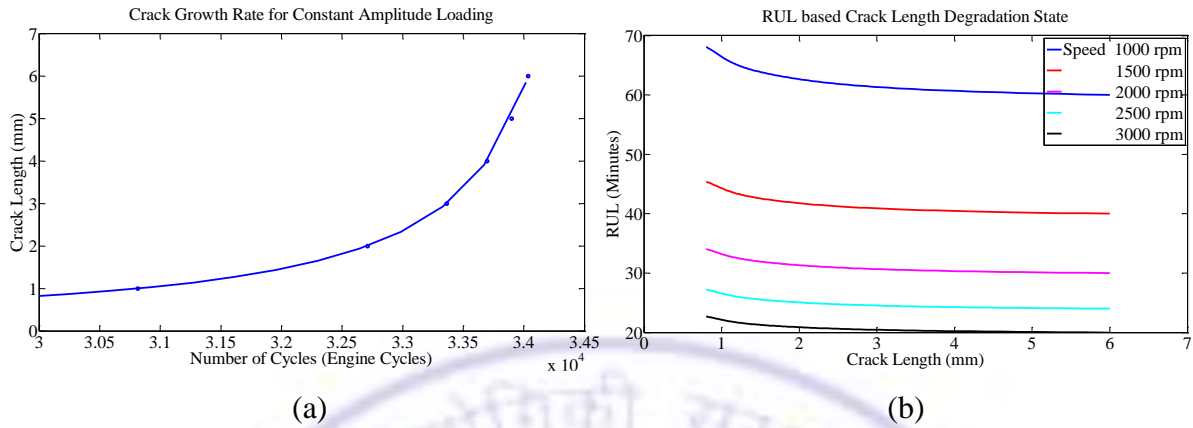


Figure 5.19: Connecting Rod Crack; (a) Constant Amplitude Loading, (b) RUL for Speeds

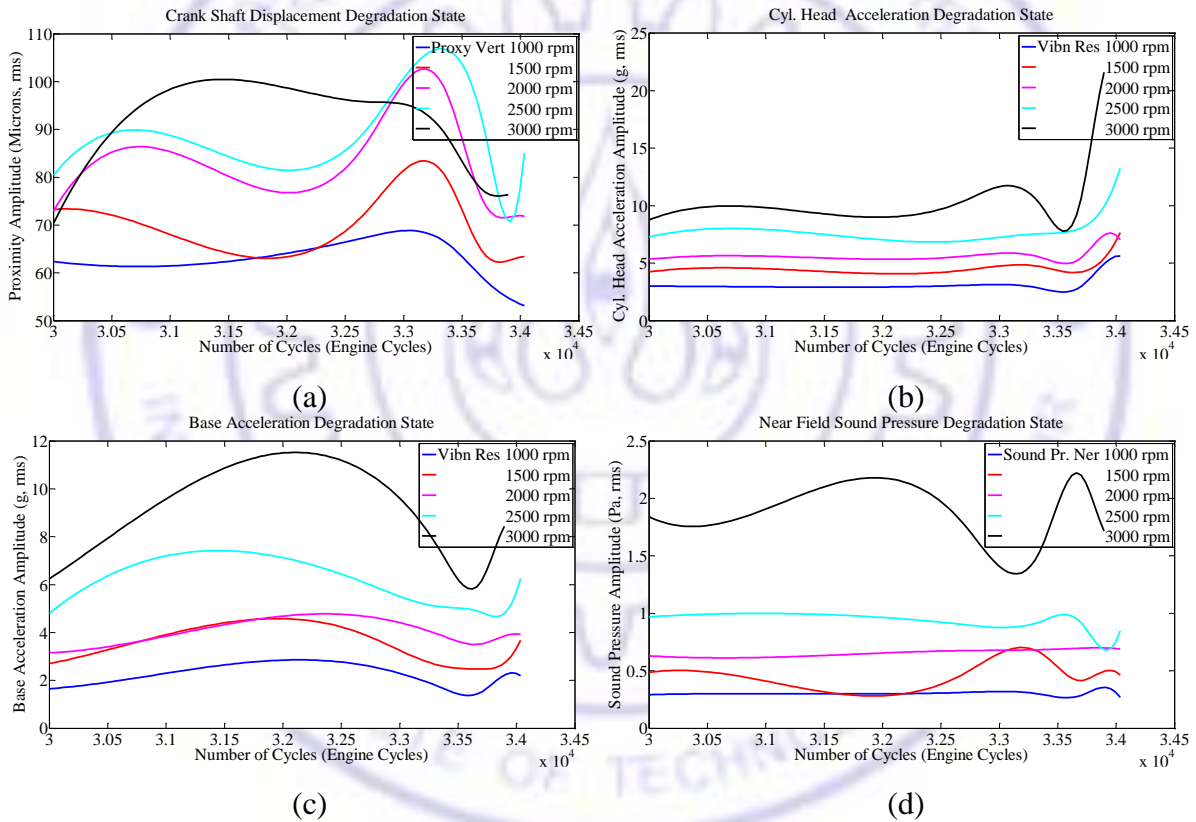


Figure 5.20: Signals Features v/s Number of Cycles: (a) Shaft Displacements; (b) Head Vibrations, (c) Base Vibrations and (d) Near and Far Field Sound Pressures

Figure 5.20 shows the plot of signal amplitudes against cycles for crack propagation. Due to non-linearity in the engine signals, bifurcation in number of cycle is observed for certain values of signal amplitudes. Correlation between the signal amplitudes and crack lengths can be conformed using correlation coefficient,

$$\rho|_a, x = \frac{E[(a-\mu_a)(x-\mu_x)]}{\sigma_a \sigma_x} \quad 5.29$$

where a is crack length and x is engine signal amplitude that follows the relation, $a = \rho x$. Table 5.16 shows the correlation values, it indicates that the cylinder head vibration amplitudes are well correlated with crack length. Cylinder head lateral vibration amplitude is highly correlated for almost all speed cases. Increased crack length has direct effect on lateral directional vibration. Proximity amplitudes have shown a negative correlation i.e. increased crack has decreased the crankshaft displacements.

Table 5.16: Correlation Coefficient between Growth of Crack and Engine Sensors

No.	Engine Sensors	1000	1500	2000	2500	3000	All
1	Proximity, Horizontal	0.453	0.529	-0.860	-0.581	-0.645	-0.221
2	Proximity, Vertical	-0.728	-0.639	-0.395	-0.212	-0.251	-0.445
3	Cyl. Head Vibration, Vertical	0.630	0.477	-0.249	0.816	0.733	0.481
4	Cyl. Head Vibration, Lateral	0.878	0.907	0.896	0.699	0.675	0.811
5	Cyl. Head Vibration, Axial	0.738	0.787	0.733	0.810	0.808	0.775
6	Base Vibration, Vertical	0.108	0.063	0.204	0.151	-0.293	0.047
7	Base Vibration, Lateral	0.360	0.169	-0.100	0.129	0.141	0.140
8	Base Vibration, Axial	-0.021	-0.165	0.274	-0.310	-0.134	-0.071
9	Near Field, Sound Pressure	0.019	-0.042	0.831	-0.725	0.088	0.034
10	Far Field, Sound Pressure	-0.292	0.578	-0.218	0.018	0.515	0.120

5.5.2 RUL from the Features

RUL is the duration that the total cycles remain for a failure. At steady engine speed i.e. constant amplitude cyclic loading, the RUL can be expressed as,

$$RUL = \frac{N_f - N_c}{N} \quad 5.30$$

where RUL is in minutes and engine speed N is in rpm. N_f and N_c are the number of cycles for fracture and consumed respectively. In Figure 5.21, RUL is plotted for different signal amplitudes and speeds. Theoretically, it exponentially decreases with increased crack length, as seen in Figure 5.19 (b), same trend has been observed for increased signal amplitudes and speeds. Cylinder head vibration curves have almost exponential decay and have less bifurcation, while proximity signals have lot of variation in amplitudes. At 1500 rpm, RUL is around 42 minutes which conforms to the value predicted by physics in Section 4.8.2.

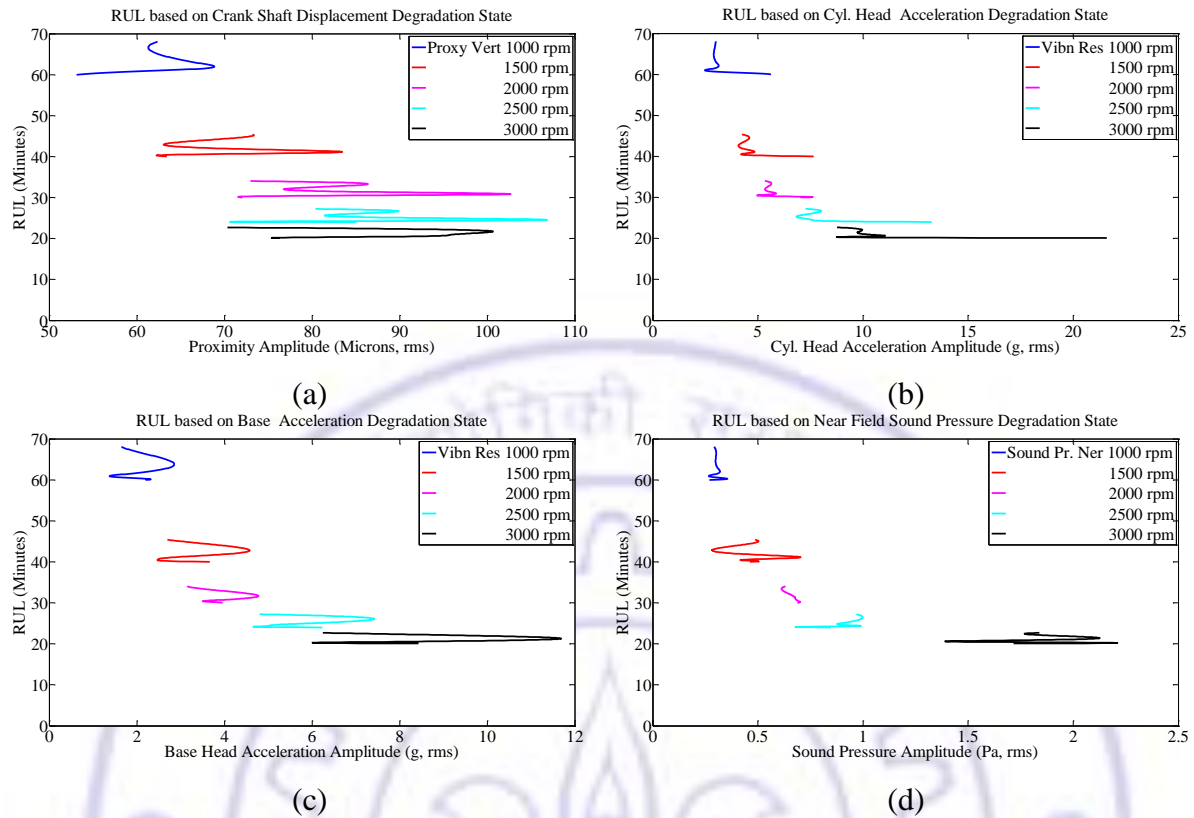


Figure 5.21: RUL for Engine Features: (a) Shaft Displacements; (b) Head Vibrations, (c) Base Vibrations and (d) Near Field Sound Pressures

5.6 Engine Failure Prediction

Figure 5.21 serve as reference curves in estimating *RUL* when engine is operated with one among the listed speed cases till the fracture. Model-based estimators such as Bayesian, Kalman or Particle filter combine physics or knowledge models with a few initial observations and uncertainty can predict general degradation states and *RULs* due to worn, cracked and bent components. They update unknown parameters in the form of probability density functions based on prior information of the unknown distribution and likelihood function. Particle filter is employed to predict fracture and *RUL* of connecting rod from a few initial measurements. Using the relation ' $a = \rho x$ ' between the crack length and engine signals, and Paris crack propagation model of engine signals can be established as,

$$\frac{d(\rho x)}{dN} = C(\Delta K)^m \quad 5.31$$

where a and x are crack length and engine signal amplitude respectively. Cadini et al. [229] have modeled the intrinsic stochasticity of the process in the above equation as,

$$\frac{d(\rho x)}{dN} = e^w C(\Delta K)^m \quad 5.32$$

where $\Delta K = \Delta\sigma\sqrt{\pi\rho x}$ is range of stress intensity factor. Rearranging the engine degradation model in the form of state transition as,

$$x_t = x_{t-1} + \frac{1}{\rho} C(\Delta\sigma\sqrt{\pi\rho x})^m \Delta N + w_t \quad 5.33$$

It represents a non-linear and non-stationary engine degradation process. The correlated degradation is predictable and directly measurable as,

$$z_t = x_t + v_t \quad 5.34$$

where w_t and v_t are the process and measurement noise respectively that can be Gaussian or non-Gaussian. The new state is estimated based on a suitable combination of the predicted states and measurements.

5.6.1 Kalman Filter based Degradation

It combines an expectation model with prior and current information optimally to estimate the parameters over time. Its process transitions can be illustrated in Figure 5.22. It assumes actions are linear and noise is Gaussian distributed. Kalman filter (KF) is based on Bayesian filter, $P(H_t|H_{t-1}, O_t)$ in which prior information is used to estimate the posterior information. It is based on Bayes' theorem:

$$P(H|O) = \frac{P(H)L(O|H)}{P(O)} \quad 5.35$$

where H is a hypothesis, O represents data, $P(H)$ is prior, $L(O|H)$ is likelihood, $P(O)$ probability of data and $P(H|O)$ is posterior probability. Kalman filter $P(H_t|H_{t-1}, \mu_t, O_t)$

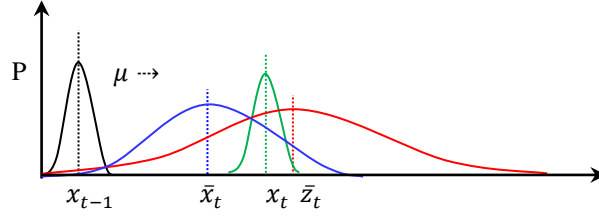


Figure 5.22: Illustration of transitions in Kalman Filter process

combines the probability of an existing state x_{t-1} , predicts state distribution \bar{x}_t under an action μ_t with Gaussian noise ε and sensor prediction \bar{z}_t to estimate its new actual state. State and sensor prediction variables which can be single or multiple as,

$$\bar{x}_t = Ax_{t-1} + Bu_t + w_t \quad 5.36$$

$$\bar{z}_t = C_z \bar{x}_t + v_t \quad 5.37$$

where A and B are state matrices, and C_z is a measurement transition matrix. $w_t \sim N(0, \sigma_x^2)$ $v_t \sim N(0, \sigma_z^2)$ are process and measurement errors, both are Gaussian white noise i.e. zero-mean normal distribution with standard deviation σ and $w_t \perp v_t$. KF estimates new states based on correction between predicted states and measurement. KF algorithm is,

Input: $A, B, C_z, x_{t-1}, u_t, E_x, E_z, z_t$

for $t = 1 \dots n$

$$\bar{x}_t = Ax_{t-1} + Bu_t$$

$$\bar{\Sigma}_t = A\Sigma_{t-1}A^T + E_x$$

$$K_t = \bar{\Sigma}_t C_z^T (C_z \bar{\Sigma}_t C_z^T + E_z)^{-1}$$

$$x_t = \bar{x}_t + K_t(z_t - C_z \bar{x}_t)$$

$$\Sigma_t = (I - K_t C_z) \bar{\Sigma}_t$$

end

where \bar{x}_t , $\bar{\Sigma}_t$ and x_t , Σ_t are predicted and final estimated state, covariance respectively. K_t is Kalman gain. For a crack correlated to engine degradation process with single variable $A=1$, $B=\frac{1}{\rho}C(\Delta K)^m$, $u_t = N_t$, $C_z = 1$. It requires an initial state distribution of the signals, process error $E_x = \sigma_x^2$ and measurement error $E_z = \sigma_z^2$ can be obtained from [Cobb et al. \[230\]](#).

Kalman filter assumes that the transitions are linear and action follows Gaussian distribution that makes the calculations rapid and accurate. However non-linear systems with Gaussian noise system can be projected into linear by extended Kalman filter. Practical problems are non-linear and have multimodal distribution so particle filter is an extension of Kalman filter that approximates transition by particles instead of functions and uses Monte Carlo simulations to avoid linear transition and models non-linear and non-Gaussian dynamics. Hence the particle filter is adopted for the prediction of engine degradation.

5.6.2 Particle Filter based Degradation

Particles are a set of randomly chosen weighted samples that approximate probability density function and update new estimated state under action and process noise. The observations are updated with measurement noise and weights are calculated with probability of the likelihood of measurement. Based on the weights, particle distribution is re-sampled to improve the estimates, which are iterated over and over for new estimate as illustrated in Figure 5.23. The particle filter model can be written as,

$$x_t = f(x_{t-1}, u_t) + w_t \quad 5.38$$

$$z_t = g(x_t) + v_t \quad 5.39$$

where x is state z is measurement, and f and g are their respective non-linear transition functions, w_t and v_t conditionally independent noise distribution and u_t is action command.

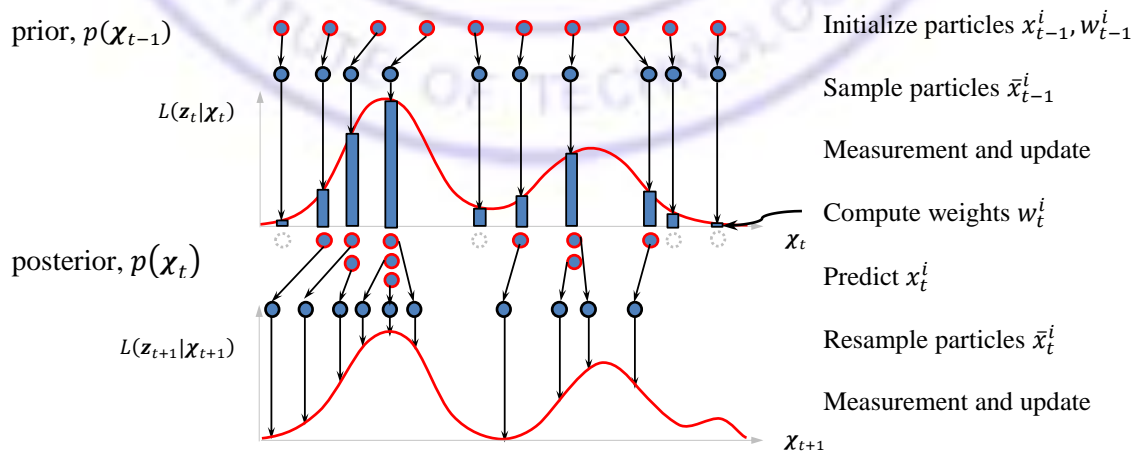


Figure 5.23: Illustration of Transitions in Particle Filter Process

Particle filter algorithm (χ_{t-1}, u_t, z_t) with an input set of particles $\chi_{t-1} = \{x_{t-1}^i, w_{t-1}^i\}$ and associated weights w_{t-1}^i are used to construct particle set χ_t as,

```

 $\bar{\chi}_t = \chi_t = \emptyset$ 
  for  $i = 1 \dots n$ 
    Sample particles according to weight  $w_{t-1}^i$ 
    Sample state  $x_t^i \sim p(x_t | x_{t-1}^i, u_t)$ 
    Reweight particles  $w_t^i = p(z_t | x_t^i)$ 
  end
  Total weight  $k = \sum_{i=1}^n w_t^i$ 
  for  $i = 1 \dots n$ 
    Normalize  $w_t^i = w_t^i / k$ 
     $\bar{\chi}_t = \bar{\chi}_t + \{x_t^i, w_t^i\}$ 
  end
   $\chi_t = \text{Resample}(\bar{\chi}_t)$ 

```

Zio and Pelsoni et al. [231] formulated the particle filter to estimate crack growth by modeling it as non-linear system affected by non-additive noises. Orchard and Vachtsevanos [232] detected crack and predicted RUL in a planetary carrier plate using particle filter. They mapped the measured vibration feature information to the actual crack size. An et al. [5 and 233] presented a particle filter MATLAB script for crack growth progression and RUL prediction. Current work adopts particle filter to model Equation 5.33 in predict engine vibration degradation. Distributions $N(7.27 \ 7.27^2)$ and $N(4.79 \ 4.79^2)$ are used to describe initial state x_0 of cylinder head and engine base signals respectively at 2500 rpm. Distribution $m_0 \sim N(3.89 \ 0.2^2)$ and $C_0 \sim N(-20.72 \ 1.12^2)$ represents Paris variables for Aluminum alloy 2219-T851. Stress range in connecting rod is 56.51MPa as listed in Table 4.3 is used. Likelihood of the measurement is assumed as Gaussian distribution as,

$$L(z_t | x_t^i, m_t^i, C_t^i) = \frac{1}{z_t \sqrt{2\pi\zeta_t^i}} \exp \left[-\frac{1}{2} \left(\frac{\ln z_t - \lambda_t^i}{\zeta_t^i} \right)^2 \right] \quad 5.40$$

where $\zeta_t^i = \sqrt{\ln[1 + \sigma/x_t^i(m_t^i, C_t^i)]}$ is the variance, σ is the standard deviation of measurement that is assumed as 0.001g and $\lambda_t^i = \ln[x_t^i(m_t^i, C_t^i)] - 1/2(\zeta_t^i)^2$ is the mean of the process.

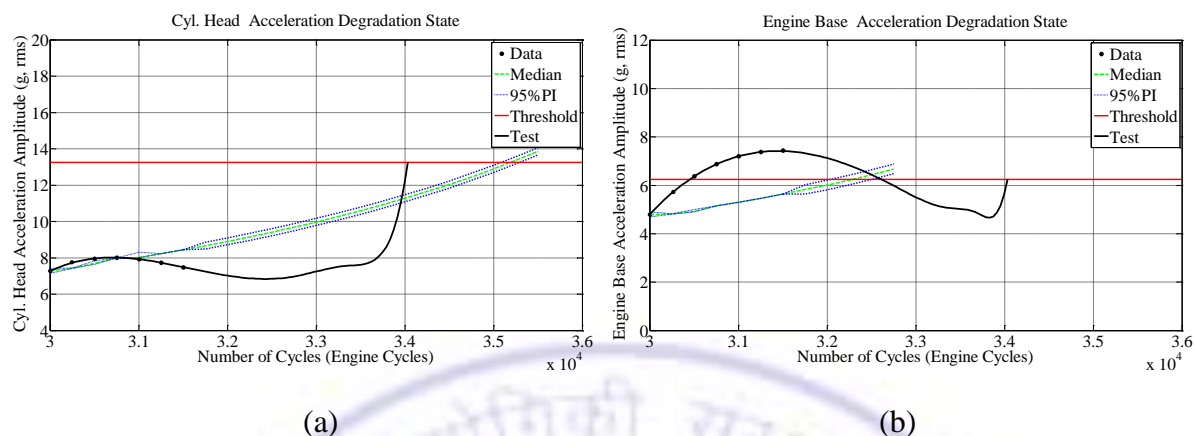


Figure 5.24: Estimation of New States using Particle Filter; (a) Cyl. Head, (b) Engine Base

In the accelerated run-to fail test, connecting rod has fractured for a cut length of 6.0 mm stage, which is equivalent to 34,035 engine cycles. Vibration amplitudes corresponding to the fracture condition are considered as threshold responses. Measured values for 0 to 2 mm cut length stage are used to train the filter and vibrations are predicted at 95% confidence interval. Figure 5.24 shows the results plotted for cylinder head and engine base, and superimposed with the respective measured degradation data. Connecting rod has actually fractured at 35,197 engine cycles, while prediction from cylinder head and engine base degradations indicated the fractured at around 32,284 engine cycles respectively. Measured degradation curves have multiple values of the cycles, while predicted curves have single values. Differences are due to non-linearity and noise in the signals. Despite of the practical complexity, the model based approach predicted values that are close to the actual fracture so it is good enough for prediction.

5.7 Conclusions:

In this chapter, a simple and novel tool for fault diagnosis and failure prognosis in an IC engine is proposed. Signals are acquired for the emulated faults and run-to-fail conditions. By re introducing faulty main bearing, cracked connecting rod, worn valve, tooth missing gear, worn cam, journal and piston ring. Symptoms to distinguish fault are studied and characteristics to predict connecting rod fracture are investigated.

Signals from faulty the components are processed using features extract from statistical moments and fast Fourier transforms. Fault diagnosis is carried out manually by comparing the features and it is then automated. Comparison of moments indicated that they are not angle to produce definite trend and features are inefficient to classify the faults manually. Comparison of Fourier and wavelet transforms for a 1500 rpm case indicated a few noticeable symptoms. However, it is found to be tedious and time consuming, so it demands an automatic classifier. In the automation process, statistical, intelligent and model-based systems are proposed. Features extracted using statistical moments and fast Fourier transforms for all speed stages are fed as inputs to the classifier and faults are classified. In statistical approach, a multiple discriminant method is used to distinguish the fault classes. In intelligent approach, an artificial neural network is built and trained for fault classification. In model-based classifier, a rule-based fuzzy logic is built to classify the engine faults. Results indicated that the model-based approach is efficient in fault classification as it has reduced the number of computations. But it requires rules, which are difficult to generate, consumes time and demands domain knowledge. ANN is easy and adaptive tool, but it has poor performance. MDA is effective, since it requires several cases and uses manual comparison of each plot formed by set of two variables.

Failure prognosis is carried-out using run-to-fail experiments and model-based predictor. Cut length information of run-to-fail trials on cracked connecting rod is related to the crack length of fracture mechanics, which are correlated to measurable signals. The engine degradation in terms of remaining useful life is estimated from proximity, vibration and noise signals. RUL curves constructed from the measured signals indicated at lower amplitudes and speed they have high life while at higher speeds and signal amplitudes they have lower life. It serves as a reference in estimating *RUL* when engine is operated with one among the listed speed cases. A model-based particle filter predicted the cycles for connecting rod failures, engine degradation states and symptoms with a few initial measurements. Results indicates that the proposed methodology has a good correlation with its physics based model results, so it is efficient to predict the degradation state for monitoring connecting rod failure.



CHAPTER 6

HYBRID METHODOLOGY HEALTH MANAGEMENT

Art is the lie that helps us to see the truth.

- Picasso (1881 – 1973)

6.1 Introduction

In Chapters 4, faults and failures are predicted using physics-based models. They provided a quick and complete insight, but demand an in-depth theoretical knowledge and their accuracy depend on simplicity, and certainty of the systems. Real faults and failures are too complex, affected by highly uncertain process and mathematical models are less effective to predict actual behaviors (Heng et al. [19] and Pascual [20]). Chapters 5 discussed data-driven and modal-based decision support systems to deal, large database due to changing environment or uncertainty and imprecision. These approaches suffer some or other deficiencies. Rigorous data and enormous experiment restricts the study to a particular machine; it is challenging to make them generic. Rules are extracted from the observations, they require domain knowledge to either derive through physics theory or condensing experience into empirical. Actual system requires decision support systems that resemble the human's way of reasoning, i.e. use of inexact, imprecise, incomplete and knowledge learning, which can be accomplished using Computational Intelligence (CI). It hybridizes five main complementary techniques: fuzzy logic to understand natural language, artificial neural network to learn from experiential data, evolutionary computing for the process of natural selection, learning theory, and probabilistic methods for dealing with uncertainty and imprecision. Hybrid system combines high-fidelity theoretical and low-fidelity data driven models for learning

and making decision from the data. It is suitable to monitor complex system with optimal resources and less computational time. It can reason, classify and make useful predictions of various engine faults and failures effectively. In this chapter, data-driven and model-based techniques are combined into hybrid models for exploring the engine condition monitoring. Purpose of this chapter is to,

1. Formulate the hybrid approach for classification.
2. Build the hybrid models and classify the engine faults.
3. Explore the fault symptoms from each classifier.
4. Compare and explore most sensitive models for classification.

Section 6.2 describes the theoretical background of hybrid systems. A theoretical background of wavelet neural network and adaptive fuzzy inference system are reviewed for the fault classification. In Section 6.3, these systems are proposed for engine fault classification; the features are trained and classified using these networks, and the fault characteristics are assessed. Last section of this chapter lists the conclusions.

6.2 Hybrid Models

A hybrid system provides flexibility to integrate different data driven, model-based and physics-based systems. [Siddique and Adeli \[22\]](#), [Lin and Lee \[234\]](#), and [Engelbrecht \[235\]](#) demonstrated the integration of various CI schemes. They presented a suitable framework for hybridization of CI paradigms. Hybrid models such as Wavelet Neural Network (WNN) and Adaptive Neuro-Fuzzy Inference System (ANFIS) are gaining increased attention due to their flexibility, promising results and optimally using very few resources. [Adeli and Jiang \[236\]](#) indicated that combining fuzzy and wavelet neural network into fuzzy wavelet neural network (FWNN) are highly accurate in modeling of dynamic characteristics of a system. [Palade et al. \[237\]](#) and [Marwala \[238\]](#) discussed the use of such models for the condition monitoring of various machineries. This section introduces the theoretical bases of WNN and ANFIS, and proposes them for fault diagnosis of study engine. The purpose of these models is to detect important characteristics of the faults for determining the abnormality and predict failure rates. It explores various models and their performance for fault classification.

6.2.1. Wavelet Neural Networks

Machinery signals are composed with spikes and wavelets like oscillations for finite durations. Due to multi resolution nature of wavelets, they are naturally suitable for analysis of the machinery signals. The artificial neural network approximates and learns the non-linear function without use of any model, so hybridizing them can form a powerful technique for machinery health management. A WNN combines the properties of wavelet decomposition along with the characteristics of neural networks. It scatters the uniformly distributed wavelets based on the signal complexity. Alexandridis and Zaprani 2013 [239] presented model identification methods for a classification using WNNs. Vachtsevanos et al. [240], and Wang and Vachtsevanos 2001 [241] demonstrated a WNN framework for the diagnosis and prognosis of complex engineered systems. They concluded that the WNN can accommodate both on-line and off-line learning routines.

Figure 6.1 shows a forward WNN, it consist of three layers; input layer, hidden layer of wavelons and output layer. Input layer takes the dependent variables, wavelon represents the signal with single neuron and output layer approximates the desired value. Nodes in each layer are interconnected by weighted sum of nodes of previous layer nodes. An external input vector $x(t)$ of m nodes is applied to the network, n is number of wavelons in hidden layer. $y(t)$ represents output of the network, $w_{jk}(t)$ is the weight between j^{th} wavelon and input unit k , $w_{ij}(t)$ is weight connection between output unit i and j^{th} wavelon, $s_j(t)$ and $\tau_j(t)$ represents dilation and translation coefficients of hidden layer at discrete time t respectively.

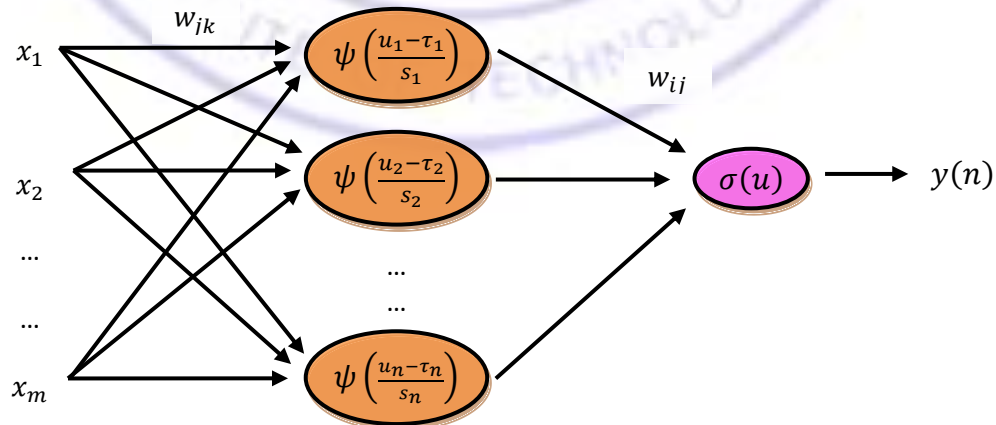


Figure 6.1: Wavelet Neural Network

Net internal activity of j^{th} wavelon at time t , is given by sum of inputs to the j^{th} wavelon, $u_j(t)$,

$$u_j(t) = \sum_{k=0}^m w_{jk}(t) x_k(t) \quad 6.1$$

where $x_k(t)$ is the k^{th} input at time t . Output of the j^{th} wavelon is computed by passing $u_j(t)$ through the wavelet i.e. $\psi_{s,\tau}[u_j(t)] = \psi_{s,\tau}\left(\frac{u_j(t)-\tau_j(t)}{s_j(t)}\right)$. Output neuron is obtained by,

$$u(t) = \sum_{j=0}^n w_{ij}(t) \psi_{s,\tau}[u_j(t)] \quad 6.2$$

Output of the network is computed by passing $u(t)$ through the nonlinear activation function,

$$o(t) = \sigma[u(t)] \quad 6.3$$

Learning algorithm for WNN: The instantaneous sum of squared error at time t is,

$$E(t) = \frac{1}{2} [d(t) - o(t)]^2 \quad 6.4$$

Where $d(t)$ is the desired response of output at time t . The method of steepest descent is used to minimize the above cost function and weight between hidden unit j and input unit k can be adjusted according to,

$$\begin{aligned} \Delta w_{jk}(t+1) &= -\eta \frac{\partial E(t)}{\partial w_{jk}(t)} + \mu \Delta w_{jk}(t) \\ &= -\eta e(t) \cdot \sigma'[u(t)] \cdot w_{ij}(t) \cdot \psi'_{s,\tau}[u_j(t)] \cdot \frac{x_k(t)}{s_j(t)} + \mu \Delta w_{jk}(t) \end{aligned} \quad 6.5$$

where η is learning rate, Connection weight between the output unit i and hidden unit j is,

$$\Delta w_{ij}(t+1) = -\eta \frac{\partial E(t)}{\partial w_{ij}(t)} + \mu \Delta w_{ij}(t) \quad 6.6$$

$$= -\eta e(t) \cdot \sigma[u(t)] \cdot \dot{\psi}_{s,\tau}[u_j(t)] + \mu \Delta w_{ij}(t) \quad 6.7$$

The translation coefficient in hidden layer can be adjusted according to,

$$\Delta \tau_j(t+1) = -\eta \frac{\partial E(t)}{\partial \tau_j(t)} + \mu \Delta \tau_j(t) \quad 6.8$$

$$= -\eta e(t) \cdot \sigma[u(t)] \cdot w_{ij}(t) \cdot \dot{\psi}_{s,\tau}[u_j(t)] \cdot \frac{1}{s_j(t)} + \mu \Delta \tau_j(t) \quad 6.9$$

The dilation coefficient in the hidden layer is updated as follows,

$$\Delta s_j(t+1) = -\eta \frac{\partial E(t)}{\partial s_j(t)} + \mu \Delta s_j(t) \quad 6.10$$

$$= -\eta e(t) \cdot \sigma[u(t)] \cdot w_{ij}(t) \cdot \dot{\psi}_{s,\tau}[u_j(t)] \cdot \frac{u_j(t) - \tau_j(t)}{s_j(t)^2} + \mu \Delta s_j(t) \quad 6.11$$

Morlet $\cos(1.75) e^{-x^2/2}$ or Mexican hat $(1 - x^2) e^{-x^2/2}$ function can be used as wavelet function $\psi(x)$. Root-Mean-Square-Error (RMSE) is calculated for each data sample, a non-zero value indicates inconsistency between actual and desired behaviour due to the disturbances. For n number of faults, it can be expressed as:

$$RMSE = \sqrt{\frac{1}{n} \sum_{i=1}^n (d_i - o_i)^2} \quad 6.17$$

A permissible value can be used to check the network convergence. WNN is well suited for classification of the fault symptoms that are generated using analytic symptom generation methods like parameter estimation, state estimation, parity equations and sampled signals. However still there is a lack of a generally accepted framework for applying wavelet networks. Some observable symptoms that have cause-effect relations are quite difficult to represent by analytic models. A rule-based approach is more suitable to acquire, represent and process the fault diagnostic knowledge base (Ayoubi and Isermann [242]). A hybrid neuro-fuzzy scheme can cope-up with uncertainty and to allow automatic knowledge extraction from experimental data, and can be used for the classification of faults.

6.2.2. Adaptive Neuro Fuzzy Inference System

An ANFIS is a kind of artificial neural network that is based on Takagi–Sugeno Fuzzy Inference System (FIS) that maps the input to an output using fuzzy sets. It increases the human interpretability and understandability to condense knowledge and experience into few rules, learns and tunes the rules of a system. [Zio and Gola \[243\]](#) validated neuro-fuzzy technique on Iris flowers classification and then successfully applied to the diagnosis of motor bearing faults. [Lou and Loparo \[244\]](#), and [Wu et al. \[245\]](#) used wavelet features with ANFIS for fault diagnosis of bearing and gear respectively. They found that the wavelet features combined with fuzzy logic are useful in detecting the continual increase in fault severity. [Chen et al. \[246\]](#) trained an ANFIS and integrated in a high-order particle filter as a model to describe the crack fault progression of a planetary gear carrier plate. [Wang et al. \[247\]](#) used neuro-fuzzy system for the prognosis of gear health condition. They found it as a robust real-time predictor. [Lei et al. \[248\]](#) implemented EMD features combining with ANFIS and genetic algorithms to identify different abnormal cases in the bearing. [Funsten \[249\]](#) employed neuro-fuzzy system to detect heartbeats. He concluded that under subtractive clustering the ANFIS has a higher performance. [Soualhi et al. \[250\]](#) applied HMM and ANFIS for prognosis of bearing failures. Research indicates that the hybridization of these techniques is more effective in handling the complex systems.

An ANFIS starts with mapping the experimental data by degree of belongingness through membership functions. A set of rules that models the system behavior are extracted by grid partitioning or clustering the input space. Weights are assigned to each rule, normalized in comparison to all the rules and aggregated the outputs of each rule into a single fuzzy set, which are then converted into a meaningful single variable. Finally the overall output is computed as the summation of all incoming signals. The partitioning determines the weight parameters. Grid partitioning divides the input space into equal intervals but its limits do not necessarily have any physical meaning. It has a computational limitation due to exponential complexity of the number of rules and produces a FIS, where each rule has zero coefficients in its output equation. Subtractive clustering estimates the number of clusters and selects a cluster center such that high density data points lie within the radius of a particular cluster. Radius specifies the range of influence of cluster center for each input and output dimension.

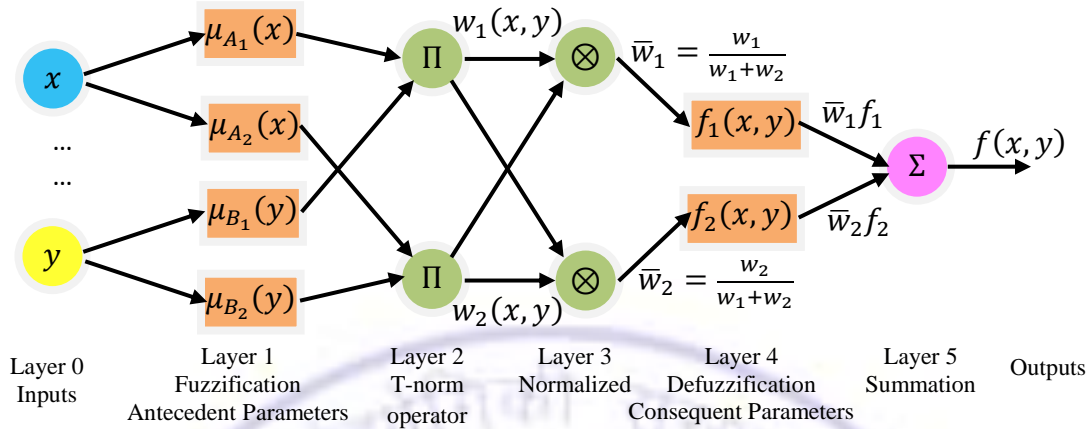


Figure 6.2: ANFIS Network

The number of rules and antecedent membership functions are determined and then linear least squares estimation is used to determine each rule's consequent equations.

The clustering time depends on the number of samples. Outcomes are predicted and defuzzified. FIS system can be based on Sugeno or Mamdani. Mamdani is intuitive, suitable for human response and computationally inefficient because of additional parameters for human interpretability. Sugeno is efficient and well suited for mathematical analysis. Learning of ANFIS is done using hybrid learning procedure, which combines back-propagation gradient descent and least squares method for identification of antecedent and consequent parameters. ANFIS network consist of five layers as shown in Figure 6.2; n is the number of inputs and p is the number of membership functions of each input, j is the number of layers with output O_{ji} , i.e. output of i^{th} node of j^{th} layer. In the layer 1, the inputs are fuzzified into output degree of membership that satisfies the fuzzy set A_k represented by membership functions. Output of this layer O_{1i} is,

$$O_{1i} = \mu_{A_k}(x_m; S_{1i}) \quad 6.12$$

where $S_{1i} = \{a_i \ b_i \ c_i \ \dots\}$ are the antecedent parameters that makes layer adaptive and x_m is a feature. Sugeno structure uses Gaussian, bell, triangle or trapezoid membership

functions. In layer 2, rules are defined by AND or OR operator to minimize or maximize the incoming signals. Let W_i be the weights from the rule nodes, so output of this layer becomes,

$$O_{2i} = W_i = \text{rule}\{A_k\}; W_1 = \mu_{A_1}(x)\mu_{B_1}(y) \quad 6.13$$

The normalization of this weight is carried out in layer 3 to ensure stable convergence and biases to avoid time consumption process of defuzzification. Output of this layer is the normalized weight of each rule \bar{W}_i given by,

$$O_{3i} = \bar{W}_i = \frac{W_i}{W_1 + W_2 + \dots + W_i} \quad 6.14$$

Normalized weights are defuzzified in Layer 4. Let $S_{1i} = \{q_{1i} \ q_{2i} \ \dots \ r\}$ be the consequent parameters. Output of this layer is O_{4i} , which is the product of normalization firing strength \bar{W}_i and a linear function f_i ,

$$O_{4i} = \bar{W}_i f_i \quad 6.15$$

where linear function $f_i = q_{1i}x_1 + q_{2i}x_2 + \dots + r_i$ is the multiplication of consequent and input parameters. Defuzzified outputs of layer 4 is aggregated in layer 5 represented by output O_{5i} , where $i = \{1\}$ due to single output.

$$O_{51} = \sum_i O_{4i} = \frac{\sum_i W_i f_i}{\sum_i W_i} = \sum_{i,n} \bar{W}_i x_n q_{ni} + \bar{W}_i r_i \quad 6.16$$

Equation 6.16 forms a set of n number of linear algebraic equations whose parameters can be estimated through sum of least squared error; unknown consequent parameters are identified by performing iterations on the training data. After obtaining consequent parameters, a gradient descent back propagation is used to determine the error measured at each output node towards the input node. Optimal values of ANFIS parameters are made from a hybrid learning, which combines least square estimator and back propagation gradient decent algorithms. The antecedent and consequent parameters are assumed to be fixed in the

forward and backward pass respectively. Least-squares estimator and gradient descent algorithm are used in forward and backward pass respectively. In case of Sugeno fuzzy model the rules and rule consequents are the linear functions that are defined as,

$$R_i: \text{if } x_1 \text{ is } A_{i1} \text{ and } x_n \text{ is } A_{in} \text{ then } o_i = p_{i1}x_1 + \dots + p_{in}x_n + p_{i(n+1)}, \quad i = 1 \dots M \quad 6.17$$

where $x = \{x_1, x_2 \dots x_n\}$ is the input vector, o_i is the output and R_i is the i^{th} rule. A_{i1}, \dots, A_{in} are fuzzy sets defined in the antecedent space by membership functions $\mu_{A_{ij}}(x_j)$ and $p_{i1}, \dots, p_{i(n+1)}$ represent the consequent parameters and M is the number of rules. The defuzzification is carried out by checking the degree of fulfilment $\beta_i = \prod_{j=1}^n \mu_{A_{ij}}(x_j), i = 1 \dots M$ of the i^{th} rule in the antecedent-consequent product space. Output y of the model is computed through the center of gravity of the final fuzzy set:

$$y = \frac{\sum_{i=1}^M \beta_i o_i}{\sum_{i=1}^M \beta_i} \quad 6.18$$

ANFIS models the prior knowledge optimally into a set of intuitive and flexible rules that are unaffected to other layers. It can effectively handle few inputs or few memberships function, but consume exponentially high time for larger number of inputs. Increased number of fuzzy rules can cause convergence issues, which can be controlled by validation error to converge at over fitting or loss of generality. Rules of ANFIS cannot share the same output membership function.

ANFIS has few rules and few connections so it convergence faster than the ANN. In fuzzy system, the rules are constructed manually while ANFIS searches for most effective inference rules. In this work, MATLAB inbuilt function ‘anfis’ of fuzzy logic toolbox is used for engine fault classification and subtractive clustering method is adopted in the simulation.

6.3 Engine Fault Classification using Hybrid Models

In this section, two hybrid models i.e. ANFIS and WNN are built for the engine fault classification. Their performance is evaluated for the classification of engine fault features at entire operating condition.

6.3.1. WNN for Engine Fault Classification

WNN is proposed as a diagnostic approach for the engine features extracted in the Section 5.3, which are fed as inputs to the WNN and outputs are used to classify the faults. In the diagnosis process, network fault class is compared with the target class. WNN is trained for the low RMSE. Architecture with different number of wavelons in the hidden layer is studied and selected architecture is used for engine fault classification. The first architecture is constructed with total 25 number of wavelons in the hidden layer, trials for wavelons that are lower than 25 indicated the architecture is insensitive with giving a constant RMSE of value 21.25. In the second architecture, total 50 wavelons are used. Inputs are normalized because the non-normalized inputs consumed significant time for convergence. First architecture recorded a lowest RMSE with a value 2.595, while the second one has a value 0.055. The computational time for the first architecture is small but to get lowest RMSE it consumed large number of iterations. Figure 6.3 shows network performance of the second architecture for FFT features at 1500 rpm, that convergence at 40 epochs.

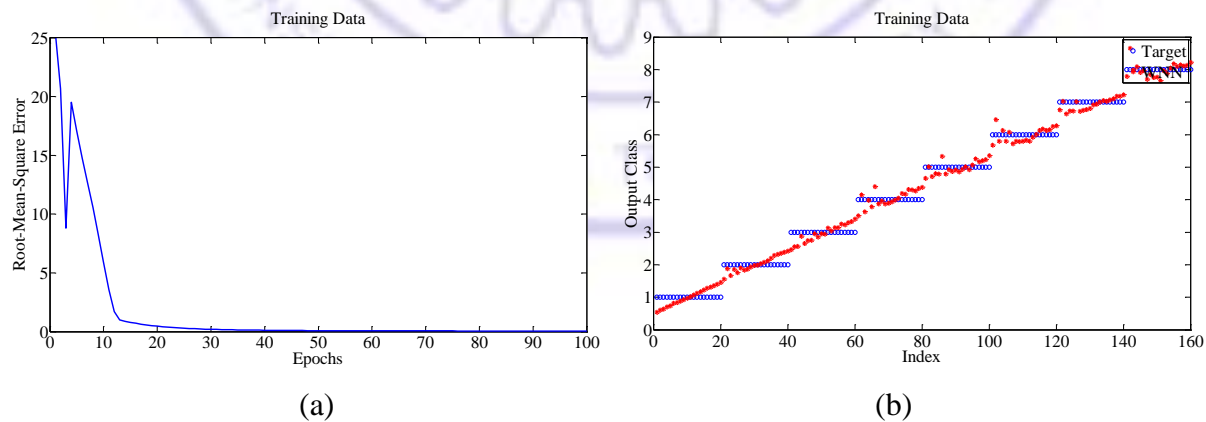


Figure 6.3: WNN Performance; (a) RMSE, (b) Output Classification

Table 6.1: WNN Classification Performance (%) at 1500 rpm

Set	Architecture 160-25-8								Architecture 160-50-8							
	Nor	MBF	CCR	WEV	MGT	WCL	WCJ	WPR	Nor	MBF	CCR	WEV	MGT	WCL	WCJ	WPR
Nor	100	0	0	0	0	0	0	0	100	0	0	0	0	0	0	0
MBF	5	85	5	5	0	0	0	0	0	100	0	0	0	0	0	0
CCR	30	35	20	15	0	0	0	0	0	5	95	0	0	0	0	0
WEV	5	0	20	25	20	25	0	5	0	0	0	100	0	0	0	0
MGT	0	0	10	35	30	5	20	0	0	0	0	0	100	0	0	0
WCL	0	5	0	20	40	15	5	15	0	0	0	0	0	100	0	0
WCJ	0	0	0	30	20	15	15	20	0	0	0	0	0	0	100	0
WPR	0	0	10	0	10	20	25	35	45	0	0	0	0	0	0	100

Table 6.2: WNN Classification Performance (%) for Sensor Cases

No.	Inputs Sensor	Statistical	FFT	Statistical	FFT
		160-40-8	160-25-8	160-80-8	160-50-8
1	Proximity, Horizontal	30.00	30.00	65.00	15.00
2	Proximity, Vertical	65.00	65.00	40.00	60.00
3	Cyl. Head Accelerometer, Vertical	65.00	65.00	35.00	60.00
4	Cyl. Head Accelerometer, Lateral	65.00	65.00	35.00	60.00
5	Cyl. Head Accelerometer, Axial	65.00	65.00	35.00	75.00
6	Base Accelerometer, Vertical	35.00	35.00	65.00	25.00
7	Base Accelerometer, Lateral	35.00	35.00	65.00	25.00
8	Base Accelerometer, Axial	65.00	65.00	35.00	75.00
9	Near Field, Microphone	65.00	65.00	35.00	75.00
10	Far Field, Microphone	65.00	65.00	35.00	75.00

It is able to correctly classify almost all faults. Table 6.1 shows the % misclassification of the fault data into other classes. The first architecture has some misclassification with 42.85% of overall correct classification; the second architecture is highly efficient with 99.34 % of classification performance. It shows the network for 1500 rpm with FFT inputs has high performance. Classification by sensor listed in Table 6.2 indicates the features from accelerometer are reliable for correct classification while proximity indicated low reliability in fault classification. Trials for overall WNN classification performance for speed cases showed a 1500 rpm with FFT inputs has high performance; the statistical inputs are not able to provide any clear trend.

6.3.2. ANFIS for Engine Fault Classification

The research on neuro-fuzzy based machinery fault diagnosis is gaining increased attention. In engine applications, neuro-fuzzy and fuzzy models are mainly used in process diagnosis. ANFIS is proposed as a diagnostic approach for engine features extracted in the Section 5.3.

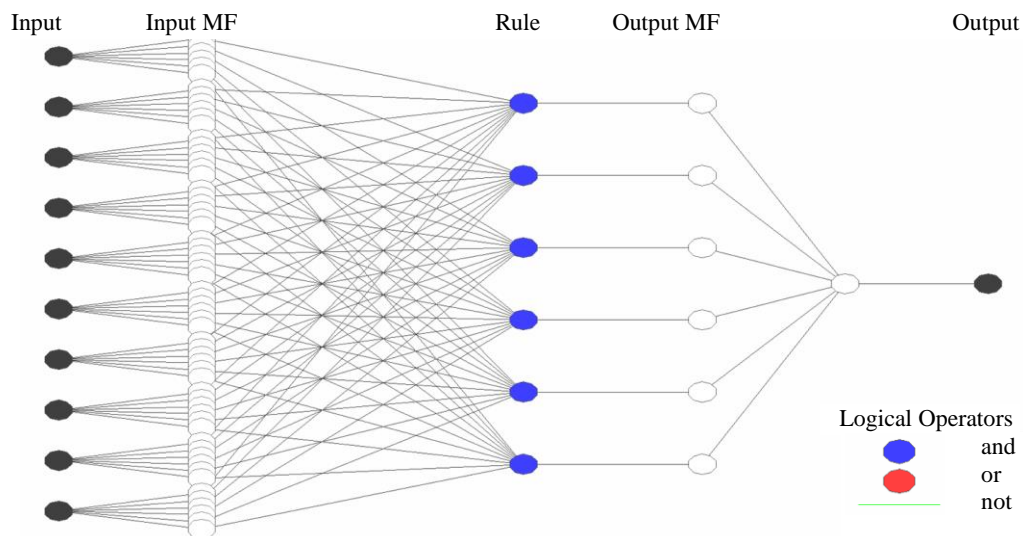


Figure 6.4: Engine ANFIS Structure

A Sugeno based ANFIS is built and its performance is evaluated, Figure 6.4 shows the general block diagram for classifying the fault features; left side of the network shows the input features. The signal features are extracted from statistical analysis and FFT of proximity, vibration and sound pressure with procedure discussed in the Section 3.4. They are fed to the ANFIS structure. The features are modelled using Gaussian type membership functions. Since the ANFIS has a single output node, so the fault output class is labeled by numbers 1-8 to represent normal, main bearing, cracked connecting rod, worn exhaust valve, tooth missing gear, worn cam, worn journal, worn piston ring faults respectively. The output of the network is then classified into one among the labeled group. A threshold value of output class ± 0.5 is used to separate each fault. The outputs of other class falling in this range are considered as misclassified and the % of misclassification is computed. The performance of ANFIS model is evaluated for different signal features, cluster radius and range of the operation. Structure that has lowest training error is selected for studying the engine fault classification. There are ten input features, twenty samples for each fault and feature, the grid partition based FIS was capable of handling up to five features with three membership functions. Number of fuzzy rules are: p^n , where n is number of inputs for grid partitioning, p is the number of membership functions that are chosen for grid partitioning i.e. 243 rules were generated. With increasing the number of inputs, number of rules are becomes very large that resulted in computational complexity. The subtractive clustering gave eight rules and

accommodated the input feature matrix. A trial for optimal radius gave 0.75, 0.53, 0.86 and 1.84 RMSE for cluster radius 0.2, 0.3, 0.4 and 0.5 respectively. The radius 0.3 is considered as optimized cluster radius and results are presented for the default 0.5 case and 0.3 radius case. Rule layer was chosen to be an AND function i.e. output of the rule layer is a minimum of two membership functions as opposed to the maximum through the OR function. It is desirable to have a decrease in RMSE or converge as the number of iterations increases. RMSE of the checking data is used to prevent over fitting, which occurs when the RMSE of the checking data increases. It is a result of fitting the fuzzy system to the training data that it no longer fits the testing data effectively, which leads to a loss of generality.

If an over fitting exists, prior to fitting the ANFIS algorithm chooses model parameters associated with the minimum error. Once RMSE of the training data is shown to decrease as the number of iterations increases and over fitting is eliminated. For the evaluation of the ANFIS, a total 200 epochs are considered. Figure 6.5 (a) shows the RMSE has a stable convergence after around 180 epochs. Figure 6.5 (b) shows the classification performed by the trained ANFIS; it indicates that the ANFIS is able to perform successful classification.

Table 6.3 shows the percentage of fault being correctly (blue bold) classified and misclassified (un-bold) by the ANFIS for 1500 rpm case. It indicates that the cluster radius 0.5 has shown 20% capability, while the optimized radius 0.3 has 82.85% capability of correct classification. It shows high cluster radius has high misclassification due to the overlap of the fault features, while too low radius is unable to classify the faults.

Correct classification performance for a particular speed case is obtained by averaging the individual percentages. ANFIS is able to clearly classify the faults in the order: Nor, MGT, WCL, MBF, WEV, WPR, WCJ and CCR. Normal case signal have low noise so it is easily classified. Table 6.4 shows the correct classification percentage by each sensor. In most of the cases, cluster radius 0.5 and statistical features have shown poor capability. FFT features have shown a better capability to separate the faults. The accelerometer sensor has overall highest fault separation capability, while proximity shows a poor capability. Table 6.5 shows the network with FFT features with cluster radius 0.3 at 1500 rpm have highest performance.

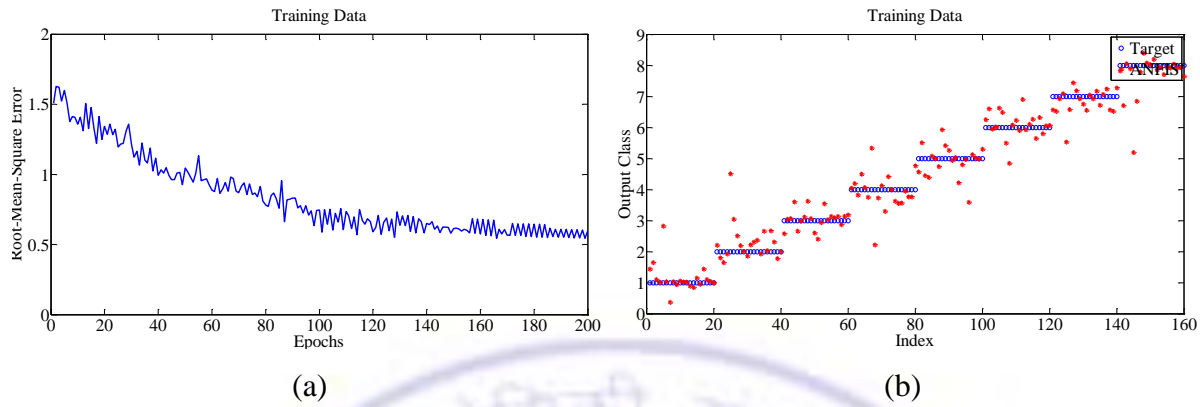


Figure 6.5: ANFIS Performance; (a) RMSE, (b) Output Classification

Table 6.3: ANFIS Classification Performance (%) at 1500 rpm

Set	Cluster Radius 0.5								Cluster Radius 0.3							
	Nor	MBF	CCR	WEV	MGT	WCL	WCJ	WPR	Nor	MBF	CCR	WEV	MGT	WCL	WCJ	WPR
Nor	10	20	0	50	20	0	0	0	95	5	0	0	0	0	0	0
MBF	5	25	10	40	15	5	0	0	0	85	5	5	5	0	0	0
CCR	0	10	40	30	15	5	0	0	0	15	65	20	0	0	0	0
WEV	0	0	10	60	15	15	0	0	0	5	5	85	5	0	0	0
MGT	0	0	10	30	30	20	10	0	0	0	0	5	90	5	0	0
WCL	0	0	10	25	30	20	15	0	0	0	0	0	5	90	5	0
WCJ	0	0	0	15	55	20	10	0	0	0	0	0	0	20	70	10
WPR	0	0	0	10	35	25	25	5	0	0	0	5	0	0	10	85

Table 6.4: ANFIS Classification Performance (%) for Sensor Cases

No.	Inputs Sensor	Statistical Radius 0.5	FFT Radius 0.5	Statistical Radius 0.3	FFT Radius 0.3
1	Proximity, Horizontal	11.88	13.13	11.88	10.63
2	Proximity, Vertical	11.88	15.00	11.88	15.00
3	Cyl. Head Accelerometer, Vertical	11.88	14.38	11.88	16.25
4	Cyl. Head Accelerometer, Lateral	11.88	11.88	11.88	15.00
5	Cyl. Head Accelerometer, Axial	11.88	11.88	11.88	11.88
6	Base Accelerometer, Vertical	11.88	13.13	11.88	15.00
7	Base Accelerometer, Lateral	11.88	-	11.88	14.38
8	Base Accelerometer, Axial	11.88	13.13	13.75	16.25
9	Near Field, Microphone	11.88	21.25	15.00	13.75
10	Far Field, Microphone	11.88	18.75	17.50	14.38

Table 6.5: Overall ANFIS Classification Performance (%) for Speed Cases

No.	Inputs	Model	1000	1500	2000	2500	3000
1	Statistical	Radius 0.5	25.00	21.25	23.75	22.50	21.25
2	FFT	„	28.75	20.00	14.37	17.50	20.00
3	Statistical	Radius 0.3	27.50	25.00	20.00	21.85	27.50
4	FFT	„	55.00	82.85	43.37	51.88	47.50

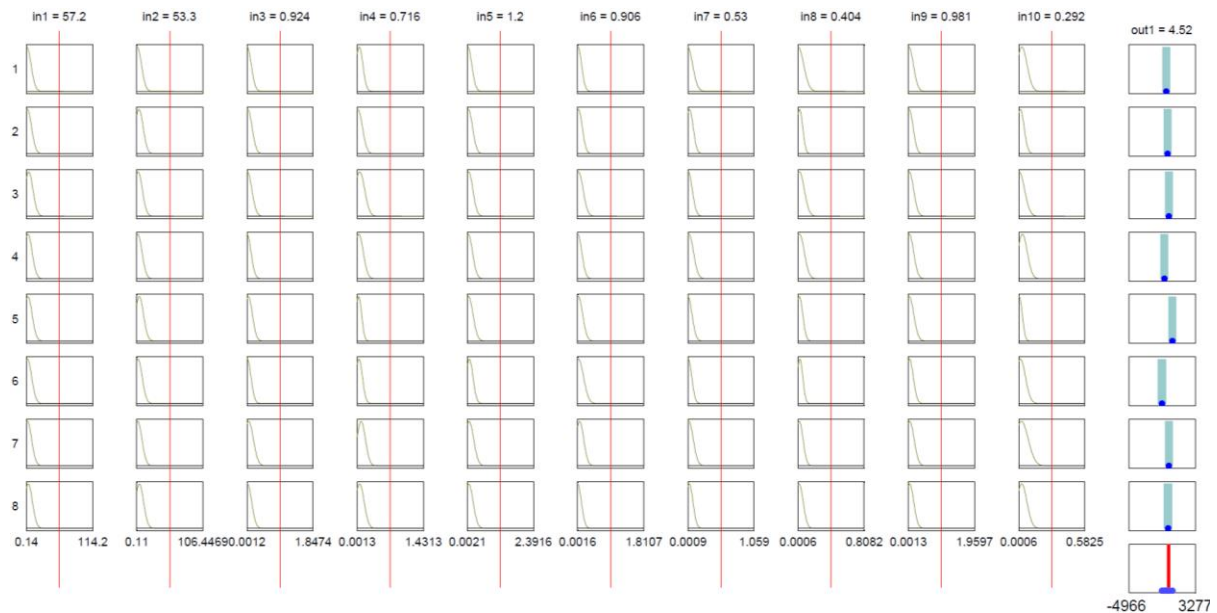
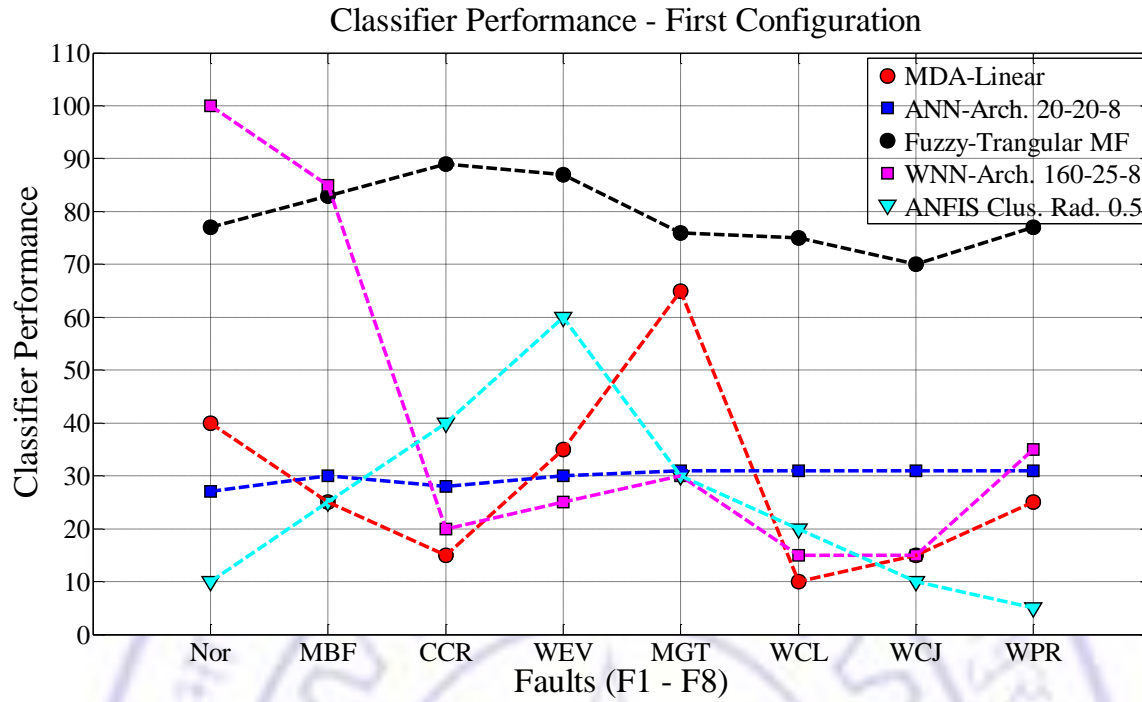


Figure 6.6: Rules Generated by the ANFIS Model for Entire FFT Data

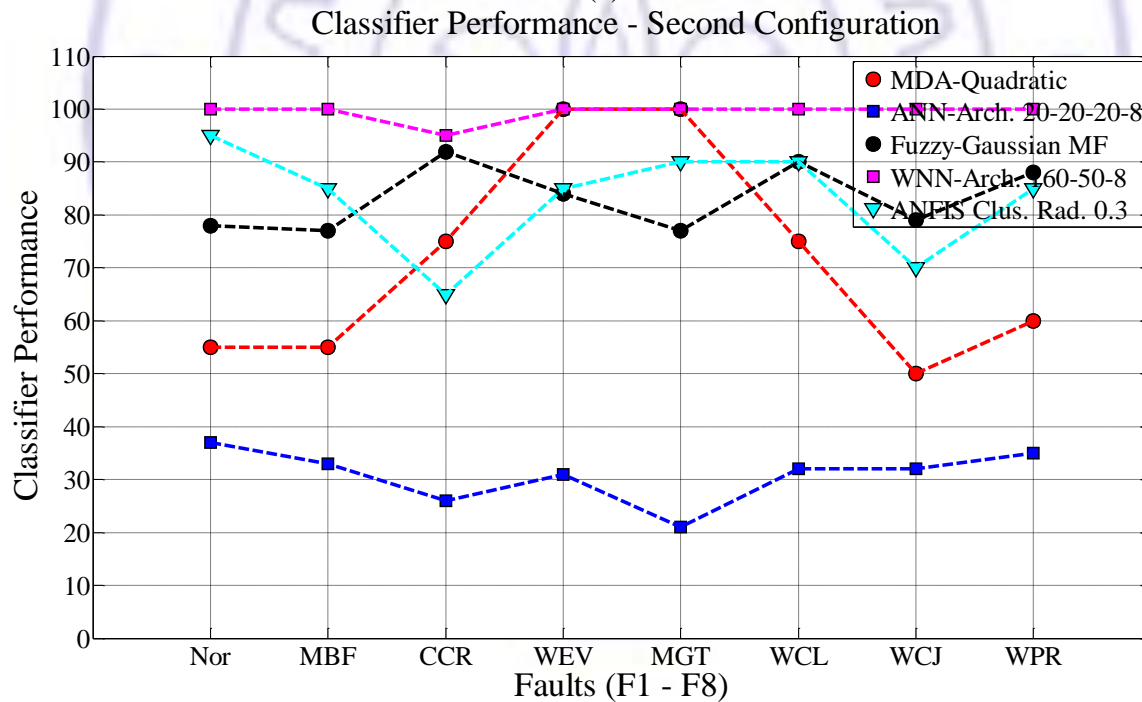
Figure 6.6 shows the rules and parameters based on subtractive clustering partition for entire FFT features and ten input variables data set. They indicate that adjusting the parameters of each variable in the specified range will give output class of fuzzy reasoning. A crisp value shown in the right-hand side lower corner is obtained by applying defuzzification method. ANFIS model generated total eight rules for subtractive clustering of radius 0.18 with RMSE value 1.89, while for grid partition produced total 243 numbers of rules with RMSE value 0.27 and took significant computational time when trained with the first five variables of 1500 rpm case. Hence a subtractive clustering based ANFIS model is effective in handling the engine fault diagnostic system.

6.4 Comparison of Classifiers

This section compares performance of the selected classifiers. In each classifier, both configurations are compared. Figure 6.7 (a) shows first configuration that uses simple un-optimized model. Figure 6.7 (b) shows second one that has been optimized for best performance and suitability of its use. Classifiers have shown different performance values for each fault. To compare classifier stability, values of each classifier are interconnected to get the general trend. Ideally a stable classifier should have a horizontal trend as shown by



(a)



(b)

Figure. 6.7: Classifier Performance; (a) First Configuration, (b) Second Configuration

ANN in first configuration. In second configuration, classifiers showed a better stability trend that indicates a less variation in performance with respect to faults. In MDA based classification, average performance of linear and quadratic discriminators are 28.75 %, and

71.25 % respectively. This indicates that the quadratic discrimination is more superior. Average performance of single and two hidden layer ANNs are 29.88% and 30.88% respectively. This shows the effect of number of hidden layers have not made much difference in the ANN performance. Average performance of Fuzzy classifier with triangular membership function is 79.25%, while with Gaussian it is 83.12%. Performance stability of Fuzzy and ANN has not changed over the configurations for all the faults. In WNN based classification, the average performance of 25 wavelons is 40.62%, while for 50 wavelons, it is 99.37%. So, increased number of wavelons has significantly changed the network performance. ANFIS with cluster radius 0.5 has average performance 25.00%, while with cluster radius 0.3 it is 83.12%. This indicates cluster radius have significantly changed the classifier performance.

The highest performance indicated by the MDA, ANN, Fuzzy, WNN and ANFIS are 71.25%, 30.88%, 83.12%, 99.37% and 83.12% respectively. WNN has highest performance, while it took large number of iterations and gives less information about classification, fuzzy has superior performance but building of inference rules is a tedious task for the engine features. The ANFIS has offered a sufficiently good performance value with automatic generation of rules and less computational time. Hence it can be selected as an effective classifier for engine faults.

Computational CPU time for above classifiers is in the order of 2-5 minutes, which is small and not significant in the practical implementation point of view. The classifier offers other important capabilities such as fault tolerant, adaptive, accurate, and handling of uncertainty and imprecision. But time consumed to build a method i.e. time from first trial to arrive its final version is significant as it takes several iterations constantly to seek better parameters. So, total time consumed for complete modeling of each method seems to be more useful in their selection. On a rough four month time scale (as used in actual modeling), ANN model is built with consuming four weeks duration, FS took sixteen weeks, MDA took about eight weeks and WNN consumed two weeks while ANFIS took a week. So ANFIS has a less model building time. Deciding a method only on basis of computational time was felt less valuable so its flexibilities are taken into consideration.

6.5 Conclusions

The hybridization provides a simple and effective tool for handling large data base, and found to be more appropriate in the analysis of fault characteristics in an IC engine. FFT features are effective in fault classification in comparison to the statistical features.

Proposed WNN and ANFIS classifier are successful in classifying the engine faults. WNN and ANFIS classifier results are comparable. In the comparison between WNN and ANFIS classifier, WNN showed a high success rate in fault classification, and has ensured low RMES, but it took significant time for training. However, it consumed significant number of iterations to match the class with minimum error. ANFIS gives rules to handle the variable parameters. Subtractive clustering in resulted in optimal rules, while grid partitioning is unable to handle the engine data base. WNN has stabilized over the increased configurations, while Fuzzy and ANN has shown not much change.

In comparison to all classifiers, ANFIS has demonstrated as an effective tool for handling the engine data, it has a lowest model building time. It offered a very simple methodology that ensures a systematic procedure for the classification. It classified the data quickly without much user involvement and provided few rules for assessment.

CHAPTER 7

CONCLUSIONS AND SUGGESTIONS

I have seen the future; and it works.

- Lincoln Steffens (1866 – 1936)

7.1 Summary

This chapter draws the overall conclusions of the research ‘Hybrid Methodologies for Health Management of Internal Combustion Engines’ and discusses the future scope. Section 7.2 re-draws the conclusions from individual chapters. Section 7.3 discusses overall conclusions of this research. Last section suggests the possible future work.

7.2 Chapter wise Conclusions

It discusses the summary of each chapter: purpose, contribution and its connection to other chapters. The conclusions from each chapter are re-drawn in context to research topic.

7.2.1 Chapter 1 Introduction

Need for a vehicle health management is introduced in this chapter. Typical fault cycle and few methods to monitor health are outlined. Research topic, objectives, outline, approach and validation, significance of this research are formulated and thesis structure is organized.

Growing dependence, functional complexity and increased accidents are forcing to ensure the vehicle reliability. Faults are the minute defects that grow over the time and lead to catastrophic failures. Managing the potential failure requires a timely attention to detect and eliminate its faults. There exist some methodologies for health monitoring, which can detect few faults of certain size well in advance to failure. Engine is a primary source in the vehicle

breakdown; due to complex structure, process and limitation in the existing methodologies, it is crucial and challenging to manage the engine health.

Modern IC engine is a complex multi-disciplinary system that carries several rotating and reciprocating components; they operate in changing environment and varying configurations. Its fault originates in several locations and affects different ways. Detection and isolation of faults, and forecast their failure requires to investigate, enhance and combine several techniques. Hence this research attempts to formulate a health management methodology.

This work signifies an attempt to enhance physics-based, statistical, intelligent and modal-based techniques. Research objectives are divided into areas/models and tasks based the literature review that has been conducted in the Chapter 2. They are outlined in the form of flow chart and listed as cases in the trial matrix for their execution. Approaches adopted to validate these models are briefed.

Thesis has been organized into seven chapters. They introduced vehicle health management, covered state-of-the-art for engine health management, built and evaluated a setup and formulated parameter estimation procedure, built and performed physics-based fault diagnosis and failure prognosis, built and performed data-driven and model-based fault diagnosis and failure prognosis, combined data-driven and model-based models into a hybrid method and performed fault diagnosis, overall conclusions are drawn and suggests future work, respectively.

7.2.2 Chapter 2 Literature Review

It reviews the literature and formulates a methodology for machinery health management; finds state-of-the-art, identifies research gaps and issues in existing techniques.

A wide verity of topics and techniques are reviewed and grouped into four quadrants: Models, Evaluation, Diagnostics and Prognostics. Models/techniques are listed in first quadrant, methods to evaluate for selection, introducing the faults in the selected models and techniques for progression of faults into failures are discussed in subsequent quadrants.

Process and structural faults of the engine are listed according to their frequency of occurrence. Such faults can be monitored using various techniques at various stages by installing performance, tribological and structural indicators. Symptoms of a few rotating component faults at steady speed are listed. Capability and suitability of these indicators to monitor the variation in engine component behavior are discussed.

An overview of health management system is briefed to understand the requirements of EHM system. Components are categorized into knowledge, diagnosis, prognosis, and maintenance management. Knowledge management extracts knowledge from the data, which involves data acquisition, signal processing and feature extraction. Various transformation techniques are compared and their current state in context to engine application is reviewed. Diagnosis involves detection of a fault and isolating it to a particular component. Prognosis is the prediction of chance of survival for the detected fault. It is carried out by assessing failure mode effects and criticality analysis, component life tracking, remaining life analysis, performance trending and fault prediction. Maintenance management initiates the suitable maintenance and logistics decisions or options based on the diagnostic and prognostic information. It assesses and reports the fault, activates supply chain integration and accommodates the fault in a worst condition. Various reasoning techniques such as model, case, rule and data based are reviewed, their features are compared applications are discussed to handle the engine system effectively.

This study provides a general health management reference with describing its basic components. Transforms and techniques are compared and framework is formulated, which is applicable to general machines. Technological gaps in each component are identified and reviewed. Research gap shows that, currently externally introduced faults are being investigated in an engine and majority of them are process faults, which can be detected easily and curable in a regular service. Internal faults such as crack and worn defects are chronic; they originate over the period and grow gradually into failure. They are crucial to detect from conventional methods. It concludes that the combined vibro-acoustic signals are good indicators of engine structural health and hybridizing of superior techniques can resolve actual issues of an IC engine effectively.

7.2.3 Chapter 3 Engine Set-Up, Evaluation and Estimation

In this chapter, an experimental set-up is built, instrumented and calibrated to study emulated faults and failures of the engine. Various monitoring configurations and operating conditions are evaluated to select effective conditions. Data analytics is carried out. Database is reduced and parameters are estimated through different time-frequency analysis. They are further employed in the subsequent chapters to manage the engine health.

Engine is coupled to magnetic brake dynamometer through speed reduction unit. Tachometer, keyphasors, proximity probes, accelerometers and microphones are installed on the fixtures and instrumented with data acquisition hardware. Set-up is calibrated by adjusting the engine mounting positions and pre-tensions to minimize the inherent unbalance and coupling misalignment faults. Repeatability over the events and data sets has been checked. Sensors, locations, directions and operating conditions are varied with fuel, stage and speeding environments. Events are identified by superimposing operational information. Acquired signals are processed and compared to select effective conditions; Cylinder head accelerometer in vertical direction at 2000 rpm with diesel fuel found to be more sensitive. Dimensionality of database is reduced using multivariate principal and independent component analysis, which confirmed to cylinder head vibration signals for exclusive information. Short duration, long duration and ramp signals are acquired for entire operating range to capture cycle variations, steady conditions and transient phenomena respectively. The short duration and ramp signals are used to explore parameter estimation techniques and features from steady signals are used for diagnosis and prognosis in subsequent chapters.

Orbit, Wavelet transform, Hilbert-Huang transform and Vold Kalman filter are evaluated on numerically simulated signals by assuming the parameters that resemble actual events, modes and noise nature of shaft motion and vibro-acoustic signals at steady speed. Transient signals are simulated under constant acceleration rate with known orders. They are re-estimated using proposed methodology and estimation error is reported. This procedure is employed in actual engine signals; system parameters of cycle events and running orders are estimated. Numerical construction of engine signals indicated the need for detailed physics-based modelling for realistic simulation and that can also useful to explore the engine health.

Simulation on numerical signals indicated operational speed lies below the shaft resonance limit so the orbit analysis of filtered signal found less useful to provide system information. HHT proved to be a simple tool as it has less computation, does not have any resolution issues and estimates background noise effectively. However IMFs amplitudes are fluctuating, and unable to separate the mode and order segments, that make interpretation difficult. HHT ridges are not continuous so they are difficult for parameter estimation and have high error. Improved HHT has eliminated uncorrelated IMFs, reduced the number of IMFs and ensured better computational efficiency. WT proves to be more robust and efficient method in parameter estimation and separates the nearby modes and orders. However it is computationally less efficient as it takes exponentially high time for increased resolution in analysis. VKF has tracked the orders easily, but requires rough information on instantaneous frequency.

Procedure has been implemented successfully on the actual engine signals; despite practical situation, dominant event features and noise level are identified, separated and quantified. Vibro-acoustic parameters provide the capabilities in monitoring the critical health of an engine. Events in the acoustic signals are less clear due to noise level so they are difficult to quantify. WT, HHT and VKF plots are comparable. The combustion and exhaust valve opening events are dominant. High modes provide poor estimation due to certain overlap of events and modes. Estimated parameters give exclusive criteria in separating the engine events, ability to reconstruct the signal with few parameters. Signal reconstruction indicates that the first two dominant modes and IMFs are sufficient to represent each event with the calculated correlation coefficient. Results indicate that the proposed parameter monitoring procedure is effective in identifying the events, and quantifying the structural faults and health of an engine.

This study concludes that WT is a superior tool for engine parameter estimation. Cylinder head vibrations are most sensitive signals for engine parameterization. WT based ramp-up analysis separated the orders and identifies some critical speeds. Due to the large number of events, orders and modes in the engine signals; it consume significant time and have practical issue in implementation. An automated parameter estimation tool can solve this problem.

7.2.4 Chapter 4 Physics-based Health Management

This chapter formulated a physics-based framework for engine fault diagnosis and failure prognosis. Lumped mass and flexible MBD models are built and evaluated for free and forced vibration, and fatigue response. Different configurations are analysed and responses are compared with the experiments. Reduced models are selected to study faults and failures.

In lumped mass approach, structural dynamics models of the engine with a few DOF are enhanced with including rotor dynamics developments. In multibody, a detailed rigid multibody dynamics model is developed in MSC/ADAMS platform and is converted into flexible for an optimal model reduction. Validation of thermodynamic, hydrodynamic, and engine dynamic models using test, literature and commercial tools, respectively, indicated that these loads are comparable. Material hysteresis is modelled using Rayleigh damping. Certain physics-based models indicated that they have good correlation with experiments and good enough to predict vibration response.

The selected models are further used to investigate the fault diagnosis and failure prognosis. Common faults such as unbalance and lack of lubrication defects are introduced in the LMD models, while crack and bend defects are introduced in FMBD models. The time domain and wavelet transform plots of each fault are compared. Results indicated that the models are successful in giving different fault characteristics. Comparison of physics-based diagnostic process with experimental indicated a few similarity in both the process. Results from above powertrain models are taken to MSC/FATIGUE, where life for crack initiation and propagation are predicted. A strain-based fatigue and fracture life information is used to extract the component survivability in terms of RUL. The fracture life obtained from physics-based model is compared with experiments and a close match is obtained.

Study shows that the formulated procedure is sufficiently good enough to predict faults and failures. Physics based models provided detailed insight, inputs and eliminated experiments, Lumped mass approach reported simple and less computational time, provided user interface to model and solve governing equations, but it has some restriction to model geometrical faults. FMBD consumed high computational time but able to model geometrical faults.

7.2.5 Chapter 5 Data-driven and Model-based Health Management

In this chapter, a health management methodology is proposed for real faults and failures of the IC engine under controlled conditions. Fault characteristics for defective main bearing, cracked connecting rod, tooth missing gear, worn parts of valve, cam, journal and piston ring are studied. Failure progressions for a connecting rod cut into fracture are investigated.

Statistical, fast Fourier and Wavelet transform plots are compared manually for 1500 rpm case. Statistical plots are unable to give clear symptoms, while Fourier and Wavelet plot showed some symptoms. Manual fault diagnosis found to be tedious and time consuming; it demanded for automation. So, statistical, intelligent and model-based multiple discriminant analysis, artificial neural network and fuzzy logic, respectively, classifiers are automated for the statistical and Fourier features. Models distinguished the fault features and provided clearly symptoms. Fuzzy model is highly efficient but generating its rules is tedious and time consuming. ANN provided a simple model, but showed a poor performance for engine signals. MDA is effective, as it works only with two variables and requires several cases for entire data set.

Failure characteristics are assessed with run-to-fail experiments conducted under accelerated damage. A cut in the connecting rod is varied by increasing its cut length every time in a step size of 1 mm till it fractures. Cut length and crack length are related, and correlated to measured signals. Engine degradation in terms of remaining useful life is estimated. Degradation states due to connecting rod failures are predicted by a model-based particle filter. It indicates that the procedure is efficient in predicting or monitoring the degradation state of connecting rod failure.

Study concludes that the formulated methodology is simple and novel for fault diagnosis and failure prognosis. Its validation on engine, whose structure is highly complex and processes are highly stochastic, indicates its capability for general use. Extracted feature provided noticeable symptoms of a fault and failure. Different classifiers are successfully distinguished the faults. Engine degradation due to connecting rod fracture is successfully measured and predicted.

7.2.6 Chapter 6 Hybrid Methodology Health Management

In this chapter, two different hybrid classifiers i.e. signal-based and model-based have been explored to study the fault characteristics. Classifiers have been formulated and employed for fault diagnosis of IC engine faults.

Classifiers are successful in classifying the engine faults and results from both the classifiers are comparable. In the comparison between WNN and ANFIS classifier, WNN showed a high success rate in fault classification, and has ensured low RMES, while it took significantly large time for training, consumed significant number of iterations to match the class with minimum error. ANFIS has offered very simple and systematic procedure for the classification and giving the rules to handle the variables and classify the faults.

Hybridization proved to be simple and effective tool for handling large data base, and found to be more appropriate in engine fault diagnosis. FFT features are effective than the statistical features. Comparison of MDA, ANN, FS, WNN and ANFIS classifiers confirms ANFIS as an effective tool for handling the engine data. It has a lowest model building time, classified the data quickly with less user involvement and provided few rules for assessment.

7.3 Overall Conclusions

In this research, state-of-the-art is carried-out; a health management methodology is formulated. Physics-based, data-driven and model-based schemes are investigated enhanced and combined in hybrid methodology. Experimental and physics-based models are built and the methodology is validated using a small single cylinder IC engine.

State-of-the-art concluded that engine health is affected by a verity of factors and controlled at several stages. It requires a methodology, which demands selection, enhancement, and integration of knowledge, diagnostic, prognostic and maintenance techniques. Data reduction transforms and reasoning techniques are compared and selected to evaluate. Survey indicated that highest failures of an engine occur in its powertrain components. Vibro-acoustic signals, superior data reduction techniques and transforms, parameterization and hybridization of reasoning techniques can provide effective results.

An engine set-up is built and instrumented to acquire vibration, noise and shaft motion signals at various conditions. Set-up is capable of acquiring signals and emulating the fabricated structural faults and failure conditions. Signals are acquired and evaluated for sensor, types, locations directions, under different fuels and speed conditions; it gives distinct responses that are most reliable conditions for effective health management. The cylinder head accelerometer signals in vertical direction for 2000 engine speed with diesel fuel conformed to be most reliable conditions.

Different signal processing techniques are explored to quantify engine system and fault using parameter estimation approach. Successful validation of these techniques on numerical signals gives the acceptance of estimated engine system parameters. Estimated parameters provided a simple few degree, mode and event systems that can represent complicated engine system with certain error. Wavelet transform found to be more effective in parameter estimation and requires less prior knowledge.

Physics-based simple lumped mass discretization and detailed flexible multibody powertrain models are built, calibrated and evaluated for model reduction and compared with experimental results. Simulation framework proved to be good enough to predict certain faults and failures. Results revealed that few models are successful to simulate the engine faults and failures. Lumped mass models provided quick results, while flexible multibody models simulated few minute geometrical defects. Low life in piston pin indicated the need for an earliest logistic support. Physics-based crack propagation estimated the connecting rod fracture around 7 mm crack length, while intermittent cut based accelerated fatigue test conformed its fracture in the 6 mm cut length trial stage. Close match between these approaches conform their validation and potentiality for further use.

Unclear trend and difficulty in manual comparison of actual fault features demanded for an automatic diagnosis tool. Classifiers have successfully separated the features of all seven actual faults from their healthy condition. Neural network proved to be a simple engine classification with less user involvement, while it recorded low performance. Fuzzy logic classified the engine faults with less computational time but requires rules which are difficult

to generate. Cut lengths correlated to the measured signals gave a methodology to detect crack directly and assess degradation. State predictor offered a novel method for prediction of remaining survivability of the engine under the given conditions. Particle filter predicted degradation states indicate the model is sufficiently good enough to predict remaining survivability of the engine.

Proposed hybrid classifiers are successfully classified the IC engine faults with fewer resources. Investigated data-driven, model-based and hybrid methodology concluded that certain techniques are highly reliable in fault classification and failure prediction. Hybridization proved to be simple and effective tool for handling large data base, and found to be more appropriate in the engine fault diagnosis. Hybrid ANFIS found to be reliable and effective tool with few simple rules.

7.4 Suggestions for Future Work

Research demonstrated the effective diagnostic and prognostic schemes for managing the IC engine structural health. They need to be implemented on board for real time use. Studies on embedding these schemes for real-time interface (HIL, SIL and MIL simulations), on-board monitoring, emergency assistance and maintenance in an integrated vehicle health management seek immediate attention.

Current study involves eight faults and a failure. In addition to the selected faults and failure, engine has several other faults and failures. It requires a consideration of all faults and failures for a robust health management process.

Study extracts the FFT and statistical features for the selected faults in entire speed range. Orbit, WT and HHT features are obtained for normal/healthy case at 1500 rpm. Parameter estimation using wavelet and HHT observed to be tedious, as real signals have infinite modes and events. Hence the current procedure adopts manual selection of first few dominant modes, events and orders; and estimates their features. Parameters of large number of modes, events and orders can increase the classifier capability, so it requires a development of an automated feature extractor.

Physics-based models can be used to investigate other common defects. Characteristics library of fault and failure can be built and used in IVHM model. Model reduction with different configurations is investigated; optimizing the model size can be iterated. Physics-based cranktrain response is compared with experiments; the response of valvetrain and geartrain are omitted. A realistic comparison can be made by modeling the entire powertrain as flexible and computing the total flexible response. In the physics-based modeling, a verity of rotor dynamic effects is considered; their effectiveness has to be explored.

Experimental set-up can be explored further to study several other faults and failures. Diagnosis and prognosis is investigated by taking most successful techniques. However, the other techniques need to be evaluated. The diagnosis and prognosis work is carried out using FFT and statistical features, while the effectiveness of orbit, WT and HHT features need to be explored.

In hybrid health management methodology, two different models are investigated. It requires a detailed study on the capability of several other hybrid models. The information from physics based models is not taken to the hybrid models; there is a scope to study the combination of physics-based features in hybrid methodology health management. Hybridization seems to have a promising feature; fusion of logical networks such as BBN with physics and data-driven inputs shall meet the growing demands.

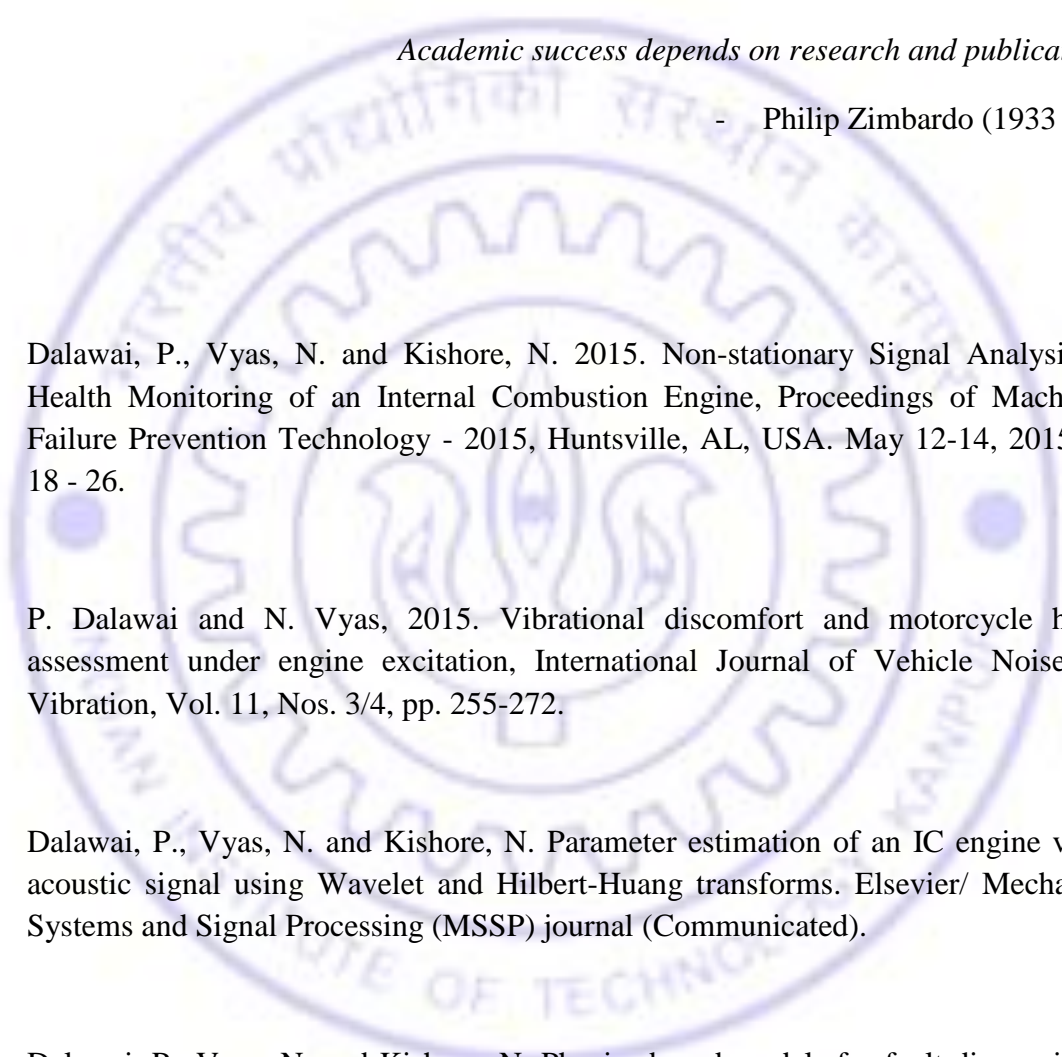
Diagnostic and prognostic schemes are validated using a small single cylinder engine. Its validation and implementation for a multi-cylinder engine, preferably a four cylinder engine, is useful for majority of commercial and passenger vehicles; and the corresponding study on a gas turbine can serve for aircraft vehicles.



PUBLICATIONS

Academic success depends on research and publications.

- Philip Zimbardo (1933 –)

- 
- [1]. Dalawai, P., Vyas, N. and Kishore, N. 2015. Non-stationary Signal Analysis for Health Monitoring of an Internal Combustion Engine, Proceedings of Machinery Failure Prevention Technology - 2015, Huntsville, AL, USA. May 12-14, 2015. pp. 18 - 26.
- [2] P. Dalawai and N. Vyas, 2015. Vibrational discomfort and motorcycle health assessment under engine excitation, International Journal of Vehicle Noise and Vibration, Vol. 11, Nos. 3/4, pp. 255-272.
- [3]. Dalawai, P., Vyas, N. and Kishore, N. Parameter estimation of an IC engine vibro-acoustic signal using Wavelet and Hilbert-Huang transforms. Elsevier/ Mechanical Systems and Signal Processing (MSSP) journal (Communicated).
- [4]. Dalawai, P., Vyas, N. and Kishore, N. Physics-based models for fault diagnosis and failure prognosis of an internal combustion engine. (Under preparation).
- [5]. Dalawai, P., Vyas, N. and Kishore, N. Adaptive intelligent systems for fault diagnosis and failure prognosis of an internal combustion engine. (Under preparation).



REFERENCES

Trust, but verify.

- Ronald Reagan (1911 – 2004)

- [1]. Jardine, A.K., Lin, D. and Banjevic, D., 2006. A review on machinery diagnostics and prognostics implementing condition-based maintenance. *Mechanical Systems and Signal Processing*, 20(7), 1483-1510.
- [2]. Walker, R., Perinpanayagam, S. and Jennions, I.K., 2013. Rotordynamic faults: recent advances in diagnosis and prognosis. *International Journal of Rotating Machinery*, Article ID 856865, 12 pages.
- [3]. Lee, J., Wu, F., Zhao, W., Ghaffari, M., Liao, L. and Siegel, D., 2014. Prognostics and health management design for rotary machinery systems-Reviews, methodology and applications. *Mechanical Systems and Signal Processing*, 42(1), 314-334.
- [4]. Zhang, B., Sconyers, C., Patrick, R. and Vachtsevanos, G., 2009. A multi-fault modeling approach for fault diagnosis and failure prognosis of engineering systems. In *Annual Conference of the Prognostics and Health Management Society*, 1-9.
- [5]. An, D., Kim, N.H. and Choi, J.H., 2015. Practical options for selecting data-driven or physics-based prognostics algorithms with reviews. *Reliability Engineering & System Safety*, 133, 223-236.
- [6]. DeBotton, G., Ben-Ari, J. and Sher, E., 2000. Vibration monitoring as a predictive maintenance tool for reciprocating engines. *Proceedings of the Institution of Mechanical Engineers, Part D: Journal of Automobile Engineering*, 214(8), 895-903.
- [7]. Liu, S., Gu, F. and Ball, A., 2006. Detection of engine valve faults by vibration signals measured on the cylinder head. *Proceedings of the Institution of Mechanical Engineers, Part D: Journal of Automobile Engineering*, 220(3), 379-386.

-
- [8]. Wu, J.D. and Chen, J.C., 2006. Continuous wavelet transform technique for fault signal diagnosis of internal combustion engines. *NDT & e International*, 39(4), 304-311.
- [9]. Zheng, G.T. and Leung, A.Y.T, 2002. Internal combustion engine noise analysis with time-frequency distribution, *Transactions of ASME*, Vol.124, 645-649.
- [10]. Albarbar, A., Gu, F. and Ball, A.D., 2010. Diesel engine fuel injection monitoring using acoustic measurements and independent component analysis. *Measurement*, 43(10), 1376-1386.
- [11]. Staszewski, W.J. and Giacomini, J., 1997, February. Application of the wavelet based FRFs to the analysis of nonstationary vehicle data. In *Proceedings-SPIE the International Society for Optical Engineering*. Spie International Society for Optical, 425-431.
- [12]. Peng, Z.K., Peter, W.T. and Chu, F.L., 2005. An improved Hilbert–Huang transform and its application in vibration signal analysis. *Journal of Sound and Vibration*, 286(1), 187-205.
- [13]. Srivastava, A.N. and Han, J. eds., *Machine learning and knowledge discovery for engineering systems health management*. Chapman and Hall/CRC Press, 2011.
- [14]. Novotny, P. and Pistek, V., 2010. New efficient methods for powertrain vibration analysis. *Proceedings of the Institution of Mechanical Engineers, Part D: Journal of Automobile Engineering*, 224(5), 611-629.
- [15]. Ma, Z.D. and Perkins, N.C., 2003. An efficient multibody dynamics model for internal combustion engine systems. *Multibody System Dynamics*, 10(4), 363-391.
- [16]. Ricci, S., *Model reduction techniques in flexible multibody dynamics with application to engine cranktrain simulation*. Ph. D Thesis, Alma Mater Studiorum - Università di Bologna, Italy, 2013.
- [17]. Markert, R., Platz, R. and Seidler, M., 2001. Model based fault identification in rotor systems by least squares fitting. *International Journal of Rotating Machinery*, 7(5), 311-321.
- [18]. Friswell, M.I., Penny, J.E.T., Garvey, S.D. and Lees, S.W., *Dynamics of rotating machines*. Cambridge University Press, 2010.
- [19]. Heng, A., Tan, A.C., Mathew, J., Montgomery, N., Banjevic, D. and Jardine, A.K., 2009. Intelligent condition-based prediction of machinery reliability. *Mechanical Systems and Signal Processing*, 23(5), 1600-1614.
-

-
- [20]. Pascual, D.G., *Artificial Intelligence Tools: Decision Support Systems in Condition Monitoring and Diagnosis*. CRC Press, 2015.
- [21]. Wu, J.D., Wang, Y.H. and Bai, M.R., 2007. Development of an expert system for fault diagnosis in scooter engine platform using fuzzy-logic inference. *Expert Systems with Applications*, 33(4), 1063-1075.
- [22]. Siddique, N. and Adeli, H., *Computational intelligence: synergies of fuzzy logic, neural networks and evolutionary computing*. John Wiley & Sons, 2013.
- [23]. Becker, D., *KPMGs global automotive executive survey-2015*. KPMG International Cooperative, 2015.
- [24]. Tyler, T., *Market forecast of revenue passenger kilometers*. International Air Transport Association, 2014.
- [25]. Berger, R., *Mastering product complexity*. Roland Berger Strategy Consultants, 2012.
- [26]. Tews, J., 2014. U.S. Initial quality study - J.D. Power. www.jdpower.com/press-releases/2014-us-initial-quality-study-iqs, Accessed: 18 August 2017.
- [27]. Markl, A., 2016. ADAC breakdown statistics-2016. www.adac.de/sp/technikzentrum/en/information/default.aspx, Accessed: 18 August 2017.
- [28]. Davies, A. ed., *Handbook of condition monitoring: techniques and methodology*. Springer Science & Business Media, 2012.
- [29]. Kebabjian, R., 2015. Accident statistics, www.planecrashinfo.com/cause.htm, Accessed: 18 August 2017.
- [30]. Rumar, K., 1985. The role of perceptual and cognitive filters in observed behavior. *Human behavior and traffic safety*, Springer US, 151-170.
- [31]. Benedettini, O., Baines, T.S., Lightfoot, H.W. and Greenough, R.M., 2009. State-of-the-art in integrated vehicle health management, *Proceedings of the Institution of Mechanical Engineers, Part G: Journal of Aerospace Engg.*, 223(4), 157-170.
- [32]. Moubray, J., *Reliability-centred maintenance*, Butterworth-Heinemann, Oxford, 1997.
- [33]. Gehloff, M., 2013. PF Curve 101–Keeping it simple. www.maintenancephoenix.com/2013/10/02/pf-curve-101-keeping-it-simple, Accessed: 23 February 2018.
- [34]. Etchison, D.M., 2016. The impact of equipment reliability on human safety, www.linkedin.com/pulse/impact-equipment-reliability-human-safety-dustin-m-etchison-cmrp, Accessed: 23 February 2018.
-

-
- [35]. Patel, J., 2010. Best practices awards: reliability decision-support system lets rules dictate maintenance. www.plantservices.com/articles/2010/09bestpractices/?show=all Accessed: 23 February 2018.
- [36]. Vachtsevanos, G.J., Lewis, F., Hess, A. and Wu, B., Intelligent fault diagnosis and prognosis for engineering systems. John Wiley & Sons, Inc., New Jersey, 2006.
- [37]. Mrad, N. and Mrad, R., L., Advances in health monitoring and management. In Expert Systems for Human, Materials and Automation. InTech., 2011.
- [38]. Matthews, C., A practical guide to engineering failure investigation. Professional Engineering Pub., 1998.
- [39]. Bloch, H.P. and Geitner, F.K., Machinery failure analysis and troubleshooting: practical machinery management for process plants. Butterworth-Heinemann, 2012.
- [40]. Valve train, www.motorera.com/dictionary/pics/p/pushrodengine1.gif. Accessed: 18 August 2017.
- [41]. Yu, L., Cleary, D., Osborn, M. and Rajiv, V., 2007. Information fusion strategy for aircraft engine health management. Proceedings of the ASME Turbo Expo 2007: Power for Land, Sea and Air, 531-538.
- [42]. Wang, H. and Chen, P., 2009. A feature extraction method based on information theory for fault diagnosis of reciprocating machinery. *Sensors*, 9(4), 2415-2436.
- [43]. Zima, S. and Greuter, E., Engine failure analysis: internal combustion engine failures and their causes. SAE International, 2012.
- [44]. Denton, T., Advanced automotive fault diagnosis: automotive technology: vehicle maintenance and repair. Elsevier Butterworth-Heinemann, 2006.
- [45]. Collacott, R., Mechanical fault diagnosis and condition monitoring. Chapman and Hall, Ltd, 1977.
- [46]. Ehrlich, F.F., Handbook of rotordynamics. Krieger, 1998.
- [47]. Nyberg, M., Model based fault diagnosis: methods, theory, and automotive engine applications, Ph. D Thesis, Linköping University, Schweden, 1999.
- [48]. Ding, S., Model-based fault diagnosis techniques: design schemes, algorithms, and tools. Springer Science & Business Media, 2008.
- [49]. Isermann, R., 2005. Model-based fault-detection and diagnosis—status and applications. *Annual Reviews in control*, 29(1), 71-85.
-

-
- [50]. Kurz, R., and Brun, K., 2001. Degradation in gas turbine systems. *ASME J Eng. Gas Turbines Power* 123, 70–77.
- [51]. Li, W., Gu, F., Ball, A.D., Leung, A.Y.T. and Phipps, C.E., 2001. A study of the noise from diesel engines using the independent component analysis. *Mechanical Systems and Signal Processing*, 15(6), 1165-1184.
- [52]. Kim, J.K. and Lee, M.C., 2009. Real-time diagnostic system using acoustic emission for a cylinder liner in a large two-stroke diesel engine. *International Journal of Precision Engineering and Manufacturing*, 10(3), 51-58.
- [53] Albarbar, A., 2013. Diesel engine air-borne acoustic signals analysis using continuous wavelet transform. *Advances in Applied Acoustics*, 2(3), 77-82.
- [54]. Mohammadpour, J., Franchek, M. and Grigoriadis, K., 2012. A survey on diagnostic methods for automotive engines. *Intern. Journal of Engine Research*, 13(1), 41-64.
- [55]. Ben-Ari, J., Itzhaki, R. and Sher, E., 1999. Fault detection in internal combustion engines by the vibrations analysis method (No. 1999-01-1223). SAE Technical Paper.
- [56]. Lee, S.K. and Kim, S.J., 2008. Internal combustion engine sound-based fault detection and diagnosis using adaptive line enhancers. *Proceedings of the Institution of Mechanical Engineers, Part D: Journal of Automobile Engg.*, 222(4), 593-605.
- [57]. Eisenmann, R.C. and Eisenmann, R.C., *Machinery malfunction diagnosis and correction: vibration analysis and troubleshooting for the process industries*. Prentice Hall PTR, 1998.
- [58]. Mobley, R.K., *An introduction to predictive maintenance*. Butterworth-Heinemann, 2002.
- [59]. Williams, J.H., Davies, A. and Drake, P.R. eds., *Condition-based maintenance and machine diagnostics*. Springer Science & Business Media, 1994.
- [60]. Mohanty, A.R., *Machinery condition monitoring: principles and practices*. CRC Press, 2014.
- [61]. Elhaj, M., Gu, F., Ball, A.D., Albarbar, A., Al-Qattan, M. and Naid, A., 2008. Numerical simulation and experimental study of a two-stage reciprocating compressor for condition monitoring. *Mechanical Systems and Signal Processing*, 22(2), 374-389.
- [62]. Jun, H.B., Kiritsis, D., Gambera, M. and Xirouchakis, P., 2006. Predictive algorithm to determine the suitable time to change automotive engine oil. *Computers & Industrial Engineering*, 51(4), 671-683.
-

-
- [63]. Zhang, Y., Wang, J. and Ai, F.X., 2010. Determination of the wear of internal combustion engine components based on measurement of the oil spectrum. *Proceedings of the Institution of Mechanical Engineers, Part D: Journal of Automobile Engineering*, 224(11), 1451-1457.
- [64]. Yonghui, Y., Weihua, W., Xinpin, Y., Hanliang, X. and Chengtao, W., 2003. An integrated on-line oil analysis method for condition monitoring. *Measurement Science and Technology*, 14(11), 1973-1977.
- [65]. Macian, V., Tormos, B., Olmeda, P. and Montoro, L., 2003. Analytical approach to wear rate determination for internal combustion engine condition monitoring based on oil analysis. *Tribology International*, 36(10), 771-776.
- [66]. Randall, R.B., *Vibration-based condition monitoring: industrial, aerospace and automotive applications*. John Wiley & Sons, 2011.
- [67]. Ettouney, M.M. and Alampalli, S., *Infrastructure health in civil engineering: Theory and components (Vol. 1)*. CRC Press, 2016.
- [68]. Johnson, S.B., Gormley, T., Kessler, S., Mott, C., Patterson-Hine, A., Reichard, K. and Scandura Jr, P. eds., *System health management: with aerospace applications*. John Wiley & Sons, 2011.
- [69]. Rao, J.S., *Vibratory condition monitoring of machines*. CRC Press, 2000.
- [70]. Staszewski, W., Boller, C. and Tomlinson, G.R. eds., *Health monitoring of aerospace structures: smart sensor technologies and signal processing*. John Wiley & Sons, 2004.
- [71]. Clutz, T.C., *A framework for prognostics reasoning*. Ph. D Thesis, Air Force Institute of Technology, Wright-Patterson Air Force Base, Ohio, 2002.
- [72]. Moustapha, H., 2004. *Aircraft systems diagnostics, prognostics and health management technology insight document*, Industry Canada Contract 5011101, Vol. 2, 2004.
- [73]. ISO Standards, ISO/TC 108 - Mechanical vibration, shock and condition monitoring, International Organization for Standardization, www.iso.org, Accessed:13 June 2016.
- [74]. SAE Standards, *Guide lines for aircraft engine condition monitoring and maintenance*, www.sae.org, Accessed:13 June 2016.
- [75]. Esperon-Miguez, M., John, P. and Jennions, I.K., 2013. A review of integrated vehicle health management tools for legacy platforms: challenges and opportunities. *Progress in Aerospace Sciences*, 56, 19-34.
-

-
- [76]. Mallat, S., A wavelet tour of signal processing. Second ed., Academic Press, 1999.
- [77]. Iatsenko, D., McClintock, P.V. and Stefanovska, A., 2015. Linear and synchrosqueezed time–frequency representations revisited: Overview, standards of use, resolution, reconstruction, concentration, and algorithms. *Digital Signal Processing*, 42, 1-26.
- [78]. Huang, N.E., Hilbert-Huang transform and its applications (Vol. 16). World Scientific, 2014.
- [79]. Peng, Z.K. and Chu, F.L., 2004. Application of the wavelet transform in machine condition monitoring and fault diagnostics: a review with bibliography. *Mechanical Systems and Signal Processing*, 18(2), 199-221.
- [80]. Lei, Y., Lin, J., He, Z. and Zuo, M.J., 2013. A review on empirical mode decomposition in fault diagnosis of rotating machinery. *Mechanical Systems and Signal Processing*, 35(1), 108-126.
- [81]. Chang, J., Kim, M. and Min, K., 2002. Detection of misfire and knock in spark ignition engines by wavelet transform of engine block vibration signals. *Measurement Science and Technology*, 13(7), 1108-1114.
- [82]. Merkisz, J. and Waligórski, M., STFT and JTFA Analyses of vibroacoustic signal for the on-line combustion process assessment in direct injection turbocharged diesel engines. *Proceedings of ISMA2010 including USD 2010*, 939-953.
- [83]. Zou, J., Chen, J. and Geng, Z.M., 2001. Application of wavelet packets algorithm to diesel engines' vibroacoustic signature extraction. *Proceedings of the Institution of Mechanical Engineers, Part D: Journal of Automobile Engineering*, 215(9), 987-993.
- [84]. Li, Y., Peter, W.T., Yang, X. and Yang, J., 2010. EMD-based fault diagnosis for abnormal clearance between contacting components in a diesel engine. *Mechanical Systems and Signal Processing*, 24(1), 193-210.
- [85]. Yadav, S.K., Automatic fault diagnosis of internal combustion engine using intelligent techniques. Ph. D Thesis, Indian Institute of Technology Kanpur, India, 2009.
- [86]. Xu, H., Yuan, S. and Zong, L., 2010. Analysis of the time-frequency characteristics of internal combustion engine vibration signal based on Hilbert-Huang transform. In *Image and Signal Processing (CISP), 2010 3rd International Congress on IEEE*, Vol. 7, (2010) 3400-3404.
- [87]. Yang, W.X., 2008. Interpretation of mechanical signals using an improved Hilbert–Huang transform. *Mechanical Systems and Signal Processing*, 22(5), 1061-1071.
-

-
- [88]. Wang, Y.S., Ma, Q.H., Zhu, Q., Liu, X.T. and Zhao, L.H., 2014. An intelligent approach for engine fault diagnosis based on Hilbert–Huang transform and support vector machine. *Applied Acoustics*, 75, 1-9.
- [89]. Srivastava T., Difference between machine learning & statistical modeling, www.analyticsvidhya.com/blog/2015/07/difference-machine-learning-statistical-modeling, Accessed:19 August 2017.
- [90]. Byington, C.S., Roemer, M.J. and Galie, T., 2002. Prognostic enhancements to diagnostic systems for improved condition-based maintenance. *Aerospace Conference Proceedings, 2002. IEEE*, Vol. 6, 6-6.
- [91]. Wagner, M.B., Younan, A., Allaire, P. and Cogill, R., 2011. Model reduction methods for rotor dynamic analysis: a survey and review. *International Journal of Rotating Machinery*, 1-17.
- [92]. Ricci, S., Troncossi, M. and Rivola, A., 2011. Model reduction of the flexible rotating crankshaft of a motorcycle engine cranktrain. *International Journal of Rotating Machinery*, 2011, 1-9.
- [93]. Lee, C.W. and Han, Y.S., 1998. The directional Wigner distribution and its applications. *Journal of Sound and Vibration*, 216(4), 585-600.
- [94]. Ajovalasit, M. and Giacomini, J., 2003. Analysis of variations in diesel engine idle vibration. *Proceedings of the Institution of Mechanical Engineers, Part D: Journal of Automobile Engineering*, 217(10), 921-933.
- [95]. Chandroth, G., Sharkey, A.J.C. and Sharkey, N.E., 1999. Vibration signatures, wavelets and principal components analysis in diesel engine diagnostics. *WIT Transactions on the Built Environment*, 45.
- [96]. Gao, Q.Q., Chen, A.Y. and Jing, G.X., 2009. Research on Time-Frequency Characteristics of Engine Induction Noise and Time-Frequency Representation of the Acoustic Signals. In *Image and Signal Processing, 2009. CISP'09. 2nd International Congress on IEEE*, 1-4.
- [97]. Lakshminarasimha, A.N., Boyce, M.P. and Meher-Homji, C.B., 1994. Modeling and analysis of gas turbine performance deterioration. *Transactions-ASME Journal of Engineering for Gas Turbines and Power*, 116, 46-46.
- [98]. Tabakoff, W., Lakshminarasimha, A.N. and Pasin, M., 1990. Simulation of compressor performance deterioration due to erosion. *Journal of Turbomachinery*, 112(1), 78-83.
-

-
- [99]. Jalan, A.K. and Mohanty, A.R., 2009. Model based fault diagnosis of a rotor–bearing system for misalignment and unbalance under steady-state condition. *Journal of Sound and Vibration*, 327(3), 604-622.
- [100]. Darpe, A.K., 2007. A novel way to detect transverse surface crack in a rotating shaft. *Journal of Sound and Vibration*, 305(1), 151-171.
- [101]. Bachschmid, N., Pennacchi, P. and Vania, A., 2002. Identification of multiple faults in rotor systems. *Journal of Sound and Vibration*, 254(2), 327-366.
- [102]. Rivola, A., Troncossi, M., Dalpiaz, G. and Carlini, A., 2007. Elastodynamic analysis of the desmodromic valve train of a racing motorbike engine by means of a combined lumped/finite element model. *Mechanical Systems and Signal Processing*, 21(2), 735-760.
- [103]. Mechefske, C.K., 1998. Objective machinery fault diagnosis using fuzzy logic. *Mechanical Systems and Signal Processing*, 12(6), 855-862.
- [104]. Mukras, S., Kim, N.H., Mauntler, N.A., Schmitz, T.L. and Sawyer, W.G., 2010. Analysis of planar multibody systems with revolute joint wear. *Wear*, 268(5), 643-652.
- [105]. Flores, P., 2009. Modeling and simulation of wear in revolute clearance joints in multibody systems. *Mechanism and Machine Theory*, 44(6), 1211-1222.
- [106]. Nayak, N., Lakshminarayanan, P.A., Babu, M.G. and Dani, A.D., 2006. Predictions of cam follower wear in diesel engines. *Wear*, 260(1), 181-192.
- [107]. Hugnell, A.B.J., Bjoerklund, S. and Andersson, S., 1996. Simulation of the mild wear in a cam-follower contact with follower rotation. *Wear*, 199(2), 202-210.
- [108]. Staszewski, W.J., 1997. Identification of damping in MDOF systems using time-scale decomposition. *Journal of Sound and Vibration*, 203(2), 283-305.
- [109]. Slavič, J., Simonovski, I. and Boltežar, M., 2003. Damping identification using a continuous wavelet transform: application to real data. *Journal of Sound and Vibration*, 262(2), 291-307.
- [110]. Byington, C.S., Watson, M., Edwards, D. and Stoelting, P., 2004. A model-based approach to prognostics and health management for flight control actuators. In *Aerospace Conference, 2004. Proceedings. 2004, IEEE, Vol. 6*, 3551-3562.
- [111]. Wu, J.D. and Liu, C.H., 2008. Investigation of engine fault diagnosis using discrete wavelet transform and neural network. *Expert Systems with Applications*, 35(3), 1200-1213.
-

-
- [112]. Wu, J.D. and Liu, C.H., 2009. An expert system for fault diagnosis in internal combustion engines using wavelet packet transform and neural network. *Expert Systems with Applications*, 36(3), 4278-4286.
- [113]. Antory, D., Kruger, U., Irwin, G. and McCullough, G., 2005. Fault diagnosis in internal combustion engines using non-linear multivariate statistics. *Proceedings of the Institution of Mechanical Engineers, Part I: Journal of Systems and Control Engineering*, 219(4), 243-258.
- [114]. Celik, M.B. and Bayir, R., 2007. Fault detection in internal combustion engines using fuzzy logic. *Proceedings of the Institution of Mechanical Engineers, Part D: Journal of Automobile Engineering*, 221(5), 579-587.
- [115]. Tay, F.E. and Shen, L., 2003. Fault diagnosis based on rough set theory. *Engineering Applications of Artificial Intelligence*, 16(1), 39-43.
- [116]. Loutas, T.H., Roulias, D., Pauly, E. and Kostopoulos, V., 2011. The combined use of vibration, acoustic emission and oil debris on-line monitoring towards a more effective condition monitoring of rotating machinery. *Mechanical Systems and Signal Processing*, 25(4), 1339-1352.
- [117]. Orsagh, R., Roemer, M., Sheldon, J. and Klenke, C.J., 2004, June. A comprehensive prognostics approach for predicting gas turbine engine bearing life. In *Proceedings of the ASME Turbo Expo*, Vol. 2, 777-785.
- [118]. Liu, X., Machinery fault diagnosis based on fuzzy measure and fuzzy integral data fusion techniques. Ph.D Thesis, Queensland University of Technology, Brisbane, Australia, 2007.
- [119]. Wu, J.D. and Kuo, J.M., 2009. An automotive generator fault diagnosis system using discrete wavelet transform and artificial neural network. *Expert Systems with Applications*, 36(6), 9776-9783.
- [120]. Heywood, J.B., *Internal combustion engine fundamentals* (Vol. 930). McGraw-Hill, New York, 1988.
- [121]. Tzeng, G.H., Lin, C.W. and Opricovic, S., 2005. Multi-criteria analysis of alternative-fuel buses for public transportation. *Energy Policy*, 33(11), 1373-1383.
- [122]. Ballabio, D., 2015. A MATLAB toolbox for Principal Component Analysis and unsupervised exploration of data structure. *Chemometrics and Intelligent Laboratory Systems*, 149, 1-9.
- [123]. Maaten, L.V.D., Postma, E. and Herik, J.V.D., 2009. Dimensionality reduction: a comparative review. *J Mach Learn Res*, 10, 66-71.
-

-
- [124]. Kerschen, G., Worden, K., Vakakis, A.F. and Golinval, J.C., 2006. Past, present and future of nonlinear system identification in structural dynamics. *Mechanical Systems and Signal Processing*, 20(3), 505-592.
- [125]. Tiwari, R. and Vyas, N.S., 1997. Parameter estimation in imbalanced non-linear rotor-bearing systems from random response. *Journal of Sound and Vibration*, 208(1), 1-14.
- [126]. Khan, A.A. and Vyas, N.S., 2001. Nonlinear bearing stiffness parameter estimation in flexible rotor-bearing systems using Volterra and Wiener approach. *Probabilistic Engineering Mechanics*, 16(2), 137-157.
- [127]. Chatterjee, A. and Vyas, N.S., 2004. Non-linear parameter estimation in multi-degree-of-freedom systems using multi-input Volterra series. *Mechanical Systems and Signal Processing*, 18(3), 457-489.
- [128]. Feldman, M., 2011. Hilbert transform in vibration analysis. *Mechanical systems and signal processing*, 25(3), 735-802.
- [129]. Vold, H. and Leuridan, J., 1993. High resolution order tracking at extreme slew rates, using Kalman tracking filters (No. 931288). SAE Technical Paper.
- [130]. Le, T.H. and Tamura, Y., 2009. Modal identification of ambient vibration structure using frequency domain decomposition and wavelet transform. In *Proceedings of the 7th Asia-Pacific conference on wind engineering*, Taipei, Taiwan.
- [130]. Yin, H.P., Duhamel, D. and Argoul, P., 2004. Natural frequencies and damping estimation using wavelet transform of a frequency response function. *Journal of Sound and Vibration*, 271(3), 999-1014.
- [132]. Bachschmid, N., Pennacchi, P. and Vania, A., 2004. Diagnostic significance of orbit shape analysis and its application to improve machine fault detection. *Journal of the Brazilian Society of Mechanical Sciences and Engineering*, 26(2), 200-208.
- [133]. Daubechies, I., 1990. The wavelet transform, time-frequency localization and signal analysis. *IEEE transactions on information theory*, 36(5), 961-1005.
- [134]. Kijewski, T. and Kareem, A., 2002. On the presence of end effects and their melioration in wavelet-based analysis. *Journal of Sound and Vibration*, 256(5), 980-988.
- [135]. Lardies, J. and Gouttebroze, S., 2002. Identification of modal parameters using the wavelet transform. *International Journal of Mechanical Sciences*, 44(11), 2263-2283.
-

-
- [136]. Porwal, R., Nonlinear system identification using wavelet transforms. Ph. D Thesis, Indian Institute of Technology Kanpur, India, 2009.
- [137]. Xiao-fei, S. and Xiao, Y., 2006, June. Instantaneous frequency extraction via wavelet ridge. In Communications, Circuits and Systems Proceedings, 2006 International Conference on IEEE , Vol. 1, 253-257.
- [138]. Montanari, L., Basu, B., Spagnoli, A. and Broderick, B.M., 2015. A padding method to reduce edge effects for enhanced damage identification using wavelet analysis. *Mechanical Systems and Signal Processing*, 52, 264-277.
- [139]. Zhidong, Z. and Yang, W., 2007. A new method for processing end effect in empirical mode decomposition. In Communications, Circuits and Systems, International Conference on IEEE, 841-845.
- [140] Wu, F. and Qu, L., 2008. An improved method for restraining the end effect in empirical mode decomposition and its applications to the fault diagnosis of large rotating machinery. *Journal of Sound and Vibration*, 314(3), 586-602.
- [141]. Huang, N.E. and Wu, Z., A review on Hilbert-Huang transform: Method and its applications to geophysical studies. *Reviews of Geophysics*, 46(2) (2008)
- [142]. Yan, B. and Miyamoto, A., 2006. A comparative study of modal parameter identification based on wavelet and Hilbert–Huang transforms. *Computer-Aided Civil and Infrastructure Engineering*, 21(1), 9-23.
- [143]. Peng, Z.K., Peter, W.T. and Chu, F.L., 2005. A comparison study of improved Hilbert–Huang transform and wavelet transform: application to fault diagnosis for rolling bearing. *Mechanical Systems and Signal Processing*, 19(5), 974-988.
- [144]. Herlufsen, H., Gade, S. and Konstantin-Hansen, H., 1999. Characteristics of the Vold-Kalman order tracking filter. *Sound and Vibration*, 33, 34-44.
- [145]. Brandt, A., *Noise and vibration analysis: signal analysis and experimental procedures*. John Wiley & Sons, 2011.
- [146]. Wilkens, H. IMAT+Signal toolbox, ATA Engineering Inc., www.ata-e.com/downloads/imat/all_doc/rtk/doc/#Vold-Kalman_Filter.htm, Accessed: September 4, 2016.
- [147]. Cho, M.R., Choi, J.K. and Han, D.C., 2001. Calculation of mixed lubrication at piston ring and cylinder liner interface. *KSME international journal*, 15(7), 859-865.
- [148]. www.en.wikipedia.org/wiki/Computational_intelligence, Accessed: January 11, 2017.
-

-
- [149]. Farrar, C.R. and Worden, K., Structural health monitoring: a machine learning perspective. John Wiley & Sons, 2012.
- [150]. Sinha, J.K., Lees, A.W. and Friswell M.I., 2004. Estimating unbalance and misalignment of a flexible rotating machine from a single run-down. *Journal of Sound and Vibration* 272 967–989.
- [151]. Sekhar A.S. and Prabhu B.S., 1995. Effects of coupling misalignment on vibrations of rotating machinery. *Journal of Sound and Vibration* 185(4), 665-671.
- [152]. Vyas, N.S. and Rao, J.S., 1997. Dynamic stress analysis and a fracture mechanics approach to life prediction of turbine blades. *Mechanism and Machine Theory*, 32(4), 511-527.
- [153]. Hu, K. and Vlahopoulos, N., 2002. A finite element formulation for coupling rigid and flexible body dynamics of rotating beams *Journal of Sound and vibration* 253(3), 603-630.
- [154]. Shabana, A.A., 1997. Flexible multibody dynamics: review of past and recent developments. *Multibody System Dynamics*, 1(2), 189-222.
- [155]. Wasfy, T.M. and Noor, A.K., 2003. Computational strategies for flexible multibody systems. *Appl Mech Rev Vol 56, No 6*, 553-613.
- [156]. Simeon, B., 2006. On Lagrange multipliers in flexible multibody dynamics. *Comput. Methods Appl. Mech. Engrg.* 195, 6993–7005.
- [157]. Simeon, B., Computational flexible multibody dynamics. In *A Differential-Algebraic Approach. Differential-Algebraic Equations Forum*. Springer, Heidelberg, 2013.
- [158]. Gerstmayr, J. and Schoberl, J., 2006. A 3D finite element method for flexible multibody systems. *Multibody Syst Dyn* 15:309–324
- [159]. Hydrolock, www.en.wikipedia.org/wiki/Hydrolock, Accessed: August 20, 2017.
- [160]. McGlothlin, M., Complete 7.3L Power Stroke Long-Block Build, www.trucktrend.com/how-to/engine/1005dp-complete-73-power-stroke-long-block-rebuild, Accessed August 20, 2017
- [161]. Josh L 2014. Nissan Oil Pump Replacement Solution for Skyline GTR Engine RB26DETT, www.skylife4ever.com/2011/01/real-problem-with-rb26-oil-pump.html, Accessed: January 20, 2017
- [162]. Commando, N., www.accessnorton.com/commando-crankshaft-porn-t8365-180.html, Accessed: January 20, 2017.
-

-
- [163]. Corvair crank failure, www.n56ml.com/corvair/flexplate/crankshaft/ Accessed: November 24, 2016.
- [164]. Sharp, R.S., Evangelou, S., and Limebeer, D.J.N., 2004. Advances in the modelling of motorcycle dynamics. *Multibody System Dynamics* 12: 251–283.
- [165]. Ambrósio J.A.C. and Gonçalves J.P.C., 2001. Complex flexible multibody systems with application to vehicle dynamics. *Multibody System Dynamics* 6: 163–182.
- [166]. Kanchwala, H., Studies in simplified dynamic modeling and characterization of vehicle suspensions. Ph. D Thesis, Indian Institute of Technology Kanpur, India, 2017.
- [167]. Rouillard, V. and Sek, M.A., 2001. Simulation of non-stationary vehicle vibrations. *Proceedings of the Institution of Mechanical Engineers, Part D: Journal of Automobile Engineering*, 215, 1069-1075
- [168]. Azadi, S. and Soltani, A., 2009. Fault detection of vehicle suspension system using wavelet analysis *Vehicle System Dynamics* Vol. 47, No. 4, 403–418.
- [169]. Schmidt, D.K. and Raney D.L., 2001. Modeling and simulation of flexible flight vehicles. *Journal of Guidance, Control, and Dynamics*, Vol. 24, No. 3, 539-546.
- [170]. Tsyfansky, S.L. and Beresnevich, V.I., 2000. Non-linear vibration method for detection of fatigue cracks in aircraft wings. *Journal of Sound and Vibration* 236(1), 49-60.
- [171]. Junhong, Z. and Jun, H., 2006. CAE process to simulate and optimise engine noise and vibration. *Mechanical Systems and Signal Processing*, 20(6), 1400-1409.
- [172]. Siano, D. and Citarella, R., 2014. Elastic multi body simulation of a multi-cylinder engine. *Open Mechanical Engineering Journal*, 8, 157-169.
- [173]. Offner, G. and Pribsch, H.H., 2006. Flexible multi-body dynamics simulation-a powerful method for prediction of structure borne noise of internal combustion engines. In *Proceedings of the International Conference on Noise and Vibration Engineering-ISMA2006*, 2663-2677.
- [174]. Guo, J., Zhang, W. and Zou, D., 2011. Investigation of dynamic characteristics of a valve train system. *Mechanism and Machine Theory*, 46(12), 1950-1969.
- [175]. Rivola, A., Carlini, A. and Dalpiaz, G., 2002. Modelling the elastodynamic behaviour of a desmodromic valve train. In *ISMA 2002 International Conference on Noise & Vibration Engineering*, 1417-1426.
-

- [176]. Mourelatos, Z.P., 2001. A crankshaft system model for structural dynamic analysis of internal combustion engines. *Computers and Structures* 79 (2001), 2009-2027.
- [177]. Khemili, I. and Romdhane, L., 2008. Dynamic analysis of a flexible slider–crank mechanism with clearance. *European Journal of Mechanics-A/Solids*, 27(5), 882-898.
- [178]. Tounsi, M., Chaari, F., Abbes, M.S., Fakhfakh, T. and Haddar, M., 2011. Failure analysis of a cam–follower system affected by a crack. *Journal of Failure Analysis and Prevention*, 11(1), 41-50.
- [179]. Villanueva, J.B., Espadafor, F.J., Cruz-Peragon, F. and García, M.T., 2011. A methodology for cracks identification in large crankshafts. *Mechanical systems and signal processing*, 25(8), 3168-3185.
- [180]. Dupac, M. and Beale, D.G., 2010. Dynamic analysis of a flexible linkage mechanism with cracks and clearance. *Mechanism and Machine Theory* 45, 1909–1923
- [181]. Tadjbakhsh, I.G. and Christos, C.J. 1986. Dynamic stability of the flexible connecting rod of a slider crank mechanism. *Journal of Mechanisms, Transmissions, and Automation in Design*, 1986, Vol. 108, 487-496.
- [182]. Goudas, I., Stavrakis, I. and Natsiavas, S., 2004. Dynamics of slider-crank mechanisms with flexible supports and non-ideal forcing. *Nonlinear Dynamics* 35: 205–227.
- [183]. Ha, J., Fung, R., Chen, K. and Hsien, S. 2006. Dynamic modeling and identification of a slider-crank mechanism. *Journal of Sound and Vibration* 289, 1019–1044
- [184]. Kim, S.J., Kim, S.G., Oh K.S. and Lee S.K., 2008. Excitation force analysis of a powertrain based on CAE technology. *International Journal of Automotive Technology*, Vol. 9, No. 6, pp. 703–711.
- [185]. Metallidis, P. and Natsiavas, S., 2003. Linear and nonlinear dynamics of reciprocating engines. *International Journal of Non-Linear Mechanics* 38, 723-738.
- [186]. Shih, Y. and Chung, C., 2013. Vibration Analysis of the Flexible Connecting Rod With the Breathing Crack in a Slider-Crank Mechanism. *Journal of Vibration and Acoustics*, Vol. 135 / 06100, 1-9
- [187]. Daniel, G.B. and Cavalca, K.L., 2011. Analysis of the dynamics of a slider–crank mechanism with hydrodynamic lubrication in the connecting rod–slider joint clearance *Mechanism and Machine Theory* 46 1434–1452
- [188]. Erkaya, S. and Uzmay, I., 2010. Experimental investigation of joint clearance effects on the dynamics of a slider-crank mechanism. *Multibody Syst Dyn* 24: 81–102

-
- [189]. Hou, J., Wicks, B.J. and Antoniou, R.A., 2002. An investigation of fatigue failures of turbine blades in a gas turbine engine by mechanical analysis. *Engineering Failure Analysis*, 9(2), 201-211.
- [190]. Qu, Z.Q., *Model order reduction techniques with applications in finite element analysis*. Springer Science & Business Media, 2013.
- [191]. Guyan, R.J., 1965. Reduction of stiffness and mass matrices. *AIAA journal*, 3(2), 380-380.
- [192]. Kammer, D.C. and Triller, M.J., 1996. Selection of component modes for Craig-Bampton substructure representations. *Journal of Vibration and Acoustics*, 118(2), 264-270.
- [193]. Craig, R.R. and Kurdila, A.J., *Fundamentals of structural dynamics*. John Wiley & Sons, 2006.
- [194]. Craig, R.R., 1995. Substructure methods in vibration. *Journal of Vibration and Acoustics*, 117(B), 207-213.
- [195]. Bampton, M.C. and Craig, R.R., 1968. Coupling of substructures for dynamic analyses. *AIAA Journal*, 6(7), 1313-1319.
- [196]. Kim, C. and Ro, P.I., 2002. An accurate full car ride model using model reducing techniques. *Journal of Mechanical Design*, Vol. 124, 697-705.
- [197]. Ersal, T., Kittirungsi, B., Fathy H.K. and Stein J.L., 2009. Model reduction in vehicle dynamics using importance analysis *Vehicle System Dynamics* Vol. 47, No. 7, July 2009, 851–865.
- [198]. Rao, J.S., *Rotor dynamics*. New Age International, 1996.
- [199]. MSC NASTRAN Rotordynamics User's Guide, Version 2004. The MacNeal-Schwendler Corporation, 2016.
- [200]. Adams/Flex Help, www.simcompanion.mscsoftware.com/Docs, Accessed: August 20, 2017.
- [201]. Norton, R.L., *Cam design and manufacturing handbook*. Industrial Press Inc, 2009.
- [202]. Shabana A.A., *Dynamics of multibody systems*. Cambridge University Press, 2005.
- [203]. Drab, C.B., Engl, H.W., Haslinger, J.R., Offner, G., Pfau, R.U. and Zulehner, W., 2009. Dynamic simulation of crankshaft multibody systems. *Multibody system dynamics*, 22(2), 133-144.
-

-
- [204]. Yamagata, H., The science and technology of materials in automotive engines. Elsevier, 2005.
- [205]. BOOST User's Guide, Version 3.3, AVL List GmbH, Graz, Austria, 2000.
- [206]. Ramachandran, S., 2009. Rapid thermodynamic simulation model of an internal combustion engine on alternate fuels. In Proceedings of the International MultiConference of Engineers and Computer Scientists, Vol. 2, 18-20.
- [207]. Kolchin, A.I. and Demidov, V.P., Design of automotive engines. MIR pub., 1984.
- [208]. Rangwala, A.S., Reciprocating machinery dynamics. New Age International, 2006.
- [209]. Mistry, K.N., 2009. Simulation and modeling of friction force and oil film thickness in piston ring–cylinder liner assembly of an IC engine. In Proceedings of the World Congress on Engineering, Vol. 2.
- [210]. Patir, N. and Cheng, H.S., 1978. An average flow model for determining effects of three-dimensional roughness on partial hydrodynamic lubrication. Journal of lubrication Technology, 100(1), 12-17.
- [211]. Cho, M.R., Choi, J.K. and Han, D.C., 2001. Calculation of mixed lubrication at piston ring and cylinder liner interface. KSME international journal, 15(7), 859-865.
- [212]. Takiguchi, M., Machida, K. and Furuhashi, S., 1988. Piston friction force of a small high speed gasoline engine. Journal of tribology, 110(1), 112-118.
- [213]. Mufti, R.A., Priest, M. and Chittenden, R.J., 2008. Analysis of piston assembly friction using the indicated mean effective pressure experimental method to validate mathematical models. Proceedings of the Institution of Mechanical Engineers, Part D: Journal of Automobile Engineering, 222(8), 1441-1457.
- [214]. Dimarogonas, A.D., Paipetis, S.A. and Chondros, T.G., Analytical methods in rotor dynamics. Springer Science & Business Media, 2013.
- [215]. Wang, A.S.D., Kishore, N.N. and Li, C.A., 1985. Crack development in graphite-epoxy cross-ply laminates under uniaxial tension. Composites Science and Technology, 24(1), 1-31.
- [216]. Agrawal, A.K. and Kishore, N.N., 2001. A study of free surface effects on through cracks using BEM. Engineering Fracture Mechanics, 68(11), 1297-1316.
- [217]. FATIGUE User's Guide, Version 2005. The MacNeal-Schwendler Corporation, 2005.
- [218]. Kumar, P., Elements of fracture mechanics. Tata McGraw-Hill Education, 2009.
-

-
- [219]. Ellyin, F., *Fatigue damage, crack growth and life prediction*. Springer Science & Business Media, 2012.
- [220]. Wang, P., Youn, B.D. and Hu, C., 2012. A generic probabilistic framework for structural health prognostics and uncertainty management. *Mechanical Systems and Signal Processing*, 28, 622-637.
- [221]. Achenbach, J.D., 2009. Structural health monitoring—What is the prescription? *Mechanics Research Communications*, 36(2), 137-142.
- [222]. Tishun Peng, J.H., Liu, Y., Saxena, A., Celaya, J. and Goebel, K., Integrated fatigue damage diagnosis and prognosis under uncertainties. Annual Conference of the Prognostics and Health Management Society 2012
- [223]. Vyas, N.S. and Satishkumar, D., 2001. Artificial neural network design for fault identification in a rotor-bearing system. *Mechanism and machine theory*, 36(2), 157-175.
- [224]. Fisher, R.A., 1936. The use of multiple measurements in taxonomic problems. *Annals of eugenics*, 7(2), 179-188.
- [225]. Duda, R.O., Hart, P.E. and Stork, D.G., *Pattern classification*. John Wiley & Sons, 2012.
- [226]. Ogaji, S.O.T., Marinai, L., Sampath, S., Singh, R. and Prober, S.D., 2005. Gas-turbine fault diagnostics: a fuzzy-logic approach. *Applied Energy*, 82(1), 81-89.
- [227]. Liu, X., Ma, L. and Mathew, J., 2006. Machinery fault diagnosis based on feature level fuzzy integral data fusion techniques. In 2006 4th IEEE International Conference on Industrial Informatics, 857-862.
- [228]. Jang, J.S.R., Sun, C.T. and Mizutani, E., *Fuzzy inference systems. Neuro-fuzzy and soft computing: a computational approach to learning and machine intelligence*, Prentice Hall Inc, 1997, 73-91.
- [229]. Cadini, F., Zio, E. and Avram, D., 2009. Monte Carlo-based filtering for fatigue crack growth estimation. *Probabilistic Engineering Mechanics*, 24(3), 367-373.
- [230]. Cobb, A.C., Michaels, J.E. and Michaels, T.E., 2008, March. Experimental verification of a Kalman filter approach for estimating the size of fastener hole fatigue cracks. In Proc. SPIE (Vol. 6935, No. 693533, pp. 1-12).
- [231]. Zio, E. and Pelsoni, G., 2011. Particle filtering prognostic estimation of the remaining useful life of nonlinear components. *Reliability Engineering & System Safety*, 96(3), 403-409.
-

-
- [232]. Orchard, M.E. and Vachtsevanos, G.J., 2009. A particle-filtering approach for on-line fault diagnosis and failure prognosis. *Transactions of the Institute of Measurement and Control*, 31(3-4), 221-246.
- [233]. An, D., Choi, J.H. and Kim, N.H., 2013. Prognostics 101: A tutorial for particle filter-based prognostics algorithm using Matlab. *Reliability Engineering & System Safety*, 115, 161-169.
- [234]. Lin, C.T. and Lee, C.G., 1996. *Neural fuzzy systems*. PTR Prentice Hall.
- [235]. Engelbrecht, A.P., 2007. *Computational intelligence: an introduction*. John Wiley & Sons.
- [236]. Adeli, H. and Jiang, X., 2006. Dynamic fuzzy wavelet neural network model for structural system identification. *Journal of Structural Engineering*, 132(1), 102-111.
- [237]. Palade, V., Bocaniala, C.D. and Jain, L.C., 2006. *Computational intelligence in fault diagnosis*. Springer.
- [238]. Marwala, T., 2012. *Condition monitoring using computational intelligence methods: applications in mechanical and electrical systems*. Springer & Business Media.
- [239]. Alexandridis, A.K. and Zaprani, A.D., 2013. Wavelet neural networks: A practical guide. *Neural Networks*, 42, 1-27.
- [240]. Vachtsevanos, G., Wang, P. and Echauz, J., 2001. A wavelet neural network framework for diagnostics of complex engineered systems. In *Intelligent Control, 2001.(ISIC'01). Proceedings of the 2001 IEEE International Symposium*, 79-84.
- [241]. Wang, P. and Vachtsevanos, G., 2001. Fault prognostics using dynamic wavelet neural networks. *AI EDAM*, 15(4), 349-365.
- [242]. Ayoubi, M. and Isermann, R., 1997. Neuro-fuzzy systems for diagnosis. *Fuzzy sets and Systems*, 89(3), 289-307.
- [243]. Zio, E. and Gola, G., 2009. A neuro-fuzzy technique for fault diagnosis and its application to rotating machinery. *Reliability Engineering & System Safety*, 94(1), 78-88.
- [244]. Lou, X. and Loparo, K.A., 2004. Bearing fault diagnosis based on wavelet transform and fuzzy inference. *Mechanical systems and signal processing*, 18(5), 1077-1095.
- [245]. Wu, J.D., Hsu, C.C. and Wu, G.Z., 2009. Fault gear identification and classification using discrete wavelet transform and adaptive neuro-fuzzy inference. *Expert Systems with Applications*, 36(3), 6244-6255.
-

-
- [246]. Chen, C., Vachtsevanos, G. and Orchard, M.E., 2012. Machine remaining useful life prediction: An integrated adaptive neuro-fuzzy and high-order particle filtering approach. *Mechanical Systems and Signal Processing*, 28, 597-607.
- [247]. Wang, W.Q., Golnaraghi, M.F. and Ismail, F., 2004. Prognosis of machine health condition using neuro-fuzzy systems. *Mechanical Systems and Signal Processing*, 18(4), 813-831.
- [248]. Lei, Y., He, Z., Zi, Y. and Hu, Q., 2007. Fault diagnosis of rotating machinery based on multiple ANFIS combination with GAs. *Mechanical systems and signal processing*, 21(5), 2280-2294.
- [249]. Funsten, B.T., ECG Classification with an Adaptive Neuro-Fuzzy Inference System, M. S. Thesis, California Polytechnic State University, San Luis Obispo, USA, 2015.
- [250]. Soualhi, A., Razik, H., Clerc, G. and Doan, D.D., 2014. Prognosis of bearing failures using hidden Markov models and the adaptive neuro-fuzzy inference system. *IEEE Transactions on Industrial Electronics*, 61(6), 2864-2874.
- 